

**MODELLING DRY AND WET EXTREMES OVER THE CANADIAN PRAIRIE
PROVINCES BASED ON THE DYNAMICAL DOWNSCALING AND MULTIVARIATE
FREQUENCY ANALYSIS APPROACHES**

A Thesis Submitted to the College of
Graduate Studies and Research
In Partial Fulfillment of the Requirements
For the Degree of Doctor of Philosophy
In the School of Environment and Sustainability
University of Saskatchewan
Saskatoon

By

MOHAMMAD BADRUL MASUD

© Copyright Mohammad Badrul Masud, May, 2016. All rights reserved.

PERMISSION TO USE STATEMENT

In presenting this thesis in partial fulfilment of the requirements for a Postgraduate degree from the University of Saskatchewan, I agree that the Libraries of this University may make it freely available for inspection. I further agree that permission for copying of this thesis in any manner, in whole or in part, for scholarly purposes may be granted by the professor or professors who supervised my thesis work or, in their absence, by the Head of the Department or the Dean of the College in which my thesis work was done. It is understood that any copying or publication or use of this thesis or parts thereof for financial gain shall not be allowed without my written permission. It is also understood that due recognition shall be given to me and to the University of Saskatchewan in any scholarly use which may be made of any material in my thesis.

Requests for permission to copy or to make other use of material in this thesis in whole or part should be addressed to:

Executive Director
School of Environment and Sustainability
University of Saskatchewan
Room 323, Kirk Hall
117 Science Place
Saskatoon, SK S7N 5C8, Canada
Phone: (306) 966-1985
Fax: (306) 966-2298
Email: sens.info@usask.ca

ABSTRACT

The primary tools to assess climate change are the Atmosphere–Ocean General Circulation Model (AOGCM) or Regional Climate Model (RCM) transient climate change simulations. Currently, RCMs offer higher spatial resolution than AOGCMs and therefore are preferred for assessing impact of climate change on different components of the hydrological cycle at regional domains of interest. The overall purpose of this research was to evaluate the impact of climate change on dry and wet climate extremes over the Canadian Prairie Provinces of Alberta, Saskatchewan and Manitoba using a multi–RCM ensemble from the North American Regional Climate Change Assessment Program (NARCCAP). This region of Canada is characterized by highly variable hydroclimate, with recurrent droughts and floods and localized summer convective storm activity often resulting in heavy precipitation events and thus poses many challenges for water managers.

At first, the Saskatchewan River Basin, the largest river in the study area, was evaluated and drought vulnerable parts of the basin were identified based on historical data and multivariate frequency analysis approaches. For the development of projected changes to drought characteristics, the research effort was extended over the entire study area and changes to various return levels of drought severity, duration and maximum severity were developed based on NARCCAP RCM simulations and multivariate frequency analysis approaches. It was found that the southern and south-western parts of the study area will experience increased drought severity in the future. Based on the projected bi- and trivariate joint occurrence probabilities of drought characteristics, southern parts along with the central parts of the study area were found to be highly drought vulnerable, whereas the southwestern and southeastern parts were found less vulnerable.

Though producing reliable estimates of changes in precipitation extremes remains an important challenge under climate change, this study attempted to develop projected changes to April–October short- and long-duration precipitation extremes based on the NARCCAP RCM simulations and regional frequency analysis approach. Projected changes to selected regional return levels of precipitation extremes were found mostly statistically significant, with relatively larger changes noted for the southeastern regions and smaller for the southwestern and western regions of the study area.

ACKNOWLEDGMENTS

"In the name of Allah, most Gracious, most Compassionate".

I would like to thank my supervisor, Dr. Naveed Khaliq, for his guidance and advice throughout the course of this dissertation. His input has been invaluable and contributed immensely to the success of this research. I also would like to thank my co-supervisor Prof. Howard Wheeler for his invaluable support and advice, as well as the members of my advisory committee: Prof. Jeffrey McDonnell, Prof. Suren Kulshreshtha, Dr. Yanping Li, and Dr. Mohamed Boulfiza. I would like to acknowledge Prof. Charles Maule for serving on my committee until his retirement.

My gratitude extends to the Canada Excellence Research Chair in Water Security, School of Environment and Sustainability and the Government of Saskatchewan for their financial support. Special thanks to my friends at the Global Institute for Water Security who helped in different ways during my Ph.D. research. I will inevitably forget their names, and for that I apologize, but I would like to specially thank: Dr. Muluneh Mekonnen, Dr. Kwok Chun, Dr. Ali Nazemi, Elvis Asong, Amir Sadeghian and Edward Bam.

I wish to thank all lovely people in Bangladesh who graciously supported my 18 years of education in different institutes of Bangladesh.

Last but not least, I need to thank my parents and family members who helped me a lot unconditionally throughout my life. I deeply miss my parents who are not with me to share my success and joy. But I know they are always with me. Endless support, sacrifice and encouragement from my lovely wife, Jannatul Ferdous Jui, is highly acknowledged. Without her support, I might not have been able to finish this research work. Thank you my sweet and lovely daughter 'Ryefa' who brought a significant change in my life with lots of happiness.

DEDICATION

This thesis is dedicated to
My parents (late Mohammad Ismail Mia and Khorsheda Begum),
Wife (Jannatul Ferdous Jui),
Daughter (Ryefa Jannat Masud) and
My family members

TABLE OF CONTENTS

PERMISSION TO USE STATEMENT	i
ABSTRACT.....	ii
ACKNOWLEDGMENTS	iii
DEDICATION.....	iv
LIST OF TABLES.....	ix
LIST OF FIGURES	x
LIST OF ABBREVIATIONS.....	xv
CHAPTER 1	1
INTRODUCTION	1
1.1 Research Purpose	4
1.1.1 Knowledge gaps.....	4
1.1.2 Objectives	5
1.2 Study area.....	5
1.3 Thesis outline	6
1.4 Copyright and author permissions	8
References.....	9
CHAPTER 2	13
ANALYSIS OF METEOROLOGICAL DROUGHTS FOR THE SASKATCHEWAN RIVER BASIN USING UNIVARIATE AND BIVARIATE APPROACHES	13
Abstract.....	13
2.1 Introduction.....	14
2.2 Study area and data	17
Figure 2.1:.....	18
2.3 Methodology.....	19
2.3.1 Drought indices and time scales	19

2.3.2 Computation of potential evapotranspiration (<i>PET</i>).....	21
2.3.3 Characteristics of drought events.....	23
2.3.4 Selection of marginal distributions.....	23
2.3.5. Copula functions for bivariate frequency analysis.....	25
2.3.6. Calculation of joint occurrence probabilities.....	26
2.3.7. Identification of drought sensitive geographic regions.....	26
2.3.8. Other considerations.....	27
2.4. Results and discussion.....	28
2.4.1. Choice of marginal distributions and copula functions.....	28
2.4.2. Drought characteristics.....	31
2.4.3. Univariate analyses.....	36
2.4.4. Bivariate analyses.....	36
2.4.5. Drought sensitive geographic regions.....	37
2.5. Summary and conclusions.....	40
Acknowledgements.....	43
References.....	43
CHAPTER 3.....	49
FUTURE CHANGES TO DROUGHT CHARACTERISTICS OVER THE CANADIAN PRAIRIE PROVINCES BASED ON NARCCAP MULTI-RCM ENSEMBLE.....	49
Abstract.....	50
3.1 Introduction.....	50
3.2 Study area, observed and model data, and the reference grid.....	53
3.2.1 Observed data.....	54
3.2.2 Model simulations.....	54
3.2.3 Reference grid.....	55
3.3 Methodology.....	56
3.3.1 Drought indices, drought events and their characteristics.....	56
3.3.2 Delineation of homogeneous geographic regions.....	58
3.3.3 Regional characteristics of drought severity and duration.....	58

3.3.4 Copula-based bi- and trivariate analyses	59
3.3.5 Estimation of drought risks	61
3.4 Results and discussion	62
3.4.1 Geographic homogeneous regions	63
3.4.2 Validation of RCM-simulated drought characteristics and lateral boundary forcing errors	63
3.4.3 Projected changes to drought characteristics	69
3.4.4 Drought vulnerable regions.....	74
3.4.5 Drought analysis for the agricultural growing season	75
3.5 Conclusions.....	78
Acknowledgements.....	80
References.....	80
CHAPTER 4	87
PROJECTED CHANGES TO SHORT- AND LONG-DURATION PRECIPITATION EXTREMES OVER THE CANADIAN PRAIRIE PROVINCES.....	87
Abstract.....	87
4.1 Introduction.....	88
4.2 Study area, observations and model simulations	91
4.3 Methodology.....	94
4.3.1 Reference grid.....	94
4.3.2 Precipitation extremes and their characteristics.....	94
4.3.3 Contiguous homogeneous regions and the RFA approach	95
4.3.4 Projected changes to precipitation extremes.....	96
4.4 Results and discussion	98
4.4.1 Delineation and validation of homogeneous regions.....	98
4.4.2 Validation of RCMs.....	99
4.4.3 Projected changes to precipitation extremes.....	103
4.5 Conclusions.....	115

Acknowledgements.....	117
References.....	117
CHAPTER 5	121
SUMMARY, CONCLUSIONS, AND FUTURE WORK	121
5.1 Summary.....	121
5.2 Conclusions.....	122
5.3 Future Work	125
References.....	126
APPENDIX A: APPENDICES FOR CHAPTER 3.....	127
APPENDIX B: SUPPORTING MATERIALS FOR CHAPTER 3	129
APPENDIX C: SUPPORTING MATERIALS FOR CHAPTER 4	132
APPENDIX D: ATTRIBUTES OF OBSERVATION STATIONS.....	155
APPENDIX E. PERMISSIONS FOR USE OF PUBLISHED MANUSCRIPTS	159

LIST OF TABLES

Table 2.1: Bivariate Archimedean copulas and their corresponding generator functions and parameters.....	24
Table 2.2: Watershed based averaged values of AIC and RMSE for 13 watersheds (WSs) and four copula functions fitted to drought severity and duration derived from drought events defined on the basis of SPI of 12-month time scale.	30
Table 3.1: The NARCCAP simulations used in the study.....	55
Table 4.1: The NARCCAP simulations considered in the study.....	93
Table 4.2: Percentage of 95% confidence interval comparisons wherein changes in 2-, 5-, 10-, 25-, and 50-yr regional return levels of 3-, 6-, 12-, 24-, and 48-h precipitation extremes were found statistically significant.	109

LIST OF FIGURES

Figure 1.1: Study area showing the Saskatchewan River Basin spanning the provinces of Alberta, Saskatchewan and Manitoba. The topography, major river systems and lakes are also indicated. The inset shows the location of the study area in Canada	7
Figure 2.1: The Saskatchewan River Basin (405,864 km ² drainage area) with its 13 watersheds and spatial distribution of annual precipitation developed from 10 km x 10 km gridded observed dataset for the 1961 to 2003 period. Inset shows location of the study area in Canada. The abbreviations AB, SK and MN mean Alberta, Saskatchewan and Manitoba, respectively.	18
Figure 2.2: A schematic diagram of the methodology adopted for univariate and bivariate frequency analyses of drought characteristics in the SRB.....	20
Figure 2.3: Definition sketch of drought characteristics (top panel) showing three drought events (labeled as N_1 , N_2 , and N_3) and a SPI-based observed example (bottom panel) for a representative grid point (Lat: 52.52; Lon: -109.1) from the Eagle Creek watershed.....	22
Figure 2.4: L-moment ratio diagrams of grid point based all samples of P (top row) and E (bottom row) corresponding to 3- (blue dots), 6- (cyan dots), and 12-month (black dots) time scales for the entire SRB. Yellow circles represent group averaged values. LN2, EV1 and Exp abbreviations are used to represent the two-parameter lognormal, Extreme Value Type-I (i.e., Gumbel) and exponential distributions. Other abbreviations are explained in the text.....	29
Figure 2.5: Spatial patterns of (a) average severity, (b) average duration, (c) maximum severity, and (d) number of drought events, obtained on the basis of SPI and SPEI values corresponding to 3-, 6-, and 12-month time scales.....	32
Figure 2.6: Box and whisker plots of the Spearman rank correlation coefficients for various combinations of drought characteristics for the SRB. Results for the case of SPI are shown in red and those for the case of SPEI in blue. The boxes correspond to the interquartile range (IQR), the line in the middle of the box to the median value and the whiskers to either the maximum value or the 1.5 times the IQR. Outliers that lie outside the 1.5 times IQR range are shown using the plus sign.	33

Figure 2.7: Spatial patterns of 5-, 10-, 20-, and 30-year return values of drought severity, derived on the basis of SPI/SPEI values of 3-, 6-, and 12-month time scales. 34

Figure 2.8: Spatial patterns of 5-, 10-, 20-, and 30-year return values of drought duration, derived on the basis of SPI/SPEI values of 3-, 6-, and 12-month time scales. 35

Figure 2.9: Spatial patterns of joint occurrence probability (in %) of “drought severity and duration” exceeding their respective thresholds at the same time [i.e., $P_2 = P(S > s \text{ and } D > d)$]. The thresholds (i.e., s and d) correspond to 5-, 10-, 20-, and 30-year return period values.. 38

Figure 2.10: Spatial patterns of joint occurrence probability (in %) of “drought severity or duration” exceeding their respective thresholds at the same time [i.e., $P_1 = P(S > s \text{ or } D > d)$]. The thresholds (i.e., s or d) correspond to 5-, 10-, 20-, and 30-year return period values..... 39

Figure 2.11: Drought sensitive geographic regions of the SRB identified on the basis of joint occurrence probability P_2 (shown in %) corresponding to 5- and 30-year return period thresholds of S and D . Results for both SPI and SPEI and three different time scales are shown. Similar patterns are found for other return period (i.e., 10- and 20-year) thresholds..... 41

Figure 3.1: Map of the study area overlaid with the reference grid; inset shows location of the study region (AB–Alberta; SK–Saskatchewan; MN–Manitoba) in Canada..... 53

Figure 3.2: Fifteen homogeneous regions (Region 1 to 15) delineated on the basis of hierarchical clustering and verified using the uni- and multivariate homogeneity analysis approaches..... 62

Figure 3.3: Comparison of observed and ensemble averaged RCM_NCEP simulated mean drought (a, b) severity and (d, e) duration for the 1981–2003 period. Relative differences between results shown in (b, a) and (e, d) panels are given in (c) and (f), respectively. 64

Figure 3.4: Comparison of observed and ensemble averaged RCM_NCEP simulated 20- and 50-year regional return levels of drought (a, b) severity and (d, e) duration for the 1981–2003 period. Relative differences between return levels shown in (b, a) and (e, d) are given in (c) and (f), respectively. 65

Figure 3.5: Relative difference (in %) between observed and RCM_NCEP simulated 20- and 50-yr regional return levels of drought severity for the 1981–2003 period. 66

Figure 3.6: Relative difference (in %) between observed and RCM_NCEP simulated 20- and 50-yr regional return levels of drought duration for the 1981–2003 period. 66

Figure 3.7: Scatterplots of 20- and 50-yr return levels of SPI- and SPEI-based (a) severity and (b) duration for the 1981-2000 period. The x-axis corresponds to NCEP driven RCM simulation, while the y-axis corresponds to AOGCM driven simulation. Numbers in each panel represent average percentage difference between the AOGCM- and NCEP-driven simulated return levels. Results based on SPI are shown in black and red color and those for the case of SPEI are shown in blue and pink color. 68

Figure 3.8: Projected changes (in %) to SPI and SPEI based (a) mean drought severity (b) mean drought duration for the 2041–2070 period with respect to the current 1970–1999 period. 70

Figure 3.9: Projected changes (in %) to regional 20-year return levels of drought (a) severity and (b) duration for the 2041–2070 period with respect to the current 1970–1999 period. Projected changes to drought severity at the regional level are also studied by comparing 20- and 50-year return levels derived from AOGCM-driven RCM simulations for the future 2041–2070 period with those for the current 1970–1999 period. 71

Figure 3.10: Projected changes (in %) to regional 50-year return levels of drought (a) severity and (b) duration for the 2041–2070 period with respect to the current 1970–1999 period. 72

Figure 3.11: Changes (in %) to (a) bivariate joint occurrence probabilities corresponding to 20-year return period thresholds of S and D and (b) trivariate joint occurrence probabilities corresponding to 20-year return period thresholds of S , D and S_{max} for the 2041–2070 period with respect to the current 1970–1999 period. 73

Figure 3.12: Changes (in %) to (a) bivariate joint occurrence probabilities corresponding to 50-year return period thresholds of S and D and (b) trivariate joint occurrence probabilities corresponding to 50-year return period thresholds of S , D and S_{max} for the 2041–2070 period with respect to the current 1970–1999 period. 76

Figure 3.13: Projected changes (in %) to SPI- and SPEI-based (a) mean drought severity (b) mean drought duration for the 2041–2070 period with respect to the current 1970–1999 period for the agricultural growing season. 77

Figure 4.1: Map of the study area overlaid with the reference grid. Precipitation stations for adjusted and rehabilitated observed dataset (DS1) are shown using five different symbols to highlight the corresponding homogeneous region (R1 to R5) they are associated with and location of engineering climate stations (DS2) where continuous seasonal precipitation is recorded. Inset shows location of the study area (i.e. Alberta–AB; Saskatchewan–SK; Manitoba–MN) in Canada..... 92

Figure 4.2: Comparison of 2-, 5-, 10-, 25-, and 50-yr observed and (a) MM5I_NCEP and (b) WRFG_NCEP simulated return levels of 6-, 12-, and 24-h seasonal (April to October) precipitation extremes for the current 1981–2000 reference period. 101

Figure 4.3: Comparison of 2-, 5-, 10-, 25-, and 50-yr observed and ensemble-averaged RCM_NCEP simulated return levels of 6-, 12-, and 24-h seasonal (April to October) precipitation extremes for the current 1981–2000 reference period. 102

Figure 4.4: Projected changes (in %) in selected grid-point level return levels of 3-, 6-, 12-, 24-, and 48-h precipitation extremes simulated by (a) CRCM_CCSM and (b) MM5I_CCSM for the 2041–2070 period with respect to the 1971–2000..... 105

Figure 4.5: Ensemble-averaged projected changes (in %) in selected grid-point level return levels of 3-, 6-, 12-, 24-, and 48-h precipitation extremes for the 2041–2070 period with respect to the 1971–2000..... 106

Figure 4.6: Projected changes (in %) in selected regional return levels of 3-, 6-, 12-, 24-, and 48-h extremes simulated by 11 RCM_AOGCM combinations for the 2041–2070 period with respect to the 1971–2000. Ensemble-averaged change is shown using red circle. 107

Figure 4.7: Observed precipitation intensity-duration-frequency plots (symbols) for nine selected sites from R1 to R5 regions based on precipitation extremes of 5-, 10-, 15-, 30-, 60-min, 2-, 6-, 12-, and 24-h durations (shown along the x-axis) from the engineering climate stations dataset

(DS2). Scaling relationships (lines) estimated using the least-squares algorithm for each return period are also plotted and the corresponding coefficient of determination (i.e. R^2) values are shown as well. 110

Figure 4.8: Same as in Fig. 4.7 but for observed regional precipitation intensity-duration-frequency plots (symbols) for regions R1 to R5. 111

Figure 4.9: RCM3_NCEP simulated regional precipitation intensity-duration-frequency plots (filled symbols) for regions R1 to R5 based on precipitation extremes of 3-, 6-, 9-, 12-, 15-, 18-, and 24-h durations (shown along the x-axis). Linear and non-linear scaling relationships (colored solid lines) estimated using the least-squares algorithm and the corresponding coefficient of determination (i.e. R^2) values are shown in each panel first for the linear case and then for the nonlinear case in brackets. Trajectories of extrapolated linear (solid blue lines) and nonlinear (dotted blue lines) relationships for each return period are also plotted. Estimated return levels based on the quantile mapping approach are shown using corresponding unfilled symbols for 2-, 5-, 10-, 25, and 50-yr return periods. 112

Figure 4.10: Projected changes (in %) in selected regional return levels of 5-, 10-, 15-, 30-, and 60-min extremes simulated by 11 RCM_AOGCM combinations for the 2041–2070 period with respect to the 1971–2000. Ensemble-averaged changes are shown using red circles. 113

LIST OF ABBREVIATIONS

AIC	:	Akaike Information Criterion
AOGCM	:	Atmosphere-Ocean General Climate/Circulation Model
CCSM	:	Community Climate System Model
CDF	:	Cumulative Distribution Function
CGCM3	:	Coupled General Circulation Model version 3
CORDEX	:	Coordinated Regional Climate Downscaling Experiment
CRCM	:	Canadian Regional Climate Model
D	:	Duration
DS1	:	Adjusted And Rehabilitated Daily Precipitation Dataset
DS2	:	Engineering Climate Stations Dataset
DTR	:	Diurnal Temperature Range
ECP2	:	Experimental Climate Prediction
GCM	:	General Climate/Circulation Model
GEV	:	Generalized Extreme Value
GEWEX	:	Global Energy and Water Exchanges
GFDL	:	Geophysical Fluid Dynamics Laboratory
GHG	:	Green House Gas
GLO	:	Generalized Logistic
GNO	:	Generalized Normal
GPA	:	Generalized Pareto
HADCM3	:	Hadley Centre Coupled Model version 3
HRM3	:	Hadley Regional Model 3
IDF	:	Intensity-Duration-Frequency
IPCC	:	Inter-governmental Panel on Climate Change
MM5I	:	National Centre for Atmospheric Research Mesoscale Model
NARCCAP	:	North American Regional Climate Change Assessment Program
NCEP	:	National Center for Environmental Prediction
P	:	Precipitation
PDSI	:	Palmer Drought Severity Index

PE3	:	Pearson Type-III
PET	:	Potential Evapotranspiration
PRUDENCE	:	Prediction of Regional scenarios and Uncertainties for Defining European Climate change risks and Effects
RCM	:	Regional Climate Model
RCM3	:	Regional Climate Model version 3
RFA	:	Regional Frequency Analysis
RMSE	:	Root Mean Square Error
S	:	Severity
Smax	:	Maximum severity
SPEI	:	Standardized Precipitation Evapotranspiration Index
SPI	:	Standardized Precipitation Index
SRB	:	Saskatchewan River Basin
SRES	:	Special Report on Emissions Scenarios
R1	:	Region 1
R2	:	Region 2
R3	:	Region 3
R4	:	Region 4
R5	:	Region 5
T	:	Temperature
WMO	:	World Meteorological Organization
WRFG	:	Weather Research Forecasting Grell Model

CHAPTER 1

INTRODUCTION

Water has always been a key resource for many sectors of human society, but the concern that sufficient water may not be available is spreading to sectors that have traditionally taken water availability for granted. Increasing demand for water and uncertain climate change may lead to severe reductions in future water supply for industry, recreation, aquatic ecosystems, and households (Trenberth et al., 2007; Mu et al., 2013). Climate change and changes in climatic variables including extremes that affect surface water, as well as groundwater resources, are being recorded in higher frequency (IPCC, 2012). As climate extremes affect human society as well as the natural environment, policy makers and stakeholders rely on credible predictions of such climatic phenomena on fine temporal and spatial scales.

Climate change is identified by changes in the mean or the variability of climatic variables over decades or longer periods (IPCC, 2007). The reported increase in the average global temperature and sea level rise suggest that the earth is warming. Such global warming is strongly linked to anthropogenic modification of the atmospheric greenhouse gas (GHG) composition. These changes are projected to increase in the future because of the continuous increase in GHG emissions, population growth, continuous industrialization, and rapid urbanization. In general, the impact of climate change is felt more by changes in the frequency, duration, and intensity of extreme climatic events because they are largely liable for climate-related damage and fatalities (Easterling et al., 2000; Meehl et al., 2000).

Extreme climate events are defined as the upper or lower values over a threshold of a climate variable, and these events are located in the upper or lower tail of a distribution. The definition of an extreme climate event is complex and depends on the stakeholder involved. By nature, extreme events are severe and rare, and are determined by their spatial and temporal scales, and their complexity. These events could be minute-lasting tornado, the week-lasting flood, year- or decade-lasting drought, etc. As extreme events are always complex in nature, sometimes they are the products of interactions between related or unrelated phenomena. In fact, an individual phenomenon can also act as a climate extreme. For example, the impact of climate change can produce extreme surges and can cause a gradual sea level rise, compounding floods in the future (IPCC, 2012). Similarly, due to the same cause, precipitation may decrease for a

long period and evapotranspiration may increase over the same period, resulting in extreme droughts.

Information on changes to climate extremes is important for water resources and agricultural decision support systems. Like many other countries, Canada is also experiencing changes in various climate variables. For example, the annual mean temperature and precipitation have increased, respectively, by 0.5 to 1.5°C and 5 to 35% in southern Canada during the 1900 to 1998 period (Zhang et al., 2000; Vincent et al., 2012). During the second half of the 20th century, the daily minimum temperature has increased more than the daily maximum temperature which in turn has decreased the diurnal temperature range (DTR) (Zhang et al. 2000; Bonsal et al., 2001). Vincent and Mekis (2006) analyzed homogenized daily precipitation and temperatures in order to calculate cold and hot climate extremes; they found that occurrence of cold extremes (e.g., cold nights, cold days, and frost days) were less frequent than occurrences of warm extremes (e.g., warm nights, warm days, and summer days) from 1950 to 2003. Barrow et al. (2004) studied Canada's future climate variability using the Coupled Global Climate Model 2 considering 1961–1990 as a base period. Their research projected an increase in average annual temperature over Canada of 1 to 9°C by the 2080s. Kharin et al. (2013) reported that the current occurrence of extreme hot days is one-in-20-year, which will become a one-in-5-year event in the middle of the 21st century over most of Canada. The projections of climate extremes from current to future periods can help identify regional characteristics and assess future climate changes which will be helpful as a key input for future planning of socioeconomic infrastructure and development of strategic adaptation measures for the water and agricultural sectors, which play an important role in the economy of Canada.

The most suitable tools for identifying the potential impacts of climate change at global or regional scales are General Circulation Models (GCMs) that describe complex atmospheric processes using mathematical equations. GCMs represent Earth system components such as atmosphere, oceans, land surfaces, and sea-ice (Fowler et al., 2007) and have been evolving steadily over the past several decades. A regional climate model (RCM) is a downscaling tool that adds higher resolution (e.g. 50 km or less) to a large scale projection of a GCM. RCMs can represent many features that are not possible with a GCM, such as complex topography and coastlines. RCMs are physically-based tools that can represent most of the processes available in the climate system of smaller regional domains. Complicated design and computational costs

sometimes limit the use of RCMs (Tripathi et al., 2006), although these constraints will no longer be problematic as different research organizations are producing RCM outputs and ensuring their free distribution. Consequently, the use of RCM projections for regional impact assessment is growing rapidly (e.g. Beniston, 2007; May, 2008; Nikulin et al., 2011; Mladjic et al., 2011; Mailhot et al., 2012; Monette et al., 2012; van Pelt et al., 2012; Khaliq et al., 2014, Jeong et al., 2014, 2015).

Downscaling approaches emerge due to the need for climate projections (Carter et al., 2007). Applying a downscaling technique, a method to derive local to regional-scale information from a large-scale model, is recommended for regional-scale analysis in the IPCC's Fourth Assessment Report (Christensen et al., 2007). More recently, downscaling has been widely applied in climatology for scenario construction and simulation/prediction of mean, minimum, and maximum air temperatures and their extremes among other climatic variables (Kettle and Thompson, 2004). Various approaches proposed for downscaling GCMs can be classified broadly into two categories: dynamical downscaling and statistical/empirical downscaling. In the dynamical downscaling approach, RCMs are essentially used with boundary conditions taken from a GCM. The advantage of using a dynamical downscaling technique is the application of very high resolution models, albeit not as high as required by some practical applications. There are some uncertainties in using a dynamical downscaling approach that depend on the spatial domain, region, and season, but the main uncertainty comes from the driving GCM. However, nowadays, models with longer duration and higher spatial resolution outputs are available for different parts of the world through different projects such as the European FP5 Prediction of Regional scenarios and Uncertainties for Defining European Climate change risks and Effects (PRUDENCE; Christensen et al., 2007; Fowler et al., 2007), ENSEMBLES (Christensen et al., 2009), Coordinated Regional Climate Downscaling Experiment (CORDEX; Jacob et al., 2013) and the North American Regional Climate Change Assessment Program (NARCCAP; Mearns et al., 2009). The second way of downscaling GCM outputs is statistical downscaling which uses a statistical framework to establish relationships between large-scale variables (predictors), such as the driving factors derived from GCMs, to local level climate conditions (predictands) that have been derived from the observed data. The advantage of statistical downscaling is that the simulation capacity is in finer scale than that of the dynamical downscaling and that extreme seasonal indices can be simulated without simulating the daily time series (e.g. Haylock et al.,

2006; Seneviratne et al., 2012). This technique holds some disadvantages as well. A long record of time series data is essential for this technique, and predictor variables that give the best fit for the historical record may not be suitable for all applications. Statistical downscaling is simpler than dynamical downscaling, but it can underestimate variance and poorly downscale extreme events (Fowler et al., 2007). In this study, dynamically downscaled outputs from the NARCCAP multi-RCM ensemble were used to explore projected changes to dry and wet climate extremes.

1.1 Research Purpose

1.1.1 Knowledge gaps

Future water scarcity and increased aridity is one of the main climate change concerns that will have severe implications for the Canadian Prairies region. Reduced water availability has major impacts on several sectors which include agriculture, forestry, energy, and many others (Natural Resources Canada, 2014). In general, water shortage ultimately leads to droughts, which are frequently observed in the southern parts of the Canadian Prairie provinces. Droughts are multifaceted extreme events that can inflict considerable damage to humans and the environment. Therefore, better understanding of the spatial and temporal characteristics of historical and future droughts is needed to ensure proper water resource and agriculture planning and management in order to mitigate the harmful effects of droughts on communities. Although there has been considerable research on various aspects of drought, to the author's knowledge, little or no work has been dedicated to the probabilistic analysis of drought characteristics within a multivariate setting using the copula approach. From the viewpoint of probabilistic analysis, specifically, the regional frequency analysis approach (RFA) is helpful in regionalization of drought risk indicators and subsequently identifying drought vulnerable regions. Also, probabilistic characterization of droughts using only precipitation based indices and those based on temperature and precipitation together for the future climate would provide an opportunity to assess impacts of rising temperatures on droughts in the study area. This is one of the main focus areas of this research.

Floods are also a major concern in the study area as the floods in recent years were caused by an increase in precipitation at times when rivers were already in high flow situations and basin saturation level was higher than average leaving the land with little storage capacity available to take up additional water from rain and melting snow (Environment Canada, 2014).

As the climate changes, the effects of extreme precipitation might vary in the future from past effects, and new methods might need to be in place for basin-wide water management in this region (Shepherd et al., 2003; Khaliq et al., 2014). Therefore, information on changes in the characteristics of precipitation extremes of short- and long-duration is highly desirable for future planning of urban drainage infrastructure, better management of water resources, ensuring sustainability of ecosystems, and maintaining regional socioeconomic activities in a changing climate. To develop this information is another main focus area of this research because, to date, such information has been lacking in the study area.

1.1.2 Objectives

The overall objective of this research was to investigate spatial patterns of historical droughts in the Saskatchewan River Basin and characteristics of current and future dry and wet extremes in the Canadian Prairie Provinces using the multi-RCM ensemble available through the NARCCAP and uni- and multivariate frequency analysis approaches. Specific objectives of the study were to:

1. Characterize historical drought events in terms of drought severity, duration, and maximum severity in the SRB using conventional univariate and copula-based bivariate frequency analyses and identify drought vulnerable geographic regions across the SRB;
2. Investigate projected changes in regional drought characteristics (severity, duration, and maximum severity) using the RFA approach and copula-based bivariate and trivariate frequency analyses to assess climate change induced impacts on drought characteristics and to evaluate the impact of rising future temperatures on drought characteristics;
3. Develop climate change informed short- and long-duration (from minutes to several hours) precipitation magnitude-frequency relationships using the RFA approach and transient climate change simulations from the NARCCAP multi-RCM ensemble.

1.2 Study area

The Alberta, Saskatchewan and Manitoba Provinces of Canada were chosen for this study (Figure 1.1). This area features a complex topography, ranging from flat land to the Rocky Mountains, with elevation varying from 1 to 3434 m above mean sea level. This region contains the SRB, the largest river basin in the area. The SRB has a total drainage area of 405,864 km² and contains various watersheds of small to large size. It is located in the cold interior of Western

Canada that spans southern parts of Alberta, Saskatchewan, and Manitoba. Southern parts of these provinces, particularly the Prairies ecozone, are important for agriculture that accounts for around 80% of the Canadian agricultural production (Wheater and Gober, 2013). The Prairies region is considered to be Canada's agricultural powerhouse, and contains more than 37 million hectares (80% of Canada's farmland) of land under cultivation.

The ecosystem of this region is heavily dependent on precipitation. The annual average precipitation is about 454 mm (less than the Canada-wide average of 535 mm) because cyclonic precipitation from the west or east coast rarely reaches these provinces (Phillip, 1990). The frequent presence of dry arctic air also plays a role in the low precipitation received across the region (Gan, 2000). A latitude effect generally dominates the spatial distribution of temperature in the absence of any dramatic change in topography (Borchert, 1950; Bonsal et al., 2012). Specifically, this region is characterized by a highly variable hydroclimate, with recurrent droughts (such as the prolonged droughts of 1988 and 1999–2004), floods (such as the severe floods of 2011, 2013, and 2014), and localized convective storm activity, resulting in heavy precipitation events, often observed during the warm season of the year. Due to varying topographic landscape and complex hydroclimatology, the study region presents many scientific research challenges and therefore offers an interesting testbed for new scientific advancements in climatology and hydrology and other closely associated fields.

1.3 Thesis outline

This thesis follows a manuscript-style structure according to the College of Graduate Studies and Research guidelines. After an introduction in chapter one, chapters 2, 3, and 4 represent three individual manuscripts. The first manuscript (Chapter 2), "Analysis of meteorological droughts for the Saskatchewan River Basin using univariate and bivariate approaches" explores the spatial and temporal characteristics of historical droughts across the SRB, which is confronted with immense water-related challenges due to rapid increases in the water demands for industrial, agricultural and domestic usages. In this chapter, a methodological approach based on two drought indices and multivariate frequency analysis approaches to develop drought risk indicators for delineating drought vulnerable parts of the basin are presented.

The second manuscript (Chapter 3), “Future changes to drought characteristics over the Canadian Prairie Provinces based on NARCCAP multi-RCM ensemble” examines projected changes to drought characteristics and future drought risks over the Canadian Prairie Provinces of Alberta, Saskatchewan, and Manitoba. Chapter 3 addresses the need to use a multivariate homogeneity analysis approach instead of a univariate approach for the delineation of homogeneous regions. Multivariate analyses of drought characteristics were developed using the copula approach and projected changes to joint occurrence probabilities based on bi- and trivariate approaches were used to identify drought-sensitive regions in the study area.

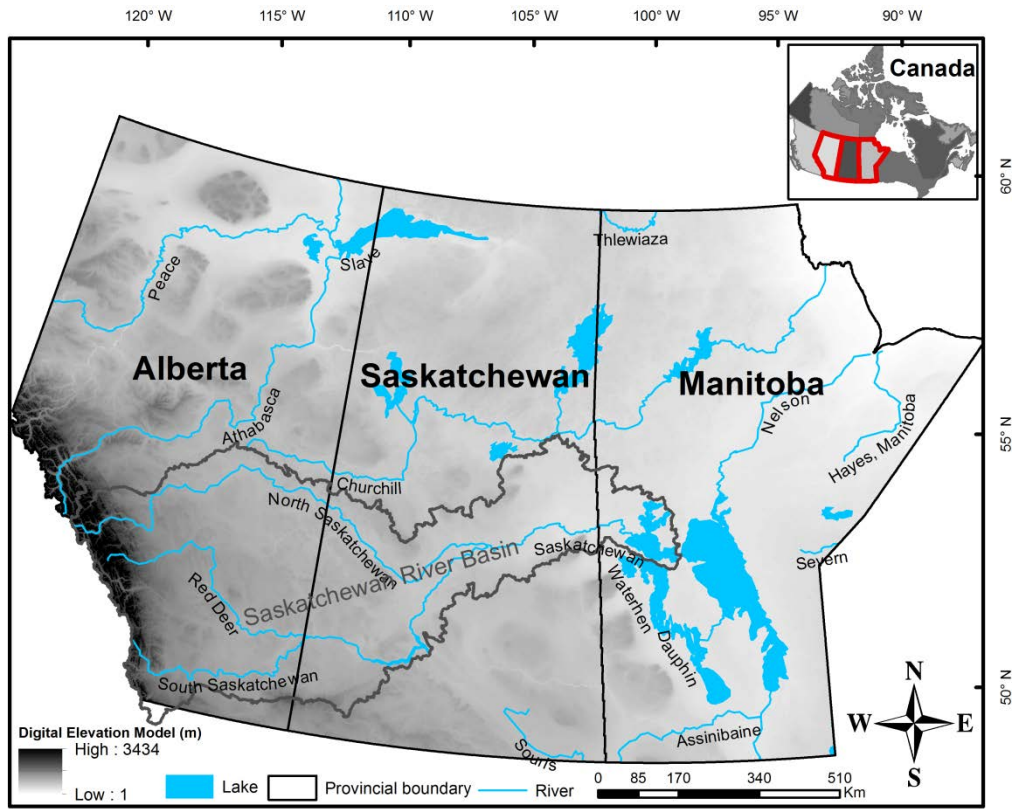


Figure 1.1: Study area showing the Saskatchewan River Basin spanning the provinces of Alberta, Saskatchewan and Manitoba. The topography, major river systems and lakes are also indicated. The inset shows the location of the study area in Canada

The third manuscript (Chapter 4), “Projected changes to short- and long-duration precipitation extremes over the Canadian Prairie Provinces” presents projected changes to short- and long-duration, ranging from 5 minutes to 48 hours, precipitation extremes over the Canadian Prairie Provinces based on the multi-RCM ensemble available through the NARCCAP. The RFA approach was applied to develop projected changes to selected 2-, 5-, 10-, 25-, and 50-yr return

levels of precipitation extremes. To assess statistical significance of the projected changes for each case investigated, confidence intervals were developed for current and future periods using the nonparametric vector bootstrap resampling method. Finally, Chapter 5 discusses the major findings reported in Chapters 2, 3, and 4 and provides recommendations for future work.

1.4 Copyright and author permissions

Chapters 2 through 4 of this thesis consist of manuscripts that have been published or submitted for publication. Consistent with the copyright and author rights of each publisher, the manuscript citations are provided below. Permission to use or author rights from each publisher allowing use of the manuscripts in this thesis is included in Appendix E. For all manuscripts, as per the College of Graduate Studies and Research, guidelines for manuscript-style theses, the student is the first author and supervisor (s) the second author (s).

Chapter 2: Masud MB, Khaliq MN, Wheater HS (2015) Analysis of meteorological droughts for the Saskatchewan River Basin using univariate and bivariate approaches. *Journal of Hydrology*, 522:452-466. DOI: <http://dx.doi.org/10.1016/j.jhydrol.2014.12.058>

Chapter 3: Masud MB, Khaliq MN, Wheater HS (2016) Future changes to drought characteristics over the Canadian Prairie Provinces based on NARCCAP multi-RCM ensemble. Submitted to *Climate Dynamics* on 31st December 2015; submission no. CLDY-D-16-00003

Chapter 4: Masud MB, Khaliq MN, Wheater HS (2016) Projected changes to short- and long-duration precipitation extremes over the Canadian Prairie Provinces. Submitted to *Climate Dynamics* on 9th March 2016; submission no. CLDY-D-16-00239

Contributions of the candidate: In the work presented in Chapters 2 to 4, which form the core of this thesis, the candidate (Masud, MB) developed conceptual ideas and theoretical frameworks, carried out simulations and performed various analyses, and designed and prepared all manuscripts. The co-authors (Dr. Khaliq and Prof. Wheater) provided advice on various aspects of the research and critical reviews of the results and their interpretations. The candidate used *R* statistical programming software and developed *R*-scripts for performing various data analyses ranging from statistical modeling to graphical plots.

References

- Barrow E, Maxwell B, Gachon P (Eds) (2004) Climate variability and change in Canada: past, present and future, ACSD Science Assessment Series No. 2, Meteorological Service of Canada, Environment Canada, Toronto, Ontario, 114p.
- Beniston M, Stephenson DB, Christenson OB, Ferro CAT, Frei C, Goyette S, Halsnaes K, Holt T, Jylhä K, Koffi B, Palutikof J, Schöll R, Semmler T, Woth K (2007) Future extreme events in European climate: an exploration of regional climate model projections. *Climatic Change* 81:71–95.
- Bonsal BR, Aider R, Gachon P, Lapp S (2012) An assessment of Canadian prairie drought: past, present, and future. *Climate Dynamics* DOI 10.1007/s00382-012-1422-0.
- Bonsal BR, Zhang X, Vincent LA, Hogg WD (2001) Characteristics of daily and extreme temperatures over Canada. *Journal of Climate* 14:1959–1976.
- Borchert JA (1950) The Climate of the Central North American grassland, *Annals of the Association of American geographers* 40:1-39.
- Carter MR, Little PD, Mogues T, Negatu W (2007) Poverty traps and natural disasters in Ethiopia and Honduras. *World Development* 35(5):835-856.
- Christensen JH, Hewitson B, Busuioc A, Chen A, Gao X, Held I, Jones R, Kolli RK, Kwon W, Laprise R, Rueda VM, Mearns L, Menéndez CG., Räisänen J, Rinke A, Sarr A, Whetton P (2007) Regional climate projections. In: *Climate Change 2007: The Physical Science Basis. Contribution of Working Group I to the Fourth Assessment Report of the Intergovernmental Panel on Climate Change* [Solomon, S., D. Qin, M. Manning, Z. Chen, M. Marquis, K.B. Averyt, M. Tignor, and H.L. Miller (eds.)]. Cambridge University Press, Cambridge, UK, pp. 847-933.
- Christensen JH, Rammukainen R, Lenderink G (2009) Formulation of very-high-resolution regional climate model ensembles for Europe. *ENSEMBLES: Climate Change and Its Impacts: Summary of Research and Results from the ENSEMBLES Project*, P. Van der Linden, and J. F. B. Mitchell, Eds., Met Office Hadley Center, 47–58.
- Easterling DR, Meehl GA, Parmesan C, Chagnon SA, Karl T, Mearns LO (2000) Climate extremes: observation, modeling and impacts. *Science* 289:2068–2074.

- Environment Canada (2014) Canada's top ten weather stories for 2014. <https://www.ec.gc.ca/meteo-weather/default.asp?lang=En&n=C8D88613-1&offset=4&toc=show>. Access date: 5th February 2016.
- Fowler HJ, Kilsby CG, Stunell J (2007) Modelling the impacts of projected future climate change on water resources in north-west England. *Hydrology and Earth System Sciences* 11(3):1115-1124.
- Gan TY (2000) Reducing vulnerability of water resources of Canadian prairies to potential droughts and possible climatic warming. *Water Resources Management* 14(2), 111–135.
- Haylock MR, Cawley GC, Harpham C, Wilby RL, Goodess CM (2006) Downscaling heavy precipitation over the United Kingdom: A comparison of dynamical and statistical methods and their future scenarios. *International Journal of Climatology* 26(10):1397-1415.
- IPCC (2012) Managing the risks of extreme events and disasters to advance climate change adaptation. A special report of working groups i and ii of the intergovernmental panel on climate change [Field, C.B., V. Barros, T.F. Stocker, D. Qin, D.J. Dokken, K.L. Ebi, M.D. Mastrandrea, K.J. Mach, G.-K. Plattner, S.K. Allen, M. Tignor, and P.M. Midgley (eds.)]. Cambridge University Press, Cambridge, UK, and New York, NY, USA, 582 pp.
- IPCC (2007) Climate Change 2007: The physical science basis. Contribution of working group i to the fourth assessment report of the intergovernmental panel on climate change [Solomon, S., D. Qin, M. Manning, Z. Chen, M. Marquis, K.B. Averyt, M. Tignor and H.L. Miller (eds.)]. Cambridge University Press, Cambridge, United Kingdom and New York, NY, USA, 996 pp.
- Jacob D, Petersen J, Eggert B, et al. (2013) EURO-CORDEX: new high-resolution climate change projections for European impact research, *Regional Environmental Change*, 14, 2, 563-578, doi: 10.1007/s10113-013-0499-2, 2013.
- Jeong DI, Sushama L, Diro GT, Khaliq MN, Beltrami H, Caya D (2015) Projected changes to high temperature events for Canada based on a regional climate model ensemble. *Climate Dynamics*. DOI 10.1007/s00382-015-2759-y.
- Jeong DI, Sushama L, Khaliq MN (2014) The role of temperature in drought projections over North America. *Climatic Change* 127 (2): 289–303.
- Kettle H, Thompson R (2004) Statistical downscaling in European mountains. verification of reconstructed air temperature. *Climate Research* 26(2): 97–112.

- Khaliq MN, Sushama L, Monette A, Wheeler H (2014) Seasonal and extreme precipitation characteristics for the watersheds of the Canadian Prairie Provinces as simulated by the NARCCAP multi-RCM ensemble. *Clim Dyn*. DOI 10.1007/s00382-014-2235-0.
- Kharin VV, Zwiers FW, Zhang X, Wehner M (2013) Changes in temperature and precipitation extremes in the CMIP5 ensemble. *Climatic Change* 119:345-357. DOI 10.1007/s10584-013-0705-8.
- May W (2008) Potential future changes in the characteristics of daily precipitation in Europe simulated by the HIRHAM regional climate model. *Climate Dynamics* 30:581–603.
- Mearns LO, Gutowski WJ, Jones R, Leung L-Y, McGinnis S, Nunes AMB, Qian Y (2009) A regional climate change assessment program for North America. *Eos, Trans. Amer. Geophys. Union*, 90, 311, doi:10.1029/2009EO360002.
- Meehl GA, Zwiers FW, Evans J, Knutson T, Mearns L, Whetton P (2000) Trends in extreme weather and climate events: Issues related to modeling extremes in projections of future climate change. *Bulletin of the American Meteorological Society* 81(3): 427-436.
- Mladjic B, Sushama L, Khaliq MN, Laprise R, Caya D, Roy R (2011) Canadian RCM projected changes to extreme precipitation characteristics over Canada. *Journal of Climate* 24:2565–2584.
- Monette A, Sushama L, Khaliq MN, Laprise R, Roy R (2012) Projected changes to precipitation extremes for Northeast Canadian watersheds using a multi-RCM ensemble. *Journal of Geophysical Research: Atmosphere* 117:D13106. doi:10.1029/2012JD017543.
- Mu Q, Zhao M, Kimball JS, McDowell NG, Running SW (2013) A remotely sensed global terrestrial drought severity index. *Bulletin of American Meteorological Society* 94, 83-98. <http://dx.doi.org/10.1175/BAMS-D-11-00213.1>.
- Nikulin G, Kjellström E, Hansson U, Strandberg G, Ullerstig A (2011) Evaluation and future projections of temperature, precipitation and wind extremes over Europe in an ensemble of regional climate simulations, *Tellus, Ser. A*, 63(1), 41–55, doi:10.1111/j.1600-0870.2010.00466.x.
- Phillips D (1990) *The Climates of Canada*. Cat. No. En56-1/1990E, Supply and Services Canada.
- Seneviratne SI, Nicholls N, Easterling D, Goodess CM, Kanae S, Kossin J, Luo Y, Marengo J, McInnes K, Rahimi M, Reichstein M, Sorteberg A, Vera C, Zhang X (2012) Changes in climate extremes and their impacts on the natural physical environment. In: *Managing the*

- Risks of Extreme Events and Disasters to Advance Climate Change Adaptation [Field, C.B., V. Barros, T.F. Stocker, D. Qin, D.J. Dokken, K.L. Ebi, M.D. Mastrandrea, K.J. Mach, G.-K. Plattner, S.K. Allen, M. Tignor, and P.M. Midgley (eds.)]. A Special Report of Working Groups I and II of the Intergovernmental Panel on Climate Change (IPCC). Cambridge University Press, Cambridge, UK, and New York, NY, USA, pp. 109-230.
- Shepherd P, Neale T, Cohen S (2003). Chapter 5: Water Management. In Cohen and Neale (eds.), 68-86.
- Trenberth E, Smith L, Qian T, Dai A, Fasullo (2007) Estimates of the global water budget and its annual cycle using observational and model data. *Journal of Hydrometeorology-Special Section 8*: 758-769.
- Tripathi S, Srinivas VV, Nanjundiah RS (2006) Downscaling of precipitation for climate change scenarios: A support vector machine approach. *Journal of Hydrology*, 330:621– 640.
- van Pelt SC, Beersma JJ, Buishand TA, van den Hurk, BJJM, Kabat P (2012) Future changes in extreme precipitation in the Rhine basin based on global and regional climate model simulations. *Hydrology and Earth System Sciences* 16:4517-4530.
- Vincent LA, Mekis E (2006) Changes in daily and extreme temperature and precipitation indices for Canada over the twentieth century, *Atmosphere-Ocean* 44:2, 177-193, DOI: 10.3137/ao.440205.
- Vincent LA, Want XL, Milewaska EJ, Wan H, Yang F, Swali V (2012) A second generation of homogenized Canadian monthly surface air temperature for climate trend analysis. *Journal of Geophysical Research: Atmosphere* 117(D18): D18110, doi:10.1029/2012JD017859.
- Wheatler HS, Gober P (2013) Water security in the Canadian prairies: science and management challenges, *Philosophical Transaction of the Royal Society of A*. doi:10.1098/rsta.2012.0409.
- Zhang X, Vincent LA, Hogg WD, Niitsoo A (2000) Temperature and precipitation trends in Canada during the 20th Century. *Atmosphere-Ocean*, 38: 395–429.

CHAPTER 2

ANALYSIS OF METEOROLOGICAL DROUGHTS FOR THE SASKATCHEWAN RIVER BASIN USING UNIVARIATE AND BIVARIATE APPROACHES

Humans must find ways to divert Earth's water to irrigate crops, meet domestic and municipal water needs, and support industrial developments. Areas of the planet that experience lack of precipitation often suffer from droughts. However, droughts can also be caused by inappropriate land and water management practices. During the second half of the 20th century, natural variability of the climate has been trending toward a dryer pattern and that has led to a decline in available water resources in many parts of the world. Gradual increase in human population and industrial activities are also adding additional stresses on water resources. One region of Canada that has drawn global attention due to water related challenges is the Saskatchewan River Basin (SRB), which is located in southern parts of Alberta, Saskatchewan and Manitoba provinces of Canada. During 1931, 1988 and 1999–2004, this region experienced major droughts, which resulted in considerable economic losses. Proper management and utilization of water resources is heavily dependent on the spatiotemporal characteristics of historical droughts. In this chapter, probabilistic drought risk indicators based on uni- and multivariate frequency analysis approaches and two different drought indices were developed to delineate drought sensitive areas of the SRB to inform water management-related decision-making. This chapter contains the following published manuscript:

1. **Masud MB**, Khaliq MN, Wheater HS (2015) Analysis of meteorological droughts for the Saskatchewan River Basin using univariate and bivariate approaches. *Journal of Hydrology*, 522:452-466. DOI: <http://dx.doi.org/10.1016/j.jhydrol.2014.12.058>

Abstract

This study was focused on the Saskatchewan River Basin (SRB) that spans southern parts of Alberta, Saskatchewan and Manitoba, the three Prairie Provinces of Canada, where most of the country's agricultural activities are concentrated. The SRB is confronted with immense water-related challenges and is now one of the ten GEWEX (Global Energy and Water

Exchanges) Regional Hydroclimate Projects in the world. In the past, various multi-year droughts have been observed in this part of Canada that impacted agriculture, energy and socio-economic sectors. Therefore, proper understanding of the spatial and temporal characteristics of historical droughts is important for many water resources planning and management related activities across the basin. In the study, observed gridded data of daily precipitation and temperature and conventional univariate and copula-based bivariate frequency analyses were used to characterize drought events in terms of drought severity and duration on the basis of two drought indices, the Standardized Precipitation Index (SPI) and the Standardized Precipitation Evapotranspiration Index (SPEI). Within the framework of univariate and bivariate analyses, drought risk indicators were developed and mapped across the SRB to delineate the most vulnerable parts of the basin. Based on the results obtained, southern parts of the SRB (i.e., western part of the South Saskatchewan River, Seven Persons Creek and Bigstick Lake watersheds) were found to be associated with a higher drought risk, while moderate risk was noted for the North Saskatchewan River (except its eastern parts), Red Deer River, Oldman River, Bow River, Sounding Creek, Carrot River and Battle River watersheds. Lower drought risk was found for the areas surrounding the Saskatchewan-Manitoba border (particularly, the Saskatchewan River watershed). It was also found that the areas characterized with higher drought severity were also associated with higher drought duration. A comparison of SPI- and SPEI-based analyses suggested only little effect of considering temperature, in the form of evapotranspiration, on identifying drought vulnerable areas. It is expected that the findings of the study will be helpful in the management and efficient utilization of the water resources of this important river basin in Canada.

Keywords: Canadian Prairies; Copula function; Drought risk analysis; SPEI; SPI; Saskatchewan River Basin

2.1 Introduction

Droughts can be defined from various perspectives including meteorological, hydrological, agricultural, and socio-economic. In general, a drought is defined as a dry weather period that lasts over several weeks to months, with no or little accumulated rainfall. Such dry weather events have significant impacts on water resources, agriculture, forestry, hydro-power, health, and socio-economic activities. A reduced amount of accumulated rainfall leads to low soil moisture and river flows, reduced storage in reservoirs and less groundwater recharge (Tallaksen

and van Lanen, 2004). According to Salinger (1995), drought-like conditions occur when the supply of moisture from precipitation or stored in the soil or hydrological reservoir is insufficient to fulfill the optimum water requirements of plants, water supply for urban dwellers, and inflows into hydro-power lakes. The start of a drought is not easy to ascertain, although its end may be. Droughts appear suddenly, spread in an unstructured manner, and can end in various ways (Wilhite, 2000).

Although many areas of Canada experience droughts from time to time, southern parts of Alberta, Saskatchewan and Manitoba Provinces of Canada, specifically the Prairies eco-region, are relatively more drought-prone, for reasons such as location in the lee of the western cordillera, distance from large water bodies and extremely high rainfall variability (Bonsal et al., 2012). Several multi-year droughts for the 1890s, 1910s, 1930s, late 1950s, early 1960s and 1980s have been reported for this region (e.g., Chipanshi et al., 2006; Bonsal et al., 2011; Stewart et al., 2011). Compared to these drought events, the drought experienced during 1999 to 2004 was the most severe drought on record (e.g., Evans et al., 2011; PaiMazumder et al., 2012). During this drought, Saskatchewan crop yields and harvested areas were below average in both 2001 and 2002, resulting in \$3.6 billion drop in agricultural production. Nationally, the gross domestic product fell some \$5.8 billion during 2001 and 2002 (Wheaton, 2011; Wheater and Gober, 2013). In the United States, economic losses of around US\$6–8 billion are estimated annually due to droughts that are far beyond any other meteorological disasters (Wilhite, 2000).

Recently, Bonsal et al. (2012) analyzed Canadian Prairies' summer drought for pre-instrumental, instrumental and future periods until 2100 using the Standardized Precipitation Index (SPI) and Palmer Drought Severity Index (PDSI). Their results revealed that the Prairies had observed drought-like conditions in the 1930s, 1958–1962, 1983–1989, and 1999–2004, and severe drought will be more perpetual in some areas of the southwestern Prairies in future. Sushama et al. (2010) also suggested that the southern Prairies might be a sensitive region with respect to droughts with projections showing less precipitation and a higher number of dry days during the growing season (April–September) in future.

Droughts are considered to be multi-faceted extreme events that can inflict considerable damage to the human society in many ways. Therefore, proper understanding of the spatial and temporal characteristics of historical droughts is needed for many water resources and agriculture planning and management related activities in order to mitigate their harmful effects on

communities. This study was focused specifically on the Saskatchewan River Basin (SRB; Figure 2.1) that is located in southern parts of the three rapidly developing Prairie Provinces of Canada (i.e., Alberta, Saskatchewan and Manitoba), where most of the country's agricultural activities are concentrated. The SRB is experiencing huge water demands and stresses due to increased usage of water for agriculture, industrial and domestic purposes. These demands and stresses require efficient water management strategies for the SRB. Recently, this river basin has drawn global attention due to challenging water related issues and it is now one of the ten GEWEX (Global Energy and Water Exchanges) Regional Hydroclimate Projects in the world.

In this study, the behavior of so called meteorological droughts was investigated at the level of 13 watersheds that represent natural subdivisions of the SRB (Figure 2.1). Observed gridded data of daily precipitation and temperature and conventional univariate and newly emerging copula-based bivariate frequency analyses were used to characterize historical drought events in terms of drought severity, duration and maximum severity on the basis of SPI (McKee et al., 1993), a purely precipitation-based index, and Standardized Precipitation Evapotranspiration Index (SPEI; Vicente-Serrano et al., 2010), a temperature and precipitation-based index. The SPEI is relatively a new drought index and it has the advantage of being multiscale over the PDSI, which was used in some of the previous studies (e.g., Bonsal et al., 2012). The PDSI is not generally suitable for mountainous regions with frequent climatic extremes and it is unable to capture emerging droughts compared to the SPI (Zargar et al., 2011). Other drought indices that have been used in some parts of the study area include the Z-Index (Quiring and Papakryiakou, 2003), Multi-Index Drought Index (Sun et al., 2011), and Drought Severity Index (PaiMazumder et al., 2012). It must be noted that several studies have been done across the world to study droughts using just the precipitation based drought index, the SPI, which has also been recommended by the World Meteorological Organization (WMO, 2009) for analyzing periods of moisture deficit. In addition, it is important to point out that no clear guidelines are available in the literature on the choice of a drought index. In most cases, availability of relevant data drove the choice of a drought index (Mishra and Singh, 2010).

The use of both SPI and SPEI for characterizing drought events for the SRB furnished an opportunity to directly evaluate the influence of temperature and hence of evapotranspiration in defining drought events. This is an important research question for drought risk analysis. In addition, none of the previous studies on droughts in this region has examined the frequency-

magnitude relationships of drought characteristics and their probabilistic behavior, particularly in both univariate and multivariate settings. Also, investigation of spatial patterns of drought risk indicators for identifying drought-sensitive geographic regions was not attempted earlier. These were some of the main objectives of this study, in addition to developing various methodological guidelines for probabilistic drought risk analysis.

This paper is organized as follows: description of the study area and observed gridded dataset used in the study is given in Section 2.2 Detailed description of the methodology for characterizing drought events and for performing univariate and copula-based bivariate frequency analyses is provided in Section 2.3, followed by results of the study and their discussion in Section 2.4. Finally, main conclusions of the study are provided in Section 2.5.

2.2 Study area and data

This study was focused on the SRB (Figure. 2.1), which has a total drainage area of 405,864 km² and contains various watersheds of small to large size. It is located in the cold interior of Western Canada that spans southern parts of Alberta, Saskatchewan and Manitoba provinces, where most of the country's agricultural activities (~80%) are concentrated. It is the major water resource in the region, which is fed mainly by snowmelt water from the Rocky Mountains. The SRB is confined by the boreal forest to the north and east, grassland and agricultural land to the south and the Rocky Mountains to the west (Liu and Stewart, 2003). It experiences the cold continental climate which is typical in the North American Central plains. Winter is long compared to summer but sunny, while summer is short but warm. Most of the annual precipitation falls as rain in spring (MAM) and summer (JJA), thus helping to replenish soil moisture and improve agricultural production. Sometimes evaporation exceeds precipitation in the SRB resulting in moisture deficits (Partners FOR the Saskatchewan River Basin, 2009).

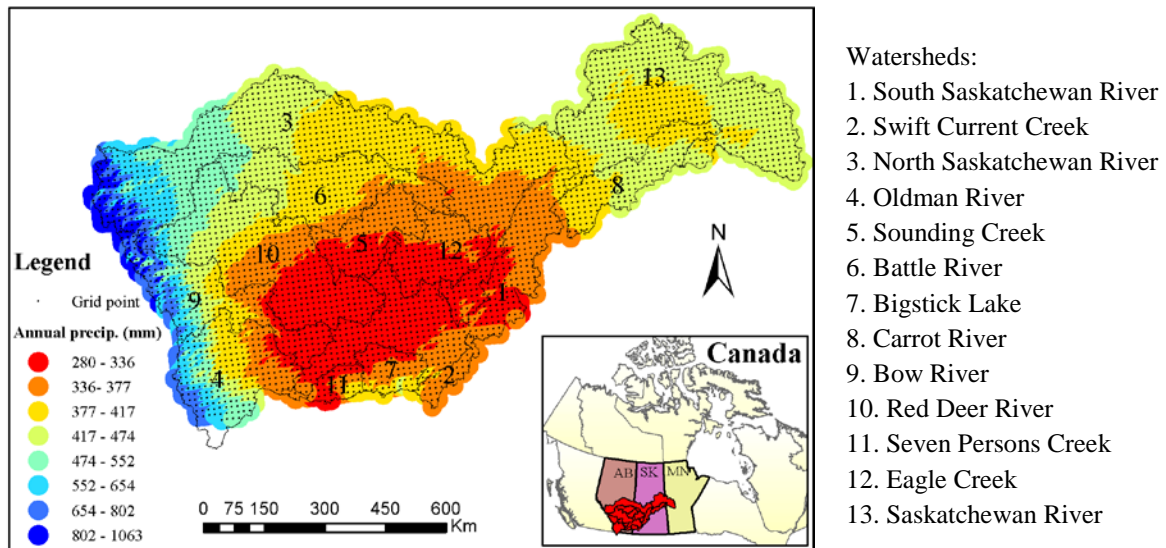


Figure 2.1: The Saskatchewan River Basin (405,864 km² drainage area) with its 13 watersheds and spatial distribution of annual precipitation developed from 10 km x 10 km gridded observed dataset for the 1961 to 2003 period. Inset shows location of the study area in Canada. The abbreviations AB, SK and MN mean Alberta, Saskatchewan and Manitoba, respectively.

Observed gridded data of daily maximum temperature (°C), daily minimum temperature (°C) and total daily precipitation (mm) for the 1961–2003 period were obtained from Agriculture and Agri-Food Canada for the SRB. There are about 4,041 grid points of 10 km × 10 km areal extent that cover 13 watersheds of different sizes in the entire SRB. The gridded datasets were interpolated from daily Environment Canada climate station observations using a thin plate smoothing spline surface fitting method implemented by ANUsplin V4.3 (Hutchinson, 2004). In comparison to other interpolation techniques, this method has been shown to perform well when interpolating noisy climate data across complex terrain (McKenney et al., 2006). Compared to station-based observations, high-resolution gridded datasets are useful specifically to explore spatial pattern of droughts. By using high-resolution datasets, one can avoid the need to interpolate spatially drought characteristics derived from station-based analyses. The latter approach would be a reasonable choice in the absence of high-resolution datasets.

2.3 Methodology

A concise overview of the methodology adopted for drought risk analysis for the SRB is illustrated in Figure 2.2, while detailed description of various components of the methodology is provided below.

2.3.1 Drought indices and time scales

A good number of indices have been suggested and used for detection and monitoring of meteorological, agricultural, hydrological and socio-economical drought (Heim, 2002; Keyantash and Dracup, 2002; Mishra and Singh, 2010; Mu et al., 2013). These indices include the PDSI (Palmer, 1965), Palmer Hydrological Drought Index (Palmer, 1965), Z-Index (Palmer, 1965), Rainfall Anomaly Index (van Rooy, 1965), self-calibrated-PDSI (Wells et al., 2004), Surface Water Supply Index (Shafer and Dezman, 1982), SPI (McKee et al., 1993), Soil Moisture Index (Sridhar et al., 2007), Standardized Runoff Index (Shukla and Wood, 2008), SPEI (Vicente-Serrano, 2010), Rainfall Variability Index (Oguntunde et. al., 2011), Multivariate Standardized Drought Index (Hao and AghaKouchak, 2013), and other variants of some commonly used drought indices. As already indicated, there is no consensus among the scientific community engaged in drought research on the selection of a drought index. Generally, the choice of an index is driven by the availability of relevant observed data and ease of computation and interpretation of the results obtained. Also, to some extent, the choice of the index is driven by the desired targets of a given project (Mishra and Singh, 2010).

In the present study, two drought indices, namely the SPI and SPEI, were used. Both indices represent the so called meteorological drought. McKee et al. (1993) developed SPI in order to quantify precipitation deficit, which, according to Guttman (1998), gives a better representation of drought-like conditions than the PDSI because it is the precipitation deficit that ultimately leads to hydrological and agricultural droughts. As mentioned earlier in the introduction section, the SPI has also been recommended by WMO (WMO, 2009) for drought analysis. The very first step in the calculation of SPI was the selection of a probability distribution (along with its parameter estimation procedure) that best fit the monthly precipitation (P) data. Next, the cumulative distribution function (cdf) of P was calculated. The normal inverse cumulative distribution function was applied to the cdf in order to obtain standard normal quantiles, which represents the SPI values. A negative SPI (positive) value indicates

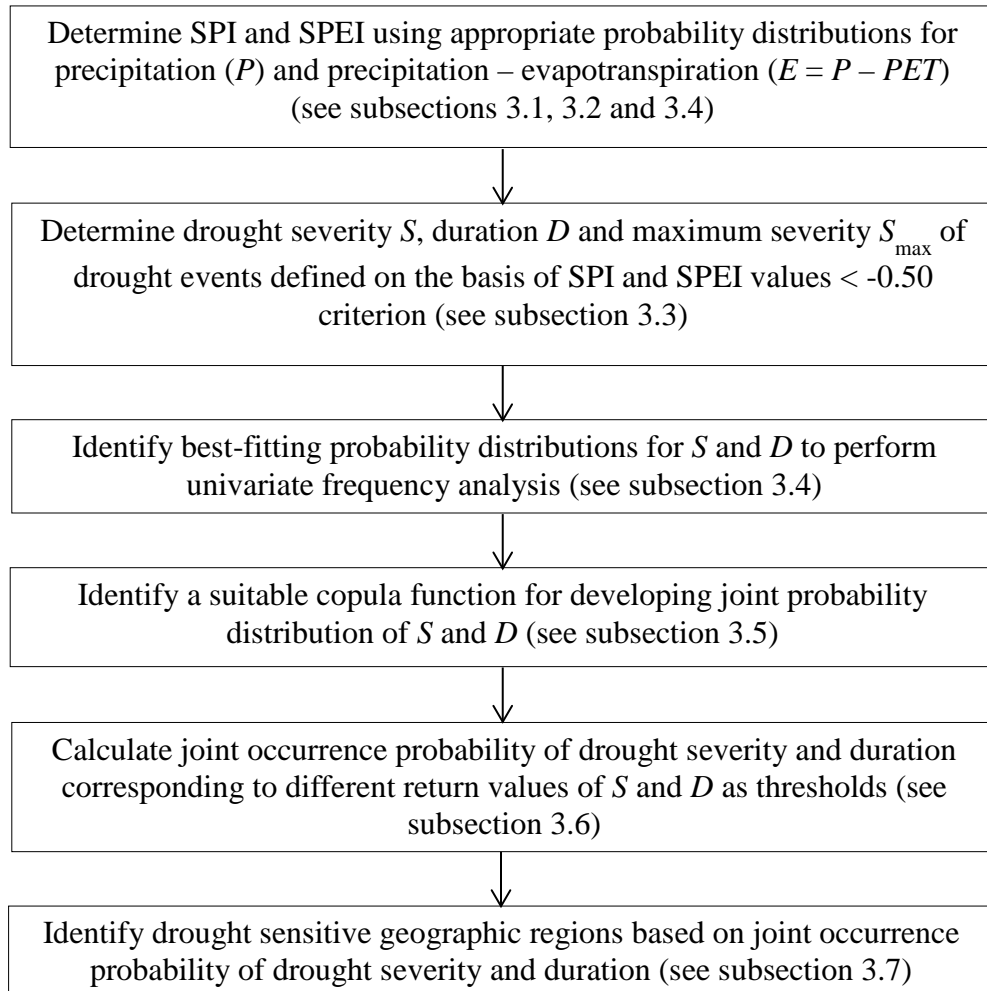


Figure 2.2: A schematic diagram of the methodology adopted for univariate and bivariate frequency analyses of drought characteristics in the SRB.

dryness (wetness). The SPEI is mathematically similar to the SPI but it includes the effect of monthly temperature in addition to precipitation. In the case of SPEI, the first step was to calculate monthly potential evapotranspiration (PET) by using a feasible method and then subtracting this from the monthly precipitation to obtain $E = P - PET$. A suitable probability distribution was selected to describe values of E . The rest of the procedure was the same as for the SPI calculation.

For investigating drought characteristics, time scale plays an important role. Selection of a suitable time scale is entirely dependent on the purpose for which the research is being undertaken (Dracup et al., 1980). McKee et al. (1993) explained that time scale functionally

separates different type of droughts. For example, a 3-month precipitation deficit may have drastic influence on agricultural production, but may not have any significant impact on city water supplies. The SPI of 6-month time scale may have more effect on water supplies than on agriculture. For the present study, 3-, 6-, and 12-month time scales for both the SPI and SPEI are used to provide short, intermediate and relatively long-term perspectives on drought characteristics.

2.3.2 Computation of potential evapotranspiration (*PET*)

The *PET* is a complex process due to the involvement of a number of atmospheric and ground-based physical parameters. Both simple and complex methods exist for estimating *PET*, e.g., Blaney-Criddle (Blaney and Criddle, 1950), Hargreaves (Hargreaves and Samani, 1982, 1985; Hargreaves et al., 1985), Thornthwaite (Thornthwaite, 1948), Lowry-Johnson (Lowry and Johnson, 1942), Priestley-Taylor (Priestley-Taylor, 1972), Modified Penman (Doorenbos and Pruitt, 1977), and Penman method (Penman, 1948). Nonetheless, the use of simple or complex methods to calculate *PET* does not affect drought analysis much as noted by Mavromatis (2007). In the present study, Hargreaves method was used which simply used the maximum and minimum temperature for estimating *PET*. This method was ranked at the top among the temperature-based methods in the American Society of Civil Engineers Manual 70 analysis (Jensen et al., 1990). Also, this method was recommended for estimating *PET* for the Canadian Prairies region in the inter-comparative study of Maulé et al. (2006). The form of the 1985 Hargreaves equation is:

$$PET = 0.0023M_{\text{day}}(T_{\text{max}} - T_{\text{min}})^{0.5}(T_{\text{mean}} + 17.8)(R_a) \quad (2.1)$$

where *PET* is the monthly potential evapotranspiration, M_{day} is the number of days in a month, T_{max} and T_{min} are respectively the average monthly maximum and minimum temperatures (°C), T_{mean} is the average monthly temperature (°C), and R_a is the water equivalent of the extraterrestrial radiation in mm day^{-1} ($1 \text{ MJ/m}^2/\text{day} = 0.408 \text{ mm/day}$) computed according to Allen et al. (1998). The R_a is usually calculated theoretically as a function of latitude and month of the year:

$$R_a = \frac{24(60)}{\pi} G_{\text{sc}} d_r [\omega_s \sin(\varphi) \sin(\delta) + \cos(\varphi) \cos(\delta) \sin(\omega_s)] \quad (2.2)$$

where G_{sc} is the solar constant = $0.0820 \text{ MJ m}^{-2} \text{ min}^{-1}$, d_r is the inverse relative distance factor for the Earth-Sun (unitless), ω_s is the sunset hour angle (rad), φ is the latitude (rad), and δ is the solar declination (rad).

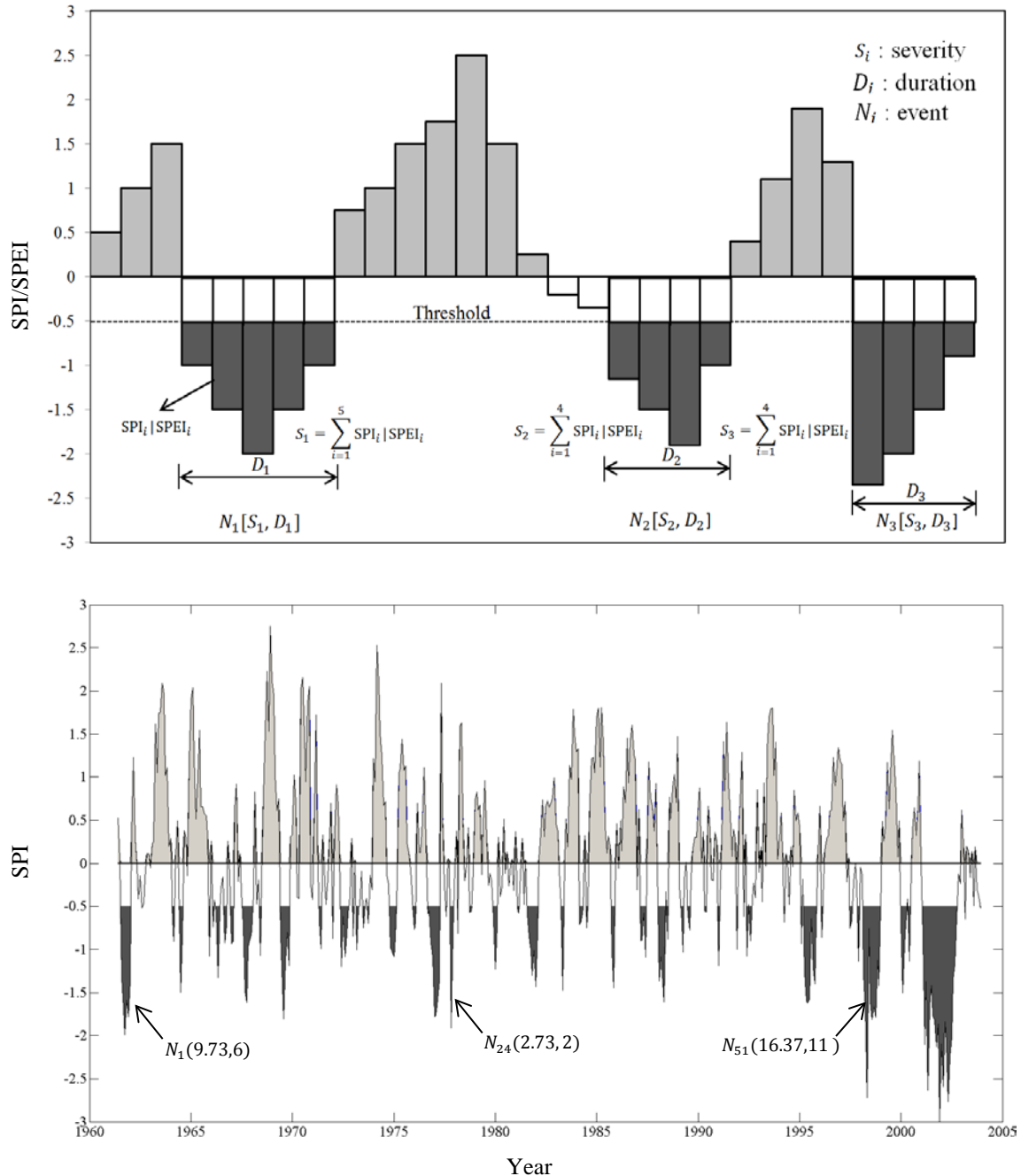


Figure 2.3: Definition sketch of drought characteristics (top panel) showing three drought events (labeled as N_1 , N_2 , and N_3) and a SPI-based observed example (bottom panel) for a representative grid point (Lat: 52.52; Lon: -109.1) from the Eagle Creek watershed.

2.3.3 Characteristics of drought events

In this study, drought events were characterized in terms of severity, duration and maximum severity. To minimize the effect of minor droughts, drought events were identified considering a threshold of -0.50 for both SPI and SPEI, i.e., a drought event occurred when the value of SPI/SPEI was smaller than this threshold. Drought duration D was identified as a continuous sequence of SPI/SPEI values that satisfied the above threshold criterion. Drought severity S was defined as the cumulative sum of all SPI/SPEI values over the duration D :

$$S = - \sum_{i=1}^D \text{SPI}_i \text{ (or SPEI}_i) < -0.50 \quad (2.3)$$

As shown in the above equation, for calculation convenience, drought severity was multiplied by -1 . For each grid point, average severity, average duration and maximum severity were calculated as:

$$S_{\text{avg}} = \frac{\sum_{i=1}^N S_i}{N} \quad (2.4)$$

$$D_{\text{avg}} = \frac{\sum_{i=1}^N D_i}{N} \quad (2.5)$$

$$S_{\text{max}} = \max_{1 \leq i \leq N} S_i \quad (2.6)$$

where N is the total number of drought events observed for the period of study. A schematic illustration of the procedure of defining drought events and their related characteristics is shown in Figure 2.3. A SPI-based example for a representative grid point is also provided in this figure.

2.3.4 Selection of marginal distributions

In order to evaluate drought characteristics on the basis of SPI and SPEI, selection of appropriate probability distributions and their parameter estimation methods were required for modeling P and E series corresponding to 3-, 6-, and 12-month time scales. For this purpose, the suitability of some commonly used probability distributions was explored using the L-moments ratio diagrams and Kolmogorov-Smirnov (KS) test. The KS test is a nonparametric goodness-of-fit test, which has been extensively used in the literature (e.g., Vicente-Serrano et al., 2010; Liu et al., 2011). The L-moments ratio diagram represents L-kurtosis as a function of L-skewness. In this diagram, single- and two-parameter distributions appear as points, while three-parameter distributions appear as curves. From the behavior of the plotted points on this diagram, one can judge the suitability of a specific candidate distribution. In this study, the distributions

investigated include the Generalized Logistic (GLO), Generalized Normal (GNO), Generalized Extreme Value (GEV), Generalized Pareto (GPA), Pearson Type-III (PE3) and Wakeby distributions. The first five of these distributions are commonly used for statistical modeling of hydrological variables. The method of L-moments was used for fitting these distributions to drought characteristics as this method has many theoretical advantages over the conventional moments to characterize a wider range of distributions with less bias in estimation (Hosking, 1990). Detailed procedure for parameter estimation of the above selected distributions can be found in Hosking and Wallis (1997).

For performing univariate frequency analyses of drought characteristics, it was also important to select appropriate probability distributions for drought severity and duration characteristics. The exponential distribution for drought duration and the gamma distribution for drought severity have been used in previous drought related studies (e.g., Shiau and Shen 2001; Shiau, 2006; Shiau and Modarres, 2009; Chen et al., 2011; Liu et al., 2011; Lee et al., 2012). In the present study, the exponential, gamma, log-normal and GPA distributions were tested for modeling samples of drought severity and duration. The KS goodness-of-fit test was used to facilitate an overall best choice in this case also.

Table 2.1: Bivariate Archimedean copulas and their corresponding generator functions and parameters.

Copula, $C_{\theta}(u, v)$	$\theta \in$	Copula generator, $\varphi(t)$	Kendall's τ
Ali-Mikhail-Haq: $\frac{uv}{[1 - \theta(1-u)(1-v)]}$	$[-1, 1)$	$\ln \left\{ \frac{(1 - \theta(1-t))}{t} \right\}$	$\left[\frac{3\theta - 2}{\theta} \right] - \left[\frac{2}{3} (1 - \theta^{-1})^2 \ln(1 - (1 - \theta^{-1})) \right]$
Gumbel-Hougaard: $\exp \left\{ -[(-\ln u)^{\theta} + (-\ln v)^{\theta}]^{1/\theta} \right\}$	$[1, \infty)$	$(-\ln t)^{\theta}$	$(1 - \theta^{-1})$
Clayton: $(u^{-\theta} + v^{-\theta} - 1)^{-\frac{1}{\theta}}$	$(0, \infty)$	$\frac{[(t)^{-\theta} - 1]}{\theta}$	$\frac{\theta}{(\theta + 2)}$
Frank: $-\frac{1}{\theta} \ln \left[1 + \frac{(e^{-\theta u} - 1)(e^{-\theta v} - 1)}{(e^{-\theta} - 1)} \right]$	\mathbb{R}	$-\ln \frac{(e^{-\theta t} - 1)}{(e^{-\theta} - 1)}$	$1 + \frac{4}{\theta} \left[\frac{1}{\theta} \int_0^{\theta} \frac{t}{e^t} dt - 1 \right]$

* u and v are the marginal distribution functions of two variables and θ is the copula parameter.

2.3.5. Copula functions for bivariate frequency analysis

Copulas have been used in some previous studies for the analysis of hydrometeorological extremes including droughts (e.g., Shiau and Shen 2001; Shiau, 2006; Shiau and Modarres, 2009; Chen et al., 2011; Liu et al., 2011; Lee et al., 2012). Based on Sklar's (1959) theorem, the joint cumulative distribution function of two or more correlated variables can be expressed as:

$$H(\mathbf{x}_1, \mathbf{x}_2, \dots, \mathbf{x}_n) = C[F_1(\mathbf{x}_1), F_2(\mathbf{x}_2), \dots, F_n(\mathbf{x}_n)] \quad (2.7)$$

where x_1, x_2, \dots, x_n are the random variables with continuous marginal distributions, $F_1(x_1), F_2(x_2), \dots, F_n(x_n)$, and C is the copula function. Some important single-parameter families of Archimedean copulas are described in Nelsen (1999) along with their generators, the range of parameters and some limiting cases. Archimedean copulas can easily be constructed and applied when the correlation among variables is positive or negative (Zhang and Singh, 2007). A very concise description of the selected copulas and their characteristics considered in this study for modeling bivariate distributions of drought severity and duration are given in Table 2.1.

To identify the best copula from the Archimedean family, a nonparametric estimation procedure, proposed by Genest and Rivest (1993), was adopted and the same has been used in numerous other studies (e.g., Zhang and Singh, 2006; Karmakar and Simonovic, 2009; Topçu and Arslan, 2012):

1. Estimate Kendall's correlation coefficient τ as:

$$\tau = \binom{n}{2}^{-1} \sum_{i < j} \text{sign}[(x_i - x_j)(y_i - y_j)] \quad (2.8)$$

where n is the number of observations in the sample; $i, j = 1, 2, \dots, n$; if $x_i \leq x_j$ and $y_i \leq y_j$, $\text{sign}[\cdot] = 1$ else $\text{sign}[\cdot] = -1$.

2. Calculate the copula parameter θ and finally the copula function (see Table 2.1).
3. Define an intermediate random variable $T = T(x, y)$ which has a distribution function $K(t) = P(T \leq t)$, where t is a specific value of T . Let $K(t) = P[C\{F_X(x), F_Y(y)\} \leq t]$, $t \in (0, 1)$, be the parametric estimate of this distribution function. Its relationship with the copula generating function is given by:

$$K(t) = t - \frac{\varphi(t)}{\dot{\varphi}(t)} \quad (2.9)$$

where $\dot{\varphi}$ is the derivative of φ with respect to t .

4. Obtain $K_n(t)$, which is a nonparametric estimate of the distribution function $K(t)$, as follows: (i) estimate $T_i = F_n(x_i, y_i) = \sum_j^n I[\{x_j \leq x_i \text{ and } y_j \leq y_i\}] / (n + 1)$, $i = 1, 2, \dots, n$, and then (ii) $K_n(t) = \frac{\text{number of } T_i \leq t}{n+1}$.
5. Calculate the Root Mean Square Error (RMSE) and Akaike Information Criterion (AIC; Akaike, 1974) to find the best copula function. The RMSE can be expressed as:

$$\mathbf{RMSE} = \sqrt{E[(x_c - x_o)^2]} = \left\{ \frac{1}{n - k} \sum_{i=1}^n [x_c(i) - x_o(i)]^2 \right\}^{0.5} \quad (2.10)$$

where $E[.]$ is the expectation operator; $x_c(i)$ denotes the i th computed value; $x_o(i)$ denotes the i th observed value; k is the number of parameters used in obtaining the computed value and n is the number of observations. The AIC can be obtained as follows:

$$\text{AIC} = n \log(\text{MSE}) + 2k \quad (2.11)$$

where $\text{MSE} = E[(x_c - x_o)^2]$. The best model is the one which has the minimum value of the RMSE and AIC.

2.3.6. Calculation of joint occurrence probabilities

In this study, two type of joint occurrence probabilities of drought severity S and duration D were considered: (1) either drought duration or drought severity exceeds a certain value at the same time (i.e., $D > d$ or $S > s$) and (2) drought duration and drought severity both exceed a certain value at the same time (i.e., $D > d$ and $S > s$). Here, d and s denote the duration and severity values corresponding to selected 5-, 10-, 20-, and 30-year return periods. Corresponding relationships of these probabilities are given below:

$$P_1 = P(D > d \text{ or } S > s) = P(D > d \cup S > s) = 1 - F(d, s) \quad (2.12)$$

$$P_2 = P(D > d \text{ and } S > s) = P(D > d \cap S > s) = 1 - F_D(d) - F_S(s) + F(d, s) \quad (2.13)$$

Further details about these relationships can be found in the work of Yue and Rasmussen (2002). The use of such probabilities for joint occurrence of drought and flood characteristics have been documented in the recent studies by Liu et al. (2011) and Jeong et al. (2013), respectively.

2.3.7. Identification of drought sensitive geographic regions

An important objective of this study was to identify drought sensitive geographic areas within the SRB. This objective was accomplished on the basis of 13 watersheds shown in Figure 2.1. The advantage of this strategy is that natural subdivisions of the SRB are preserved in their entirety. In order to develop a drought probability scenario at the regional scale in the SRB,

every watershed (out of 13) was checked for similarity of grid-based drought characteristics. Where possible, a watershed (specifically a larger one) was divided into smaller geographic regions with similar drought characteristics using cluster analysis, which is one of the most commonly used statistical multivariate analysis techniques. Using this technique, one combines a set of sites (or grid points in the present study) into groups with similar characteristics or features of interest (Hosking and Wallis, 1997; Rao and Srinivas, 2008). Herein, hierarchical clustering (Kaufman and Rousseuw, 1990) was applied to each watershed separately to perform cluster analysis. Although different methods, including single, average and complete linkage, and Ward's minimum variance method, are available for hierarchical clustering, the last one was used extensively in different fields (Ramos, 2001). Watersheds were divided into different geographic regions by identifying clusters in the space of grid characteristics, i.e., geographic location (latitude, longitude and elevation) and statistical parameters (mean, L-CV, L-skewness and L-kurtosis) of drought severity and duration. As observed scales of these variables are different and standard methods of clustering are susceptible to these different scales, the variables were rescaled before performing cluster analysis. The Ward's minimum variance method cannot always provide exact formation of groups and therefore some subjective adjustments are imperative in order to arrive at meaningful geographic regions, wherein grid characteristics behave in a similar manner. After this similarity analysis, the values of probabilistic drought risk indicators (i.e., P_1 and P_2) were spatially mapped to identify drought sensitive geographic regions within the SRB. It is hoped that following this methodology, geographic regions with similar drought sensitivities will group together, which will furnish a reasonable basis for drought planning and water management related activities.

2.3.8. Other considerations

It is important to note that most of the analyses were performed at the level of individual grid points within the SRB. However, to ease presentation, the results of the analyses are discussed with respect to 13 watersheds shown in Figure 2.1.

2.4. Results and discussion

2.4.1. Choice of marginal distributions and copula functions

The very first step in the analysis was to select appropriate probability distributions for P and E samples in order to drive calculations of the selected drought indices, i.e., the SPI and SPEI (Figure 2.2). To have an initial understanding of the statistical characteristics of P and E samples, L-moment ratio diagrams were developed for the SRB considering 4,041 grid points that span the entire basin and all P and E samples corresponding to 3-, 6-, and 12-month time scales (Figure 2.4). The large scatter of L-skewness vs. L-kurtosis suggests that the type of the distribution varies spatially across the SRB and, to some extent, is also associated with the time scale. In short, none of the commonly used distributions appear to be capable of describing all samples of P and E for the entire study area. However, based on the overall averaged values of L-skewness and L-kurtosis, there is some evidence that the PE3, GNO and GEV distributions could be strong candidates for modelling P and E samples. Here, it is also important to point out that McKee et al. (1993), who introduced SPI, suggested the use of the gamma distribution for modeling P samples and Vicente-Serrano et al. (2010), who introduced SPEI, suggested the log-logistic distribution for modeling E samples. Their suggestions have been followed in some studies in different parts of the world. With reference to the results shown in Figure 2.4, these two distributions do not appear to be flexible enough for addressing the large spatial variability observed in P and E samples for the SRB.

In the light of the above discussion, it would be ideal to select a distribution that can accommodate the changing behavior of the distribution type across the entire SRB, for modeling samples of both P and E . According to Hosking and Wallis (1997), the five-parameter Wakeby distribution can mimic the shapes of many commonly used skew distributions (e.g., GEV, GNO, PE3, etc.). The parameterization technique of the Wakeby distribution explicitly exhibits a generalization of the GPA distribution. Having five parameters, which are more than any of the commonly used distributions, the Wakeby distribution can attain a wider range of distributional shapes and therefore this distribution is used for modeling P and E samples in this study. This choice is supported further based on the KS test. The results of this test indicate that the Wakeby is the only distribution that fits better than any other distribution for the majority of the samples. For the Wakeby distribution, about 87%, 84% and 82% of P and E samples, corresponding to 3-,

6- and 12-month time scales, passed this test, compared to 67% (65%), 70% (68%) and 70% (69%), respectively, for the PE3 (GNO) distribution. In addition, none of the values for all samples of P and E is found below the location parameter of the Wakeby distribution, which is an important requirement to be met by this distribution. GPA and GLO are the least suitable distributions as the number of samples that passed the KS test is $<50\%$. Following the choice of the Wakeby distribution, drought events based on the SPI and SPEI values are defined and their characteristics (i.e., severity, duration and maximum severity) are derived for further analyses.

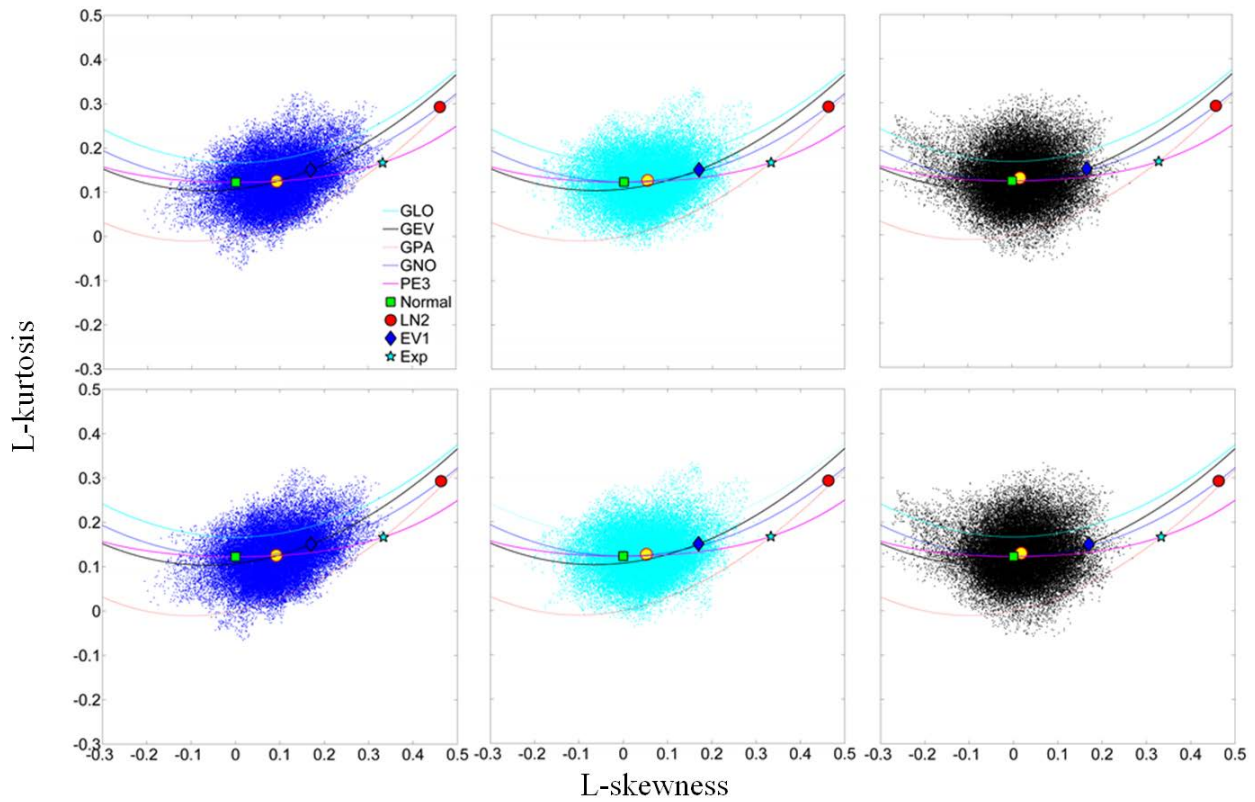


Figure 2.4: L-moment ratio diagrams of grid point based all samples of P (top row) and E (bottom row) corresponding to 3- (blue dots), 6- (cyan dots), and 12-month (black dots) time scales for the entire SRB. Yellow circles represent group averaged values. LN2, EV1 and Exp abbreviations are used to represent the two-parameter lognormal, Extreme Value Type-I (i.e., Gumbel) and exponential distributions. Other abbreviations are explained in the text.

Table 2.2: Watershed based averaged values of AIC and RMSE for 13 watersheds (WSs) and four copula functions fitted to drought severity and duration derived from drought events defined on the basis of SPI of 12-month time scale.

WS No.	No. of grid points	Copula family							
		Frank		Gumbel-Hougaard		Clayton		Ali-Mikhail-Haq	
		AIC	RMSE	AIC	RMSE	AIC	RMSE	AIC	RMSE
1	475	-205.06	0.029	-194.25	0.034	-188.83	0.038	-90.58	0.204
2	40	-210.71	0.025	-195.92	0.032	-190.64	0.035	-89.07	0.204
3	944	-197.02	0.035	-189.81	0.039	-177.98	0.039	-91.72	0.203
4	261	-207.58	0.028	-196.04	0.034	-190.63	0.037	-90.88	0.204
5	156	-227.57	0.030	-217.84	0.035	-211.68	0.038	-102.74	0.202
6	299	-209.96	0.035	-203.14	0.039	-197.21	0.042	-98.39	0.202
7	77	-186.93	0.029	-176.26	0.035	-171.45	0.038	-81.96	0.205
8	181	-223.88	0.028	-212.14	0.034	-206.05	0.037	-99.02	0.202
9	258	-210.94	0.034	-203.85	0.038	-198.89	0.042	-98.49	0.203
10	509	-207.08	0.031	-197.91	0.036	-184.98	0.063	-93.68	0.203
11	46	-169.03	0.030	-159.42	0.036	-155.12	0.039	-74.47	0.207
12	164	-218.24	0.032	-209.91	0.036	-203.82	0.040	-100.18	0.202
13	631	-234.41	0.034	-227.45	0.037	-220.85	0.041	-109.63	0.201
Average		-208.34	0.031	-198.77	0.036	-192.16	0.041	-93.91	0.203

Note: Similar results are found for SPEI-12 and other time scales of both SPI and SPEI

The next step was to identify a suitable probability distribution for samples of drought severity S and duration D abstracted from drought events for each grid point. The KS test results strongly suggest that drought severity and duration samples are consistent with the three-parameter GPA distribution. Since S and D values are derived based on a threshold approach as opposed to the block maxima approach, wherein only one value per block (i.e., a year or a season) is considered, the choice of the GPA distribution can also be supported on theoretical grounds to some extent. According to Coles (2001), the GPA distribution is a natural modeling choice for threshold based samples. Parameters of the GPA distribution were estimated using the method of L-moments. The fitted distributions were used for univariate frequency analyses of drought severity and duration.

Watershed based averaged values of RMSE and AIC for the severity-duration pair of drought characteristics, derived on the basis of SPI and SPEI values of only 12-month time scale for 13 watersheds and for four selected copula functions, are shown in Table 2.2. These goodness-of-fit measures indicate that the Frank copula provides overall the best results for all watersheds, followed by the Gumbel-Hougaard, Clayton and Ali-Mikhail copulas. Therefore, for performing bivariate frequency analysis of drought severity and duration at each grid point, the Frank copula was selected.

2.4.2. Drought characteristics

Figure 2.5 shows spatial patterns of drought characteristics (i.e., average severity and duration, maximum severity and number of drought events) corresponding to the SPI and SPEI values of 3-, 6-, and 12-month time scale. Based on the three time scales of both indices, the pattern of average drought severity shows that the southern parts of the basin tend to experience relatively more severe droughts (Figure 2.5a). Also, severe droughts are found in the middle parts of the basin, which mainly cover the Alberta-Saskatchewan border, whereas less severe droughts are found in areas surrounding the Saskatchewan-Manitoba border (particularly, the Saskatchewan River watershed). The differences between spatial patterns of average drought duration are more obvious compared to any other drought characteristic (Figure 2.5b). Based on the pattern of average drought duration, long lasting droughts are found in the northern and southern parts of the basin, whereas short duration droughts are found in the eastern part of the basin. For the 12-month time scale, the spatial patterns suggest that the North and South Saskatchewan River watersheds experience long lasting drought events. Remarkably, the Saskatchewan River watershed tends to experience droughts of short duration at all three time scales.

No explicit spatial pattern is found for the maximum severity characteristic of drought events. Nonetheless, Figure 2.5c suggests that the eastern parts of the North Saskatchewan River watershed and, more generally, the middle parts of the SRB have experienced some of the more intense droughts; this pattern is specifically visible for 3- and 6-month time scales. With respect to the number of drought events, higher number of events is found in the eastern and north-eastern parts of the basin, while lower number of events is found in the southern and north-western parts of the basin for all time scales (Figure 2.5d). As with the average drought severity, spatial coverage of higher number of drought events decreases with increasing time scales.

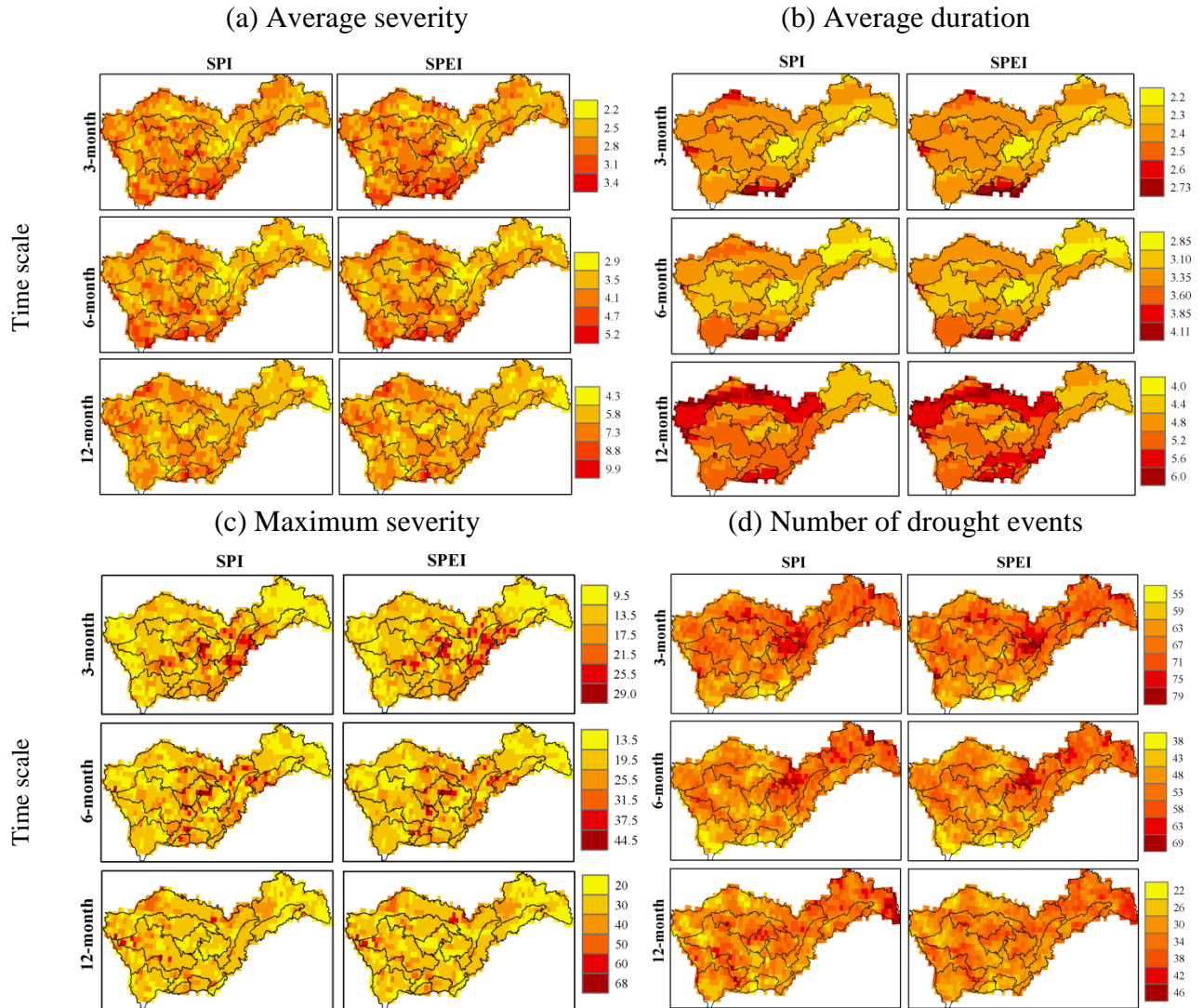


Figure 2.5: Spatial patterns of (a) average severity, (b) average duration, (c) maximum severity, and (d) number of drought events, obtained on the basis of SPI and SPEI values corresponding to 3-, 6-, and 12-month time scales.

The box and whisker plots of Spearman rank correlation coefficient, for different combinations of drought characteristics, are shown in Figure 2.6. There is a very strong association between drought severity and duration, with maximum number of correlations falling within the 0.80 to 0.99 range for all time scales. The values of correlation between severity and maximum severity are also quite strong as most of them fall within the slightly wider 0.52 to 0.99 range, followed by relatively moderate correlations between maximum severity and duration that lie within a relatively wider range, 0.23 to 0.95. An increasing trend in the values of correlation coefficient with increasing time scale of drought indices is observed.

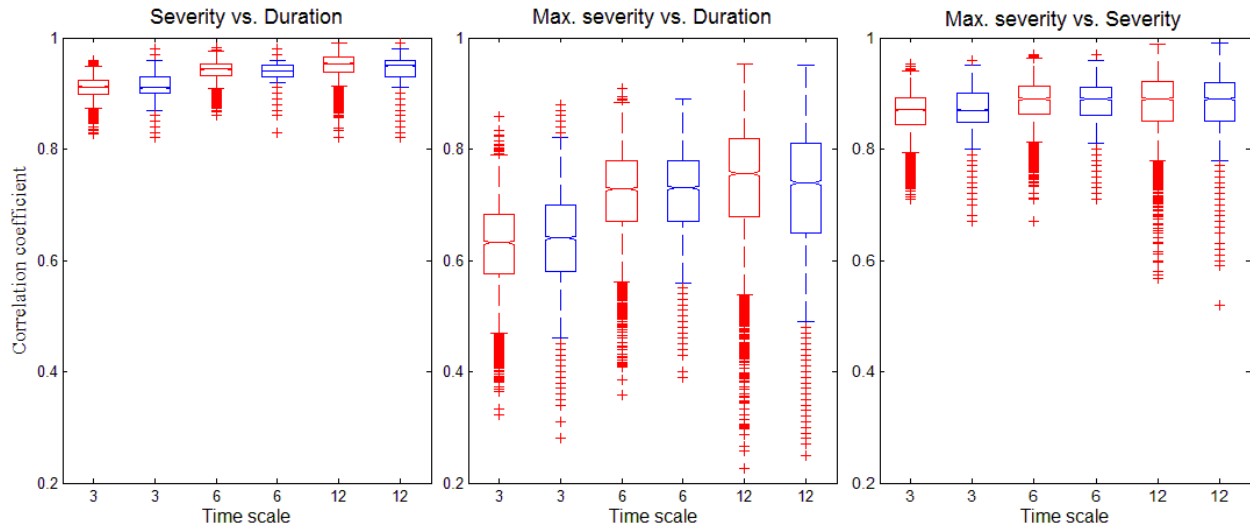


Figure 2.6: Box and whisker plots of the Spearman rank correlation coefficients for various combinations of drought characteristics for the SRB. Results for the case of SPI are shown in red and those for the case of SPEI in blue. The boxes correspond to the interquartile range (IQR), the line in the middle of the box to the median value and the whiskers to either the maximum value or the 1.5 times the IQR. Outliers that lie outside the 1.5 times IQR range are shown using the plus sign.

It is also found that the concurrent values of SPI and SPEI are highly correlated for all time scales, which is also evident from the spatial patterns shown in Figure 2.5. This result is not surprising, since similar behavior was also noted by Vicente-Serrano et al. (2010), who found that the SPI and SPEI values show stronger correlations than their correlations with the PDSI values.

A comparison of SPI and SPEI based results shown in Figure 2.5 suggests that there is little effect of considering temperature in the form of evapotranspiration in the drought index in delineating spatial patterns of drought characteristics. Nonetheless, drought characteristics show slightly higher spatial coverage in the case of SPEI than SPI. It is anticipated that under the future warming conditions, the importance of including temperature in the drought index for assessing drought characteristics could become significant as the evapotranspiration is projected to increase due to projected increases in temperature in this region (Bonsol et al., 2012).

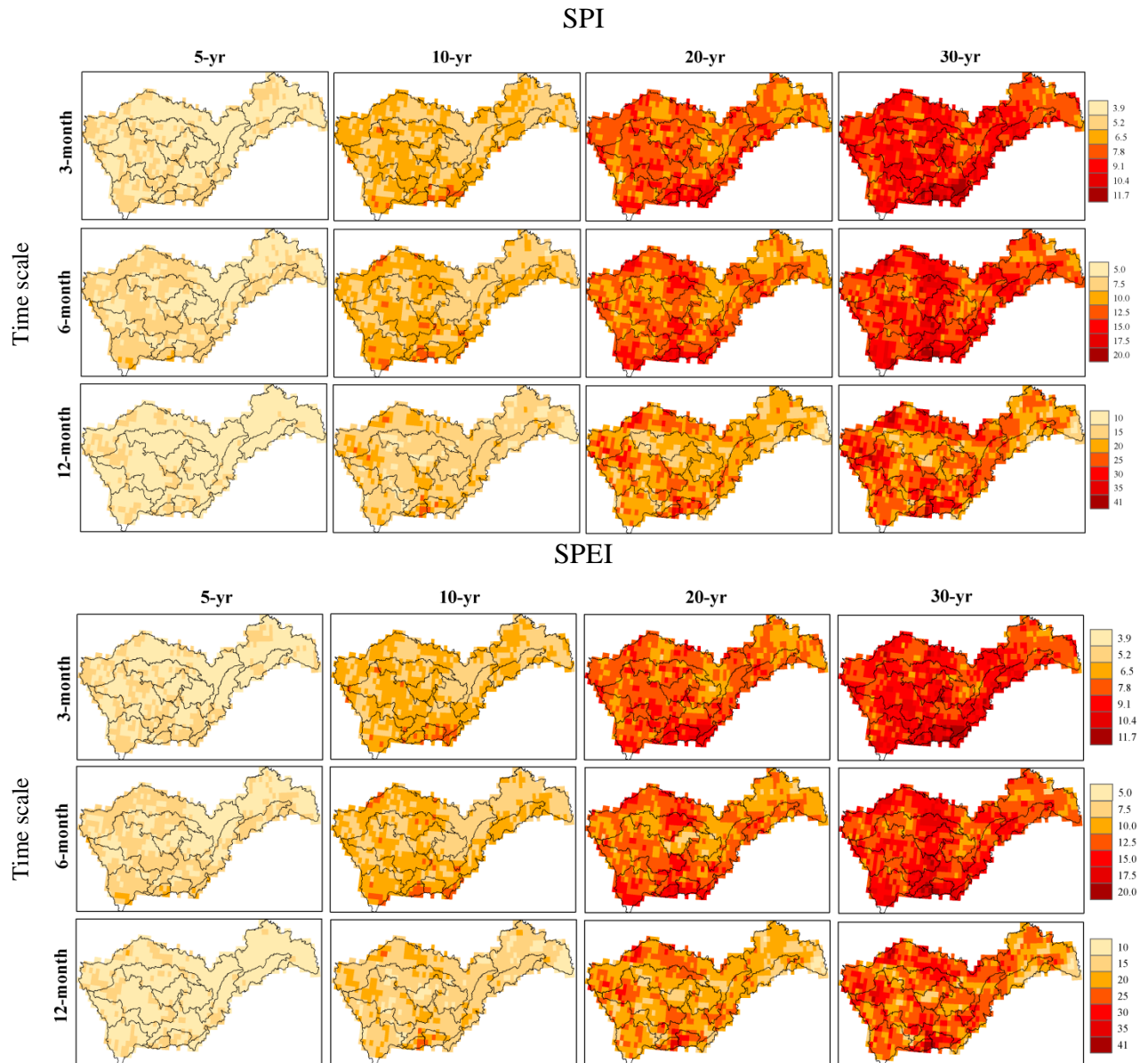


Figure 2.7: Spatial patterns of 5-, 10-, 20-, and 30-year return values of drought severity, derived on the basis of SPI/SPEI values of 3-, 6-, and 12-month time scales.

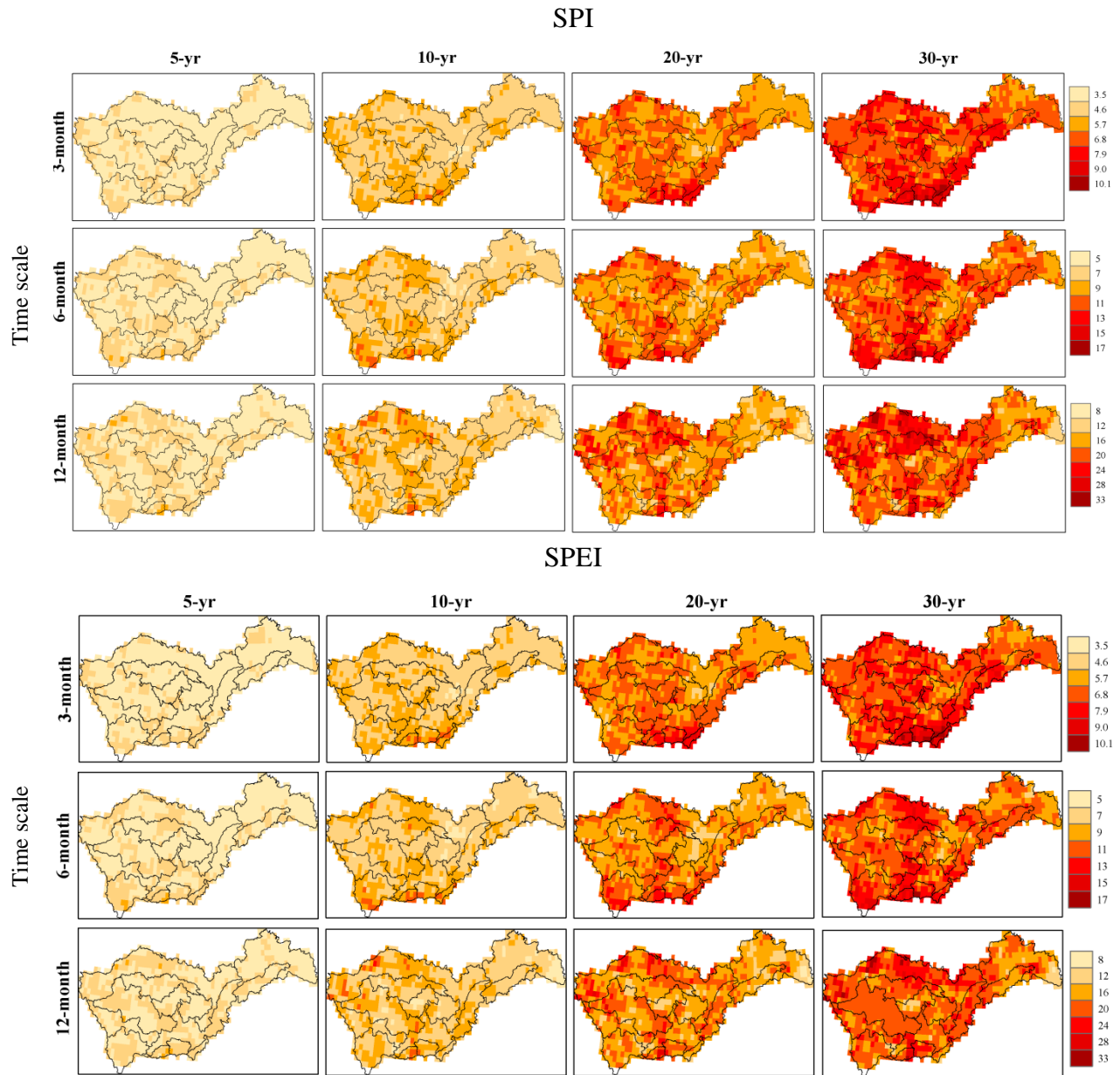


Figure 2.8: Spatial patterns of 5-, 10-, 20-, and 30-year return values of drought duration, derived on the basis of SPI/SPEI values of 3-, 6-, and 12-month time scales.

2.4.3. Univariate analyses

Figure 2.7 shows spatial patterns of 5-, 10-, 20-, and 30-year return values of drought severity for the SPI and SPEI of 3-, 6-, and 12-month time scales. As expected, the intensity of drought severity increases with increasing return period for different time scales. However, decreases in the intensity of droughts with increasing time scales can also be seen in this figure. For the 3-month time scale, droughts with higher severity can be found in most of the watersheds, except the eastern part of the North Saskatchewan River, Eagle Creek and Saskatchewan River watersheds. Similar spatial pattern of drought severity is observed for the 6-month time scale however, the spatial extent of areas affected by severe droughts is reduced compared to the 3-month time scale. For the 12-month time scale, the north-western and central areas of the southern part of the SRB are more sensitive to droughts, where drought severity increases with longer return periods. The spatial patterns of 5-, 10-, 20-, and 30-year return values of drought duration are shown in Figure 2.8. It can be seen from this figure that the areas characterized by longer duration of droughts are also associated with more severe droughts (cf. Figure 2.7). Therefore, it can be stated that a longer duration of drought means a higher drought severity and vice versa. According to the results shown in Figures 2.7 and 2.8, severe and longer drought events are detected mainly in the North Saskatchewan River watershed, Red Deer River watershed, and the southern and middle parts of the SRB, whereas less intense and shorter drought events are found mainly in the eastern part of the SRB (particularly the Saskatchewan River watershed and areas surrounding the Saskatchewan-Manitoba border).

2.4.4. Bivariate analyses

As the drought severity and duration are highly correlated, bivariate analysis of drought severity and duration seems imperative to assess drought risks across the SRB. In this respect, two joint probabilities are assessed: $P_1 = P(S > s \text{ or } D > d)$ and $P_2 = P(S > s \text{ and } D > d)$. The former probability represents the joint occurrence probability of “drought severity or duration” exceeding their respective thresholds at the same time, while the latter represents the joint occurrence probability of “drought severity and duration” exceeding their respective thresholds at the same time. The results for P_2 are presented first followed by P_1 . The spatial patterns of P_2 are illustrated in Figure 2.9. The thresholds s and d correspond to 5-, 10-, 20-, and 30-year return values derived from univariate analyses. The probability P_2 corresponding to 5-

year return period threshold is that drought severity is higher than the value of the 5-year return period and drought duration is longer than the duration of the 5-year return period.

Similar interpretation for the probability P_1 can be made also. A discernible spatial pattern is found in the SRB for the joint occurrence probability P_2 for all time scales and return periods. The western part of the North Saskatchewan River watershed, a major portion of the Red Deer River watershed and almost the entire southern part of the SRB are completely dominated by relatively larger P_2 values, suggesting a higher drought risk in these areas. On the contrary, the eastern part of the SRB (i.e., the eastern part of the North Saskatchewan River, Saskatchewan River and Carrot River watersheds) is dominated by lower P_2 values, suggesting relatively lower drought hazards in these areas. The southern parts of the Bow River and a minor portion of the Red Deer River watersheds are also found to be less sensitive to drought risk. The spatial patterns of joint occurrence probability P_1 are shown in Figure 2.10. The areal coverage of P_1 is quite similar to that of P_2 , except some increased adjacent spatial extent revealed by P_2 .

2.4.5. Drought sensitive geographic regions

To delineate drought sensitive regions in the SRB, each watershed was checked individually for similarity of drought severity and duration characteristics for both SPI and SPEI cases through hierarchical clustering. Based on the results of this technique, some watersheds are subdivided into smaller geographic regions, with similar drought features. The results of similarity analyses are about the same for both drought severity and duration characteristics. In addition, almost the same geographic divisions are identified using the values of probabilistic drought risk indicators P_1 and P_2 . After identifying geographic regions with similar features of drought events, regionally averaged values of P_1 and P_2 are mapped across the SRB in order to synthesize some useful information for planning and management purposes. The results corresponding to only P_2 are shown in Figure 2.11. These results reveal that drought sensitive regions are about the same for SPI and SPEI of 3- and 6-month time scales, regardless of return period considered. The Oldman River, Seven Persons Creek, Bigstick Lake, Swift Current Creek, western part of the South Saskatchewan River, and a major portion of the Red Deer River watersheds in the southern parts of the SRB are found to be more vulnerable to drought.

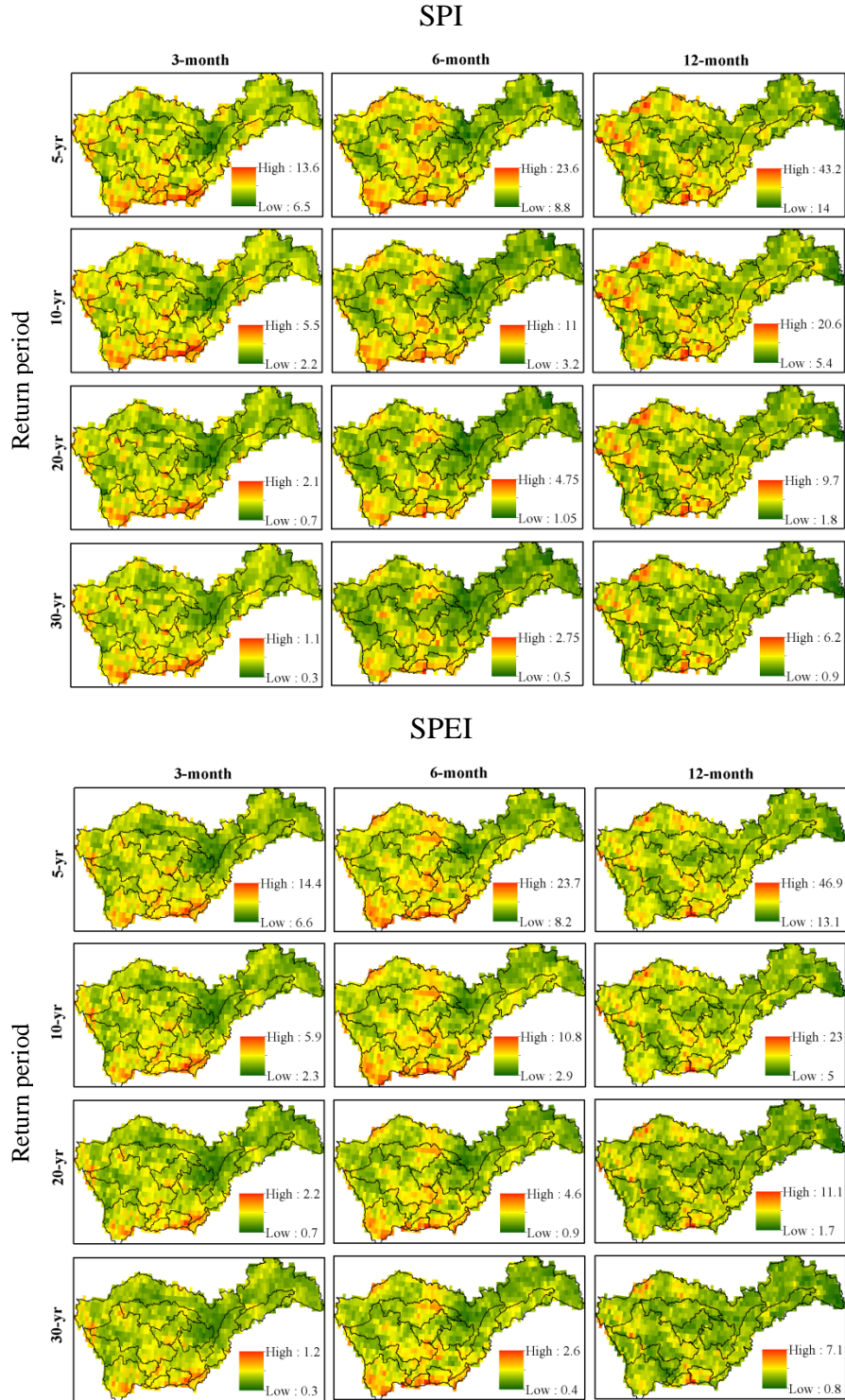


Figure 2.9: Spatial patterns of joint occurrence probability (in %) of “drought severity and duration” exceeding their respective thresholds at the same time [i.e., $P_2 = P(S > s \text{ and } D > d)$]. The thresholds (i.e., s and d) correspond to 5-, 10-, 20-, and 30-year return period values.

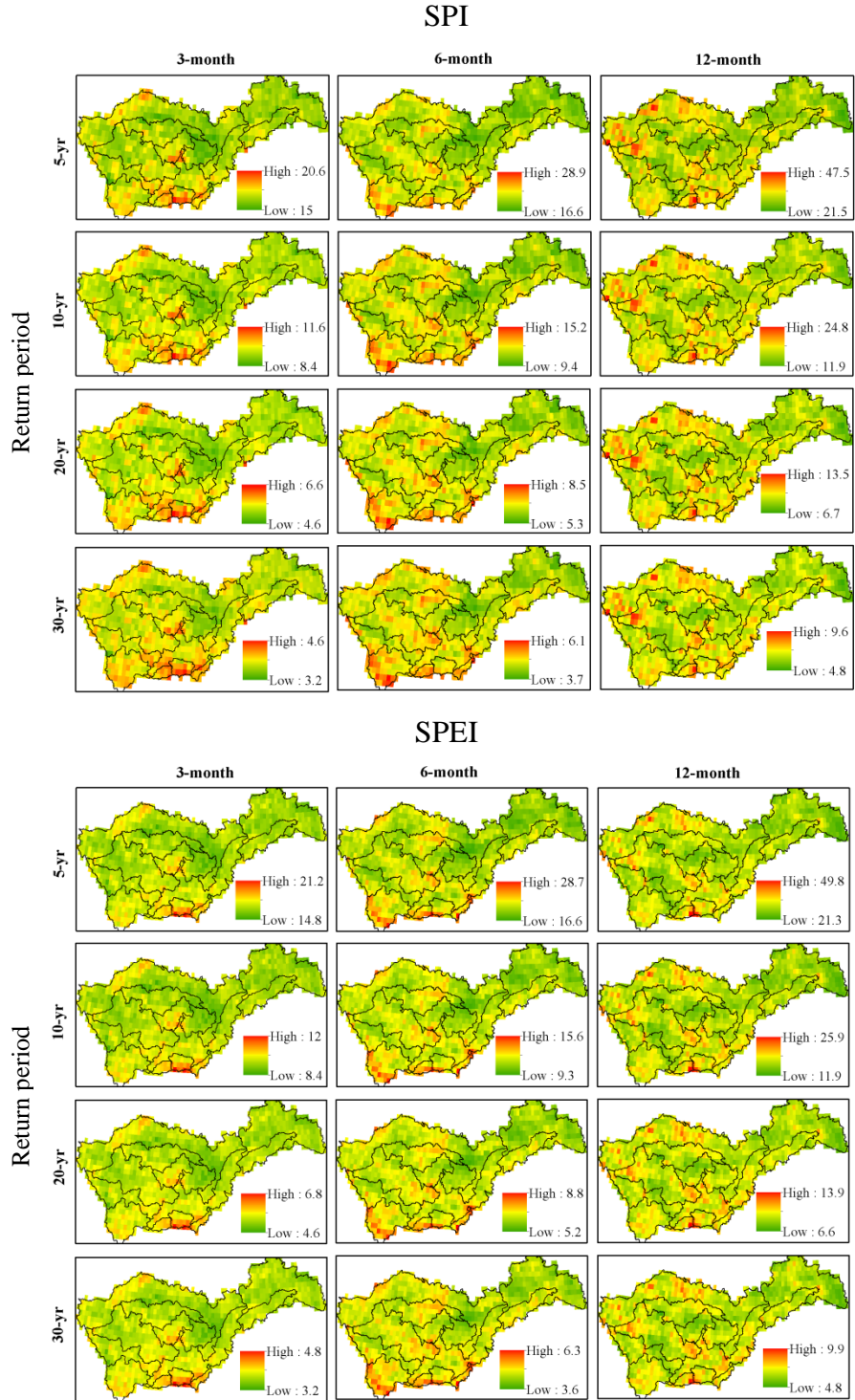


Figure 2.10: Spatial patterns of joint occurrence probability (in %) of “drought severity or duration” exceeding their respective thresholds at the same time [i.e., $P_1 = P(S > s \text{ or } D > d)$]. The thresholds (i.e., s or d) correspond to 5-, 10-, 20-, and 30-year return period values.

The Bow River, Sounding Creek, Carrot River, and North Saskatchewan River watersheds are found relatively less sensitive to drought. At the 12-month time scale, the sensitive regions are slightly different than those identified at the other two time scales. At this time scale, the Seven Persons Creek, Bigstick Lake, western part of the South Saskatchewan River, and a major portion of the North Saskatchewan River watersheds are found more sensitive to drought, while the Swift Current Creek, Oldman River and a major portion of the Red Deer River watersheds are associated with moderate risks. Also, at this time scale, the western part of the North Saskatchewan River watershed is highly vulnerable to drought in the case of SPEI than SPI that dictates clearly the effect of temperature in identifying drought sensitive regions. The eastern parts of the North Saskatchewan River watershed and the Saskatchewan River watershed are generally found less sensitive to drought risks at the three time scales of both SPI and SPEI indices.

2.5. Summary and conclusions

Characteristics of so called meteorological droughts were defined on the basis of two drought indices, the SPI and SPEI, using $10 \text{ km} \times 10 \text{ km}$ gridded observed data for the 1961 to 2003 period for the entire SRB. An exclusive feature of the current study is that it is the first attempt to examine characteristics of historical droughts in a probabilistic manner using both the conventional univariate and newly emerging copula-based bivariate approaches. Different marginal distributions were tested for calculating SPI and SPEI values, respectively from the monthly precipitation and difference of monthly precipitation and evapotranspiration using L-moments ratio diagrams and the KS goodness-of-fit test. None of the commonly used three-parameter distributions was found satisfactory for describing these monthly quantities corresponding to 3-, 6-, and 12-month time scales and therefore, the five-parameter Wakeby distribution is used for this purpose. In a similar manner, various marginal distributions were tested for univariate frequency analysis of drought severity and duration; the three-parameter GPA distribution was found to be the best candidate for modeling these characteristics. From the family of Archimedean copulas, Frank copula was selected on the basis of minimum values of the RMSE and AIC for performing bivariate frequency analysis of drought severity and duration. Main conclusions of the study are summarized below:

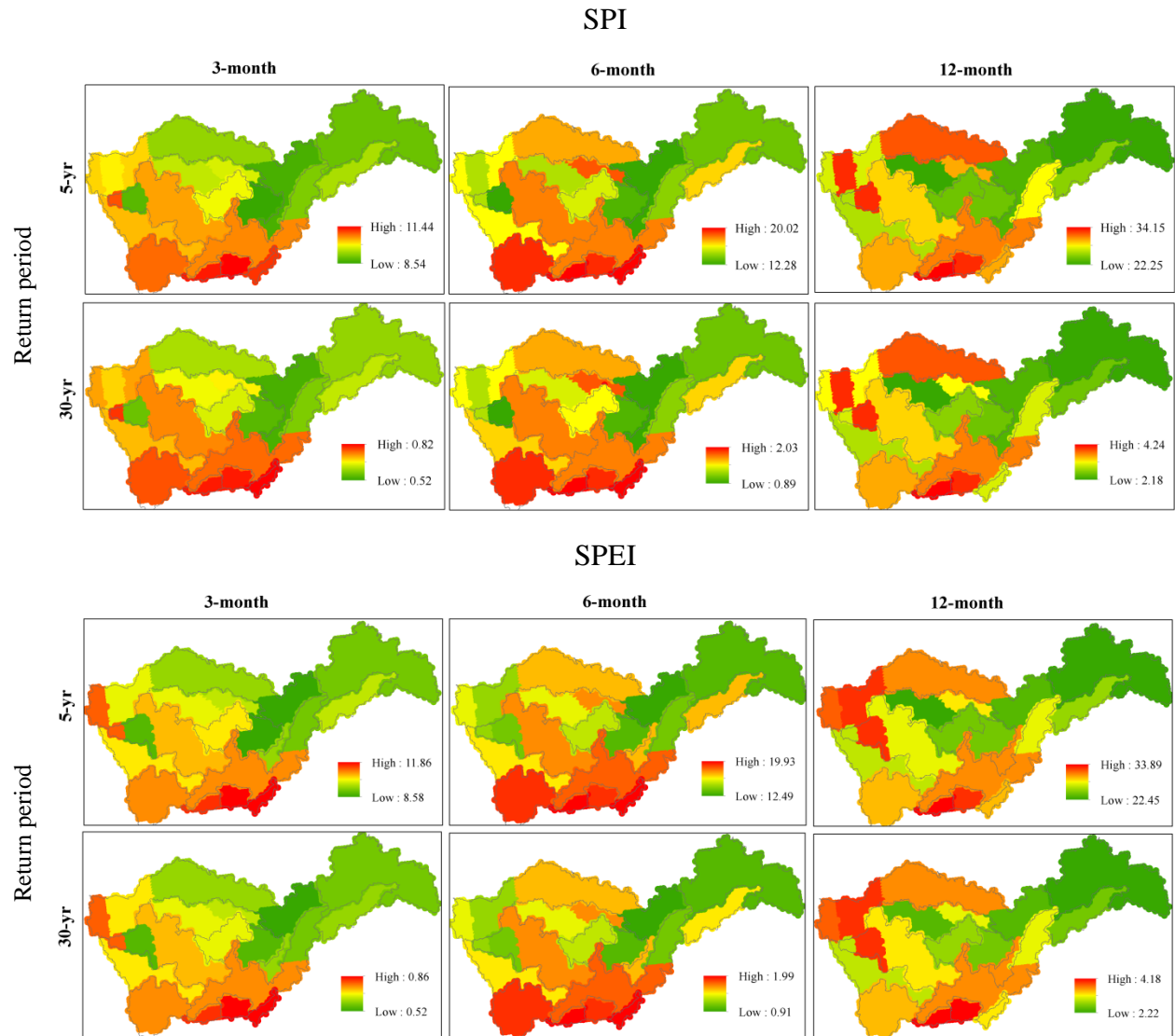


Figure 2.11: Drought sensitive geographic regions of the SRB identified on the basis of joint occurrence probability P_2 (shown in %) corresponding to 5- and 30-year return period thresholds of S and D . Results for both SPI and SPEI and three different time scales are shown. Similar patterns are found for other return period (i.e., 10- and 20-year) thresholds.

- The spatial patterns of drought characteristics, severity and duration, show that the North Saskatchewan River watershed, southern parts of the SRB and the areas surrounding the Alberta-Saskatchewan border experience intense droughts. The magnitude of the drought severity and duration are largely consistent, that is, drought events of higher severity normally last longer and vice versa. The areas surrounding the Saskatchewan-Manitoba

border (specifically the Saskatchewan River watershed) have experienced more frequent droughts but of relatively mild severity.

- There is no substantial difference in the spatial extent of drought affected areas identified on the basis of various return values of drought severity and duration derived from the SPI and SPEI of 3-, 6-, and 12-month time scales. This suggests little effect of temperature (in the form of evapotranspiration) inclusion in the drought index in delineating drought sensitive regions. However, it is anticipated that the SPEI could prove a useful index for the analysis of future droughts in the SRB using outputs from climate models due to the predicted increases in temperature that will play an important role in drought analysis as noted in Jeong et al. (2014).
- The areas characterized by longer drought duration are also dominated by more severe droughts, an indication that both drought severity and duration are positively correlated. This type of behavior can best be described using a bivariate frequency analysis.
- The results of the bivariate frequency analyses based on the Frank copula suggest that the western part of the North Saskatchewan River watershed, a major portion of the Red Deer River watershed and almost the entire southern part of the SRB are associated with larger values of the joint occurrence probability P_2 , that is, when the drought severity and duration exceed their corresponding 5-, 10-, 20-, and 30-yr return values at the same time. Eastern part of the North Saskatchewan River, Saskatchewan River and Carrot River watersheds are associated with smaller values of the joint occurrence probability P_2 , suggesting low risk of droughts in these areas.
- To identify drought sensitive geographic regions within the SRB, estimates of the probability P_2 are spatially mapped on the basis of regions, with similar characteristics of droughts, identified using the hierarchical clustering. The results of the analyses suggest that, at the 3- and 6-month time scales, the Oldman River, Seven Persons Creek, Bigstick Lake, Swift Current Creek, western part of the South Saskatchewan River, and a major portion of the Red Deer River watersheds in southern parts of the SRB are more vulnerable to droughts followed by the Bow River, Sounding Creek, Carrot River, and North Saskatchewan River watersheds, which are associated with relatively moderate drought risks. At the 12-month time scale, Seven Persons Creek, Bigstick Lake, western parts of the South Saskatchewan River, and a major portion of the North Saskatchewan River watersheds are found relatively

more drought sensitive than the other watersheds. The Swift Current Creek, Oldman River and a large portion of the Red Deer River watersheds are relatively less sensitive to droughts at the 12-month time scale. Eastern parts of the North Saskatchewan River and Saskatchewan River watersheds are found to be less sensitive to droughts at all three time scales.

Finally, as the drought severity is highly correlated with drought duration, results based on the joint occurrence probability P_2 of drought characteristics will play a significant role for planning drought risk management strategies for the SRB. Future work should investigate droughts within the realm of trivariate frequency analysis, thus considering another level of sophistication for spatial mapping of drought risk indicators. In addition, a bivariate regional frequency analysis may also provide some additional insights about the spatial structure of droughts.

Acknowledgements

The authors would like to acknowledge Agriculture and Agri-Food Canada for providing observed gridded data of daily precipitation and temperature used in this study. The financial support from the Canada Excellence Research Chair in water security and School of Environment and Sustainability, University of Saskatchewan is also acknowledged. The authors would like to thank three anonymous referees and the editors for their helpful comments.

References

- Akaike H (1974) A new look at the statistical model identification. *IEEE Transactions on Automatic Control* 19(6), 716-723.
- Allen R, Pereira L, Raes D, Smith M (1998) Crop evapotranspiration: guidelines for computing crop requirements. *Irrigation and drainage*, paper 56. FAO. Roma. Italia.
- Blaney HF, Criddle WD (1950) Determining water requirements in irrigated areas from climatological and irrigation data. U.S. Department of Agriculture, Soil Conservation Service. Technical paper 96.
- Bonsal BR, Wheaton EE, Chianshi AC, Lin C, Sauchyn DJ, Wen L (2011) Drought research in Canada: A review. *Atmospheric-Ocean* 49(2), 303-319. <http://dx.doi.org/10.1080/07055900.2011.555103>.

- Bonsal BR, Aider R, Gachon P, Lapp S (2012) An assessment of Canadian prairie drought: past, present, and future. *Climate Dynamics* DOI 10.1007/s00382-012-1422-0.
- Coles S (2001) An introduction to statistical modeling of extreme values. Springer publishers. Great Britain.
- Chen L, Singh VP, Guo S (2011) Drought analysis based on Copulas. 2011 Symposium on Data-Driven Approaches to Droughts. Paper 45. <http://docs.lib.purdue.edu/ddad2011/45>.
- Chipanshi AC, Findlater KM, Hadwen T, O'Brien EG (2006) Analysis of consecutive droughts on the Canadian Prairies. *Climate Research* 30,175-187.
- Doorenbos J, Pruitt WC (1977) Crop water requirements. *Irrigation and Drainage* 24, 15-54
- Dracup JA, Lee KS, Paulson EG Jr (1980) On the statistical characteristics of drought events. *Water Resources Research* 16, 289-296.
- Evans E, Stewart RE, Henson W, Saunders K (2011) On Precipitation and Virga over three locations during the 1999-2004 Canadian Prairie drought. *Atmosphere-Ocean* 49(4), 366-379.
- Genest C, Rivest LP (1993) Statistical inference procedures for bivariate Archimedean copulas. *Journal of The American Statistical Association Theory and Methods* 88(423), 1034-1043.
- Guttman NB (1998) Comparing the palmer drought index and the standardized precipitation index. *Journal of the American Water Resources Association* 34(1), 113-121.
- Hao Z, AghaKouchak A (2013) Multivariate standardized drought index: A parametric multi-index model. *Advances in Water Resources* 57, 12-18.
- Hargreaves GH, Samani ZA (1982) Estimating potential evapotranspiration. Technical Note. *Journal of Irrigation and Drainage Engineering* 108(3), 225-230.
- Hargreaves GH, Samani ZA (1985) Reference crop evapotranspiration from temperature. *Applied Engineering in Agriculture* 1(2), 96-99.
- Hargreaves GL, Hargreaves GH, Riley JP (1985) Agricultural benefits for Senegal River Basin. *Journal of Irrigation and Drainage Engineering* 111, 113-124.
- Heim RR (2002) A review of twentieth-century drought indices used in the United States. *Bulletin of American Meteorological Society* 83, 1149-1165.
- Hosking JRM (1990) L-moments: Analysis and estimation of distributions using linear combinations of order statistics. *Journal of Royal Statistical Society* 52(1), 105-124.
- Hosking JRM, Wallis JR (1997) Regional frequency analysis. Cambridge University Press.

- Hutchinson MF (2004) ANUsplin Version 4.3: User Guide, The Australian National University, Centre for Resource and Environmental Studies, Canberra, Australia. (<http://cres.anu.edu.au/outputs/anusplin.php>).
- Jensen ME, Burman RD, Allen RG, eds. (1990) Evapotranspiration and Irrigation Water Requirements. ASCE Manual 70. Reston, Va.: American Society of Civil Engineers.
- Jeong DI, Sushama L, Khaliq MN, Roy R (2013) A copula-based multivariate analysis of Canadian RCM projected changes to flood characteristics for northeastern Canada. *Climate Dynamics* DOI: 10.1007/s00382-013-1851-4.
- Jeong DI, Sushama L, Khaliq MN (2014) The role of temperature in drought projections over North America. *Climatic Change* 127(2), 289-303.
- Karmakar S, Simonovic SP (2009) Bivariate flood frequency analysis. Part 2: a copula-based approach with mixed marginal distributions. *Journal of Flood Risk Management* 2, 32-44.
- Kaufman L, Rousseuw PJ (1990) Finding groups in data: An introduction to cluster analysis, Wiley-interscience, New York. 344 pp.
- Keyantash A, Dracup JA (2002) The quantification of drought: An evaluation of drought indices. *Bulletin of American Meteorological Society* 83, 1167-1180.
- Lee T, Modarres R, Ouarda TBMJ (2012) Data-based analysis of bivariate copula tail dependence for drought duration and severity. *Hydrological Processes* DOI:10.1002/hyp.9233.
- Liu C-L, Zhang Q, Singh VP, Cui Y (2011) Copula-based evaluations of drought variations in Guangdong, South China. *Natural Hazards* 59, 1533-1546.
- Liu J, Stewart RE (2003) Water vapor fluxes over the Saskatchewan River Basin. *Journal of Hydrometeorology* 4, 944-959.
- Lowry RL, Johnson AF (1942) Consumptive use of water for agriculture. *American Society of Civil Engineers Transactions* 107, 1243-1266.
- Maulé C, Helgalson W, McGinn S, Cutforth H (2006) Estimation of standardized reference evapotranspiration on the Canadian Prairies using simple models with limited weather data. *Canadian Biosystems Engineering/Le génie des biosystèmes au Canada* 48, 1.1 - 1.11.
- Mavromatis T (2007) Drought index evaluation for assessing future wheat production in Greece. *International Journal of Climatology* 27, 911-924.

- McKee TB, Doesken NJ, Kleist J (1993) The relationship of drought frequency and duration to time scales. Preprints 8th Conference on Applied Climatology, Anaheim, CA. American Meteorological Society 179-184.
- McKenney DW, Pedlar JH, Papadopolk P, Hutchinson MF (2006) The development of 1901-2000 historical monthly climate models for Canada and the United States. *Agricultural and Forest Meteorology* 138, 69-81.
- Mishra AK, Singh VP (2010) A review of drought concepts. *Journal of Hydrology* 391, 202-216.
- Mu Q, Zhao M, Kimball JS, McDowell NG, Running SW (2013) A remotely sensed global terrestrial drought severity index. *Bulletin of American Meteorological Society* 94, 83-98. <http://dx.doi.org/10.1175/BAMS-D-11-00213.1>.
- Nelsen RB (1999) An introduction to copulas. Springer-Verlag: New York; pp 217.
- Oguntunde PG, Abiodun JB, Gunnar LG (2011) Rainfall trends in Nigeria, 1901-2000. *Journal of Hydrology* 411, 207-218.
- PaiMazumder D, Sushama L, Laprise R, Khaliq MN, Sauchyn D (2012) Canadian RCM projected changes to short- and long-term drought characteristics over the Canadian Prairies. *International Journal of Climatology*, DOI: 10.1002/joc.3521.
- Palmer WC (1965) Meteorological drought. Research Paper No. 45. Weather Bureau, Washington, DC.
- Partners FOR the Saskatchewan River Basin (2009) From the mountains to the sea. The state of the Saskatchewan River Basin. Basin overview (Chapter two) http://www.saskriverbasin.ca/page.php?page_id=70; Date of access: 14th June 2013.
- Penman HL (1948) Natural evaporation from open water, bare soil, and grass. *Proceedings, Royal Society, London* 193, 120-146.
- Priestley CHB, Taylor RJ (1972) On the assessment of surface heat flux and evaporation using large scale parameters. *Monthly Weather Review* 100, 81-92.
- Quiring SM, Papakryiakou NT (2003) An evaluation of agricultural drought indices for the Canadian prairies. *Agricultural and Forest Meteorology* 118, 49-62.
- Ramos MC (2001) Divisive and hierarchical clustering techniques to analyse variability of rainfall distribution patterns in a Mediterranean region. *Atmospheric Research* 57, 123-138
- Rao AR, Srinivas VV (2008) Regionalization of watersheds – An approach based on cluster analysis, Springer publishers, Germany.

- Salinger J (1995) Conditions leading to drought in New Zealand. *Water and Atmosphere* 3 (1): 11–12.
- Shafer BA, Dezman LE (1982) Development of a Surface Water Supply Index (SWSI) to assess the severity of drought conditions in snowpack runoff areas. In: Preprints, Western Snow Conference, Reno, NV, Colorado State University, pp. 164-175.
- Shiau JT (2006) Fitting drought duration and severity with two-dimensional Copulas. *Water Resources Management* 20, 795-815.
- Shiau JT, Shen HW (2001) Recurrence analysis of hydrological droughts of differing severity. *Journal of Water Resources Planning Management* 127(1), 30-40.
- Shiau JT, Modarres R (2009) Copula-based drought severity-duration-frequency analysis in Iran. *Meteorological Applications* 16,481-489. DOI:10.1002/met.145.
- Shukla S, Wood AW (2008) Use of a standardized runoff index for characterizing hydrologic drought. *Geophysical Research Letters* 35:L02405. DOI:10.1029/2007/GL032487.
- Sklar K (1959) Fonctions de repartition `a n dimensions et leurs marges. *Publications de l'Institut de Statistique de l'Universit'e: Paris* 8, 229-231.
- Sridhar V, Hubbard KG, You J, Hunt E (2007) Development of the soil moisture index to quantify agricultural drought and its “User Friendliness” in severity-area-duration assessment. *Journal of Hydrometeorology* 9, 660-676.
- Stewart RE, Pomeroy J, Lawford R (2011) The drought research initiative: a comprehensive examination of drought over the Canadian Prairies. *Atmospheric Ocean* DOI:10.1080/07055900.2011.622574.
- Sun L, Mitchell SW, Davidson A (2011) Multiple drought indices for agricultural drought risk assessment on the Canadian Prairies. *International Journal of Climatology* DOI: 10.1002/joc.2385.
- Sushama L, Khaliq MN, Laprise R (2010) Dry spell characteristics over Canada in a changing climate as simulated by the Canadian RCM. *Global and Planetary Change* 74, 1-14.
- Tallaksen LM, van Lanen, HAJ (2004) *Hydrological Drought: Processes and estimation methods for streamflow and groundwater*. *Developments in Water Science* 48. Elsevier, Amsterdam. P.579.
- Thornthwaite CW (1948) An approach toward a rational classification of climate. *The Geographical Review* 38(1), 55-94.

- Topçu Ç, Arslan F (2012) Selecting the suitable copula function when only values of distribution functions are available. *Selçuk Journal of Applied Mathematics* 13(2), 35-41.
- van Rooy MP (1965) A rainfall anomaly index independent of time and space. *Notos* 14, 43.
- Vicente-Serrano SM, Beguería S, López-Moreno JI (2010) A Multi-scalar drought index sensitive to global warming: The Standardized Precipitation Evapotranspiration Index. *Journal of Climate* 23(7), 1696-1718.
- Wells N, Goddard S, Hayes MJ (2004) A self-calibrating Palmer drought severity index. *Journal of Climate* 17, 2335-23561.
- Wheater HS, Gober PA (2013) Water security in the Canadian Prairies: science and management challenges, *Philosophical Transactions of Royal Society A* 371, 20120409. doi: 10.1098/rsta.2012.0409.
- Wheaton E (2011) What effects do droughts have in Canada? Highlights of the repercussions of a major multi-year drought. In: *Drought Research Initiative*, Stewart, R. and Lawford, R. (Eds.), Department of Environment and Geography, University of Manitoba, Winnipeg, Manitoba, pp 23–24.
- Wilhite DA (2000) Drought as a natural hazard: concepts and definitions. In: *Drought: a global assessment*, Wilhite, D.A. (Ed.), Routledge, London, pp 3-18.
- WMO (2009) Inter-Regional workshop in indices and early warning systems for drought (Lincoln, NE, Dec. 2009) (Geneva: World Meteorological Organization).
- Yue S, Rasmussen P (2002) Bivariate frequency analysis: discussion of some useful concepts in hydrological application. *Hydrological Processes* 16, 2881-2898. DOI: 10.1002/hyp.1185.
- Zargar A, Sadiq R, Naser B, Khan FI (2011) A review of drought indices. *Environmental Reviews* 19, 333-349.
- Zhang L, Singh VP (2006) Bivariate flood frequency analysis using the copula method. *Journal of Hydrologic Engineering* 11(2), 150-164.
- Zhang L, Singh VP (2007) Bivariate rainfall frequency distributions using Archimedean copulas. *Journal of Hydrology* 332, 93-109.

CHAPTER 3

FUTURE CHANGES TO DROUGHT CHARACTERISTICS OVER THE CANADIAN PRAIRIE PROVINCES BASED ON NARCCAP MULTI-RCM ENSEMBLE

Reliable information on expected changes to various water cycle components due to climate change at various spatial and temporal scales is important for water resources and agricultural decision support systems. Atmosphere-Ocean General Climate Models (AOGCMs) and Regional Climate Models (RCMs) are the primary tools to assess impacts of anticipated climate change. AOGCMs can deliver useful information on large spatial and temporal scales. However, climate on regional scales is strongly modified by features like cloud cover, land-water contrasts, steep topographic gradients, and land cover changes on scales that are poorly resolved by AOGCMs, if they are resolved at all. Synoptic, meso- and microscale weather systems may interact in complex, nonlinear ways, further undermining the utility of AOGCM outputs. To translate coarse scale information available from AOGCMs to regional, catchment and local scale hydroclimatic variables such as precipitation and temperature, either dynamical or statistical downscaling techniques are used. The former involves the use of a Regional Climate Model (RCM) and the latter depends on establishing statistical relationships between large scale predictors and local scale variables of interest. In the work presented in this chapter, multi-RCM simulations, available through the North American Regional Climate Change Assessment Program, were used to assess impacts of climate change on drought characteristics on the basis of 15 geographic contiguous regions covering the three Prairie Provinces of Canada. These regions were identified through univariate and multivariate homogeneity analysis approaches and form the basis for the developed projected changes to drought characteristics, presented in this chapter. This chapter contains the following submitted manuscript:

2. **Masud MB**, Khaliq MN, Wheeler HS (2016) Future changes to drought characteristics over the Canadian Prairie Provinces based on NARCCAP multi-RCM ensemble. Submitted to *Climate Dynamics* on 31st December 2015; submission no. CLDY-D-16-00003

Abstract

This study assessed projected changes to drought characteristics in Alberta, Saskatchewan and Manitoba, the prairie provinces of Canada, using a multi-Regional Climate Model (RCM) ensemble available through the North American Regional Climate Change Assessment Program. Simulations considered include those performed with six RCMs driven by National Centre for Environmental Prediction reanalysis II for the 1981–2003 period and those driven by four Atmosphere–Ocean General Circulation Models for the 1970–1999 and 2041–2070 periods (i.e. eleven current and the same number of corresponding future period simulations). Drought characteristics were extracted using two drought indices, namely the Standardized Precipitation Index (SPI), which is solely based on precipitation, and the Standardized Precipitation Evapotranspiration Index (SPEI), which is based on both precipitation and temperature in the form of evapotranspiration. Regional frequency analysis was used to project changes to selected 20- and 50-yr regional return levels of drought characteristics for fifteen homogeneous regions, covering the study area. In addition, multivariate analyses of drought characteristics, derived on the basis of 6-month SPI and SPEI values, were developed using the copula approach for each region. Analysis of multi-RCM ensemble-averaged projected changes to mean and selected return levels of drought characteristics show increases over the southern and south-western parts of the study area. Based on bi- and trivariate joint occurrence probabilities of drought characteristics, the southern regions along with the central regions are found highly drought vulnerable, followed by the southwestern and southeastern regions. These projections will be useful in the development of appropriate adaptation strategies for the water and agricultural sectors, which play an important role in the economy of the study area.

Keywords: Drought characteristics; Copula; Multivariate frequency analysis; Multivariate homogeneity testing; Regional Climate Model; NARCCAP; Canadian Prairie Provinces

3.1 Introduction

Drought is considered to be a continuous dry weather phenomenon with abnormally low precipitation for a period of time ranging from several months to years. It can cause severe damage to both the natural environment and human lives. For example, the 2012–2013 U.S. drought in the Central Plains caused more than US \$12 billion in damages in the U.S., while the 1995 drought in Spain and the 1982 drought in Australia cost US \$4.5 and US \$6 billion,

respectively (Touma et al., 2015). In spite of having world's largest fresh water resources, Canada is not drought proof. Several multi-year droughts for the 1890s, 1910s, 1930s, late 1950s, early 1960s and 1980s have been reported for the southern parts of the Alberta, Saskatchewan and Manitoba provinces of Canada. The drought experienced during the 1999–2004 period was the most severe over the last 100 years (Evans et al., 2011). Gross domestic product declined respectively by \$2.1 and \$3.6 billion in the years 2001 and 2002, with the total loss estimated over the same period pegged at \$5.8 billion (Wheater and Gober, 2013). Considering the massive impact of droughts, it is important to know how anticipated climate change will influence drought characteristics in this region. Projections of future droughts will be useful for the assessment of climate change impacts on water infrastructure and agriculture and in the development of efficient adaptation strategies.

The primary tool to assess future climate change is to use simulations of coupled global and regional climate models when these models are integrated from the recent past to some time-point in the future (IPCC, 2007). Currently, Regional Climate Models (RCMs) offer higher spatial resolution than Global Climate Models (GCMs) and therefore RCMs can help represent many finer scale features and atmospheric processes which are not possible using GCMs (e.g. see Giorgi, 2006; May 2008; Torma et al., 2015). RCMs are physically based tools and can represent most of the processes of the climate system over smaller regional domains. Due to these merits, many studies have used RCM simulations for the assessment of future changes to drought characteristics (e.g. Jeong et al., 2014; Diasso and Abiodun, 2015; Huang et al., 2015).

This study explored projected changes to drought characteristics and future drought risks over the Canadian Prairie Provinces of Alberta, Saskatchewan and Manitoba based on the North American Regional Climate Change Assessment Program (NARCCAP) multi-RCM ensemble. Drought events were defined on the basis of Standardized Precipitation Index (SPI; McKee et al., 1993), which is a purely precipitation-based index, and Standardized Precipitation Evapotranspiration Index (SPEI; Vicente-Serrano et al., 2010), which is a temperature and precipitation-based index. The use of SPI and SPEI together helps to better understand the impact of future rises in temperature on drought characteristics. Drought events were characterized in terms of three associated characteristics, i.e. drought severity, duration and maximum severity. These characteristics were modelled using the univariate regional frequency analysis (RFA) approach of Hosking and Wallis (1997) and copula based multivariate

approaches. Within the multivariate frequency analysis framework, copula based bi- and trivariate frequency analyses are performed to study projected changes to drought characteristics. Compared to univariate approaches, copula-based multivariate approaches are useful in modelling inter-dependence of drought characteristics and thus could provide more realistic information for drought risk analysis and in the identification of drought sensitive geographic regions.

Examples of previous studies wherein copula-based bivariate analysis of drought characteristics was undertaken include the studies by Shiau and Modarres (2009), Serinaldi et al. (2009), Kao and Govindaraju (2010), Halwatura et al. (2015), and Masud et al. (2015). Most of these studies were performed using observational data. Quite a few drought-related studies have also used a trivariate analysis approach. For example, Wong et al. (2010) analyzed droughts in Australia based on rainfall data categorized into three climatic states (i.e. El-Nino, Neutral and La-Nina) and using the Gumbel-Hougaard and t -copulas to model these states. Madadgar and Moradkhani (2013) explored drought risks under climate change using Gumbel and t -copula in Oregon's Upper Klamath River Basin. They found less frequent droughts in the future compared to the historical period. Ganguli and Reddy (2013a) performed multivariate frequency analysis of droughts for three meteorological subdivisions of western India using multivariate copula functions and demonstrated the importance of trivariate frequency analysis, which provided significant additional insights for drought risk management over the univariate approaches. Ma et al. (2013) applied copula-based trivariate approach to investigate changing behavior of drought events in the Weihe River Basin, China.

Frequency analysis of drought characteristics has mostly been performed on the basis of non-regional univariate and/or multivariate approaches and on the basis of regional univariate approaches only. Some forms of regional multivariate approaches are beginning to emerge for other hydro-meteorological variables (e.g. Chebana and Ouarda, 2007; Sadri and Burn, 2011; Rajsekhar et al., 2013). In the present study, both univariate and multivariate approaches were explored for the analysis of projected changes to drought characteristics on a regional basis by defining and validating homogeneous regions based on cluster analysis and multivariate L-moments, developed by Serfling and Xiao (2007), and multivariate homogeneity tests developed by Chebana and Ouarda (2007).

This paper is organized as follows: description of the study area, observed datasets, and RCM simulations used in the study are described in Section 2. Detailed description of the methodology for characterizing drought events, performing univariate RFA and copula-based multivariate frequency analyses are provided in Section 3. Validation of RCM simulations and development of projected changes to drought characteristics and some other useful results of the study are presented and discussed in Section 4, followed by the main conclusions in Section 5.

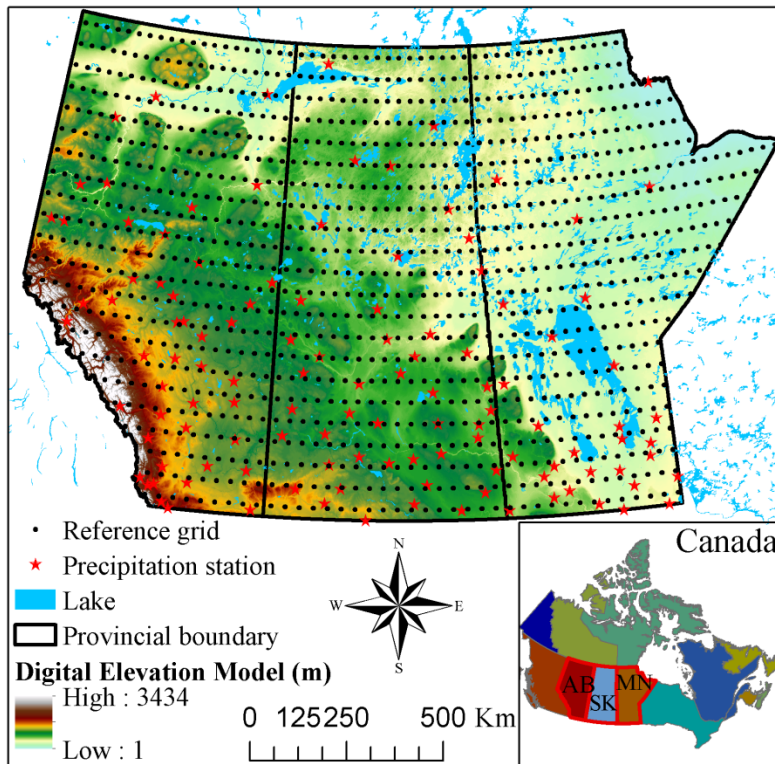


Figure 3.1: Map of the study area overlaid with the reference grid; inset shows location of the study region (AB–Alberta; SK–Saskatchewan; MN–Manitoba) in Canada.

3.2 Study area, observed and model data, and the reference grid

The study area consists of Alberta, Saskatchewan and Manitoba, provinces of Canada (Figure 3.1). Southern parts of these provinces, particularly the Prairies ecozone, are important for agricultural activities and account for around 80% of the Canadian agricultural production (Wheater and Gober, 2013). The ecosystem of this region is heavily dependent on precipitation. The mean annual precipitation for the Prairies ecozone is 454 mm, which is much less than the Canada-wide average of 535 mm (McGinn, 2010). The spatial distribution of temperature is generally dominated by a latitude effect in the absence of any dramatic change in topography and

mitigating impact of oceans (Bonsal et al., 2012). The average annual maximum and minimum temperature in this region are respectively 8.1 and -4.1 °C (McGinn, 2010). Due to the high variability of precipitation in both time and space and relatively higher summer temperatures, this region is more susceptible to droughts (Pomeroy, 2011). Also, it has been found that circulation patterns in the upper atmosphere are associated with onset of droughts. Historically, this region was highly affected by various single- and multi-year droughts, including the most recent drought of 1999-2004.

3.2.1 Observed data

Observed data used in this study consist of 10 km × 10 km gridded data of daily maximum and minimum temperatures (°C) and total daily precipitation (mm) for the 1961–2003 period. This dataset, available from Agriculture and Agri-Food Canada for the entire country south of sixty degrees north latitude, was interpolated from daily Environment Canada climate station observations using a thin plate smoothing spline surface fitting method implemented by ANUsplin V4.3 (Hutchinson, 2004). In the present study, this dataset was used for dividing the study area into smaller homogeneous regions to facilitate development of uni- and multivariate frequency analysis approaches, to be discussed in the methodology section. In addition, a second set of station-based data consisting of daily precipitation and maximum and minimum temperatures, available from Environment Canada for the 1961–2003 period for a network of 120 stations located across the study area, was also considered (Table D.1. in Appendix D). This station-based dataset, which is commonly referred to as adjusted and rehabilitated dataset (Mekis and Vincent, 2011), was used as an additional source for validating statistical homogeneity of regions identified on the basis of the gridded dataset discussed above. It is important to mention that some of the underlying stations in both datasets are the same, but not necessarily the data due to the incorporated adjustments in the second dataset.

3.2.2 Model simulations

Outputs from six different RCMs, driven by National Center for Environmental Prediction (NCEP) reanalysis II and four different Atmospheric-Ocean General Circulation Models (AOGCMs), available through the NARCCAP were considered in this study (see Table 3.1). The aim of NARCCAP was to produce RCM simulations for a common period and domain (Mearns et al., 2009) to aid in systematic evaluation of various sources of uncertainty in future climate projections. These simulations were produced in two phases. In Phase I, simulations from

CRCM, ECP2, HRM3, MM5I, RCM3 and WRFG RCMs were produced with boundary conditions from NCEP reanalysis II for a 25 year reference period (1981–2003). In Phase II, RCM simulations with boundary conditions taken from four different AOGCMs (i.e. CCSM, CGCM3, GFDL and HADCM3) for the 1970–1999 current and 2041–2070 future climates, with Special Report on Emissions Scenarios (SRES) A2 scenario (Nackicenovic et al., 2000), were produced. The NCEP-driven simulations were used to assess performance of individual RCMs, while the AOGCM-driven current and future period 11 simulation pairs were used in the assessment of projected changes to selected drought characteristics, discussed in the section on methodology. In this study, various RCM simulations will be referred to as ‘RCM_LBC’, where RCM stands for the acronym of the RCM and LBC for the lateral boundary condition, i.e. NCEP reanalysis or the AOGCM driving the RCM at its boundaries. For example, CRCM simulation driven by CGCM3 will be referred to as CRCM_CGCM3. Though the simulation domains of the RCMs cover most of North America, as noted above, this study focuses only on Alberta, Saskatchewan and Manitoba provinces of Canada.

Table 3.1: The NARCCAP simulations used in the study.

RCM	Driving AOGCM				Acronym for each model
	GFDL	CGCM3	HADCM3	CCSM	
CRCM	--	√	--	√	CRCM_CGCM3; CRCM_CCSM
ECP2	√	--	--	--	ECP2_GFDL
HRM3	√	--	√	--	HRM3_GFDL; HRM3_HADCM3
MM5I	--	--	√	√	MM5I_HADCM3; MM5I_CCSM
RCM3	√	√	--	--	RCM3_GFDL; RCM3_CGCM3
WRFG	--	√	--	√	WRFG_CGCM3; WRFG_CCSM
Details of RCMs and AOGCMS					
CRCM	Canadian Regional Climate Model (Caya and Laprise, 1999)				
ECP2	Experimental Climate Prediction (Juang et al., 1997)				
HRM3	Hadley Regional Model 3 (Jones et al., 2003)				
MM5I	NCAR mesoscale model (Grell et al., 1993)				
RCM3	Regional Climate Model version 3 (Pal et al., 2007)				
WRFG	Weather Research and Forecasting Grell Model (Grell and Devenyi, 2002)				
GFDL	Geophysical Fluid Dynamics Laboratory (GFDL GAMDT, 2004)				
CGCM3	Third General Coupled Global Climate Model (Flato, 2005)				
HADCM3	Hadley Centre Coupled Model version 3 (Gordon et al., 2000)				
CCSM	Community climate System Model (Collins et al., 2006)				

3.2.3 Reference grid

All RCMs have roughly the same horizontal resolution (i.e. 50-km) but different projections on the spherical earth. Therefore, a common reference grid (i.e. half-degree University of Delaware grid; Figure 3.1) was considered in order to ease inter-comparison of

results. All model outputs were interpolated to this reference grid using spline interpolation, while observed gridded data were aggregated to this reference grid before doing any analysis. This reference grid has been used in some previous studies wherein NARCCAP RCM simulations were used (e.g. Mearns et al., 2012).

3.3 Methodology

This section provides information on the framework used for deriving future changes to drought characteristics based on the NARCCAP multi-RCM simulations. It is important to note that most of the analyses were targeted at the level of individual grid cells which then feed into regional level analyses for the entire study area. Thus, first the procedures for deriving drought events are described, followed by identification of homogeneous regions of the study area and univariate and multivariate frameworks for frequency analysis of drought characteristics.

3.3.1 Drought indices, drought events and their characteristics

Various drought indices are available to detect and monitor droughts. However, the choice of indices depends mainly on the desired objectives of the study, available data, ease of computation, and interpretation of the results obtained. In this study, two different drought indices namely the SPI, which is solely based on precipitation, and SPEI, which is based on the difference between precipitation and potential evapotranspiration, were used to define drought events. According to Guttman (1998), the SPI, which is also recommended by WMO (2009), gives a better representation of drought-like conditions than the Palmer Drought Severity Index because it is the precipitation deficit that ultimately leads to hydrological and agricultural droughts. The SPEI has great potential to represent drought-like conditions as it considers a broader measure of the climatic water balance in the context of global warming compared to SPI (Potop et al., 2012; Jeong et al., 2014; Stagge et al., 2015). Both indices can be calculated for various time scales, e.g. 1-, 3-, 6-, 12-, 24-month etc., depending upon the nature of application. Based on the results reported in a related previous study (Masud et al., 2015), SPI and SPEI values corresponding to the 6-month time scale were used in this study. SPI of 6-month time scale uses 6-month cumulative precipitation P obtained from monthly total precipitation amounts. The calculation procedures of both SPI and SPEI are the same except the input variable. SPEI is calculated using the difference between precipitation and potential evapotranspiration (PET) (hereafter this difference is represented by E). Both simple and

complex methods exist for calculating *PET*, however, the use of any method to calculate *PET* does not affect drought analysis much as noted by Mavromatis (2007). In this study, Hargreaves method (Hargreaves and Samani, 1985), which simply uses the maximum and minimum temperature for estimating *PET*, was used. This method was ranked at the top among the temperature-based methods in the American Society of Civil Engineers Manual 70 analysis (Jensen et al., 1990). Wang et al. (2012) evaluated five temperature based approaches (i.e. Thornthwaite, Hargreaves, Linacre, Hamon and a vapor deficit method) to calculate monthly *PET* for Western North America and found Hargreaves method the best. Also, this method was recommended for estimating *PET* for the Canadian Prairies region in the inter-comparison study of Maulé et al. (2006) and is an integral part of the distributed WATFLOOD hydrological model which is commonly used for simulating streamflow in a wide variety of watersheds across Canada (Kouwen, 2014). It is also important to note that Hargreaves and Samani (1982) and Mohan (1991) found that the Hargreaves method consistently produces accurate estimates of *PET* as compared to using the energy balance techniques, the Penman combination equation and the lysimetric methods.

Following a detailed comparative investigation based on the Kolmogorov-Smirnov (KS) and Z goodness-of-fit tests, the five parameter Wakeby distribution (Hosking and Wallis, 1997; Masud et al., 2015) was selected to model *P* and *E* samples. The Wakeby distribution can mimic the shapes of many other commonly used skew distributions (e.g., Generalized Extreme Value (GEV), Generalized Normal (GNO), Pearson Type-III (PE3), Generalized Logistic (GLO), Generalized Pareto (GPA) etc.; Hosking and Wallis, 1997) and therefore, has the potential to adapt to whichever distribution is suitable for a certain region/area/station. After estimating the distribution function of *P* and *E* samples corresponding to six month time scale, cumulative probabilities of *P* and *E* values were calculated. The SPI (SPEI) time series were produced by mapping the cumulative probabilities of *P* (*E*) series onto the standard normal distribution function for each case considered (i.e. observed and RCM_LBC simulations). It is important to note that for calculating SPI and SPEI series for future climate, the cumulative probabilities of the future precipitation series were calculated from the fitted distribution functions for the current climate at the same grid cell of the same RCM_AOGCM simulation. To minimize the effect of minor droughts, drought events were identified considering a threshold of -0.50 for both SPI and SPEI, i.e., a drought event occurs when the value of SPI/SPEI is smaller than this

threshold. Three important drought characteristics, i.e. duration (i.e. continuous sequence of SPI/SPEI values that satisfy the above threshold criterion), severity (i.e. cumulative sum of all SPI/SPEI values over the duration) and maximum severity (i.e. the largest drought severity within a drought event), were extracted for each drought event. Additional details of this procedure can be found in Masud et al. (2015).

3.3.2 Delineation of homogeneous geographic regions

The study area has been shown to be heterogeneous due to variations in climatic patterns and topographic features (Armstrong et al., 2015) and therefore was divided into smaller statistical homogeneous regions using cluster analysis, which is one of the commonly used statistical multivariate analysis techniques. Individual grid characteristics, i.e. geographic location (latitude, longitude and elevation), average drought severity and duration and mean annual precipitation were used as input attributes. Using this technique, one combines a set of sites (i.e. grid locations in the present study) into groups with similar characteristics or features of interest (Hosking and Wallis, 1997; Rao and Srinivas, 2008). Herein, hierarchical clustering (Kaufman and Rousseeuw, 1990) was used for the entire study area. This technique cannot always provide exact formation of groups and therefore some subjective adjustments were applied in order to arrive at meaningful contiguous geographic regions (Hosking and Wallis, 1997; Masud et al., 2015). Once such regions are delineated, their statistical homogeneity is required to be tested. For this purpose, Hosking and Wallis (1997) proposed an L-moments-based univariate test. According to this test, statistics of only one drought characteristic (e.g. either drought severity or drought duration) can be considered. The regions found homogeneous on the basis of the univariate test may not always be homogeneous within the space of multiple drought characteristics. This problem is resolved by using multivariate L-moments-based multivariate homogeneity tests of Chebana and Ouarda (2007) (see Appendix A.2). Multivariate L-moments were developed by Serfling and Xiao (2007) (see Appendix A.1). Thus, both univariate and multivariate tests were used for testing homogeneity of a region.

3.3.3 Regional characteristics of drought severity and duration

After verifying statistical homogeneity of all delineated regions based on uni- and multivariate approaches discussed above, the next step was to select an appropriate regional distribution for each homogeneous region from some suitable candidate distributions in order to develop regional growth curves. A regional growth curve represents a dimensionless relationship

between frequency and magnitude of the selected drought characteristic. The distributions considered in this study included GEV, GLO, GPA, PE3, GNO, and Wakeby, which are commonly used for frequency analysis of hydro-climatic extremes. The Z test of Hosking and Wallis (1997) and KS test were used to pick the most appropriate regional distribution. Based on these criteria, multiple candidates (i.e. PE3, GPA and Wakeby) were found suitable for most of the regions. It is important to mention that the distribution of annual or seasonal maxima of the variable of interest asymptotically converges to the GEV distribution and that of the thresholded samples to the GPA distribution (Coles, 2001). Based on this theoretical reasoning and the empirical support from the Z and KS tests, the GPA distribution was selected for modeling regional growth curves of selected characteristics of observed drought events. The same distribution was used to model growth curves of RCM_NCEP and RCM_AOGCM current and future period simulated characteristics of drought events however, with parameters re-estimated for each case considered.

Observed regional 20- and 50-yr return levels of drought characteristics for each homogeneous region were computed by multiplying regional growth factors, derived from respective regional growth curves with the respective regionally-averaged grid-cell based mean values of drought characteristics. When deriving growth factors, the impact of rate of annual exceedances was taken into account using regionally-averaged grid-cell based values of rate of exceedances (i.e. the number of extreme values per year). Exactly, the same procedure was used for RCM_AOGCM current and future period simulations.

3.3.4 Copula-based bi- and trivariate analyses

The copula is a multivariate distribution function with all the univariate marginal distributions being uniform on the interval [0,1]. Based on Sklar's (1959) theorem, the joint cumulative distribution function of two or more correlated variables can be expressed as:

$$H(x_1, x_2, \dots, x_n) = C[F_1(x_1), F_2(x_2), \dots, F_n(x_n)] \quad (3.1)$$

where x_1, x_2, \dots, x_n are random variables with marginal distributions, $F_1(x_1), F_2(x_2), \dots, F_n(x_n)$, and C is the copula function. The n -dimensional Archimedean copula (Nelsen, 2006) can be expressed as:

$$C^n(u) = \varphi^{[-1]}(\varphi(u_1) + \varphi(u_2) + \dots + \varphi(u_n)) \quad (3.2)$$

where the superscript on C denotes dimension; $u_i = F_i(X_i)$ is the marginal cumulative distribution function (cdf) of variable X_i ($i = 1, 2, 3, \dots, n$); $\varphi(\cdot)$ = copula generator which needs

to be completely monotonic and φ^{-1} is the pseudo inverse of $\varphi(\cdot)$. A symmetric copula is enough to describe the dependency between two variables, but it is restrictive to describe the dependence when there are more than two variables as the correlation between any pair of variables is identical. For many hydro-climatic variables, this assumption is difficult to satisfy. To overcome this issue, a fully nested Archimedean copula is constructed by nesting symmetric copulas (Embrechets et al., 2003; Savu and Trede, 2010; Wong et al., 2010), expressed as:

$$\begin{aligned} C(u_1, \dots, u_n) &= C_1\{u_n, C_2[u_{n-1}, \dots, C_{n-1}(u_2, u_1) \dots]\} \\ &= \varphi_1^{-1}\left[\varphi_1(u_n) + \varphi_1\left(\varphi_2^{-1}\left(\varphi_2\{u_{n-1} + \dots + \varphi_{n-1}^{-1}[\varphi_{n-1}(u_2) + \varphi_{n-1}(u_1)] \dots\}\right)\right)\right] \end{aligned} \quad (3.3)$$

For the trivariate case, equation (3) can be expressed as:

$$\begin{aligned} C(u_1, u_2, u_3) &= C_1[C_2(u_1, u_2), u_3] \\ &= \varphi_1^{-1}\left(\varphi_1\left\{\varphi_2^{-1}\left[\varphi_2(u_1) + \varphi_2(u_2)\right] + \varphi_1(u_3)\right\}\right) \end{aligned} \quad (3.4)$$

where C_1 and C_2 are two bivariate one-parameter copulas; C_2 is the copula describing the dependence between variables u_1 and u_2 and the outer copula C_1 is a function of the inner copula and u_3 . In order to apply the trivariate Archimedean copula, the rank correlation coefficients between the inner pair (u_1, u_2) is required to be higher than the correlation between the other pairs (u_1, u_3) and (u_2, u_3) .

The Gumbel-Hougaard (GH) copula is a common choice for many hydro-climatic applications, because it includes multivariate extreme distributions which exhibit tail dependence and has been found to provide reasonable fit to field data (Serinaldi and Grimaldi, 2007; Wong et al., 2010). Nelsen (2006) stated that the GH copula is the only Archimedean extreme value copula. The GH copula with two- and three-variable versions is given by:

$$C(u_1, u_2) = \exp\left\{-\left[(-\ln u_1)^\theta + (-\ln u_2)^\theta\right]^{1/\theta}\right\}, \text{ and} \quad (3.5)$$

$$\begin{aligned} C_1[C_2(u_1, u_2), u_3] &= \exp\left\{-\left(\left[(-\ln u_1)^{\theta_2} + (-\ln u_2)^{\theta_2}\right]^{\theta_1/\theta_2} + (-\ln u_3)^{\theta_1}\right)^{\frac{1}{\theta_1}}\right\} \\ &\theta_1 < \theta_2, \theta \in (1, \infty) \end{aligned} \quad (3.6)$$

To evaluate the fitted copula, goodness-of-fit tests are often used. Genest and Favre (2007) described several goodness-of-fit tests including graphical diagnostics and formal tests. One of the simplest ways to evaluate the copula is to compare the observed data with the copula density. Another possible way proposed by Genest et al. (2009), which has been used in some studies on

floods and droughts, is to compare the theoretical and empirical copula (C_n) calculated from pseudo-observations U_1, \dots, U_n (e.g. Ganguli and Reddy, 2013a, b):

$$C_n(u) = \frac{1}{n} \sum_{i=1}^n I(U_{i,1} \leq u_1, \dots, U_{i,d} \leq u_d), \quad u = (u_1, \dots, u_d) \in [0,1]^d \quad (3.7)$$

For bi- and trivariate analyses the empirical copula can be expressed as:

$$C_n(u, v) = \frac{1}{n} \sum_{i=1}^n I(U_{i,n} \leq u, V_{i,n} \leq v) \quad (3.8)$$

$$C_n(u, v, w) = \frac{1}{n} \sum_{i=1}^n I(U_{i,n} \leq u, V_{i,n} \leq v, W_{i,n} \leq w), \quad (u, v, w) \in [0,1] \quad (3.9)$$

where $(U_{i,n}, V_{i,n}, W_{i,n})$ are pseudo-observations computed from the collected observational data $(X_1, Y_1, W_1), \dots, (X_n, Y_n, W_n)$ and $U_{i,n} = \frac{1}{n+1} \sum_{j=1}^n 1(X_j \leq X_i)$, $V_{i,n} = \frac{1}{n+1} \sum_{j=1}^n 1(Y_j \leq Y_i)$, $W_{i,n} = \frac{1}{n+1} \sum_{j=1}^n 1(W_j \leq W_i)$, $i \in \{1, \dots, n\}$. The last procedure was used in this study.

3.3.5 Estimation of drought risks

In this study, first the joint occurrence probabilities of drought severity S and duration D were considered, i.e. drought severity and duration both exceed a certain threshold value at the same time (i.e. $S > s$ and $D > d$). Corresponding relationships of the joint occurrence probabilities are given below:

$$\begin{aligned} P_1 &= P(S > s \text{ and } D > d) = P(S > s \cap D > d) = 1 - F_S(s) - F_D(d) + F(s, d) \\ &= 1 - F_S(s) - F_D(d) + C\{F_S(s), F_D(d)\} \end{aligned} \quad (3.10)$$

Similar relationships can be developed for “duration and max severity” and “severity and maximum severity” pairs. All three types of joint bivariate occurrence probabilities were evaluated in order to identify drought sensitive regions.

Similarly, trivariate joint occurrence probabilities of drought severity, duration and maximum severity were also evaluated, i.e. drought severity and duration and maximum severity exceeding respective specific thresholds at the same time (i.e. $S > s$ and $D > d$ and $S_{\max} > s_{\max}$). Here, s , d and s_{\max} denote the severity, duration and maximum severity values corresponding to selected 20-, and 50-yr return periods. The joint occurrence probability is given by:

$$\begin{aligned} P_2 &= P(S > s \text{ and } D > d \text{ and } S_{\max} > s_{\max}) = P(S > s \cap D > d \cap S_{\max} > s_{\max}) \\ &= 1 - F_S(s) - F_D(d) - F_{S_{\max}}(s_{\max}) + F(s, d) + F(s, s_{\max}) + F(d, s_{\max}) \\ &\quad - F(s, d, s_{\max}) \\ &= 1 - F_S(s) - F_D(d) - F_{S_{\max}}(s_{\max}) + C\{F_S(s), F_D(d)\} + C\{F_S(s), F_{S_{\max}}(s_{\max})\} \\ &\quad + C\{F_D(d), F_{S_{\max}}(s_{\max})\} - C\{F_S(s), F_D(d), F_{S_{\max}}(s_{\max})\} \end{aligned} \quad (3.11)$$

Based on the results of the KS test and theoretical reasons behind thresholded samples (Coles, 2001), the GPA distribution was selected to model drought severity, drought duration, and maximum severity. The same distribution was also used in the work of Masud et al. (2015), where historical droughts were investigated for the Saskatchewan River basin, which is the largest river basin of the current study area and serves many needs of Alberta, Saskatchewan and Manitoba.

3.4 Results and discussion

In this section, identification of statistical homogeneous regions is presented first, followed by other important analyses including validation and boundary forcing analysis of RCMs, projected changes to drought characteristics, and identification of drought sensitive regions. Analysis of drought severity and duration provide similar results and therefore detailed results are presented for drought severity and only selected results for drought duration. For the validation of RCM simulated drought characteristics, we concentrate mostly on the behavior of ensemble-averaged values and less on individual model performance due to space limitations. However, for the analysis of future droughts, detailed analyses are presented and discussed.

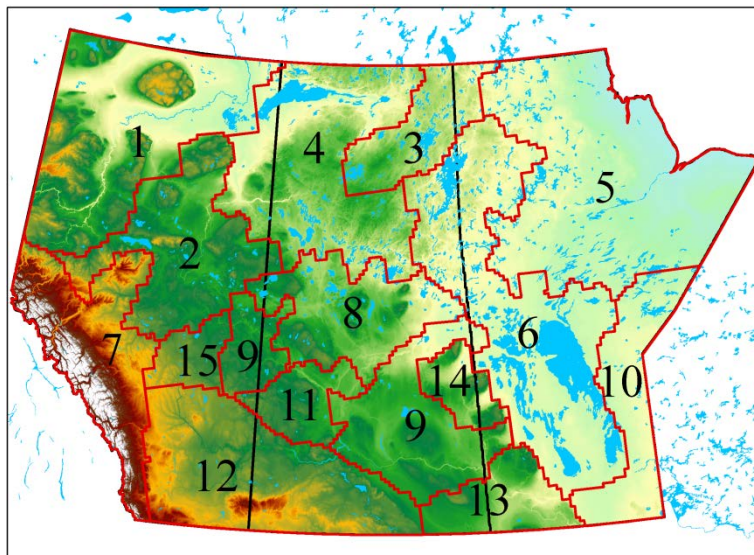


Figure 3.2: Fifteen homogeneous regions (Region 1 to 15) delineated on the basis of hierarchical clustering and verified using the uni- and multivariate homogeneity analysis approaches.

3.4.1 Geographic homogeneous regions

Based on similarity of drought characteristics, the study area is divided into 15 geographic regions/partitions using hierarchical clustering (Figure 3.2). Statistical homogeneity of these regions is verified first using the univariate L-moment ratio-based regional homogeneity testing procedure of Hosking and Wallis (1997) for drought severity and duration separately and then using the bivariate homogeneity approach of Chebana and Ouarda (2007). The results of univariate analysis for drought severity suggest that most of the regions could be considered homogeneous or acceptably homogeneous, except Region 1 and 15. A few regions are found non-homogeneous (i.e. Region 2, 4, and 13) for drought duration.

However, based on the results of the bivariate homogeneity test of drought severity and duration together, all regions are found homogeneous. Furthermore, in addition to the drought characteristics derived from observed gridded data, homogeneity of all 15 regions is also tested using drought characteristics derived from station-based adjusted and rehabilitated data available from 120 stations for the 1961-2003 period. Results from this validation also reveal that all regions could be considered homogeneous based on drought severity. Similar results are noted for drought duration for most of the regions, except two (Region 1 and 2), which are found to be within an acceptably homogeneous category. On the basis of this station-based dataset, results of bivariate homogeneity testing also suggest that all regions could be considered homogeneous.

In addition to the above presented validations, homogeneity of the identified regions is tested using drought characteristics derived from observed 50-km resolution gridded data and NCEP-driven RCM simulated data. For these cases, similar results are found as noted above. Validation of homogeneous regions using drought characteristics derived from multiple datasets provides a sound basis to develop additional analyses based on these regions.

3.4.2 Validation of RCM-simulated drought characteristics and lateral boundary forcing errors

First, spatial patterns of observed values of mean drought severity, shown in Figure 3.3(a), are discussed before validation of RCMs. From this figure, it can be noticed that three southern regions (i.e. Region 11, 12 and 15) and three northwestern regions (i.e. Region 1, 2 and 4) are associated with larger values of drought severity compared to the other regions – meaning that these regions appear to be relatively more drought prone. RCM-simulated ensemble-averaged mean drought severity is shown in Figure 3.3(b) and the relative differences from the

corresponding observed values in Figure 3.3(c). In general, ensemble-averaged drought severity for both SPI and SPEI cases differ from that obtained from observed data for various regions. RCMs tend to produce relatively more severe droughts for central and eastern regions. Typical differences lie within the -20 to 50% range. Similar spatial patterns are found for mean values of drought duration for various regions (Figure 3.3(d, e)), however, with differences lying typically within the $\pm 10\%$ range (Figure 3.3(c)).

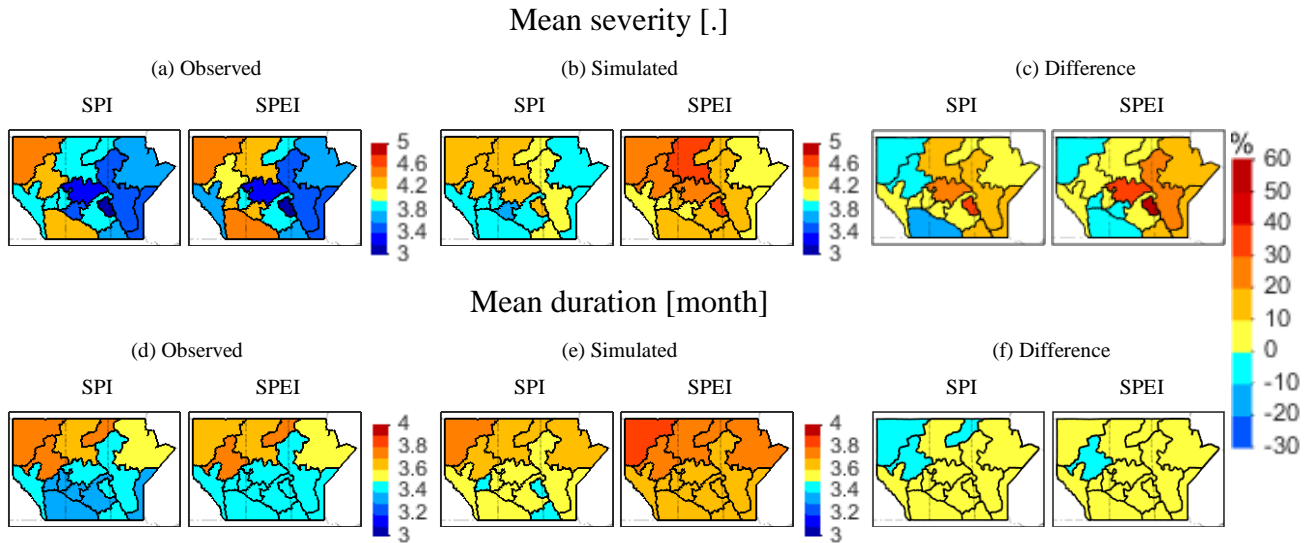


Figure 3.3: Comparison of observed and ensemble averaged RCM_NCEP simulated mean drought (a, b) severity and (d, e) duration for the 1981–2003 period. Relative differences between results shown in (b, a) and (e, d) panels are given in (c) and (f), respectively.

The spatial patterns of observed and NCEP-driven RCM simulated regional return levels of drought severity are shown in Figure 3.4. Figure 3.4(a) shows that the spatial patterns of observed return levels are very similar to those of mean severity shown in Figure 3.3(a). Overall, smaller return levels are found for many eastern and a few south-western regions (e.g. Region 7). The performance errors of all RCMs is assessed by comparing regional return levels of drought severity derived from NCEP-driven RCM simulations to those derived from observed gridded data. Ensemble-averaged regional return levels of drought severity are shown in Figure 3.4(b) and their relative differences from the corresponding observed values in Figure 3.4(c). Like mean severity, ensemble-averaged return levels for both SPI and SPEI cases differ from those obtained from observed data for various regions. In general, RCMs tend to produce more severe

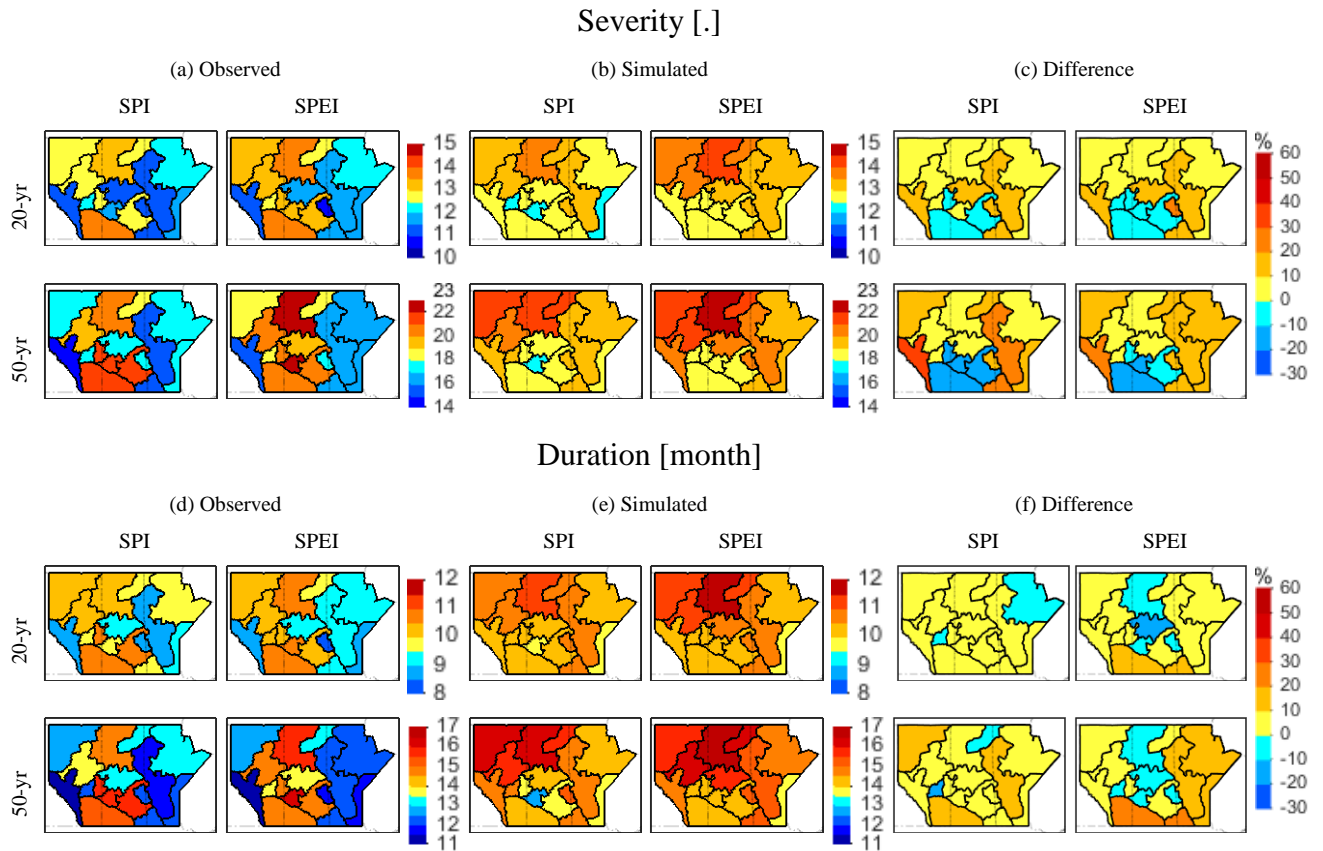


Figure 3.4: Comparison of observed and ensemble averaged RCM_NCEP simulated 20- and 50-year regional return levels of drought (a, b) severity and (d, e) duration for the 1981-2003 period. Relative differences between return levels shown in (b, a) and (e, d) are given in (c) and (f), respectively.

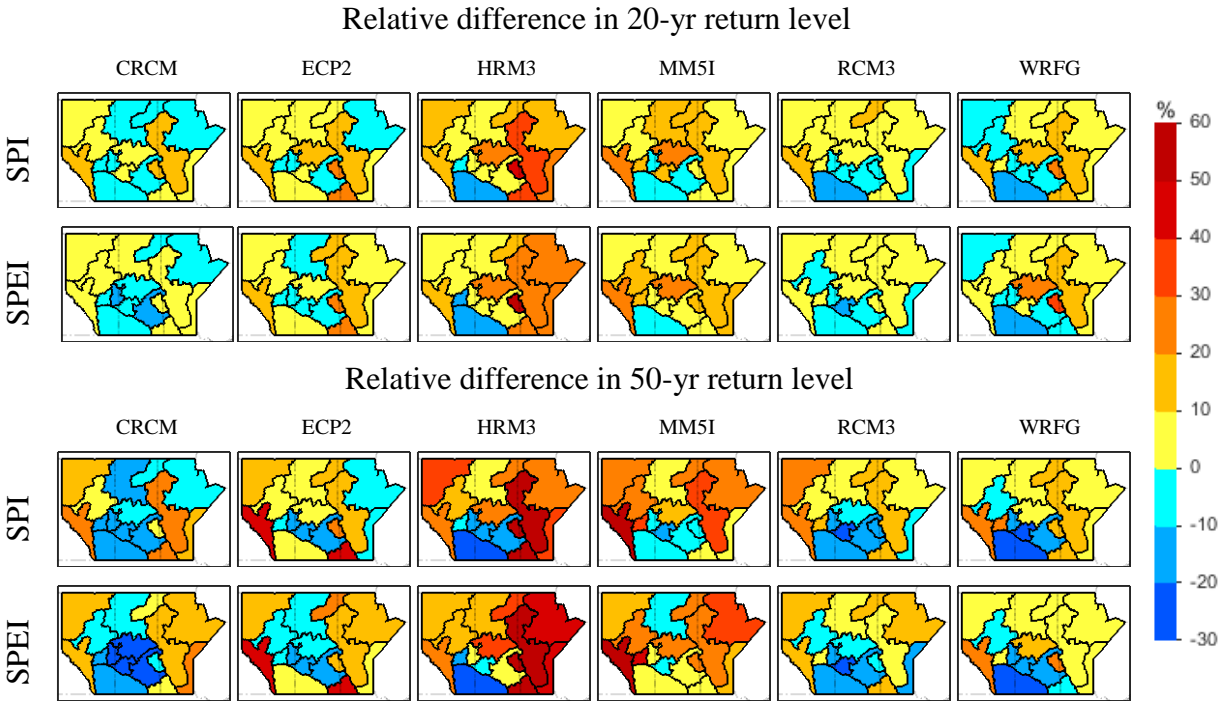


Figure 3.5: Relative difference (in %) between observed and RCM_NCEP simulated 20- and 50-yr regional return levels of drought severity for the 1981–2003 period.

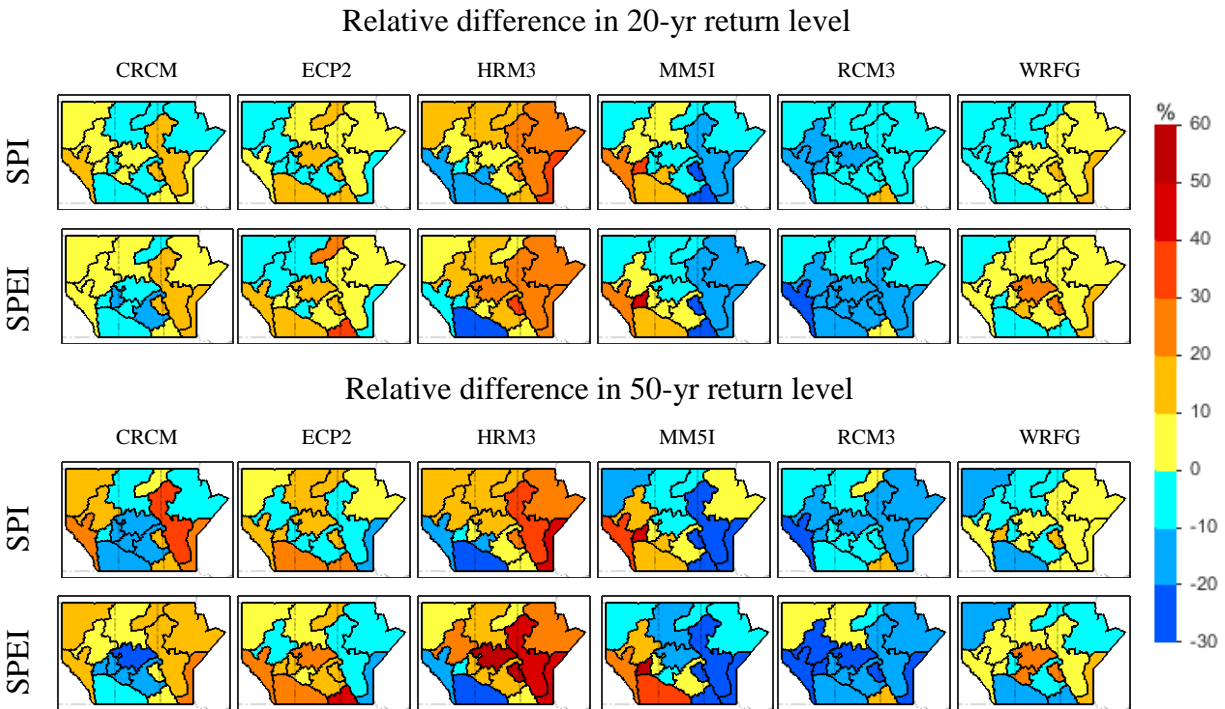


Figure 3.6: Relative difference (in %) between observed and RCM_NCEP simulated 20- and 50-yr regional return levels of drought duration for the 1981–2003 period.

droughts for many northern and eastern regions. Typical differences lie within -10 to 20% range. Overall, relative differences (i.e. performance errors) are larger for the 50-yr return level compared to the 20-yr return level. For return levels of drought duration, results are similar to those of severity except that the magnitude of over-/underestimation is relatively smaller. Now we turn to the performance of individual models. Figure 3.5 shows relative differences between 20- and 50-yr regional return levels of drought severity derived from NCEP-driven RCM simulations and observed data (Figure 3.4(a)) for each of the six RCMs separately. For the 20-yr return levels, the relative differences lie between $\pm 10\%$ for most of the regions and RCMs except HRM3 which overestimates (up to 60%) for some eastern regions. The results for the 50-yr return levels are similar to those for the 20-yr return levels, but with a wider range of relative differences (-30 to 60%). For western regions (Region 1 and 7), all six RCMs overestimate 50-yr return levels. For eastern regions (i.e. Region 5, 6 and 10), four of the six RCMs (i.e. HRM3, MM5I, RCM3 and WRF3) overestimate 50-yr return levels, while the other two (i.e. CRCM and ECP2) exhibit a mixed behavior. Like the 20-yr return level, HRM3 overestimates 50-yr return level by up to 60% for many regions. In general, ensemble-averaged positive or negative relative differences shown in Figure 3.4(c) are smaller than those noted for individual RCMs and lie within a smaller range (i.e. -20 to 40%) for the majority of the regions. The relative differences between 20- and 50-yr regional return levels of drought duration derived from NCEP-driven RCM simulations and observed data (given in Figure 3.4(d)) are shown in Figure 3.6 separately for each of the six RCMs. Here, the spatial patterns are very close to the pattern of return levels of drought severity. The physical reasons for this over- or underestimation by an individual RCM outcome may depend on model formulation and parameterization schemes of the respective RCM, which require in-depth separate analyses and therefore lie outside the scope of this article.

The impact of the driving fields (i.e. the lateral boundary forcing errors) is assessed by comparing NCEP- and AOGCM-driven simulations for the 1981-2000 period. A comparison of 20- and 50-yr return levels of SPI- and SPEI-based severity and duration is illustrated in Figure 3.7. Five out of six RCMs were driven by two different AOGCMs, while another one was driven by only one AOGCM, leading to the eleven sets of scatterplots for both SPI and SPEI cases, shown in Figure 3.7. It should be noted that for both severity and duration, the difference between AOGCM- and NCEP-driven RCM simulated 20-yr return levels are smaller than those for the 50-yr return levels. More specifically, for example, 50-yr return levels for AOGCM-

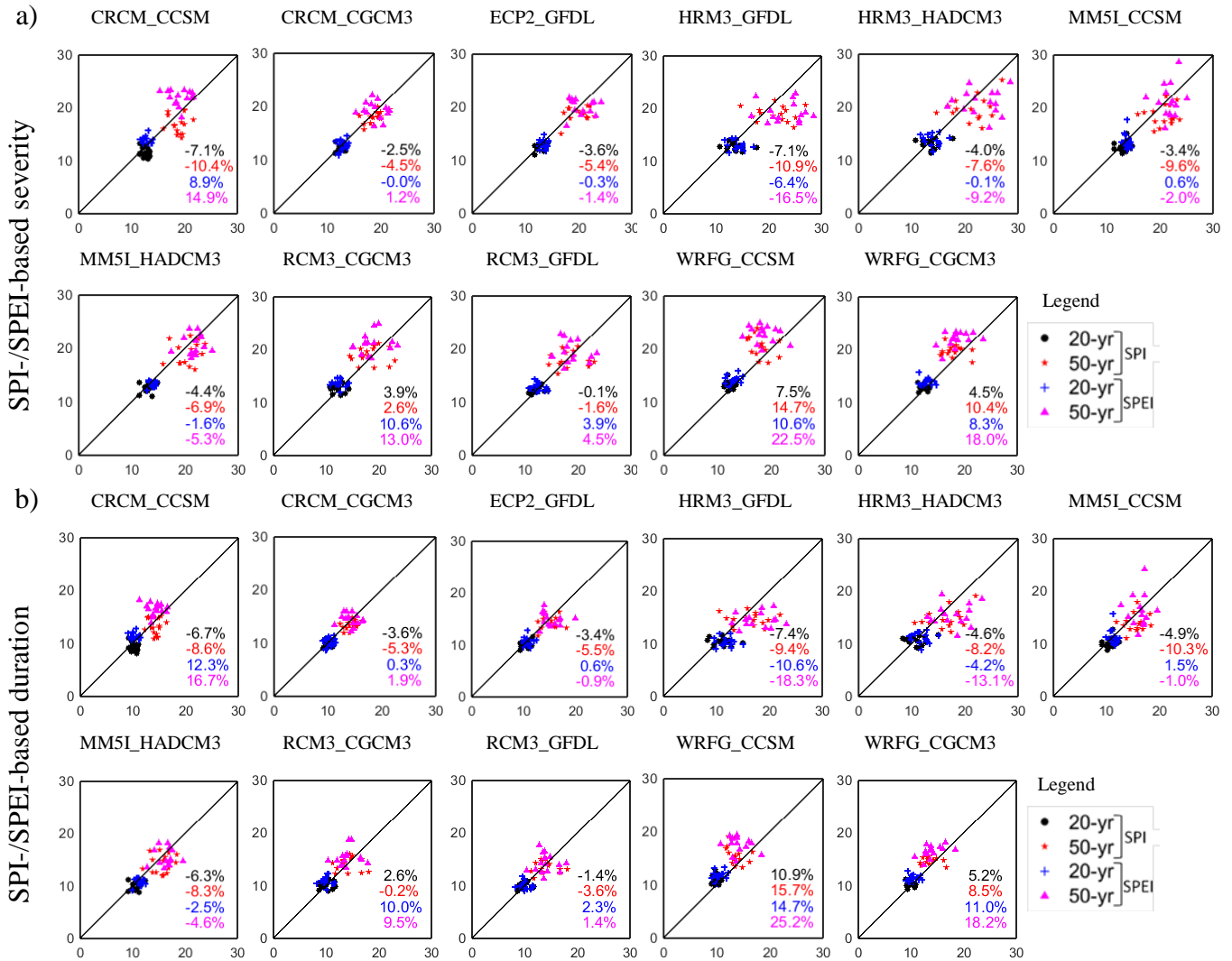


Figure 3.7: Scatterplots of 20- and 50-yr return levels of SPI- and SPEI-based (a) severity and (b) duration for the 1981-2000 period. The x-axis corresponds to NCEP driven RCM simulation, while the y-axis corresponds to AOGCM driven simulation. Numbers in each panel represent average percentage difference between the AOGCM- and NCEP-driven simulated return levels. Results based on SPI are shown in black and red color and those for the case of SPEI are shown in blue and pink color.

driven simulations are smaller than those for NCEP-driven simulations for HRM3, while for WRFG, return levels for AOGCM-driven simulations are larger than those of NCEP-driven simulations for the majority of the regions. For both HRM3 and WRFG, the lateral boundary forcing errors are slightly larger in the case of SPEI-based severity and duration than that of SPI-based severity and duration.

Overall, the average boundary forcing errors are less than 10% for the majority of the cases and larger differences are associated with longer return periods, in general. Comparison of RCM performance errors and boundary forcing errors show that performance errors are larger than the boundary forcing errors for most of the cases.

3.4.3 Projected changes to drought characteristics

Figure 3.8(a) provides projected changes to SPI and SPEI based mean severity for the 2041–2070 period relative to 1970–1999 for individual RCM_AOGCM pairs. These changes, projected by the majority of the RCM_AOGCM pairs (eight out of eleven), are mostly positive for southern parts of the study area. It can be noticed from the results of SPEI-based analysis that completely positive changes are projected by three out of eleven simulation pairs (CRCM_CCSM, HRM3_HADCM3 and MM5I_HADCM3) for all regions, while the rest of the simulation pairs project a decrease in drought severity specifically for regions located in the northern parts of the study area. Similar spatial patterns are found for mean drought duration (Figure 3.8(b)), but with changes of relatively smaller magnitude for most of the regions. Overall, SPEI based ensemble-averaged projected changes shown in Figure 3.8 indicate increases in both drought severity and duration in southern parts of the study area, with more pronounced changes in mean severity. The effect of temperature on defining drought characteristics is visible in SPEI-based results of all RCM_AOGCM pairs. The spatial patterns of mean annual precipitation suggest an increase in precipitation over the study area (see supplemental material in Appendix B). However, at the same time, mean annual *PET* has been projected to increase for most of the RCM_AOGCM combinations perhaps due to the projected increase in the mean annual temperature in the 1 to 3°C range. Thus, the projections of the underlying variables (i.e. *P*, *T* and *PET*) used for calculating drought indices generally support the changes noted in drought characteristics in the future over the study area. It is important to note that an analysis on the annual basis is just a simple way of uncovering the impact of underlying variables on changes to drought characteristics.

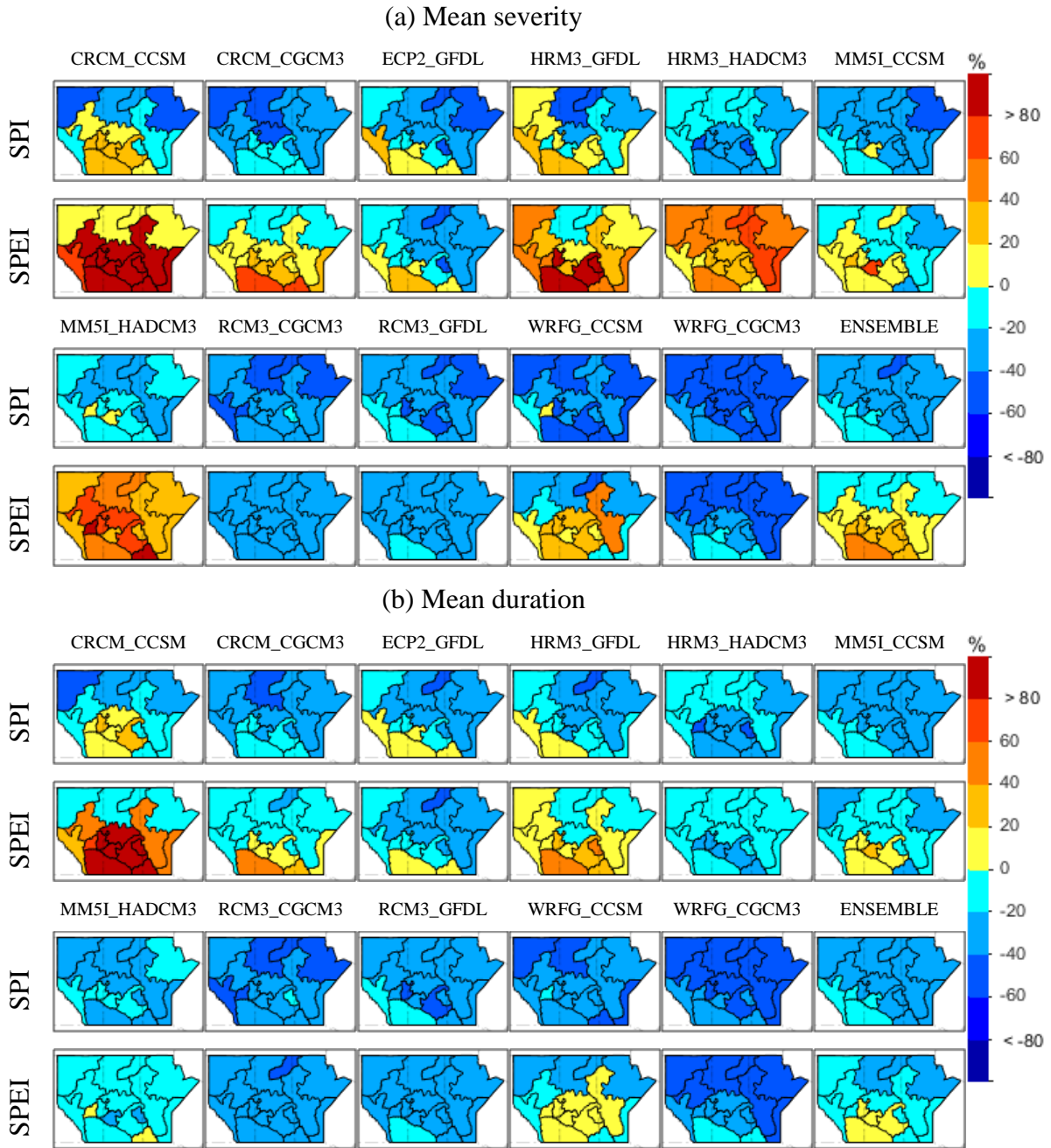


Figure 3.8: Projected changes (in %) to SPI and SPEI based (a) mean drought severity (b) mean drought duration for the 2041–2070 period with respect to the current 1970–1999 period.

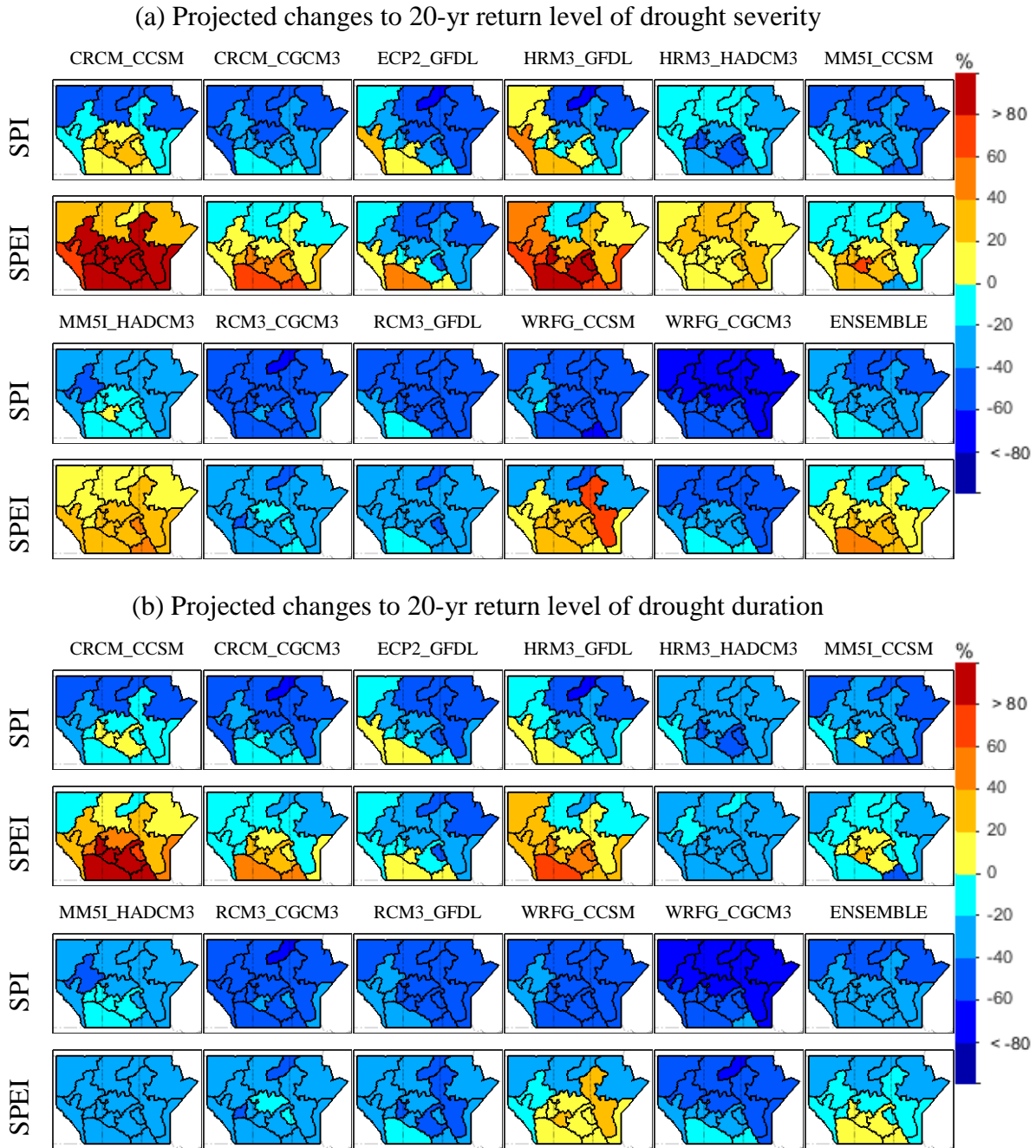


Figure 3.9: Projected changes (in %) to regional 20-year return levels of drought (a) severity and (b) duration for the 2041–2070 period with respect to the current 1970–1999 period. Projected changes to drought severity at the regional level are also studied by comparing 20- and 50-year return levels derived from AOGCM-driven RCM simulations for the future 2041–2070 period with those for the current 1970–1999 period.

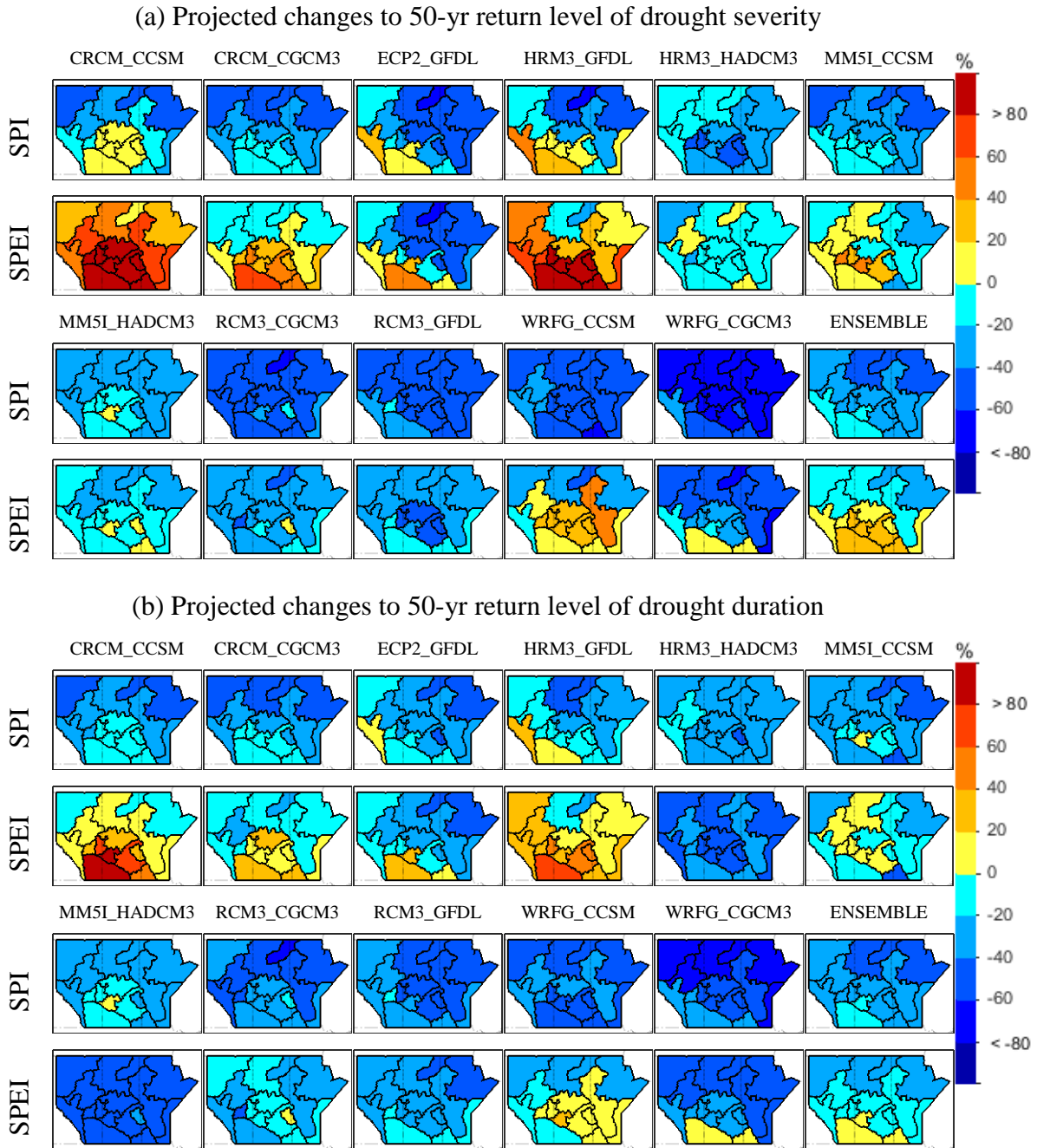


Figure 3.10: Projected changes (in %) to regional 50-year return levels of drought (a) severity and (b) duration for the 2041–2070 period with respect to the current 1970–1999 period.

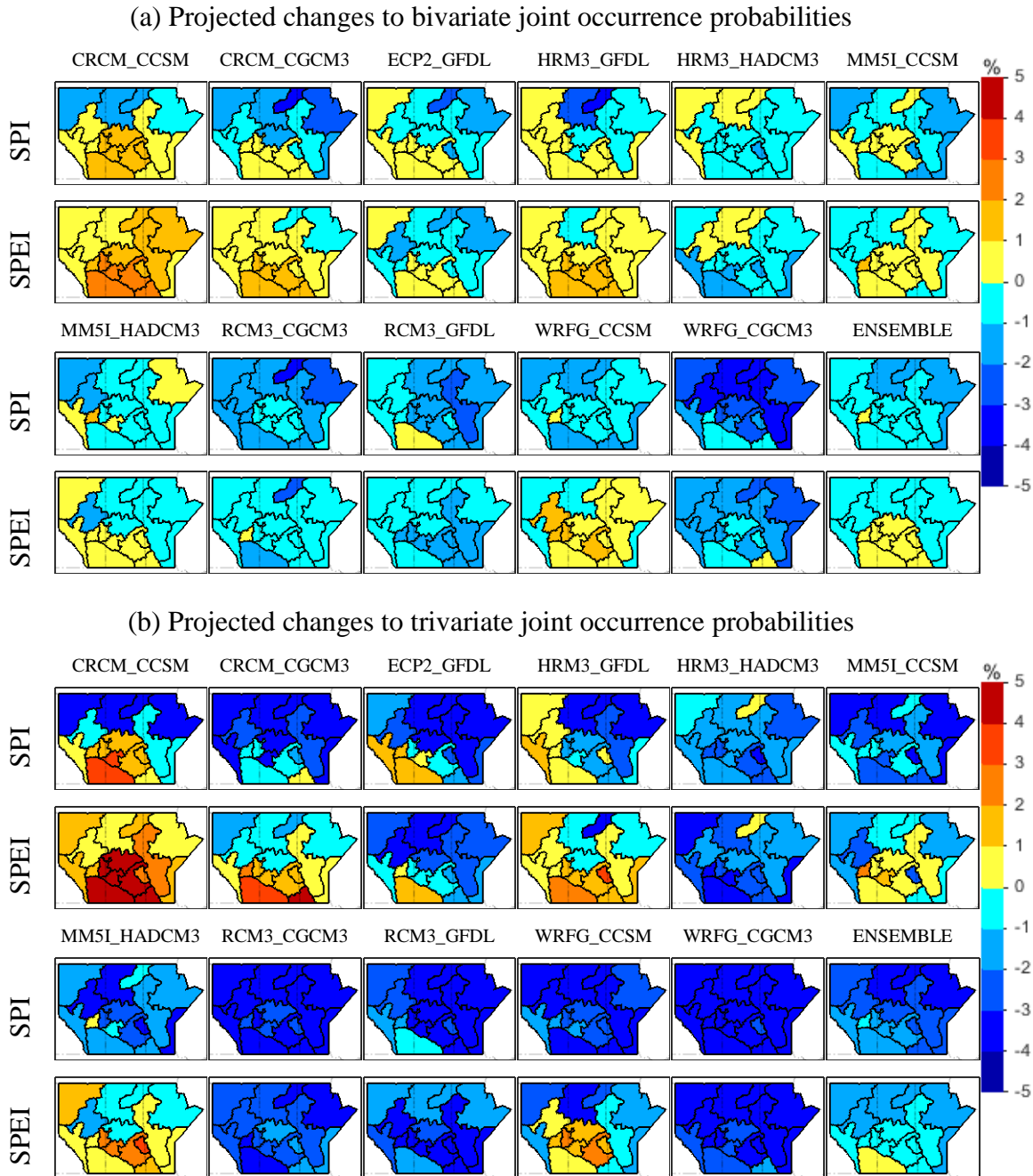


Figure 3.11: Changes (in %) to (a) bivariate joint occurrence probabilities corresponding to 20-year return period thresholds of S and D and (b) trivariate joint occurrence probabilities corresponding to 20-year return period thresholds of S , D and S_{\max} for the 2041–2070 period with respect to the current 1970–1999 period.

Figure 3.9 (a,b) shows percentage changes to 20-yr return levels of drought severity and duration at the regional scale. It is noteworthy to mention that the spatial patterns are somewhat similar to the spatial patterns found for drought severity and duration in Figure 3.8. For the case of 50-yr return levels, this behavior of AOGCM-driven RCM simulations stays about the same (see Figure 3.10). The magnitude of projected changes in 50-yr return levels is relatively smaller than that in the 20-yr return levels. Average projected change for all RCM_AOGCM pairs shows that the 20-yr return level will increase by up to 60% for drought severity and 40% for drought duration in southern regions, while 50-yr return level will increase by up to 40% for drought severity and 20% for drought duration in the same parts of the study area. A comparison of analyses shown in Figure 3.9 and 3.10 suggest considerable influence of the driving AOGCM on the magnitude and sign of the projected change. For example, results based on CRCM_CCSM suggest considerably larger increases compared to CRCM_CGCM3. Therefore, the use of multiple AOGCMs at the RCM boundaries is important for addressing uncertainties associated with the driving fields.

3.4.4 Drought vulnerable regions

As the drought characteristics are highly correlated, multivariate analysis using copulas seems important for evaluating drought risks across the study area. Therefore, two joint occurrence probabilities are considered in this study for the current and future periods: $P_1 = P(S > s \text{ and } D > d)$ and $P_2 = P(S > s \text{ and } D > d \text{ and } S_{\max} > s_{\max})$. The former probability represents the joint occurrence probability of “drought severity and duration” exceeding their respective thresholds at the same time, while the latter represents the joint occurrence probability of “drought severity, duration and maximum severity” exceeding their respective thresholds at the same time. The thresholds s , d and s_{\max} correspond to 20- and 50-year return levels obtained from univariate analyses. Figure 3.11 shows percentage changes in (a) bivariate and (b) trivariate probabilities for the case of 20-yr return period threshold.

A discernible spatial pattern of drought sensitive regions is visible in this figure, which is consistent with the findings discussed in the previous section that southern regions are more susceptible to droughts in the future compared to the northern regions. Based on bivariate analyses, seven out of eleven RCM_AOGCM pairs indicate that southern regions are associated with higher drought risks in the future. Similar analyses are also performed for other bivariate cases (i.e. severity and maximum severity; duration and maximum severity). Their results (not

shown) broadly suggest similar patterns. Southern regions emerge out even more susceptible to droughts when trivariate joint occurrence probabilities are considered, while northern regions become less susceptible (Figure 3.11(b)). Consequently, the impact of considering three instead of two drought characteristics for identifying drought sensitive regions is obvious.

Figure 3.12 shows percentage changes in (a) bivariate and (b) trivariate probabilities for the case of 50-yr return period thresholds. For this case, almost analogous spatial patterns of drought sensitive regions are found. It is interesting to note that, compared to other RCM_AOGCM pairs, only CRCM_CCSM produces highly positive changes in joint occurrence probabilities for both bi- and trivariate cases. Overall, ensemble-averaged projected changes for the case of 20-yr return period threshold show higher drought risks for southern parts of the study area (i.e. Region 8, 9, 11, 12, 13, and 14 for the bivariate case and Region 12 for the trivariate case). The pattern of drought sensitive regions for the 50-yr return period threshold case are almost identical to the 20-yr case, however, with few additional regions (Region 2, 6, 7 and 10 for the bivariate case and Region 11 for the trivariate case) are identified as vulnerable.

3.4.5 Drought analysis for the agricultural growing season

Finally to complete the analysis, we evaluate projected changes to drought characteristics specifically for the agricultural growing season (May-August) due to the fact that southern parts of the study area support a vibrant agro-based economy, which was impacted negatively due to historical droughts of 1890s, 1910s, 1930s, late 1950s, early 1960s, 1980s and 1999–2004. During the growing season, the study area receives the majority of the annual precipitation and observes higher seasonal temperatures and hence drought conditions have the greatest impacts on sectors related to water and agriculture. For this analysis, drought indices (SPI and SPEI) and drought characteristics are determined separately for the growing season. Projected changes to mean drought severity and duration are shown in Figure 3.13. In this figure, most of the SPEI based projections reveal drier conditions over most of the regions in future. These drier conditions are much stronger over the southern and southwestern regions. Similar results are projected by SPI based analysis, however, with much less severe droughts. The pattern of projected changes to drought duration follows that of drought severity. Furthermore, the projected changes in severity and duration are larger in the growing season than those for the 6-month time scale presented before. Also, the spatial extents of projected changes are larger for the growing season than that of the 6-month time scale.

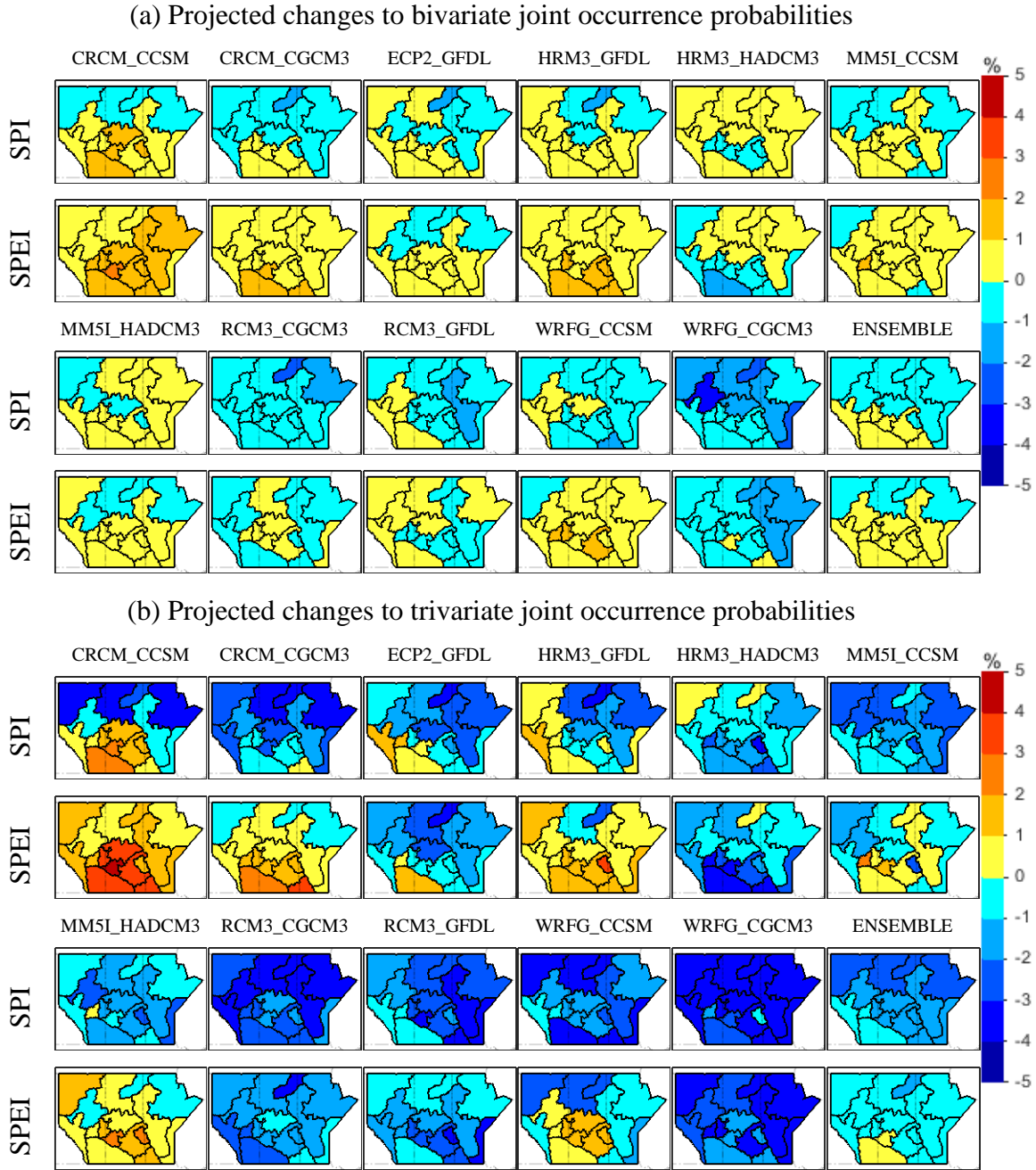


Figure 3.12: Changes (in %) to (a) bivariate joint occurrence probabilities corresponding to 50-year return period thresholds of S and D and (b) trivariate joint occurrence probabilities corresponding to 50-year return period thresholds of S , D and S_{\max} for the 2041–2070 period with respect to the current 1970–1999 period.

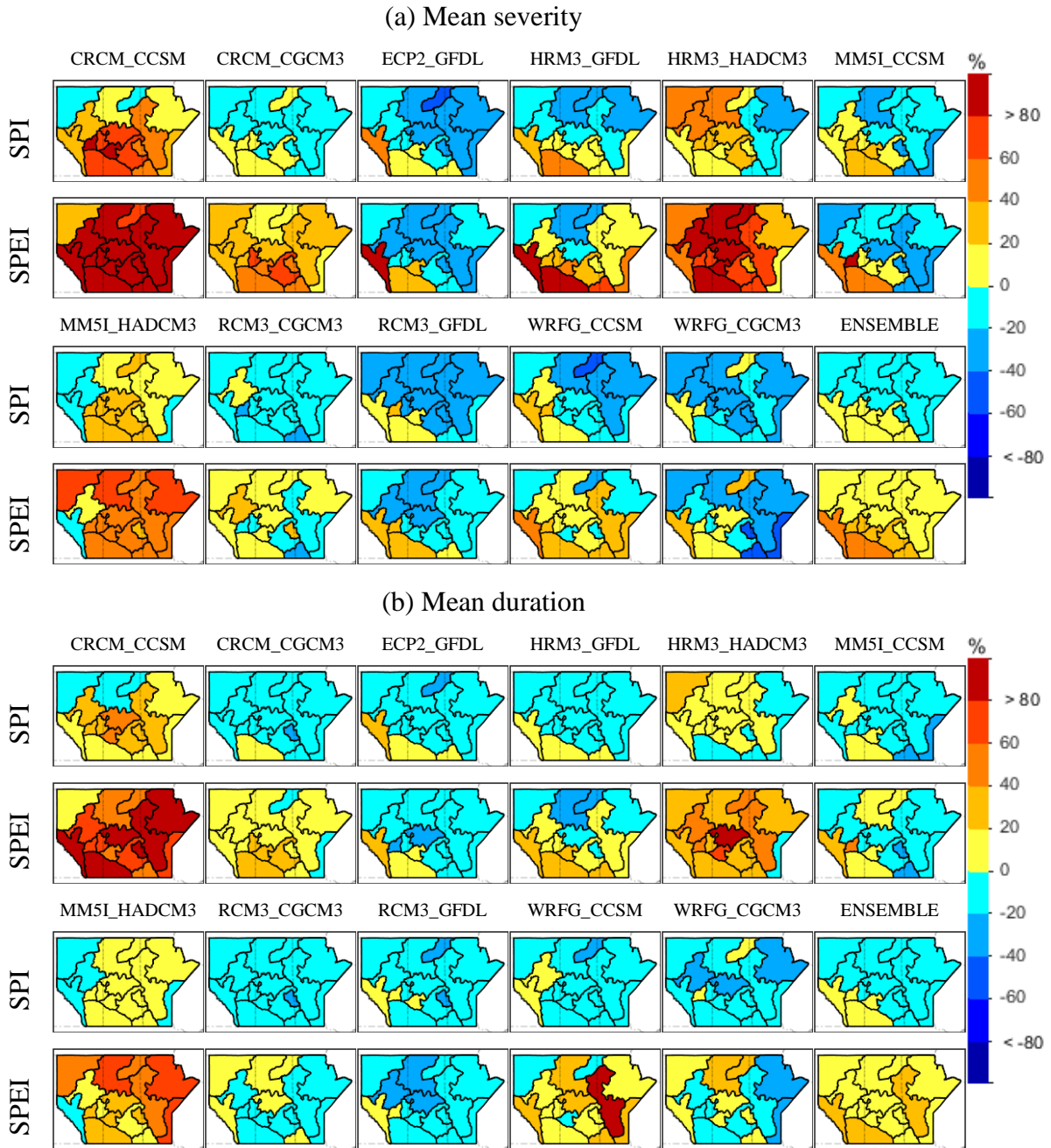


Figure 3.13: Projected changes (in %) to SPI- and SPEI-based (a) mean drought severity (b) mean drought duration for the 2041–2070 period with respect to the current 1970–1999 period for the agricultural growing season.

These results specifically for the southern Canadian Prairies region are in general consistent with the findings of Bonsal et al. (2012), who employed statistical downscaling of a few AOGCM outputs, and PaiMazumder et al. (2013), who employed a five member ensemble of a single RCM.

3.5 Conclusions

From various analyses presented and discussed in this paper, following main conclusions can be drawn:

(1) To facilitate drought risk analysis, the study area was divided into fifteen different geographic regions based on numerous trials of hierarchical clustering. Statistical homogeneity of these regions was verified based on uni- and bivariate homogeneity analysis tests. The bivariate homogeneity test suggests that all regions can be considered homogeneous compared to the univariate test, which identifies a few regions as possibly heterogeneous, particularly for the case of drought duration. Thus, the results of this study highlight the importance of considering simultaneously two highly correlated characteristics of droughts for identifying homogeneous regions. It is important to note that a homogeneous region helps to increase the effective length of data, which in turn increases the accuracy of the estimated return levels. In addition, regional analysis is useful in reducing the undesirable noise resulting from at-site analysis when identifying projected changes to variables of interest.

(2) For validating various RCMs, mean drought severity and duration values derived from NCEP-driven RCM simulations were compared with those from the observed data. This comparison indicates that RCMs tend to produce relatively more severe droughts for the central and eastern regions of the study area. The performance errors of RCMs were assessed by comparing selected regional return levels of drought severity and duration. Relative difference between 20- and 50-yr return levels derived from NCEP-driven RCM simulations and observed data suggest that the differences are highly model dependent which could be as high as 60%. However, by considering ensemble-averaged values, relative differences were found to be much smaller than for the individual models for the majority of the regions. The lateral boundary forcing errors were also assessed by comparing selected regional return levels of drought severity and duration derived from NCEP- and AOGCM-driven simulations. It was found that

the boundary forcing errors are much smaller than the performance errors for both SPI- and SPEI-based drought severity and duration.

(3) Most of the RCM_AOGCM simulations project an increase in drought characteristics for the southern parts of the study area, while some model combinations project completely positive changes for the entire study area. Comparison of analyses based on both SPI and SPEI reveal that the effect of temperature in drought characterization is important for future drought risk analysis and assessment for this region. Similar results are realized for the agricultural growing season, where the drought characteristics are projected to increase with relatively higher margins. Compared to the SPI based projections, SPEI based projections of most of the RCM_AOGCM simulations suggest drier conditions over many parts of the study area, in particular, the southern and south-western regions are found relatively more drought vulnerable. Therefore, considering potential effects from both precipitation and temperature changes is vital for assessing future drought risks.

(4) Most of the RCM_AOGCM simulations project an increase in return levels of drought severity and duration for southern regions, with some differences noted between models and between different return periods considered. More regions emerge with positive changes in drought characteristics, with higher magnitude of change in return levels corresponding to lower return period (i.e. 20-year) than higher return period (e.g. 50-year) values. On average, positive changes of up to 60% are noted for regions located in the southern and south-western parts of the study area.

(5) Projected changes in joint occurrence probabilities of droughts for bi- and trivariate cases are spatially mapped over the study area in order to identify drought vulnerable regions. Overall, central and southern regions (i.e. Region 8, 9, 11, 12, 13 and 14 for the bivariate case and Region 12 for the trivariate case) are found highly drought vulnerable compared to the northern regions, which are associated with less frequent droughts in the future. Multivariate joint occurrence probabilities from the multivariate drought distribution can describe drought events perhaps closer to the reality and therefore can reveal their properties more objectively and comprehensively. This type of information could serve as a reference for regional drought defense and agricultural resources management purposes.

Finally, results from different models show remarkable influence of the driving AOGCM on the magnitude and sign of the projected change. Perhaps, a single regional climate model

cannot describe fully the complex natural climate system, no matter how complex the model itself is. Therefore, combined information from several models can be superior to a single-model output. Besides, according to Tebaldi and Knutti (2007), combining models generally increase the skill, reliability and consistency of model projections. Therefore, it is advisable to consider climate change simulations from numerous models in future drought risk analysis studies in order to derive climate change related information in a robust manner.

Acknowledgements

The authors would like to thank the NARCCAP project team for the RCM simulations and Agriculture and Agri-Food Canada and Eva Mekis, from Environment Canada, for providing the observed datasets. The financial support from the Canada Excellence Research Chair in Water Security and School of Environment and Sustainability, University of Saskatchewan, is also acknowledged. Thanks are also due to Fateh Chebana from Institut national de la recherche scientifique (INRS) for his support with the bivariate homogeneity testing, Seth McGinnis from NARCCAP for the computational support in re-gridding model data, and Amir Sadeghian from the Global Institute for Water Security for help with the spatial maps.

References

- Armstrong RN, Pomeroy JW, Martz LW (2015) Variability in evaporation across the Canadian Prairie region during drought and non-drought periods. *J Hydrol* 521:182-195.
- Bonsal BR, Aider R, Gachon P, Lapp S (2012) An assessment of Canadian prairie drought: past, present, and future. *Clim Dyn* DOI 10.1007/s00382-012-1422-0.
- Caya D, Laprise R (1999) A semi-implicit semi-Lagrangian regional climate model: The Canadian RCM. *Mon Weather Rev* 127:341–341.
- Chebana F, Ouarda TBMJ (2007) Multivariate L-moment homogeneity test. *Water Resour Res* 43(W08406):1-14.
- Coles S (2001) An introduction to statistical modeling of extreme values. Springer Publishers, Great Britain.
- Collins WD et al (2006) The Community Climate System Model version 3 (CCSM3). *J Clim* 19:2122–2143 .

- Diasso U, Abiodun BJ (2015) Drought modes in West Africa and how well CORDEX RCMs simulate them. *Theor appl Climatol*, DOI: 10.1007/s00704-015-1705-6
- Embrechets P, Lindskog F, McNeil AJ (2003) Modelling dependence with copulas and applications to risk management. *Handbook of heavy tailed distributions in finance*, S. T. Rachev, ed., Elsevier Science, Amsterdam, The Netherlands.
- Evans E, Stewart RE, Henson W, Saunders K (2011) On precipitation and virga over three locations during the 1999–2004 Canadian Prairie drought, *Atm-Ocean*, 49(4): 366-379.
- Flato GM (2005) The Third Generation Coupled Global Climate Model (CGCM3). Available online from <http://www.ec.gc.ca/ccmac-cccma/default.asp?n=1299529F-1>.
- Ganguli P, Reddy MJ (2013a) Evaluation of trends and multivariate frequency analysis of droughts in three meteorological subdivisions of western India. *Int J Climatol* DOI: 10.1002/joc.3742.
- Ganguli P, Reddy MJ (2013b) Probabilistic assessment of flood risks using trivariate copulas. *Theor Appl Climatol* 111(1–2): 341–360. DOI: 10.1007/s00704-012-0664-4.
- Giorgi F (2006) Regional climate modeling: status and perspectives. *J Phys IV* 139:101–18.
- Genest C, Favre A-C (2007) Everything you always wanted to know about copula modeling but were afraid to ask. *J Hydrol Engg* 12: 4(347).
- Genest C, Rémillard B, Beaudoin D (2009) Goodness-of-fit tests for copulas: a review and a power study. *Insu Math Econ* 44:199–213.
- GFDL GAMDT (The GFDL Global Model Development Team) (2004) The new GFDL global atmospheric and land model AM2-LM2: evaluation with prescribed SST simulations. *J Clim* 17:4641–4673.
- Gordon C et al. (2000) The simulation of SST, sea ice extents and ocean heat transports in a version of the Hadley Centre coupled model without flux adjustments. *Clim Dyn* 16:147–168.
- Grell GA, Devenyi D (2002) A generalized approach to parameterizing convection combining ensemble and data assimilation techniques. *Geophys Res Lett* 29:1693–1697.
- Grell GA, Dudhia J, Stauffer DR (1993) A description of the fifth-generation Penn State/NCAR Mesoscale Model (MM5). NCAR Tech. Note NCAR/TN-398+1A, 107 pp.
- Guttman NB (1998) Comparing the palmer drought index and the standardized precipitation index. *Journal of the American Water Resources Association* 34(1): 113-121.

- Halwatura D, Lechner AM, Arnold S (2015) Drought severity-duration-frequency curves: a foundation for risk assessment and planning tool for ecosystem establishment in post-mining landscapes. *Hydrol Earth Syst Sci* 19: 1069-1091.
- Hargreaves GH, Samani ZA (1982) Estimating potential evapotranspiration, Technical note. *J Irrig Drain Eng* 108(3): 225–300.
- Hargreaves GH, Samani ZA (1985) Reference crop evapotranspiration from temperature. *Appl Eng Agric* 1 (2): 96–99.
- Hosking JRM, Wallis JR (1993) Some statistics useful in regional frequency analysis. *Water Resour Res* 29: 271-81.
- Hosking JRM, Wallis JR (1997) *Regional frequency analysis*. Cambridge University Press.
- Huang S, Krysanova V, Hattermann F (2015) Projections of climate change impacts on floods and droughts in Germany using an ensemble of climate change scenarios, *Reg Environ Change* 15:461-43. DOI: 10.1007/s10113-014-0606-z
- Hutchinson MF (2004) ANUsplin Version 4.3: User Guide, The Australian National University, Centre for Resource and Environmental Studies, Canberra, Australia. <<http://cres.anu.edu.au/outputs/anusplin.php>>
- IPCC (2007) *Climate change: the physical science basis—summary for policy makers*. Contribution of Working Group 1 to the Fourth Assessment Report of the Intergovernmental Panel on Climate Change (IPCC), Geneva, Switzerland.
- Jensen ME, Burman RD, Allen RG, eds. (1990) *Evapotranspiration and Irrigation Water Requirements*. ASCE Manual 70. Reston, Va.: American Society of Civil Engineers.
- Jeong DI, Sushama L, Khaliq MN (2014) The role of temperature in drought projections over North America. *Clim Change* 127 (2): 289–303.
- Jones RG, Hassell DC, Hudson D, Wilson SS, Jenkins GJ, Mitchell JFB (2003) *Workbook on generating high resolution climate change scenarios using PRECIS*. UNDP, 32 pp.
- Juang H-M, Hong S-Y, Kanamitsu M (1997) The NCEP regional spectral model: an update. *Bull Am Meteorol Soc* 78: 2125–2143.
- Kao S, Govindaraju RS (2010) A copula-based joint deficit index for droughts. *J Hydrol* 380: 121-134.
- Kaufman L, Rousseuw PJ (1990) *Finding groups in data: an introduction to cluster analysis*. Wiley-Interscience, New York, 344pp.

- Khaliq MN, Sushama L, Monette A, Wheeler H (2014) Seasonal and extreme precipitation characteristics for the watersheds of the Canadian Prairie Provinces as simulated by the NARCCAP multi-RCM ensemble. *Clim Dyn*. DOI 10.1007/s00382-014-2235-0.
- Kouwen N (2014) WATFLOOD Hydrological Model and Flood Forecasting System. User's Manual. Department of Civil Engineering. University of Waterloo, Waterloo, ON, Canada (<http://www.civil.uwaterloo.ca/watflood/manual/manualstart.htm>; accessed on December 20, 2015).
- Ma M, Song S, Ren L, Jiang S, Song J (2013) Multivariate drought characteristics using trivariate Gaussian and Student t copulas. *Hydrol Process* 27: 11754-1190.
- Madadgar S, Moradkhani H (2013) Drought analysis under climate change using copula. *J Hydrol Eng* 18: 746-759.
- Masud MB, Khaliq MN, Wheeler HS (2015) Analysis of meteorological droughts for the Saskatchewan River Basin using univariate and bivariate approaches. *J Hydrol* 522:452-466.
- Maulé C, Helgason W, McGinn S, Cutforth H (2006) Estimation of standardized reference evapotranspiration on the Canadian Prairies using simple models with limited weather data. *Canadian Biosystems Engineering/Le génie des biosystèmes au Canada* 48:1.1–1.11.
- Mavromatis T (2007) Drought index evaluation for assessing future wheat production in Greece. *Intl J Climatol* 27, 911-924.
- May W (2008) Potential future changes in the characteristics of daily precipitation in Europe simulated by the HIRHAM regional climate model. *Clim Dyn* 30:581–603.
- McGinn SM. (2010) Weather and climate patterns in Canada's Prairies grassland. In *arthropods of Canadian grasslands (Volume 1): Ecology and interactions in grasslands habitats*. Edited by J.D. Shorthouse and K.D. Floate. Biological survey of Canada, pp. 105-119; doi: 10.3752/9780968932148.ch5.
- McKee TB, Doesken NJ, Kleist J (1993) The relationship of drought frequency and duration to time scales. In: *Preprints 8th Conference on Applied Climatology, Anaheim, CA*. American Meteorological Society, 179–184.

- Mearns LO, Gutowski WJ, Jones R, Leung L-Y, McGinnis S, Nunes AMB, Qian Y (2009) A regional climate change assessment program for North America. *Eos Trans Am Geophys Union* 90:311–312.
- Mearns LO et al. (2012) The North American Regional Climate Change Assessment Program: Overview of phase I results. *Bull Amer Meteor Soc* 93:1337–1362. doi: <http://dx.doi.org/10.1175/BAMS-D-11-00223.1>.
- Mekis E, Vincent LA (2011) An overview of the second generation adjusted daily precipitation dataset for trend analysis in Canada. *Atmos Ocean* 49(2):163–177.
- Mladjic B, Sushama L, Khaliq MN, Laprise R, Caya D, Roy R (2011) Canadian RCM projected changes to extreme precipitation characteristics over Canada. *J Clim* 24:2565–2584.
- Mohan S (1991) Intercomparison of evapotranspiration estimates. *Hydrol Sci J* 36(5): 447–461.
- Monette A, Sushama L, Khaliq MN, Laprise R, Roy R (2012) Projected changes to precipitation extremes for Northeast Canadian watersheds using a multi-RCM ensemble. *J Geophys Res* 117:D13106. doi:10.1029/2012JD017543.
- Nakicenovic N et al (2000) *Special Report on Emissions Scenarios: A special report of working group III of the intergovernmental panel on climate change*, Cambridge University Press, Cambridge, U.K., 599 pp. Available online at: <http://www.grida.no/climate/ipcc/emission/index.htm>.
- Nelsen RB (2006) *An introduction to copulas*. Springer-Verlag: New York; pp 272.
- PaiMazumder D, Sushama L, Laprise R, Khaliq MN, Sauchyn D (2013) Canadian RCM projected changes to short- and long-term drought characteristics over the Canadian Prairies. *Intl J Climatol* 33: 1409-1423.
- Pal JS et al (2007) Regional climate modeling for the developing world: The ICTP RegCM3 and RegCNET. *Bull Am Meteorol Soc* 88: 1395–1409.
- Pomeroy J, Pietroniro A, Fang X, Shaw D, Armstrong R, Shook K, Comeau L, Toth B, Martz L, Westbrook C (2011) Canadian prairie drought hydrology. In: Stewart R, Lawford R (eds) *Drought Research Initiative*. ISBN No. 978-0-9868749-0-1, pp 59–62.
- Potop V, Možný M, Soukup J (2012) Drought evolution at various time scales in the lowland regions and their impact on vegetable crops in the Czech Republic. *Agricul and Forest Met* 156:121-133.

- Rajsekhar D, Mishra AK, Singh VP (2013) Regionalization of drought characteristics using an entropy approach. *J Hydrol Eng* 18:870-887.
- Rao AR, Srinivas VV (2008) Regionalization of watersheds—an approach based on cluster analysis. Springer Publishers, Germany.
- Sadri S, Burn DH (2011) A fuzzy c-means approach for regionalization using a bivariate homogeneity and discordancy approach. *J Hydrol* 401: 231-239.
- Savu C, Tiede M (2010) Hierarchies of Archimedean copulas. *Quant Finance* 10(3):295–304
- Serfling R, Xiao P (2007) A contribution to multivariate L-moments: L-commoment matrices. *J Multivariate Anal* 98:1765-1781.
- Serinaldi F, Grimaldi S (2007) Fully nested 3-copula: Procedure and application on hydrological data. *J Hydrol Eng* 12(4):420– 430.
- Serinaldi F, Bonaccorso B, Cancelliere A, Grimaldi S (2009) Probabilistic characterization of drought properties through copulas. *Phys Chem Earth* 34 (10–12):596–605.
- Shiau JT, Modarres R (2009) Copula-based drought severity- duration-frequency analysis in Iran. *J Appl Meteorol* 16(4): 481–489.
- Sklar K (1959) Fonctions de repartition ‘a n dimensions et leurs marges. *Publications de l’Institut de Statistique de l’Université de Paris* 8: 229–231.
- Stagge JH, Tallaksen LM, Gudmundsson L, Van Loon AF, Stahl K (2015) Candidate Distributions for Climatological Drought Indices (SPI and SPEI). *Int J Climatol* 35: 4027–4040 (2015). DOI: 10.1002/joc.4267.
- Tebaldi C, Knutti R (2007) The use of the multi-model ensemble in probabilistic climate projections. *Phil Trans R Soc A* 365:2053-2075.
- Touma D, Ashfaq M, Nayak MA, Kao S-C, Diffenbaugh NS (2015) A multi-model and multi-index evaluation of drought characteristics in the 21st century. *J Hydrol* 526:196-207
- Torma C, Giorgi F, Coppola E (2015) Added value of regional climate modeling over areas characterized by complex terrain—Precipitation over the Alps. *J Geophys Res Atmos* 120:3957–72.
- Vicente-Serrano SM, Beguería S, López-Moreno JI (2010) A multi-scalar drought index sensitive to global warming: the standardized precipitation evapotranspiration index. *J Clim* 23(7):1696–1718.

- Wang T, Hamann A, Spittlehouse DL, Murdock TQ (2011) ClimateWNA--High-Resolution Spatial Climate Data for Western North America. *Agricul and Forest Met* 51:16-29. DOI: 10.1175/JAMC-D-11-043.1.
- Wheater HS, Gober P (2013) Water security in the Canadian prairies: science and management challenges, *Philos Trans Roy Soc A*. doi:10.1098/rsta.2012.0409.
- WMO (2009) Inter-Regional workshop in indices and early warning systems for drought (Lincoln, NE, Dec. 2009) (Geneva: World Meteorological Organization).
- Wong G, Lambert MF, Leonard M, Metcalfe AV (2010) Drought analysis using trivariate copulas conditional on climate states. *J Hydrol Eng* 15(2): 129–141.

CHAPTER 4

PROJECTED CHANGES TO SHORT- AND LONG-DURATION PRECIPITATION EXTREMES OVER THE CANADIAN PRAIRIE PROVINCES

The effects of climate change on dry extremes (i.e., droughts) were presented in chapter 2 and 3. In addition to droughts, the study area (Alberta, Saskatchewan and Manitoba provinces of Canada) also experiences recurrent floods, sometimes caused by heavy precipitation events during the warm season of the year. Therefore, the impact of climate change on warm season wet extremes was also studied. For the research reported in this chapter, projected changes to selected return levels of short- and long-duration (ranging from minutes to several hours) precipitation extremes were developed using multi-Regional Climate Model simulations available from the North American Regional Climate Change Assessment Program (NARCCAP) and regional frequency analysis approach. These changes were developed at the level of a 50 × 50 km grid to portray more detailed spatial information and at the level of five large geographic regions covering the study area in order to deduce a robust climate change signal. These changes would be useful for developing climate change informed design standards for future development projects and for assessing adequacy of existing infrastructure facilities. This chapter contains the following submitted manuscript in the *Climate Dynamics* journal:

- 3. Masud MB, Khaliq MN, Wheater HS (2016)** Projected changes to short- and long-duration precipitation extremes over the Canadian Prairie Provinces. Submitted to *Climate Dynamics* on 9th March; submission no. CLDY-D- 16-00239

Abstract

The effects of climate change on April to October short- and long-duration precipitation extremes over the Canadian Prairie Provinces were evaluated using a multi-Regional Climate Model (RCM) ensemble available through the North American Regional Climate Change Assessment Program. Simulations considered include those performed with six RCMs driven by the National Centre for Environmental Prediction (NCEP) reanalysis II product for the 1981–2000 period and those driven by four Atmosphere–Ocean General Circulation Models (AOGCMs) for the current 1971–2000 and future 2041–2070 periods (i.e. a total of 11 current-to-future period simulation pairs). A regional frequency analysis approach was used to develop

2-, 5-, 10-, 25-, and 50-yr return values of precipitation extremes from NCEP and AOGCM-driven current and future period simulations that respectively were used to study performance of RCMs and projected changes for selected return values at regional, grid-cell and local scales. Performance errors due to internal dynamics and physics of RCMs studied for the 1981-2000 period reveal considerable variation in the performance of the RCMs. However, the performance errors were found to be much smaller for RCM ensemble averages than for individual RCMs. Projected changes for future climate to selected regional return values of short-duration (e.g. 15- and 30-min) precipitation extremes and for longer return periods (e.g. 50-yr) were found to be mostly larger than those to the longer duration (e.g. 24- and 48-h) extremes and short return periods (e.g. 2-yr). Overall, projected changes in precipitation extremes were larger for southeastern regions followed by southern and northern regions and smaller for southwestern and western regions of the study area. The changes to return values were also found to be statistically significant for the majority of the RCM-AOGCM simulation pairs. These projections might be useful as a key input for future planning of urban drainage infrastructure and development of strategic climate change adaptation measures.

Keywords: climate change, precipitation extremes, regional frequency analysis, NARCCAP, Canadian Prairie provinces

4.1 Introduction

Information on projected changes to precipitation extremes is needed for future planning of urban drainage infrastructure, better management of water resources, ensuring proper functioning of ecosystems, and sustaining regional socio-economic activities by adapting to a changing climate. Therefore, it is relevant to investigate future changes in precipitation extremes at local, regional or other scales of interest. The primary means used to assess future climate change are the transient climate change simulations produced with the coupled global and regional climate models when these models are integrated from the recent past to some time-point in the future (IPCC, 2007). Currently, Regional Climate Models (RCMs) offer higher spatial resolution than Global Climate Models (GCMs) and therefore can represent many finer scale features, which is not possible to do using GCMs, such as complex topography and its impact on precipitation forming mechanisms. Due to these obvious merits of RCMs over GCMs, recently many studies have used RCM simulations for the assessment of changes in characteristics of precipitation

extremes (e.g. Beniston, 2007; May, 2008; Nikulin et al., 2011; Mladjic et al., 2011; Mailhot et al., 2012; Monette et al., 2012; Hanel and Buishand, 2012; van Pelt et al., 2012; Khaliq et al., 2014, 2015). Though the use of a single RCM is not uncommon, the combination of results from many RCMs leads to more robust and reliable results by reducing the uncertainty associated with the projections of a single model (Hagedorn et al., 2005). Also, as pointed out by de Elía et al. (2008), RCMs are associated with various sources of uncertainties including (1) structural uncertainty associated with model formulation (e.g., domain size and location, nesting and relaxation technique, physical processes and parameterization), (2) internal variability (triggered by differences in the initial conditions), and (3) dependence on lateral boundary forcing (i.e., choice of boundary forcings). Such sources of uncertainties can be evaluated better using simulations from multi-RCM ensembles. Similar to the PRUDENCE (Christensen et al., 2007) and ENSEMBLES (Christensen et al., 2009) multi-RCM projects over Europe, the North American Regional Climate Change Assessment Program (NARCCAP) (Mearns et al., 2009) is a multi-RCM ensemble project over North America. In this study, the multi-RCM simulations available from NARCCAP are considered to evaluate some of the sources of uncertainties mentioned above and the impact of climate change on short- and long-duration precipitation extremes, which is the main focus of this study.

A previous country-wide study by Mladjic et al. (2011) assessed projected changes to single- and multiday precipitation extremes using the Regional Frequency Analysis (RFA) approach and an ensemble of Canadian Regional Climate Model (CRCM) simulations on the basis of 10 large climatic regions covering Canada. Their study revealed significant increases in regional return values for both single- and multiday precipitation extremes for the 2041–2070 period, with changes to the 20-, 50-, and 100-yr regional return values being larger (smaller) for the northern (southern) climatic regions. Following the study of Mladjic et al. (2011), Mailhot et al. (2012) developed projected changes in selected characteristics of precipitation extremes for the same climatic regions, but using the NARCCAP multi-RCM ensemble. Their findings were generally in line with those of Mladjic et al. (2011). Monette et al. (2012) also used the NARCCAP multi-RCM ensemble to study projected changes to 1-, 2-, 3-, 5-, 7-, and 10-day precipitation extremes over 21 northeastern Canadian watersheds spread mainly across the province of Quebec and extending through some parts of the provinces of Ontario and Newfoundland and Labrador. Recently, Khaliq et al. (2014) analyzed projected changes to

seasonal precipitation totals and daily precipitation extremes for 47 watersheds that span Alberta, Saskatchewan and Manitoba Provinces of Canada using the same NARCCAP multi-RCM ensemble as used in Monette et al. (2012). Their region of study was roughly the same as considered in this study. However, an exclusive feature of their study was that the RFA approach was applied for developing projected changes to 10-, 30-, and 50-yr return values of rain and snow dominated extremes (RDEs and SDEs) separately. They found projected changes to RDEs to be generally larger for watersheds located in central and southeastern parts of the study area than those located in northwestern parts, while for SDEs, larger projected changes were found for watersheds in the northern, western and southern parts than those in the southeastern parts. Other studies where simulations from NARCCAP RCMs were evaluated at various scales include Gao et al. (2012) on Colorado River discharge, Wehner (2013) on extreme seasonal precipitation in the US, Caldwell (2010) on California wintertime precipitation, Jeong et al. (2014) on future droughts at the North American continental scale, Masud et al. (2015) on projected changes to regional droughts, and Jeong et al. (2015a, b) on hot and cold spells across Canada.

This study explored projected changes to seasonal (April-October) short- and long-duration (i.e. 5-, 10-, 15-, 30-, 60-min, 3-, 6-, 12-, 24-, and 48-h) precipitation extremes over the Canadian Prairie Provinces of Alberta, Saskatchewan and Manitoba based on a larger NARCCAP multi-RCM ensemble, compared to the ones used in the studies mentioned above. This region consists of 47 diverse watersheds including the Saskatchewan, Athabasca, Peace, and Churchill River basins, which play a significant role in the economy of the region as sources to support agricultural production, domestic and industrial water supply, and hydropower generation. Seasonal precipitation extremes for the above mentioned selected durations were obtained using a moving window of a fixed duration. For the analysis, the RFA approach of Hosking and Wallis (1997) was used to calculate various return values at the regional, local and grid-point scale. The RFA approach has several advantages compared to the at-site approach. For example, the RFA approach is specifically suitable in situations where generally short records are available and was appealing for this study since the maximum sample size used was just 30 seasonal extreme values. The RFA approach was applied to current and future period simulated extremes and projected changes to 2-, 5-, 10-, 25-, and 50-yr return values were developed for 2041–2070 with respect to the 1971–2000 period. To our knowledge, no other study on projected changes to both

short- and long-duration precipitation extremes has been undertaken so far for the three Prairie Provinces of Canada. In particular, changes to short-duration (e.g. minutes to hours) extremes are highly desirable to assess adequacy of urban drainage infrastructure in the context of climate change.

This paper is organized as follows. A brief description of the study area, observed data, and NARCCAP multi-RCM simulations used in the study is provided in Section 4.2. Section 4.3 describes the methodology used for developing projected changes to selected characteristics of short- and long-duration precipitation extremes, followed by results and discussion related to the assessment of various RCMs and projected changes to short- and long-duration precipitation extremes in Section 4.4. Finally, main conclusions of the study are presented in Section 4.5.

4.2 Study area, observations and model simulations

The Canadian Prairie Provinces (Alberta, Saskatchewan and Manitoba; Figure 4.1) feature a complex topography, ranging from flat land in the East to Rocky Mountains in the West, with elevation varying from 1 to 3434 m above mean sea level. The southern parts of these provinces, particularly the Prairies ecozone, are considered as home to 80% of Canada's agricultural production (Wheater and Gober, 2013). The ecosystem of this region is highly dependent on the occurrence and timing of seasonal precipitation which is correlated with atmospheric circulation and the mid troposphere ridge (Dey, 1982; Hogg et al., 2000). The annual average precipitation (454 mm) of these provinces is less than the Canada-wide average (535 mm) because cyclonic precipitation rarely reaches to this area from the west or east coast (Phillip, 1990) and there is a frequent presence of dry arctic air (Gan, 2000). More specifically, this region is characterized by a highly variable hydroclimate, with recurrent droughts (such as the prolonged droughts of 1988 and 1999–2004), floods (such as severe floods of 2011, 2013 and 2014) and localized convective storm activity, resulting in heavy precipitation events, often observed during warm seasons of the year, posing many research challenges.

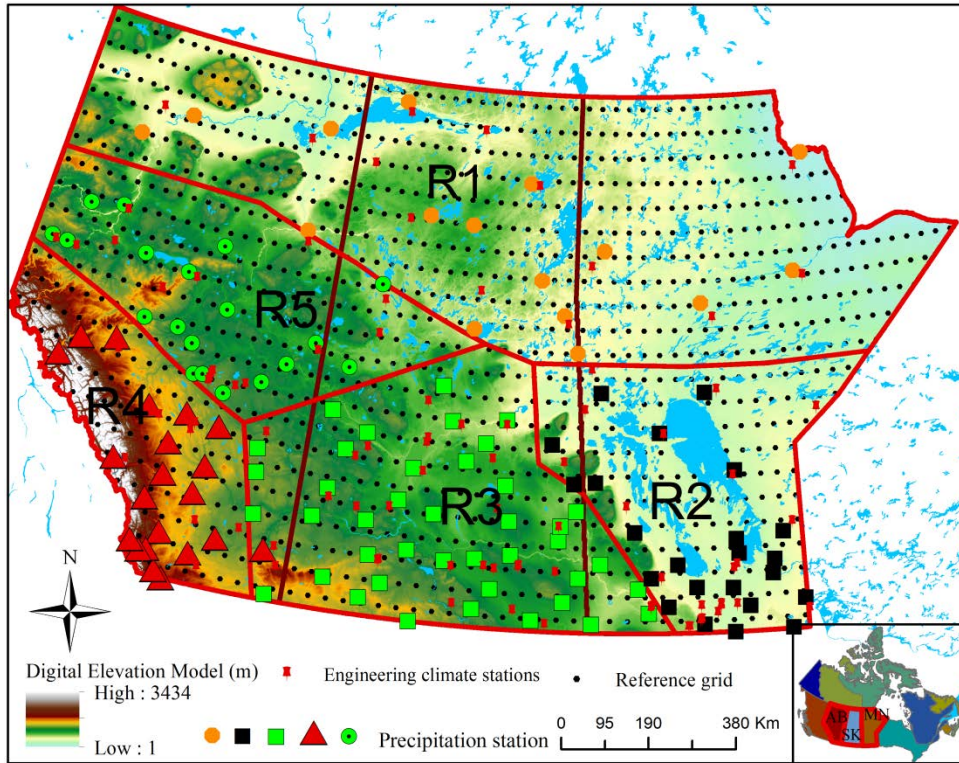


Figure 4.1: Map of the study area overlaid with the reference grid. Precipitation stations for adjusted and rehabilitated observed dataset (DS1) are shown using five different symbols to highlight the corresponding homogeneous region (R1 to R5) they are associated with and location of engineering climate stations (DS2) where continuous seasonal precipitation is recorded. Inset shows location of the study area (i.e. Alberta–AB; Saskatchewan–SK; Manitoba–MN) in Canada.

One set of observed data considered for this study consists of adjusted and rehabilitated daily precipitation data, available from Environment Canada for the 1961–2000 period for a network of 120 stations located across the study area (Figure 4.1). In the present study, the spatial patterns of daily precipitation extremes from this dataset were used for dividing the study area into contiguous homogeneous regions from previously developed soft fuzzy regions adapted from Asong et al. (2014, 2016) to facilitate RFA, to be discussed in the methodology section. Additionally, the characteristics of multiday precipitation extremes from this dataset were used to verify statistical homogeneity of identified regions. Hereafter, this dataset is referred to as DS1.

The second set of observed data considered consists of 5-, 10-, 15-, 30-, 60-min, 2-, 6-, 12-, and 24-h seasonal (April to October) precipitation extremes from 92 engineering climate stations located over the study area (Figure 4.1), obtained from Environment Canada. These extremes were compiled by Environment Canada using a moving window of fixed duration. A detailed description of this dataset can be found at http://climate.weather.gc.ca/prods_servs/engineering_e.html. Precipitation extremes from this dataset for the 1961-2000 period were used for verifying statistical homogeneity of contiguous homogeneous regions developed from fuzzy regions identified by Asong et al. (2014, 2016) and for selecting the most appropriate regional distribution for modeling precipitation extremes using the RFA approach. It is important to note that there is no duplication of data in these observed datasets and therefore, both complement each other. This second observed dataset will be referred to as DS2 in this paper. The objective of using different datasets was to ensure adequate statistical homogeneity of the identified regions.

Table 4.1: The NARCCAP simulations considered in the study

RCM	NCEP	Driving AOGCM			
		GFDL	CGCM3	HADCM3	CCSM
CRCM	√	--	√	--	√
ECP2	√	√	--	--	--
HRM3	√	√	--	√	--
MM5I	√	--	--	√	√
RCM3	√	√	√	--	--
WRFG	√	--	√	--	√

Outputs from six different RCMs (Table 4.1), driven by National Center for Environmental Prediction (NCEP) reanalysis II and four different Atmospheric-Ocean General Circulation Models (AOGCMs), available through the NARCCAP project were considered for this study. Detailed information and description of the participating RCMs and their driving AOGCMs can be obtained from the NARCCAP website (<http://www.narccap.ucar.edu>). The aim of NARCCAP was to produce RCM simulations for a common period and domain (Mearns et al., 2009) to aid in the systematic evaluation of various sources of uncertainty in future climate projections. These simulations were produced in two phases. In Phase I, simulations from CRCM, ECP2, HRM3,

MM5I, RCM3 and WRFG RCMs were produced with boundary conditions from NCEP reanalysis II for the 1981–2000, 20 year period. In Phase II, RCM simulations with boundary conditions taken from four different AOGCMs (i.e. CCSM, CGCM3, GFDL and HadCM3) for the 1971–2000 current and 2041–2070 future periods, with Special Report on Emissions Scenarios (SRES) A2 scenario (Nackicenovic et al., 2000), were produced. The NCEP-driven simulations were used to assess the performance of individual RCMs, while the AOGCM-driven current and future period 11 simulation pairs were used in the assessment of projected changes to selected return values of precipitation extremes, discussed in the methodology section. In this study, various RCM simulations are referred to as ‘RCM_LBC’, where RCM part of the abbreviation reflects the acronym of the RCM and LBC part refers to the acronym of the lateral boundary condition (i.e. NCEP reanalysis or the AOGCM driving the RCM at its boundaries). For example, CRCM simulation driven by CGCM3 is referred to as CRCM_CGCM3. Though the simulation domains of the RCMs cover most of North America, as noted above, this study focuses only on Canadian provinces of Alberta, Saskatchewan and Manitoba.

4.3 Methodology

4.3.1 Reference grid

All RCMs have roughly the same horizontal resolution (i.e. 50-km) but different projections on the spherical earth. A common reference grid (i.e. the half-degree University of Delaware grid; Figure 4.1) was considered to ease inter-comparison of results. All model outputs were interpolated to this reference grid using spline interpolation (Green and Silverman, 1993). This reference grid was also used in previous studies on NARCCAP RCM simulations (e.g. Mearns et al., 2012).

4.3.2 Precipitation extremes and their characteristics

The precipitation extremes considered in this study, for each RCM_AOGCM simulation consisted of seasonal (April–October) maximum values of 3-, 6-, 12-, 24-, and 48-h durations, while those from DS2 correspond to 5-, 10-, 15-, 30-, 60-min, 2-, 6-, 12-, and 24-h durations. Precipitation extremes considered from DS1 correspond to 1-, 2- and 3-day durations. These extremes from respective datasets were derived using a running window of a fixed duration. It is important to note that 24- and 48-h extremes are not the same as 1- and 2-day extremes due to the differences in the resolution of the underlying datasets. It is also important to point out that

the minimum temporal resolution of the RCM-simulated precipitation was just 3-h and therefore derivation of precipitation extremes of durations smaller than 3-h was not possible. The April-October period was considered as the available engineering climate stations operate only during this period. For RCM simulations, precipitation extremes correspond to the reference grid mentioned above. Characteristics of precipitation extremes in terms of 2-, 5-, 10-, 25-, and 50-yr return values were considered for evaluating the performance of various RCMs and for developing projected changes to precipitation extremes. Concerning the interpretation of return values, a 50-yr return value is the amount of precipitation that has a probability of 2% of being equaled or exceeded in a given year; a similar interpretation is applicable for other return values.

4.3.3 Contiguous homogeneous regions and the RFA approach

The three Canadian Prairie Provinces region was subdivided into five climatically homogeneous fuzzy precipitation regions based on the teleconnection patterns (e.g. indices of Pacific Decadal and Pacific North American Oscillations), large-scale atmospheric covariates (i.e. wind speed at 10-m, 500- and 850-hPa; U-component and V-component at 10-m, 500- and 850-hPa, geo-potential height, specific humidity, and relative humidity at 850- and 500-hPa; total cloud cover, mean sea level pressure, precipitable water and 2-m air temperature) and geographic site attributes (e.g. latitude and longitude) by Asong et al. (2014, 2016) using principal component and canonical correlation analyses and a Fuzzy C-Means clustering algorithm. In the current study, these fuzzy regions were hardened (i.e. separating two adjoining soft regions using a hard boundary) through numerous trials based on the spatial pattern of mean seasonal daily extremes and paying attention to the influence of local water bodies and topographic features. After delineating these regions, their statistical homogeneity was tested based on L-moment ratio based heterogeneity statistics proposed by Hosking and Wallis (1997). According to these authors, heterogeneity statistics H_i ($i = 1, 2$ and 3) include the weighted standard deviation of the L-coefficient of variation (H_1), L-skewness (H_2) and L-kurtosis (H_3). These values were derived using 2000 Monte Carlo simulations for each of the five regions. The outcome of these analyses can be explained in three different ways based on H_i values. A region can be defined as ‘acceptably homogeneous’ if $H_i < 1$, ‘possibly homogeneous’ if $1 < H_i < 2$ and ‘definitely heterogeneous’ if $H_i > 2$.

After verifying the statistical homogeneity of all delineated regions, the next step was to select an appropriate regional distribution for each homogeneous region from suitable candidate

distributions to develop regional growth curves. A regional growth curve represents a dimensionless relationship between the frequency and magnitude of selected precipitation extremes. The frequency distributions considered include the Generalized Extreme Value (GEV), Generalized Logistic (GLO), Generalized Pareto (GPA), Pearson Type-III (PE3), Generalized Normal (GNO), and Wakeby, which are commonly used for frequency analysis of hydro-climatic extremes. The Z test developed by Hosking and Wallis (1997) was used to pick the most appropriate regional distribution.

After selecting an appropriate regional distribution for modeling precipitation extremes for each duration considered, comparisons of 2-, 5-, 10-, 25-, and 50-yr return values of 6-, 12-, and 24-h precipitation extremes obtained from observations and NCEP-driven RCM simulations were carried out in a RFA setting to evaluate performance of various RCMs. This was followed by an assessment of boundary forcing errors by comparing directly return values derived from NCEP-driven and AOGCM-driven RCM simulations. Though possible, the impact of two different AOGCMs driving the same RCM was not explicitly evaluated. The at-site (grid-point level) return values of precipitation extremes were computed by multiplying regional growth factors, derived from respective observed (model simulated) regional growth curves, with respective at-site (grid-point based) mean value of extremes. For regional return values, the regional growth factors were multiplied with the respective regionally-averaged at-site (grid-point based) mean value of extremes. For deriving an ensemble-averaged regional return value, the same procedure was used but using ensemble-averaged growth factors and regionally averaged mean values of extremes. Though this procedure is consistent with those used in Mladjic et al. (2011), Monette et al. (2012), and Khaliq et al. (2014, 2015), other variations of the same procedure are also possible.

4.3.4 Projected changes to precipitation extremes

Projected changes to precipitation extremes of 3-, 6-, 12-, 24-, and 48-h durations were assessed by comparing the return values, corresponding to selected return periods, derived from current and future period simulations of 11 RCM_AOGCM combinations (Table 4.1). To assess statistical significance of projected changes in return values at the regional level, confidence intervals were developed for current and future periods using the nonparametric vector bootstrap resampling method (Efron and Tibshirani 1993; Khaliq et al., 2009). In addition to the effect of limited sample size, this method takes care of the first-order spatial correlations, which are

present within most gridded datasets, on estimates of confidence intervals. For each RCM_AOGCM combination and region, one thousand resamples were considered to construct confidence intervals for various return values using the standard error-based approach from Hall et al. (2004) and assuming 5% significance level. For each region and precipitation duration, these confidence intervals were developed first for dimensionless return values (i.e. regional growth factors) which were then multiplied by the regional mean value of extremes to get the desired intervals. An additional description of this approach can be found in the reference quoted above and also in Mladjic et al. (2011). For a given RCM_AOGCM combination, if the current and future period confidence intervals did not overlap then it was an indication that the projected change from current to future climate conditions could be considered statistically significant. For the ensemble-average case, a similar assessment was carried out using the error analysis approach from Bevington and Robinson (2002).

In the event that sub-hourly precipitation extremes, which are highly desirable for many engineering applications (such as designing urban drainage infrastructure; Haddad and Rahman, 2014), were not available from NARCCAP RCMs, the authors attempted to fill that gap by referencing the scaling behaviour of precipitation intensities (i.e. precipitation expressed as precipitation rate in mm/h) of 2-, 5-, 10-, 25-, and 50-yr return periods with the corresponding durations (in hours) of precipitation extremes. More explicitly, by scaling behavior we mean that return values of precipitation intensities for a given return period corresponding to a specific number of precipitation durations are functionally related. It is important to mention that some form of scaling behavior was noticed for Environment Canada's intensity-duration-frequency curves for the majority of the 520 stations included in their engineering climate stations (i.e. DS2). In this study, the scaling behaviour of precipitation intensities was characterized by a simple relationship of the form $y = a + bx + cx^2$, where y is the natural logarithm of precipitation intensity (mm/h), x is the natural logarithm of precipitation duration (h) and a , b and c are the coefficients, estimated using the least squares algorithm. When the third term is not valid, the above relationship reduces to a linear form within the log-log domain and was found suitable for many stations from DS2, but not for all. Consequently, the former relationship was found more inclusive and applicable for all stations. The scaling relationship was first validated for both observed and RCM_NCEP simulated return values to support the hypothesis and then similar relationships were developed separately for current and future period simulated return

values of 3-, 6-, 9-, 12-, 15-, 18-, 24-, 36-, and 48-h precipitation durations. The 9-, 15-, 18-, and 36-h durations were additionally considered in order to develop robust relationships by having additional sample points. Due to the high uncertainty associated with the true form of the scaling relationship for precipitation durations smaller than 3-hours for all RCM_NCEP and RCM_AOGCM simulations due to unavailability of relevant sub-hourly datasets and because of the very different behaviour of extrapolated return values following the scaling relationships, a quantile mapping approach (Boé et al., 2007) was used to estimate expected return values of 5-, 10-, 15-, 30-, and 60-min precipitation durations from 6-, 12- and 24-h return values separately, and then taking an average. Three separate precipitation durations were considered to avoid the influence of a single duration on the expected return values. The estimated return values for current and future periods were used to develop projected changes.

4.4 Results and discussion

In this section, first the results of the statistical homogeneity analysis of predefined soft regions are presented followed by validation of NARCCAP RCMs. The validation of RCMs is essential in order to have confidence in their ability to simulate the characteristics of precipitation extremes for a chosen reference historical period. This is followed by the results of projected changes to short- and long-duration (ranging from minutes to several hours) precipitation extremes. It is important to note that in some cases detailed results and graphical outputs are presented only for selected RCM_NCEP and RCM_AOGCM simulations, as it was difficult to accommodate all plots corresponding to multiple simulations for multiple precipitation durations and for multiple return values in this article due to space constraints. For these cases, results are summarized only and detailed results are available from the authors on request.

4.4.1 Delineation and validation of homogeneous regions

As mentioned in the methodology section, five homogeneous precipitation fuzzy regions were adapted from the work of Asong et al. (2014, 2016), who delineated these regions for the same study area. In a given fuzzy soft region, sites from neighbouring regions are allowed to have a partial membership. However, for the application of the RFA approach, contiguous homogeneous regions are required and partial representation of sites from neighbouring regions is difficult to manage. Therefore, in this study, the five fuzzy regions were hardened based on the

spatial patterns of mean values of seasonal daily precipitation extremes through a trial and error approach. After delineating contiguous regions from fuzzy regions, testing of statistical homogeneity of contiguous regions was carried out using L-moment ratio based regional homogeneity tests developed by Hosking and Wallis (1997), and described in the methodology section. This testing was performed using single- and multiday (i.e. 1-, 2- and 3-day) extremes from DS1 and 5-, 10-, 15-, 30-, 60-min, 2-, 6-, 12-, and 24-h extremes from DS2. Based on the homogeneity criteria H_1 , H_2 and H_3 for precipitation extremes corresponding to most of the above mentioned durations, all five regions were found acceptably homogeneous. On the basis of these results, the five delineated contiguous regions shown in Figure 1 were considered for the various regional frequency analyses reported in this paper.

The next task was to select an appropriate regional frequency distribution for each of the five regions to develop regional growth curves. For this purpose, observed seasonal precipitation extremes were employed and the Z test devised by Hosking and Wallis (1997) was used to pick the most appropriate regional distribution from the GEV, GLO, GPA, PE3, GNO, and Wakeby distributions. Multiple candidates (i.e. GEV, PE3 and GNO) were found equally suitable for most of the regions and precipitation durations. It is important to mention that the distribution of annual or seasonal maxima of the variable of interest asymptotically converges to the GEV distribution (Coles, 2001). Based on this theoretical reasoning and the empirical support provided by the Z test, the GEV distribution was selected for modeling regional growth curves of observed precipitation extremes and the same GEV distribution was also used to model regional growth curves for RCM_NCEP and RCM_AOGCM current and future period simulated extremes, however, with parameters re-estimated for each case considered. This choice is also consistent with Environment Canada's choice of the Gumbel distribution, which is a special case of the GEV distribution, for single-site frequency analysis.

4.4.2 Validation of RCMs

The performance errors of RCMs, i.e. due to errors in the internal dynamics and physics of each RCM (e.g. Sushama et al., 2006), were assessed by comparing 2-, 5-, 10-, 25-, and 50-yr return values of 6-, 12- and 24-h extremes derived from NCEP-driven RCM simulations to those derived from observed data (DS2) within the RFA framework. It should be noted that this comparison was feasible only for the above mentioned precipitation durations due to data unavailability (i.e. model-simulated precipitation extremes for smaller than 3 hour durations and

observed extremes for 3 hour and longer than 24 hour durations were not available). First a comparison of station-based return values was performed with the grid-cell-based return values (both derived within a RFA setting) through scatterplots and then a quantitative evaluation was carried out at the level of individual regions. The scatterplot comparisons for each of the five regions are shown in Figure 4.2 for MM5I and WRFG only and show a good correspondence between observed and simulated return values. Similar, but somewhat different results were noticed for other RCMs (i.e. CRCM and HRM3 generally underestimated and ECP2 and RCM3 generally overestimated observed return values; see Appendix C.1). The comparison between ensemble averaged simulated return values and those observed is shown in Figure 4.3 for all regions. It was found that over- or underestimation of return values was considerably reduced compared to those of individual RCMs. This can also be verified by comparing Figures 4.2 and 4.3.

The quantitative assessment of performance errors in regional return values showed significant overestimation of observed return values by ECP2 and RCM3 respectively in the range of 26 to 55% and 23 to 42% for the entire study domain. Compared to this, CRCM and HRM3 resulted in the underestimation of various return values respectively in the range of -31 to -24% and -31 to -18% for all regions. For the other two models (i.e. MM5I and WRFG), domain-averaged performance errors were found respectively in the range of -9 to -8% and -19 to -16%. It is important to note that return values associated with longer return periods were over- or under-estimated by larger relative differences by all models and for all regions compared to the return values associated with short return periods. With respect to comparisons across regions, the performance of models is relatively poor for region R2 and R4 and occasionally so for region R3. For these three regions, overestimation up to 91%, and underestimation up to -38% was noticed specifically for 6-h precipitation return values. It is important to note that grid-point based precipitation simulated by RCMs exhibit characteristics of areal average precipitation compared to point observations which thus tend to have larger values and shorter durations than the areal average. Apart from this explanation, which is supported by some RCM simulations, the precise physical reasons for over- or underestimation by an individual RCM outcome may depend on model formulation and parameterization schemes of the respective RCM, which require separate in-depth analysis and, therefore, lie outside the scope of this study.

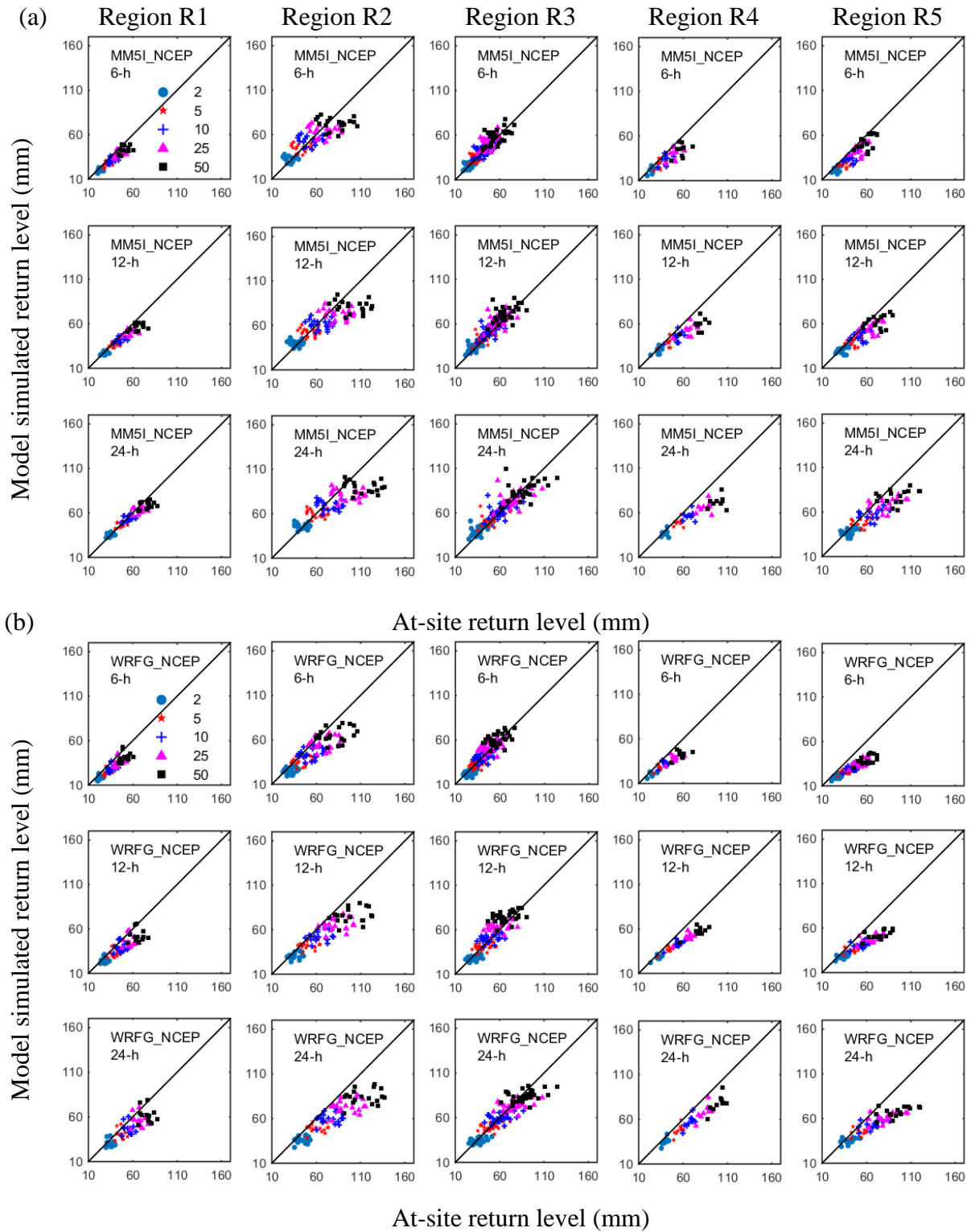


Figure 4.2: Comparison of 2-, 5-, 10-, 25-, and 50-yr observed and (a) MM5I_NCEP and (b) WRFG_NCEP simulated return levels of 6-, 12-, and 24-h seasonal (April to October) precipitation extremes for the current 1981–2000 reference period.

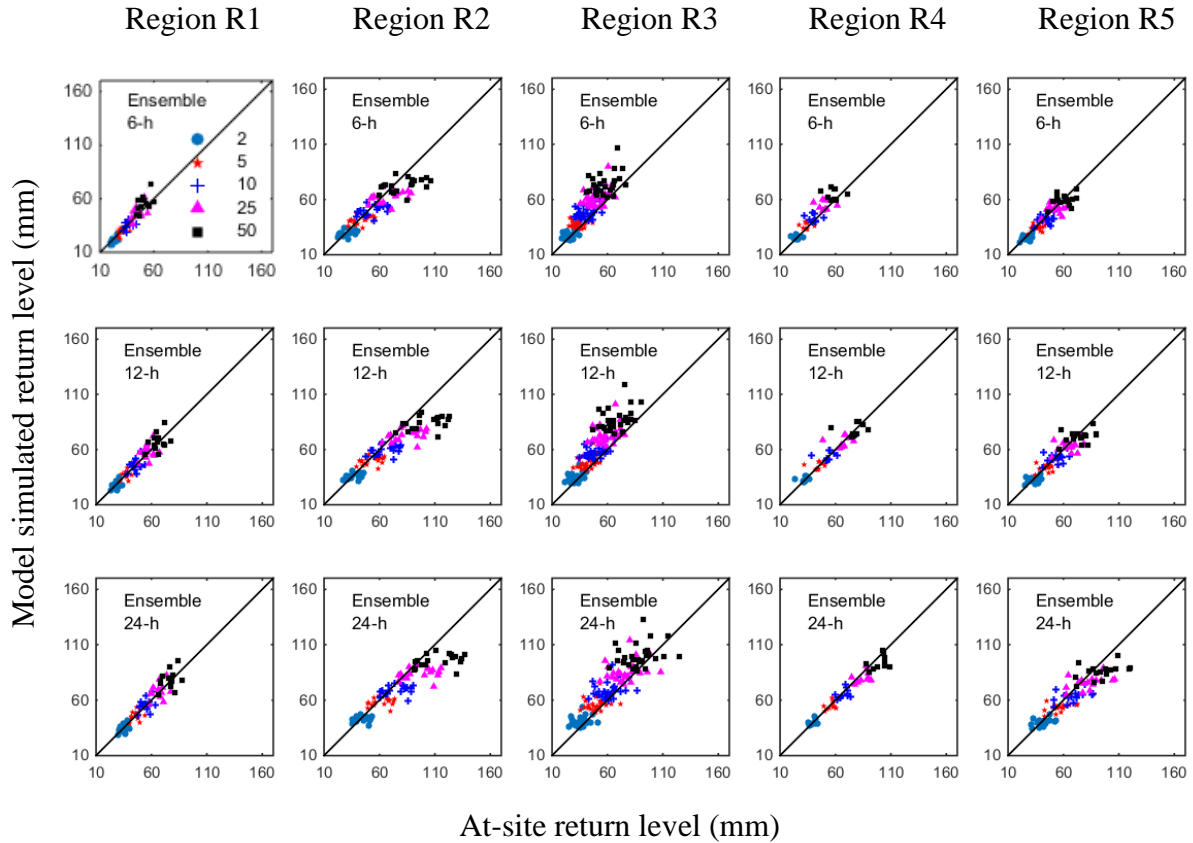


Figure 4.3: Comparison of 2-, 5-, 10-, 25-, and 50-yr observed and ensemble-averaged RCM_NCEP simulated return levels of 6-, 12-, and 24-h seasonal (April to October) precipitation extremes for the current 1981–2000 reference period.

Regardless of region and duration of precipitation, relative differences between ensemble-averaged regional return values for the NCEP-driven RCM simulations and those observed were found in the -28 to 15% range for 50-yr return period followed by -27 to 13% range for 25-yr, -26 to 12% range for 10-yr, -24% to 12% range for 5-yr, and -23 to 12% range for 2-yr return period. Irrespective of return period and precipitation duration, relative differences between ensemble-averaged and observed regional return values were found in the -21 to 1% range for region R1, -24 to -9% range for region R2, -2 to 12% range for region R3, -21 to -2% range for region R4, and -23 to -7% range for region R5. For the ensemble averaged case, the performance errors were much smaller (in absolute terms) than those reported above.

The lateral bounding forcing errors were evaluated by comparing return values from NCEP- and AOGCM-driven simulations for the 1981–2000 period. For regions R1 to R5, irrespective of return periods and precipitation durations, average relative differences between

return values of NCEP- and AGOGCM-driven simulations were found in the -28 to -24% range for CRCM_CCSM, in the -15 to -13% range for CRCM_CGCM3, in the 17 to 22% range for HRM3_GFDL, in the 24 to 30% range for HRM3_HadCM3, about -10% for MM5I_CCSM, in the 5 to 9% range for MM5I_HadCM3, in the 0 to 2% range for RCM3_CGCM3, in the -1 to 2% range for RCM3_GFDL, in the -14 to -12% range for WRF_GCCSM, about -21% for WRF_GCGCM3, and in the -6 to -4% range for ECP2_GFDL. Comparison of results from RCM performance errors and lateral boundary forcing errors presented above suggests that boundary forcing errors are much smaller than performance errors for CRCM, ECP2 and RCM3, and are of the same magnitude for HRM3, MM5I and WRF_G. Overall, the performance errors appeared to be larger than the boundary forcing errors for the study area as a whole.

4.4.3 Projected changes to precipitation extremes

Projected changes to precipitation extremes were explored at the levels of individual grid points and individual regions by comparing return values derived from RCM_AOGCM simulations for the future 2041–2070 period with respect to the current 1971–2000 period. Figure 4.4 shows projected changes in precipitation extremes at the grid-point level for two RCM_AOGCM combinations (i.e. CRCM_CCSM and MM5I_CCSM) due to space limitations (see Appendix C.2 for the results of other RCM_AOGCM combinations). Ensemble-averaged changes are provided in Figure 4.5 to provide an overall view. It can be noticed from these figures that positive changes for the majority of the grid points are associated with return values of 3- and 6-h extremes. Comparatively, positive (negative) changes become less (more) widespread with return values of 24- and 48-h extremes. In the case of the ensemble average (Figure 4.5), the changes are mostly positive and lie within the 0–20% range for 24- and 48-h extremes and within a wider range of 0–40% for 3- and 6-h extremes for most of the study area. Although these figures provide more detailed spatial information about changes, the sporadic behavior of spatial patterns substantially reduces the robustness of the derived changes. Therefore, to circumvent this situation and to derive a robust and practically more useful signal, we developed changes at the scale of the five regions discussed earlier. Figure 4.6 shows projected changes in 2-, 5-, 10-, 25-, and 50-yr return values of 3-, 6-, 12-, 24-, and 48-h precipitation extremes at the regional scale for each of the 11 RCM_AOGCM combinations. This figure provides a clear signal and suggests an increase in extreme values under future climate for most precipitation durations and range of return periods considered, although some conflicting changes can also be

noted for certain RCM_AOGCM combinations. In general, the maximum projected increase in return values is simulated by WRFG_CGCM3 for most of the regions except region R4 where the maximum increase is simulated by HRM3_GFDL for most of the precipitation durations. Decreases in return values, which are around -10%, are simulated by ECP2_GFDL for region R4 and slightly smaller changes (0 to -5%) by CRCM_CCSM for few other regions. A comparison of projected changes from the same RCM driven by two different AOGCMs (Figure 4.6) indicates considerable influence of the driving AOGCM on the magnitude of the projected change. These results support the necessity of using several AOGCMs at the boundaries to address uncertainties associated with the driving fields. A similar comparison of projected changes from different RCMs driven by the same AOGCM supports the use of the multi-RCM ensemble.

As mentioned earlier, ensemble averaged changes may perhaps provide a better signal than the individual RCM values. Therefore, ensemble-averaged projected changes in return values are also shown in Figure 4.6. In general, larger increases in return values are found for longer return periods (e.g. 50-yr). Ensemble-averaged changes are found to lie within the 6–23% range for all durations and return periods considered and are shown in Figure 4.6. However, irrespective of precipitation durations and return periods considered, region R2 is associated with larger changes in precipitation extremes and region R4 with smaller changes. Regardless of return period and duration of precipitation, the ensemble-averaged projected changes in return values are found in the range of 11–19% for region R1, 14–23% for region R2, 12–20% for region R3, 6–15% for region R4, and 8–17% for region R5, respectively.

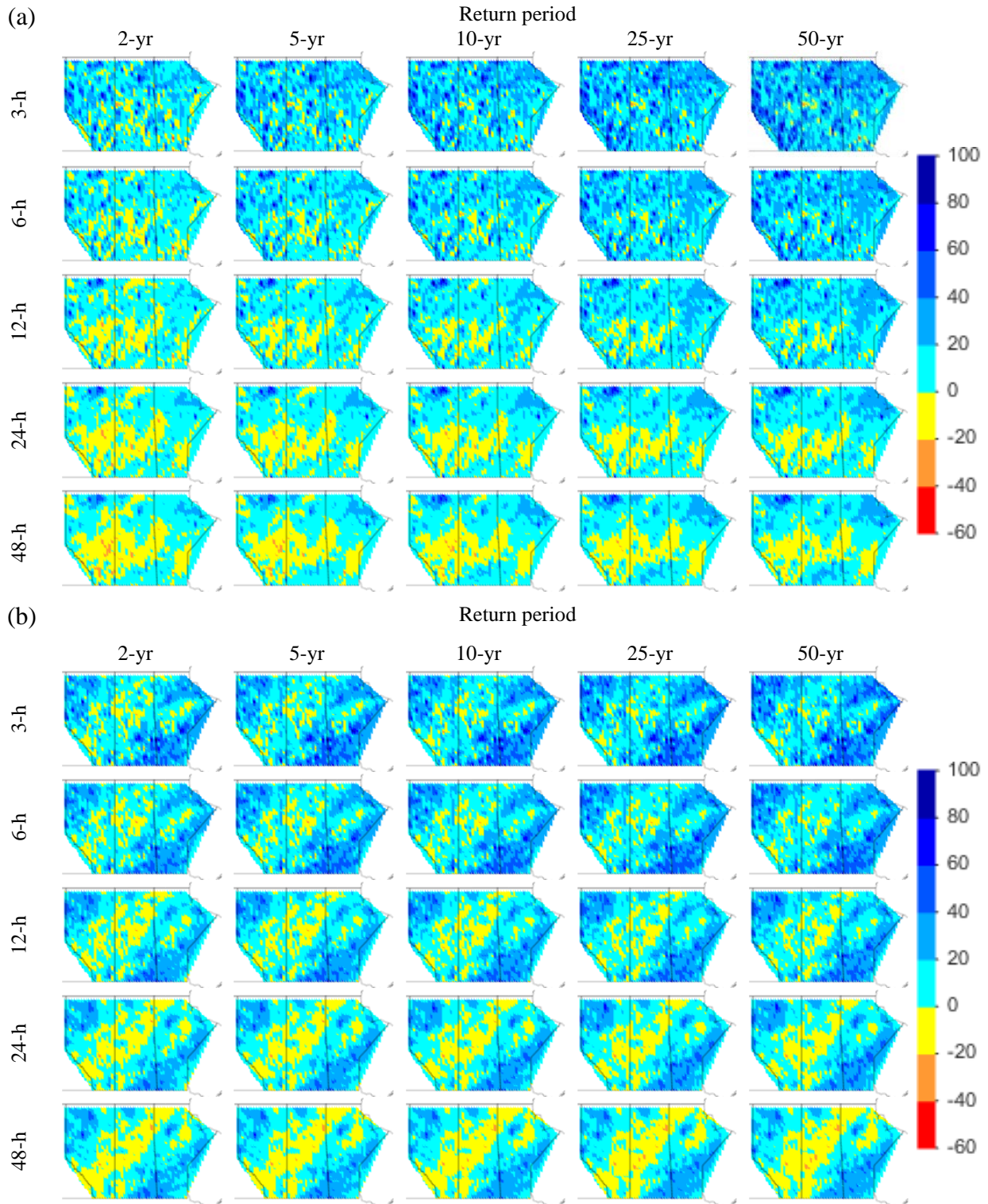


Figure 4.4: Projected changes (in %) in selected grid-point based return levels of 3-, 6-, 12-, 24-, and 48-h precipitation extremes as simulated by (a) CRCM_CCSM and (b) MM5I_CCSM for the 2041–2070 period with respect to the 1971–2000.

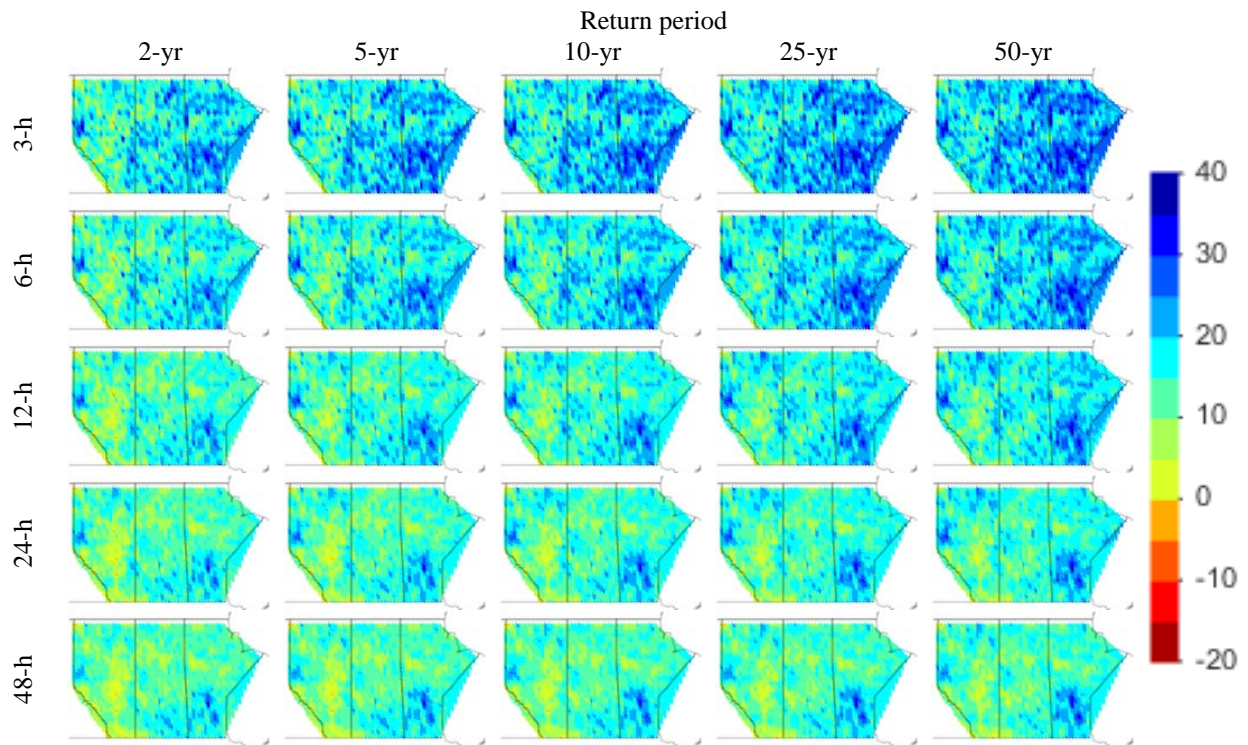


Figure 4.5: Ensemble-averaged projected changes (in %) in selected grid-point based return levels of 3-, 6-, 12-, 24-, and 48-h precipitation extremes for the 2041–2070 period with respect to the 1971–2000.

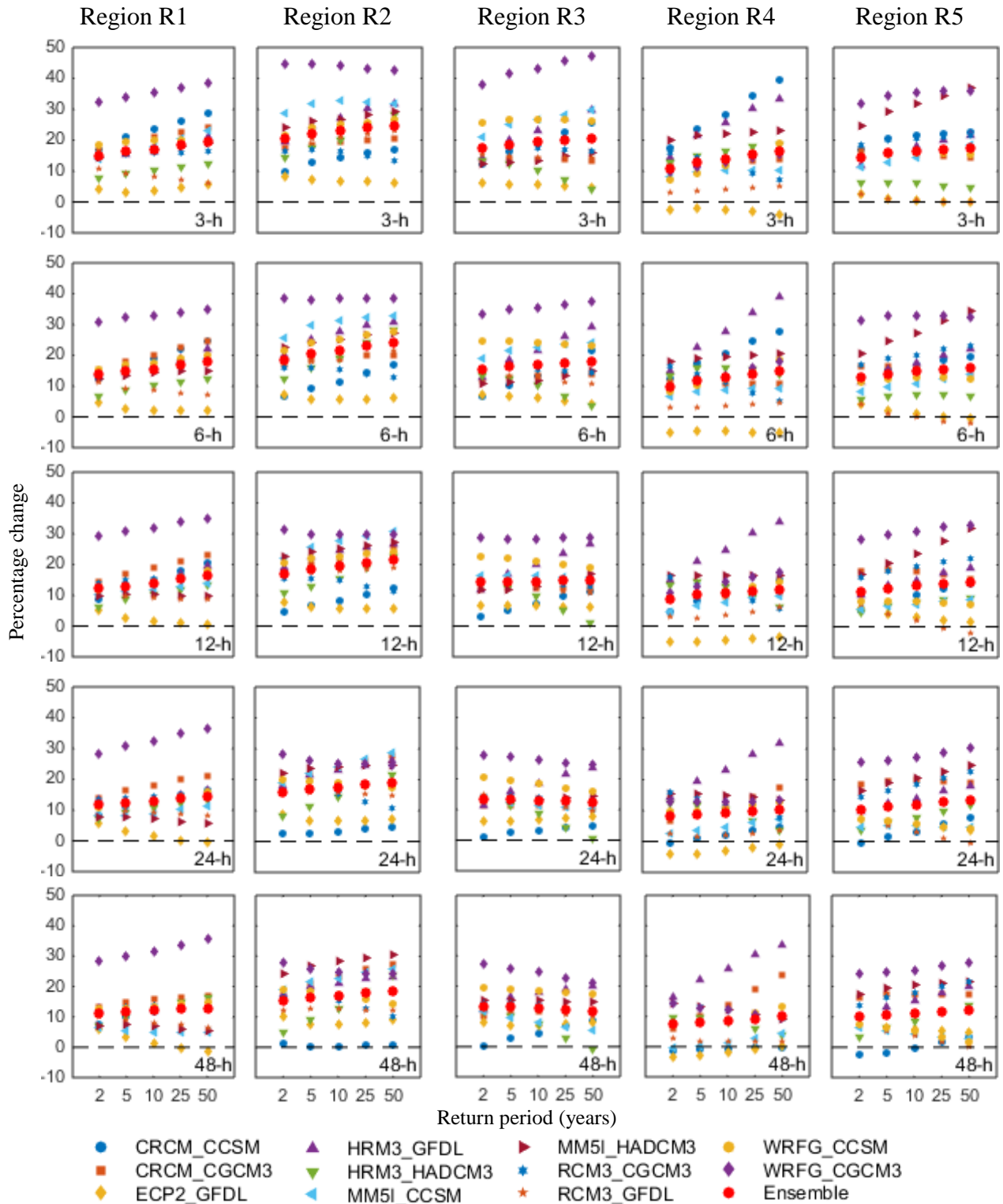


Figure 4.6: Projected changes (in %) in selected regional return levels of 3-, 6-, 12-, 24-, and 48-h extremes simulated by 11 RCM_AOGCM combinations for the 2041–2070 period with respect to the 1971–2000. Ensemble-averaged change is shown using red circle.

Analysis of significance of projected changes was performed as described in the methodology section. For all RCM_AOGCM combinations, comparisons between current and future period confidence intervals for all return periods and precipitation durations were performed individually and the percentage number of cases, where the confidence intervals did not overlap for the 11 combinations of current and future period simulations is given in Table 4.2 with respect to the return period considered. These results suggest statistically significant changes for nearly all regions, durations and return periods. For longer return periods, the percentage number is slightly less than 100% for some RCM_AOGCM combinations (Table 4.2). Only the RCM3_GFDL combination shows completely insignificant changes for region R4 for all return periods and the ECP2_GFDL combination for region R1 and R2 for some return periods. In the ensemble-averaged case, projected changes were found statistically significant for all regions, except region R4 where a slightly weaker signal was realized.

Since it was not possible to derive changes to return values of hourly and sub-hourly precipitation extremes directly based on the available simulations from the NARCCAP, the authors developed these changes based on the quantile mapping approach inspired by the scaling behavior of precipitation extremes. Therefore, before presenting projected changes to return values of hourly and sub-hourly precipitation extremes, it is useful to firstly explore the scaling behavior of observed extremes and their validation. For nine selected stations from regions R1 to R5 and based on DS2, observed return values of 2-, 5-, 10-, 25-, and 50-yr return periods were estimated for precipitation durations ranging from 5-min to 24-h and the resulting scaling behaviors are displayed in Figure 4.7. It is obvious from this figure that various return values scale within the log-log domain in both a linear and nonlinear manner, depending upon the station and return period. A similar investigation was also carried out for observed regional return values for R1 to R5 regions. The results of this investigation are shown in Figure 4.8 and the plots seem to support linear (non-linear) scaling relationships within the log-log domain for regions R1 and R4 (R2, R3 and R5). In general, return values corresponding to longer return periods (e.g. 50-yr) tend to follow nonlinear relationships. In most cases, the goodness-of-fit measure R^2 values were found close to 0.99. As the return values for RCM_NCEP simulations could not be obtained for precipitation durations smaller than 3-h due to data unavailability constraints, we evaluated the scaling hypothesis based on return values of 3-, 6-, 9-, 12-, 15-, 18-, 24-, 36-, and 48-h durations.

Table 4.2: Percentage of 95% confidence interval comparisons wherein changes in 2-, 5-, 10-, 25-, and 50-yr regional return levels of 3-, 6-, 12-, 24-, and 48-h precipitation extremes were found statistically significant.

RCM_AOGCM	Region R1					Region R2					Region R3				
	Return period (years)					Return period (years)					Return period (years)				
	2	5	10	25	50	2	5	10	25	50	2	5	10	25	50
CRCM_CCSM	100	100	100	100	100	60	60	60	60	60	40	60	60	60	60
CRCM_CGCM3	100	100	100	100	100	100	100	100	100	100	100	100	100	100	60
ECP2_GFDL	100	100	20	0	0	100	100	100	0	0	100	100	100	100	40
HRM3_GFDL	100	100	100	100	100	100	100	100	100	100	100	100	100	100	100
HRM3_HadCM3	100	100	100	100	100	100	100	100	100	100	100	100	100	0	0
MM5I_CCSM	100	100	100	80	80	100	100	100	100	100	100	100	100	80	80
MM5I_HadCM3	100	100	100	100	60	100	100	100	100	100	100	100	100	100	100
RCM3_CGCM3	100	100	100	100	100	100	100	100	100	100	100	100	100	100	100
RCM3_GFDL	100	100	100	100	40	100	100	100	100	100	100	100	100	100	100
WRFG_CCSM	100	100	100	100	100	100	100	100	100	60	100	100	100	100	60
WRFG_CGCM3	100	100	100	100	100	100	100	100	100	100	100	100	100	100	100
ENSEMBLE	100	100	100	100	100	100	100	100	100	100	100	100	100	100	100

Table 4.2 Contd.

	Region R4					Region R5				
	Return period (years)					Return period (years)				
	2	5	10	25	50	2	5	10	25	50
CRCM_CCSM	60	60	60	60	60	60	60	60	60	60
CRCM_CGCM3	100	100	100	100	80	100	100	100	100	100
ECP2_GFDL	100	100	100	20	100	80	60	40	0	0
HRM3_GFDL	100	100	100	100	100	100	100	100	100	100
HRM3_HadCM3	100	100	80	40	20	40	100	100	40	20
MM5I_CCSM	60	80	60	60	20	80	100	60	40	40
MM5I_HadCM3	100	100	100	80	60	100	100	100	100	100
RCM3_CGCM3	100	100	100	20	100	100	100	100	100	100
RCM3_GFDL	0	0	0	0	0	60	60	40	0	0
WRFG_CCSM	100	100	100	100	60	100	100	100	40	40
WRFG_CGCM3	100	100	100	100	80	100	100	100	100	100
ENSEMBLE	80	100	80	80	80	100	100	100	100	100

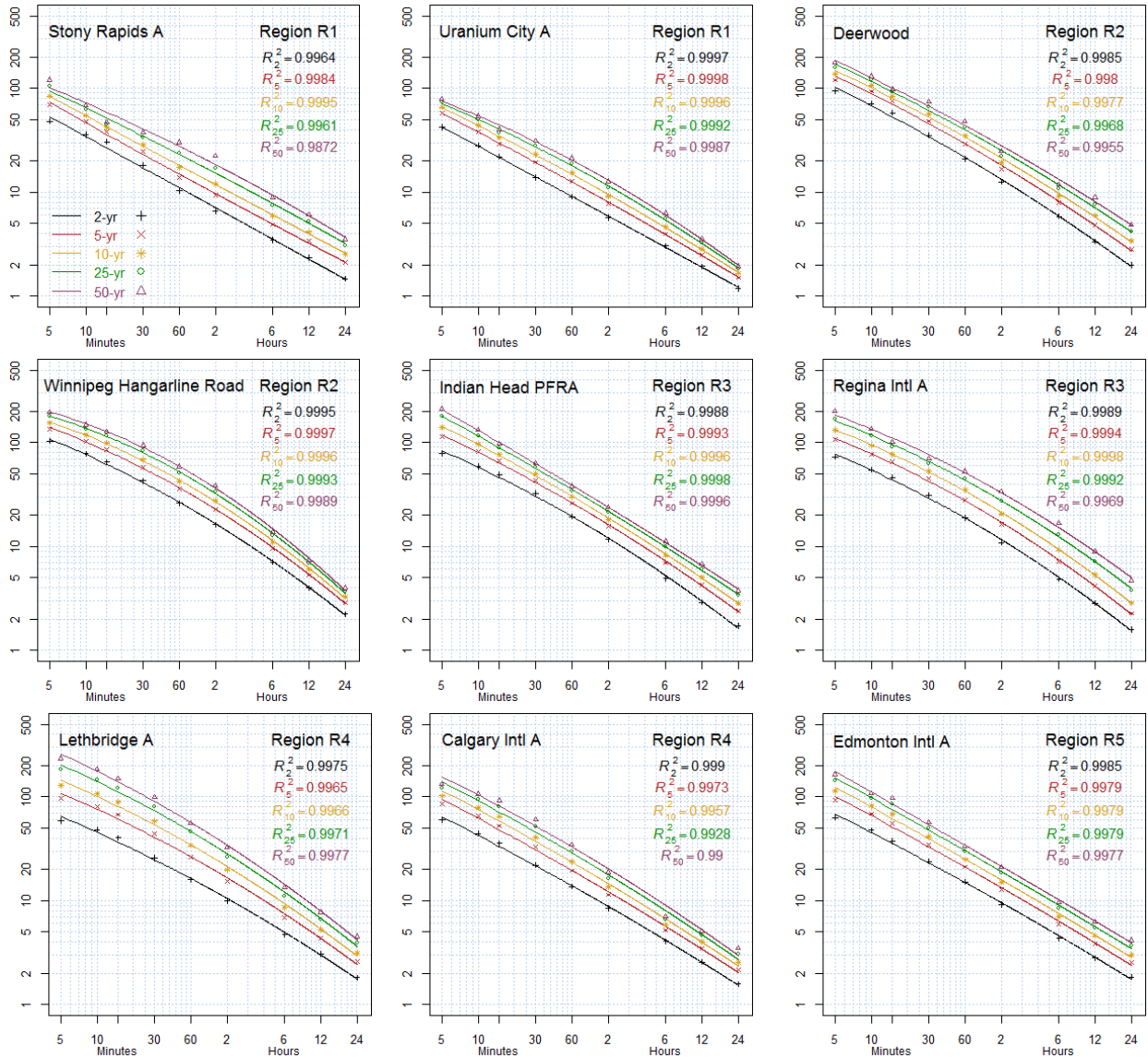


Figure 4.7: Observed precipitation intensity-duration-frequency plots (symbols) for nine selected sites from R1 to R5 regions based on precipitation extremes of 5-, 10-, 15-, 30-, 60-min, 2-, 6-, 12-, and 24-h durations (shown along the x-axis) from the engineering climate stations dataset (DS2). Scaling relationships (lines) estimated using the least-squares algorithm for each return period are also plotted and the corresponding coefficient of determination (i.e. R^2) values are shown as well.

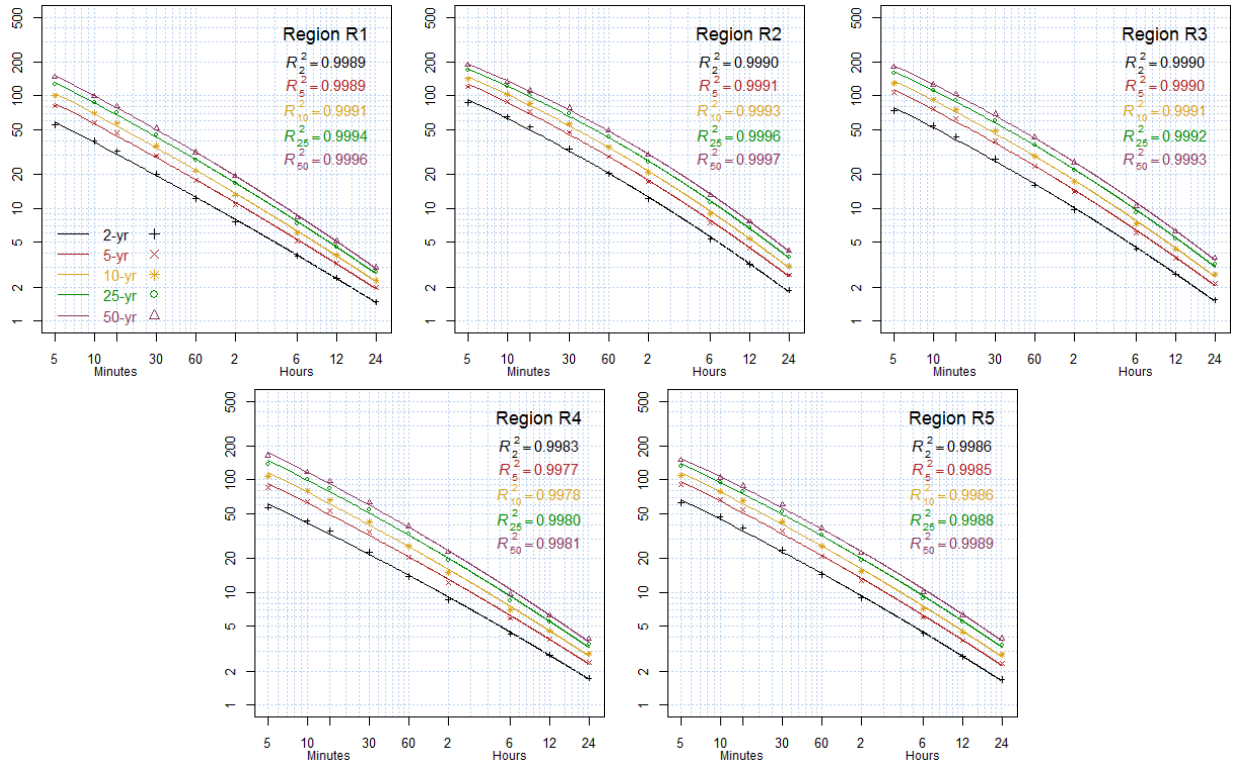


Figure 4.8: Same as in Fig. 4.7 but for observed regional precipitation intensity-duration-frequency plots (symbols) for regions R1 to R5.

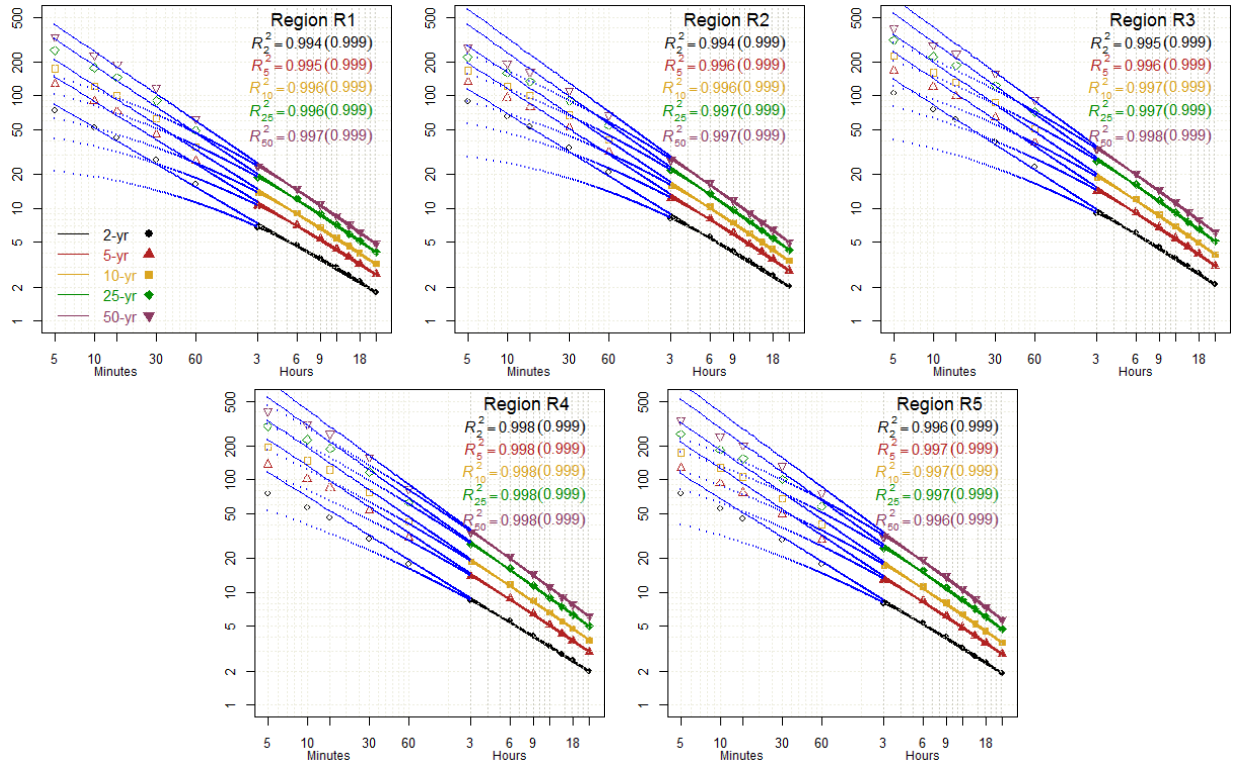


Figure 4.9: RCM3_NCEP simulated regional precipitation intensity-duration-frequency plots (filled symbols) for regions R1 to R5 based on precipitation extremes of 3-, 6-, 9-, 12-, 15-, 18-, and 24-h durations (shown along the x-axis). Linear and non-linear scaling relationships (colored solid lines) estimated using the least-squares algorithm and the corresponding coefficient of determination (i.e. R^2) values are shown in each panel first for the linear case and then for the nonlinear case in brackets. Trajectories of extrapolated linear (solid blue lines) and nonlinear (dotted blue lines) relationships for each return period are also plotted. Estimated return levels based on the quantile mapping approach are shown using corresponding unfilled symbols for 2-, 5-, 10-, 25, and 50-yr return periods.

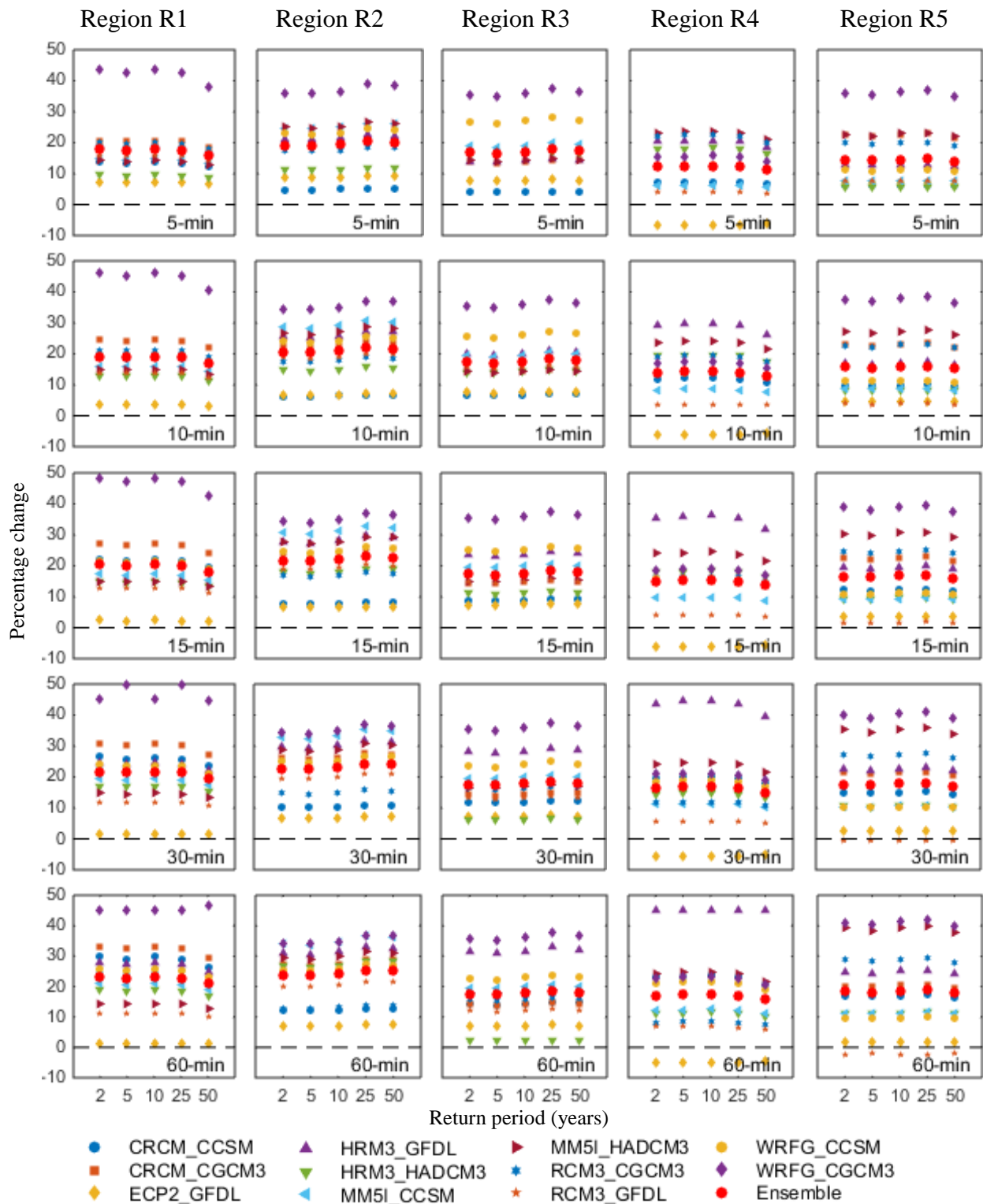


Figure 4.10: Projected changes (in %) in selected regional return levels of 5-, 10-, 15-, 30-, and 60-min extremes simulated by 11 RCM_AOGCM combinations for the 2041–2070 period with respect to the 1971–2000. Ensemble-averaged changes are shown using red circles.

Figure 4.9 shows plots of various return values (filled symbols) along with the fitted relationships (solid black, red, orange, green, and violet lines) for the RCM3_NCEP simulation. For consistency with Figure 4.7 and 4.8, return values for 36- and 48-h durations were not plotted in Figure 4.9. It is obvious from Figure 4.9 that the model-simulated return values also strongly support the scaling relationship. Similar results were noted for other RCM_NCEP simulations. However, it is not clear how the models would behave for unavailable sub-hourly extremes. Extrapolated trajectories of both linear (solid blue lines) and nonlinear (dotted blue lines) scaling relationships are also shown in Figure 4.9. These relationships are very different from each other and therefore would lead to very different extrapolated return values based on merely scaling relationships. The same observation was also found applicable for other RCM_NCEP simulations. Given this high level of uncertainty and to come up with a reasonable solution, we derived quantile mapping relationships from observed extremes for each of the five regions separately and those in turn were used to estimate expected return values of sub-hourly precipitation extremes. Sub-hourly return values were estimated by averaging estimates obtained from 6-, 12- and 24-h quantile mappings. These estimated return values are also shown in Figure 4.9 for RCM3 (unfilled symbols). Like this RCM, other RCMs also showed different scaling behaviors for different return periods and regions (see Appendix C.3); some of these were similar to the linear behavior while others showed deviations from this behavior. Almost similar results were also noted for RCM_AOGCM current and future period simulations (see Appendix C.4). Based on the above discussed results, current and future period return values for unavailable precipitation durations (i.e. 5-, 10-, 15-, 30-, and 60-min) were estimated, which in turn were used to develop projected changes to various return values. Figure 4.10 shows projected changes in various return values of hourly and sub-hourly precipitation extremes. For all simulations and regions, the percentage increase or decrease in return values is relatively larger than that presented in Figure 4.6. Larger projected changes in return values are simulated by WRFG_CGCM3 for regions R1, R2, R3 and R5 and by HRM3_GFDL for region R4. Decreases in return values, which are around -6%, are simulated by ECP2_GFDL, mainly for region R4. The range of ensemble-averaged changes for all durations and return periods is 15–23% for region R1, 18–25% for region R2, 16–18% for region R3, 11–17% for region R4, and 14–18% for region R5.

4.5 Conclusions

From the various analyses presented in this paper, the following main conclusions were reached:

1. The study area (i.e. the Alberta, Saskatchewan and Manitoba Provinces of Canada) selected for this study was divided previously into five climatically homogeneous precipitation fuzzy regions by Asong et al. (2014, 2016). These regions were adopted for this study after constraining them to form contiguous regions. These regions were also found statistically homogeneous based on characteristics of short- and long-duration precipitation extremes used in the study. This verification of climatic regions facilitated RFA of precipitation extremes for each of the five regions. To model precipitation extremes corresponding to various durations, the GEV, PE3 and GNO distributions were found equally suitable. Based on theoretical considerations and empirical evidence provided by goodness-of-fit statistical tests, the GEV distribution was selected for developing frequency-magnitude relationships at the regional, grid-cell level and local scales for both observed and RCM simulated extremes.
2. Comparison of 2-, 5-, 10-, 25-, and 50-yr return values, derived from NCEP-driven RCM simulations with those derived from observed precipitation extremes for the 1981–2000 period, showed an underestimation by most of the models (i.e. CRCM, HRM3, MM5I and WRFG), except ECP2 and RCM3, which produced overestimated return values for longer return periods, with increasingly larger differences for long-duration precipitation extremes. Among all RCMs, the return values simulated by MM5I (followed by WRFG) were found to be quite close to the return values derived from observed data. Overall, the performance errors were much smaller for the ensemble-averaged case than that for individual RCMs. Overall, the lateral boundary forcing errors, which were obtained by comparing return values from NCEP- and AOGCM-driven simulations for the 1981–2000 period, were found smaller than performance errors.
3. The projected changes to 2-, 5-, 10-, 25-, and 50-yr return values of 3-, 6-, 12-, 24-, and 48-h precipitation extremes developed for the 2041–2070 period with respect to the 1971–2000 period were mostly positive and were found as high as 50% for some RCM_AOGCM combinations and regions. Comparatively, ensemble-averaged changes were found to lie within the 6–23% range for all durations and return periods considered. Irrespective of

precipitation durations and return periods, region R2 (southeastern part of the study area) was associated with relatively larger projected changes and region R4 (southwestern part of the study area) with smaller changes. Overall, for 3- and 6-h extremes, the projected changes were found within the 10–23% range and within the 6–18% range for 24- and 48-h extremes. It is noteworthy to mention that most of these projected changes for the future period were found statistically significant for all regions and most of the precipitation durations and return periods considered.

4. The NARCCAP RCM simulations did not permit direct estimation of various return values of hourly and sub-hourly (i.e. 5-, 10-, 15-, 30-, and 60-min) precipitation extremes. Therefore, the authors filled this gap by estimating selected return values of hourly and sub-hourly precipitation extremes following the quantile mapping approach inspired by the scaling behavior of 3-, 6-, 9-, 12-, 15-, 18-, 24-, 36-, and 48-h precipitation extremes noted in both NCEP- and AOGCM-driven RCM simulations. Projected changes in return values of 5-, 10-, 15-, 30-, and 60-min precipitation extremes were developed for all RCM_AOGCM current and future period simulation pairs. Considering the ensemble averaged case, maximum increases of the order of 25% were found for 60-min precipitation extremes in region R2 and minimum increases of the order of 12% for 5-min precipitation extremes in region R4, with intermediate results for the remainder of the regions. As mentioned above, one should bear in mind that these changes were developed based on the quantile mapping approach rather than original model simulated return values and therefore, they need to be evaluated carefully for applications in high value projects.

Finally, it is worth mentioning that projected changes in the magnitude of short-duration (ranging from minutes to a few hours) extremes are highly important in ensuring proper functioning of urban drainage infrastructure and flood control structures in fast responding areas while those in the magnitude of longer duration (ranging from 24- to 48-h) extremes are important for water management and storage-related activities. As a word of caution, the results presented in this study need to be interpreted carefully due to the various sources of uncertainties associated with RCM_AOGCM simulations discussed in the paper. However, the information on projected changes will undoubtedly be useful in adaptation related decision-making.

Acknowledgements

The authors would like to thank the NARCCAP project team for the RCM simulations used in this study. The financial support from the Canada Excellence Research Chair in Water Security and School of Environment and Sustainability, University of Saskatchewan, is also acknowledged. The language editing support provided by Michelle-Andre Martel from the GIWS is much appreciated.

References

- Asong ZE, Khaliq MN, Wheeler HS (2016) Multisite multivariate modeling of daily precipitation and temperature in the Canadian Prairie Provinces using generalized linear models. *Clim Dyn* Doi:10.1007/s00382-016-3004-z
- Asong ZE, Khaliq MN, Wheeler HS (2014) Regionalization of precipitation characteristics in the Canadian Prairie Provinces using large-scale atmospheric covariates and geophysical attributes. *Stoch Environ Res Risk Assess*. Doi 10.1007/s0047-014-0918-z.
- Beniston M, Stephenson DB, Christenson OB, Ferro CAT, Frei C, Goyette S, Halsnaes K, Holt T, Jylhä K, Koffi B, Palutikof J, Schöll R, Semmler T, Woth K (2007) Future extreme events in European climate: an exploration of regional climate model projections. *Clim Change* 81:71–95.
- Beniston M, Stephenson DB, Christenson OB, Ferro CAT, Frei C, Goyette S, Halsnaes K, Holt T, Jylhä K, Koffi B, Palutikof J, Schöll R, Semmler T, Woth K (2007) Future extreme events in European climate: an exploration of regional climate model projections. *Clim Change* 81:71–95
- Boé J, Terray L, Habets F, Martin E (2007) Statistical and dynamical downscaling of the Seine basin climate for hydro-meteorological studies. *Int J Climatol* 27:1643-1655
- Caldwell P (2010) California wintertime precipitation bias in regional and global climate models. *J Appl Meteorol Climatol* 49:2147–2158
- Christensen JH, Carter TR, Rummukainen M, Amanatidis G (2007) Evaluating the performance and utility of regional climate models: the PRUDENCE project. *Clim Change* 81:1–6
- Christensen JH, Rummukainen M, Lenderink G (2009) Formulation of very-high-resolution regional climate model ensembles for Europe. In: van der Linden P, Mitchell JFB (eds)

- ENSEMBLES: climate change and its impacts: summary of research and results from the ENSEMBLES project. Met Office Hadley Centre, UK, pp 47–58
- Coles S (2001) An introduction to statistical modeling of extreme values. Springer Publishers, Great Britain
- de Elía R et al. (2008) Evaluation of uncertainties in the CRCM-simulated North American climate. *Clim Dyn* 30(2):113-132
- Dey B (1982) Nature and possible causes of drought on the Canadian prairies-case studies. *J Clim* 2:233-249
- Efron B, Tibshirani RJ (1993) An Introduction to the Bootstrap. Chapman and Hall, 436 pp.
- Gan TY (2000) Reducing vulnerability of water resources of Canadian prairies to potential droughts and possible climatic warming. *Water Resour. Manage* 14(2), 111–135.
- Gao Y, Leung LR, Salathé EP Jr, Dominguez F, Nijssen B, Lettenmaier DP (2012) Moisture flux convergence in regional and global climate models: implications for droughts in the southwestern United States under climate change. *Geophys Res Lett* 39:L09711. doi:10.1029/2012GL051560
- Green PJ, Silverman BW (1993) Nonparametric regression and generalized linear models: a roughness penalty approach. CRC press, 184 pp
- Haddad K, Rahman A (2014) Design rainfall estimation and changes. *Handbook on Engineering Hydrology, Modeling, Climate Change and Variability*. CRC press, 634 pp
- Hagedorn R, Doblas-Reyes FJ, Palmer TN (2005) The rationale behind the success of multi-model ensembles in seasonal forecasting–I. Basic concept. *Tellus* 57A:219–233
- Hall MJ, van den Boogaard HFP, Fernando RC, Mynett AE (2004) The construction of confidence intervals for frequency analysis using resampling techniques. *Hydrol Earth Syst Sci* 8:235–246
- Hanel M, Buishand TA (2012) Multi-model analysis of RCM simulated 1-day to 30-day seasonal precipitation extremes in the Czech Republic. *J Hydrol* 412-413:141-150
- Hogg EH, Price DT, Black TA (2000) Postulated feedbacks of deciduous forest phenology on seasonal climate patterns in the Western Canadian Interior, *J Clim* 13: 4229–4243
- Hosking JRM, Wallis JR (1997) *Regional frequency analysis*. Cambridge University Press.

- IPCC (2007) Climate change: the physical science basis—summary for policy makers. Contribution of Working Group 1 to the Fourth Assessment Report of the Intergovernmental Panel on Climate Change (IPCC), Geneva, Switzerland
- Jeong DI, Sushama L, Diro GT, Khaliq MN, Beltrami H, Caya D (2015a) Projected changes to high temperature events for Canada based on regional climate model ensemble. *Clim Dyn* DOI 10.1007/s00382-015-2759-y
- Jeong DI, Sushama L, Diro GT, Khaliq MN (2015b) Projected changes to winter temperature characteristics over Canada based on an RCM ensemble. *Clim Dyn* DOI 10.1007/s00382-015-2906-5
- Jeong DI, Sushama L, Khaliq MN (2014) The role of temperature in drought projections over North America. *Clim Change* 127 (2): 289–303
- Khaliq MN, Mladjic B, Sushama L (2015) Projected changes to short- and long-duration precipitation extremes over the greater montreal area based on regional climate model simulations. Proceedings of the 22nd Hydrotechnical Conference, Canadian Society for Civil Engineering, Montreal, QC, Canada, pp. 10
- Khaliq MN, Sushama L, Monette A, Wheeler H (2014) Seasonal and extreme precipitation characteristics for the watersheds of the Canadian Prairie Provinces as simulated by the NARCCAP multi-RCM ensemble. *Clim Dyn* DOI 10.1007/s00382-014-2235-0
- Khaliq MN, Ouarda TBMJ, Sushama L, Gachon P (2009) Identification of hydrological trends in the presence of serial and cross correlations: A review of selected methods and their application to annual flow regimes of Canadian rivers. *J Hydrol* 368, 117–130.
- Mailhot A, Bearegard I, Talbot G, Caya D, Biner S (2012) Future changes in intense precipitation over Canada assessed from multi-model NARCCAP ensemble simulations, *Int J Climatol* Doi:10.1002/joc.2343
- Masud MB, Khaliq MN, Wheeler HS (2015) Future changes to drought characteristics over the Canadian Prairie Provinces based on NARCCAP multi-RCM ensemble. *Clim Dyn* (CLDY-S-16-00003; under review)
- May W (2008) Potential future changes in the characteristics of daily precipitation in Europe simulated by the HIRHAM regional climate model. *Clim Dyn* 30:581–603

- Mearns LO, Gutowski WJ, Jones R, Leung L-Y, McGinnis S, Nunes AMB, Qian Y (2009) A regional climate change assessment program for North America. *Eos Trans Am Geophys Union* 90:311–312
- Mearns LO et al. (2012) The North American Regional Climate Change Assessment Program: Overview of phase I results. *Bull Amer Meteor Soc* 93:1337–1362. Doi: <http://dx.doi.org/10.1175/BAMS-D-11-00223.1>
- Mladjic B, Sushama L, Khaliq MN, Laprise R, Caya D, Roy R (2011) Canadian RCM projected changes to extreme precipitation characteristics over Canada. *J Clim* 24:2565–2584
- Monette A, Sushama L, Khaliq MN, Laprise R, Roy R (2012) Projected changes to precipitation extremes for Northeast Canadian watersheds using a multi-RCM ensemble. *J Geophys Res* 117:D13106. doi:10.1029/2012JD017543
- Nikulin G, Kjellström E, Hansson U, Strandberg G, Ullerstig A (2011) Evaluation and future projections of temperature, precipitation and wind extremes over Europe in an ensemble of regional climate simulations, *Tellus, Ser. A*, 63(1), 41–55, doi:10.1111/j.1600-0870.2010.00466.x.
- Nakicenovic N et al (2000) *Special Report on Emissions Scenarios: A special report of working group III of the intergovernmental panel on climate change*, Cambridge University Press, Cambridge, U.K., 599 pp. Available online at: <http://www.grida.no/climate/ipcc/emission/index.htm>
- Phillips D (1990) *The Climates of Canada*. Cat. No. En56-1/1990E, Supply and Services Canada.
- Sushama L, Laprise R, Caya D, Frigon A, Slivitzky M (2006) Canadian RCM projected climate-change signal and its sensitivity to model errors. *Int J Climatol* 26:2141-2159
- van Pelt SC, Beersma JJ, Buishand TA, van den Hurk, BJJM, Kabat P (2012) Future changes in extreme precipitation in the Rhine basin based on global and regional climate model simulations. *Hydrol. Earth Syst Sci* 16:4517-4530
- Wehner MF (2013) Very extreme seasonal precipitation in the NARCCAP ensemble: model performance and projections. *Clim Dyn* Doi:10.1007/s00382-012-1393-1
- Wheater HS, Gober P (2013) Water security in the Canadian prairies: science and management challenges, *Philos Trans Roy Soc A* Doi:10.1098/rsta.2012.0409

CHAPTER 5

SUMMARY, CONCLUSIONS, AND FUTURE WORK

5.1 Summary

It has become unequivocal that climate change resulting from anthropogenic modification of the GHG concentration of the atmosphere is projected to continue in the future (IPCC, 2013). Changes in climate have been the subject of extensive study considering the impact on socioeconomic infrastructure. The primary tools to assess future climate change are the Atmosphere-Ocean General Circulation Model (AOGCM) and Regional Climate Model (RCM) simulations produced when those models are integrated from the recent past to some time-point in the future (IPCC, 2007). Currently, RCMs offer higher spatial resolution than GCMs and can therefore represent finer scale features such as complex topography, land use, and cloud cover, which are hardly resolved by GCMs. Though the use of a single RCM is not uncommon, combinations of results from many RCMs with different boundary forcings can lead to a more robust and reliable outcome by reducing sources of uncertainties inherited from the driving AOGCM and deficiencies in the parameterization schemes of individual RCMs. The same paradigm was adopted in this study.

This study explored spatial patterns of historical droughts in the Saskatchewan River Basin (SRB) and developed projected changes to dry and wet climate extremes over the Canadian Prairie Provinces of Alberta, Saskatchewan, and Manitoba as simulated by the North American Regional Climate Change Assessment Program (NARCCAP) multi-RCM ensemble. Specific objectives of the study were to (1) characterize historical drought events in terms of severity, duration, and maximum severity; (2) analyze drought characteristics within the framework of a changing climate; and (3) develop projected changes to short- and long-duration precipitation magnitude-frequency relationships within the framework of regional frequency analysis (RFA) approach.

Droughts are considered to be multifaceted extreme events that can inflict considerable damage to water resources and agriculture. An understanding of spatial and temporal characteristics of historical droughts is needed to mitigate the harmful effects of droughts on communities. The first objective was focused on the SRB which is currently experiencing huge water demands due to increased usage of water for agriculture, industrial, and domestic purposes.

Recently, the SRB has drawn global attention due to challenging water related issues, and it is now one of the 10 GEWEX (Global Energy and Water Exchanges) Regional Hydroclimate Projects in the world. The behavior of meteorological droughts was investigated at the level of 13 watersheds that represent natural subdivisions of the SRB. Conventional univariate and newly emerging copula-based bivariate frequency analyses were used to characterize historical drought events in terms of drought severity, duration, and maximum severity on the basis of Standardized Precipitation Index (SPI) and Standardized Precipitation Evapotranspiration Index (SPEI). The use of both SPI and SPEI helped understand the influence of temperature in defining drought events.

As climate change is an ongoing process, it is relevant to study how climate change will impact characteristics of dry and wet extremes in a future climate. The second objective of the study was achieved using the NARCCAP multi-RCM ensemble simulations for the Canadian Prairie Provinces of Alberta, Saskatchewan, and Manitoba at the level of 15 regions the study area was divided into. These regions were validated through conventional univariate and newly emerging bivariate homogeneity testing approaches. After identifying drought events based on SPI and SPEI, drought characteristics were modelled using the univariate RFA approach and copula-based multivariate approaches. Both bi- and trivariate frequency analyses were performed to study projected changes in drought characteristics.

As mentioned above, to achieve the second objective, the impacts of climate change on dry extremes were analyzed. However, the study area is also prone to heavy precipitation events triggered by convective activity leading to occasional flooding. Therefore, impacts of climate change to wet extremes were also analyzed to achieve the third objective of the study. In this analysis, seasonal (April-October) precipitation extremes of 3-, 6-, 12-, 24-, and 48-h duration were employed and return levels corresponding to 2-, 5-, 10-, 25-, and 50-yr return periods were studied. For the calculation of return levels, a RFA approach was used. This approach was used since it can address the impact of deficiencies originating from small samples on the estimated return levels. This rationale of the RFA approach was appealing because the maximum sample size of extremes employed in this study consisted of just 30 extreme values.

5.2 Conclusions

The research reported in this thesis led to the following main conclusions:

- The analysis of spatial patterns of drought severity and duration showed that the southern parts of the SRB and the areas surrounding the Alberta-Saskatchewan border have experienced intense droughts, historically. The magnitudes of drought severity and duration were found largely consistent, that is, drought events of higher severity normally last longer and milder droughts are shorter in duration. For the historical climate, the inclusion of temperature in the SPEI drought index for delineating drought-sensitive regions showed little effect on drought characteristics. However, predicted increases in future temperatures are expected to play an important role in drought analysis and, therefore, the SPEI was retained for the analysis of projected changes to drought characteristics part of the study.
- The results of the bivariate frequency analyses suggested that the western parts of the North Saskatchewan River watershed, a major portion of the Red Deer River watershed, and almost the entire southern part of the SRB are associated with larger values of joint occurrence probability of drought severity and duration exceeding their corresponding thresholds at the same time. Compared to this, eastern parts of the North Saskatchewan River, the Saskatchewan River, and the Carrot River watersheds were found to be associated with smaller values of the same joint occurrence probability, suggesting a low risk of droughts in these areas.
- To facilitate future drought risk analysis, the study area was divided into 15 geographic regions and the statistical homogeneity of these regions was verified based on univariate and bivariate homogeneity analysis approaches. Based on the results of bivariate homogeneity analysis approach, it was found that all regions could be considered homogeneous, a result which was not supported by the univariate approach with equal strength. The latter approach flagged a few regions as possibly heterogeneous, particularly in the case of drought duration. Thus, the results of this study highlight the importance of testing a region based on the multivariate criterion and not just the univariate criterion often used in homogeneity testing related studies in different parts of the world.
- Most of the RCM_AOGCM simulations considered in the study projected an increase in mean drought severity for the southern parts of the study area, while some model combinations projected increases for the entire study area. Though similar results were found in the case of return levels of drought severity and duration for the southern regions, some differences were noted between models and between different return periods considered.

Comparison of analyses based on both SPI and SPEI revealed that the effect of temperature in drought characterization is very important for future drought risk assessment in this region. Similar results were realized for the agricultural growing season (May–August), where the drought characteristics were projected to increase with relatively higher margins.

- In an attempt to delineate drought sensitive regions, projected changes in joint occurrence probabilities of drought characteristics for bi- and trivariate analyses were spatially mapped over the study area. According to this evaluation, central and southern regions were found to be highly drought vulnerable compared to northern regions, which were associated with less frequent droughts in the future, with some differences noted between the bi- and trivariate cases and the drought indices considered. According to the current investigation, multivariate joint occurrence probabilities from the multivariate analyses can predict drought probability more objectively and comprehensively than the univariate approach.
- Projected changes to regional return levels of 3-, 6-, 12-, 24-, and 48-h seasonal (April–October) precipitation extremes were found mostly positive and were as high as 50% for some simulations and regions. Compared to this, ensemble-averaged changes were found to lie between 6 and 23% for the above mentioned precipitation durations and 2-, 5-, 10-, 25-, and 50-yr return levels. Irrespective of precipitation duration and return period, the southeastern part of the study area was associated with much larger projected changes than the southwestern part of the study region. Most of the projected changes for the future period were found statistically significant based on the results obtained with the nonparametric vector bootstrap resampling method, which is generally considered more suitable for spatially correlated datasets, such as outputs from climate models.
- As the climate model simulations used in this study did not permit sub-hourly precipitation realizations, an attempt was made to estimate return levels of sub-hourly precipitation extremes from 6-, 12-, and 24-h return levels following the quantile mapping approach. Following this approach, projected changes to precipitation extremes of 5-, 10-, 15-, 30-, and 60-min durations were developed. Ensemble-averaged projected changes to 2-, 5-, 10-, 25-, and 50-year return values were found to vary between 12 and 25% for all durations and regions. Irrespective of precipitation duration and return period, larger projected changes were found in the southeastern part while smaller changes were found in southeastern part of the study area. Because of the importance of urban centres in regional socioeconomic

activities, climate change related information for short-duration precipitation extremes is in high demand for assessing adequacy of urban drainage infrastructures in a changing climate.

5.3 Future Work

The current study could be advanced in numerous ways. Some potential avenues are discussed below:

- As the climate change scenarios have shown that hydro-meteorological regimes of a region or watershed will likely be modified significantly over the next 50–100 years (IPCC, 2013), a future study might consider applying a non-stationary frequency analysis approach using much longer, but continuous, simulations than used in this study.
- Future research could investigate explicitly the impact of wind speed, humidity, solar radiation, and soil moisture on drought characterization using more complex potential evapotranspiration estimation methods. It is anticipated that the results of such a study will hardly change the results of this study but it will be worthwhile to explore this methodology in order to ratify general findings of this study.
- In this study, considerable influence of the driving AOGCM on the magnitude of projected changes to dry and wet extremes was noticed. Therefore, the use of a much bigger AOGCM ensemble than used in this study at the RCM boundaries would be helpful in addressing the uncertainties associated with the magnitude and sign of projected changes. It is hoped that the associated computing costs which often restrict such possibilities may reduce over the coming years due to advances in the computing power and data storage facilities.
- Projected changes to sub-hourly extremes were derived using the quantile mapping approach after learning from the scaling behavior of extremes of 3-h and higher durations. This technique was followed due to unavailability of RCM simulations for durations shorter than 3-h. Therefore, it would be interesting to evaluate the true behavior of sub-hourly extremes when simulations from the same RCMs as used in this study will become available in the future.
- Snow sublimation has been shown to be an important part of water balance in the Canadian Prairies where blowing snow sublimation losses have been estimated 15 to 41% of annual snowfall (MacDonald et al., 2010) and on average $57 \pm 31\%$ of snowfall ablated through the winter via some combination of evaporation, sublimation, wind redistribution, or mid-winter

melt and infiltration (J. McDonnell 2016, personal communication). Therefore, it would be interesting to explore the role of evapo-sublimation of snow for drought risk analysis using physically-based hydrological models.

References

- IPCC (2013) Climate Change 2013: The Physical Science Basis. Contribution of Working Group I to the Fifth Assessment Report of the Intergovernmental Panel on Climate Change, T. F. Stocker et al. (Eds.), Cambridge University Press, Cambridge and New York, 1–1535.
- IPCC (2007) Climate Change 2007: The physical science basis. Contribution of working group I to the fourth assessment report of the intergovernmental panel on climate change [Solomon, S., D. Qin, M. Manning, Z. Chen, M. Marquis, K.B. Averyt, M. Tignor and H.L. Miller (eds.)]. Cambridge University Press, Cambridge, United Kingdom and New York, NY, USA, 996 pp.
- MacDonald MK, Pomeroy JW, Pietroniro A (2010) On the importance of sublimation to an alpine snow mass balance in the Canadian Rocky Mountains. *Hydrology and Earth System Sciences* 14: 1401-1415. DOI: 10.5194/hess-14-1401-2010

APPENDIX A: APPENDICES FOR CHAPTER 3

A.1 Multivariate L-moments

Let $X^{(j)}$ be a random variable with distribution function F_j , for $j = 1, 2$. By analogy with the covariance representation for L-moments, and also by analogy with the central comoments, Serfling and Xiao (2007) defined k_{th} L- comoment as follows:

$$\lambda_{k[ij]} = \text{Cov}\left(X^{(i)}, P_{k-1}^*\left(F_j(X^{(j)})\right)\right), i, j = 1, 2 \text{ and } k = 2, 3, \dots \quad (\text{A1.1})$$

where P_k^* is the shifted Legendre polynomial. For example, the k_{th} L- comoment of $X^{(1)}$ with respect to $X^{(2)}$ is:

$$\lambda_{k[12]} = \text{Cov}\left(X^{(1)}, P_{k-1}^*\left(F_2(X^{(2)})\right)\right) \quad (\text{A1.2})$$

Particularly, the first L- comoment elements are (Chebana and Ouarda, 2007):

$$\lambda_{2[12]} = 2\text{Cov}\left(X^{(1)}, F_2(X^{(2)})\right) \quad (\text{A1.3})$$

$$\lambda_{3[12]} = 6\text{Cov}\left(X^{(1)}, (F_2(X^{(2)}) - 1/2)^2\right)$$

$$\lambda_{4[12]} = \text{Cov}\left(X^{(1)}, 20(F_2(X^{(2)}) - 1/2)^3 - 3\left(F_2(X^{(2)}) - \frac{1}{2}\right) + 1\right)$$

which are the L- covariance, L- coskewness and L- cokurtosis, respectively. Therefore, L- comoment coefficients are given by:

$$\tau_{k[12]} = \frac{\lambda_{k[12]}}{\lambda_2^{(1)}}, \text{ for } k \geq 3 \text{ and} \quad (\text{A1.4})$$

$$\tau_{2[12]} = \frac{\lambda_{2[12]}}{\lambda_1^{(1)}}, \text{ for } k \geq 2$$

The matrix Λ_k of the L- comoment coefficients is written as:

$$\Lambda_k^* = (\tau_{k[ij]})_{i,j=1,2} = \begin{pmatrix} \tau_{k[11]} & \tau_{k[12]} \\ \tau_{k[21]} & \tau_{k[22]} \end{pmatrix} \quad (\text{A1.5})$$

Particularly, for $k = 2$ the L- covariation matrix is given by:

$$\Lambda_2^* = \begin{pmatrix} \tau_{2[11]} & \tau_{2[12]} \\ \tau_{2[21]} & \tau_{2[22]} \end{pmatrix} \quad (\text{A1.6})$$

According to Serfling and Xiao (2007), the L- comoments are similar in structure and behavior to the univariate L- moments (Hosking and Wallis, 1993) and capture their attractive properties.

A.2 Multivariate heterogeneity test

Chebana and Ouarda (2007) proposed multivariate heterogeneity test which is analogous to the statistic given by Hosking and Wallis (1993) for univariate heterogeneity test. According to Chebana and Ouarda (2007), the statistic $V_{\|\cdot\|}$ is defined as:

$$V_{\|\cdot\|} = \left(\left(\sum_{i=1}^{N_s} n_i \right)^{-1} \sum_{i=1}^{N_s} n_i \|\Lambda_2^{*(i)} - \overline{\Lambda_2^*}\|^2 \right)^{1/2} \quad (\text{A2.1})$$

where $\|\cdot\|$ is the norm of matrix V . $\Lambda_2^{*(i)}$ is the L -covariation matrix for site i with record length n_i , $i = 1, \dots, N_s$.

$$\Lambda_2^* = \left(\sum_{i=1}^{N_s} n_i \right)^{-1} \sum_{i=1}^{N_s} n_i \Lambda_2^{*(i)} \quad (\text{A2.2})$$

In case of one variable, the statistic $V_{\|\cdot\|}$ reduces to the V statistic of Hosking and Wallis (1993) whatever the norm taken. The heterogeneity measure of a set of sites is given by:

$$H_{\|\cdot\|} = \frac{V_{\|\cdot\|} - \mu_{V_{\text{sim}}}}{\sigma_{V_{\text{sim}}}} \quad (\text{A2.3})$$

where $\mu_{V_{\text{sim}}}$ and $\sigma_{V_{\text{sim}}}$ are the mean and standard deviation of the N_{sim} values of $V_{\|\cdot\|}$ of simulated regions. The Gumbel bivariate copula with the marginal 4-parameter Kappa distributions are the bivariate distribution on which the simulations are carried out to compute $\mu_{V_{\text{sim}}}$ and $\sigma_{V_{\text{sim}}}$. A region is said to be heterogeneous if H is sufficiently large. Hosking and Wallis (1997) suggested that a region is considered as “homogeneous” if $H_{\|\cdot\|} < 1$, “acceptably homogeneous” if $1 < H_{\|\cdot\|} < 2$ and “definitely heterogeneous” if $H_{\|\cdot\|} \geq 2$.

APPENDIX B: SUPPORTING MATERIALS FOR CHAPTER 3

B.1 Introduction

In this supplementary material projected changes to annual precipitation and potential evapotranspiration for the future compared to the current climate are presented to support the results of projected changes to drought characteristics presented in Chapter 3. The changes in precipitation and evapotranspiration are the underlying mechanisms which drive changes to drought characteristics. A comparison of Figs. B1 and B2 and Figs. 3.8(a), 3.9(a) and 3.10(a) demonstrates that positive changes to drought severity for the future 2041–2070 period appear to be driven by increases in the potential evapotranspiration for most of the RCM-AOGCM combinations. However, complex interactions between changes in potential evapotranspiration and precipitation and the memory effect induced by the time-scale of the drought indices can also be noted, particularly for the HadCM3 driven RCMs. Projected changes to the mean annual temperature over the study area range from 1 to 3°C. Though there is no direct connection between the six-month time scale used in the analysis of drought characteristics and the annual time window used in the supplementary material, the results do provide some useful insights as to the state of precipitation, evapotranspiration and temperature for the future with respect to the current climate.

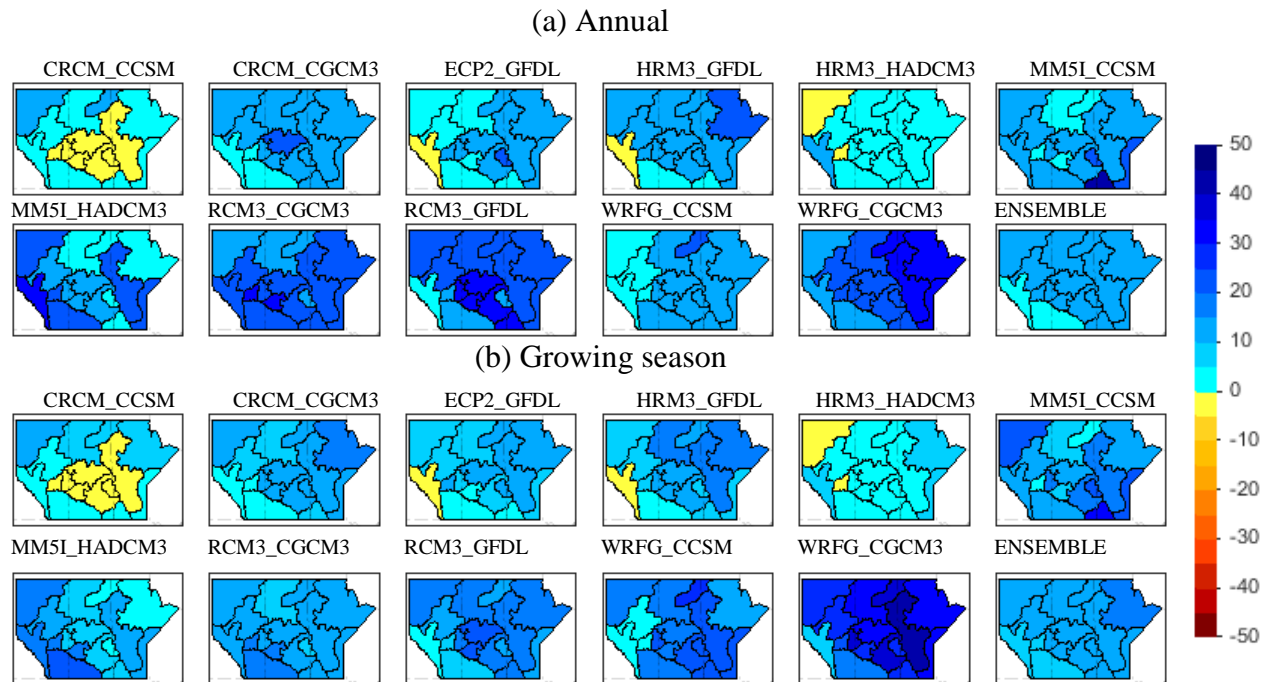


Figure B1: Projected changes (in %) to annual and growing seasonal precipitation as simulated by various RCM-AOGCM combinations along with the ensemble averaged values for the 2041-2070 period with respect to the current 1970-1999 period.

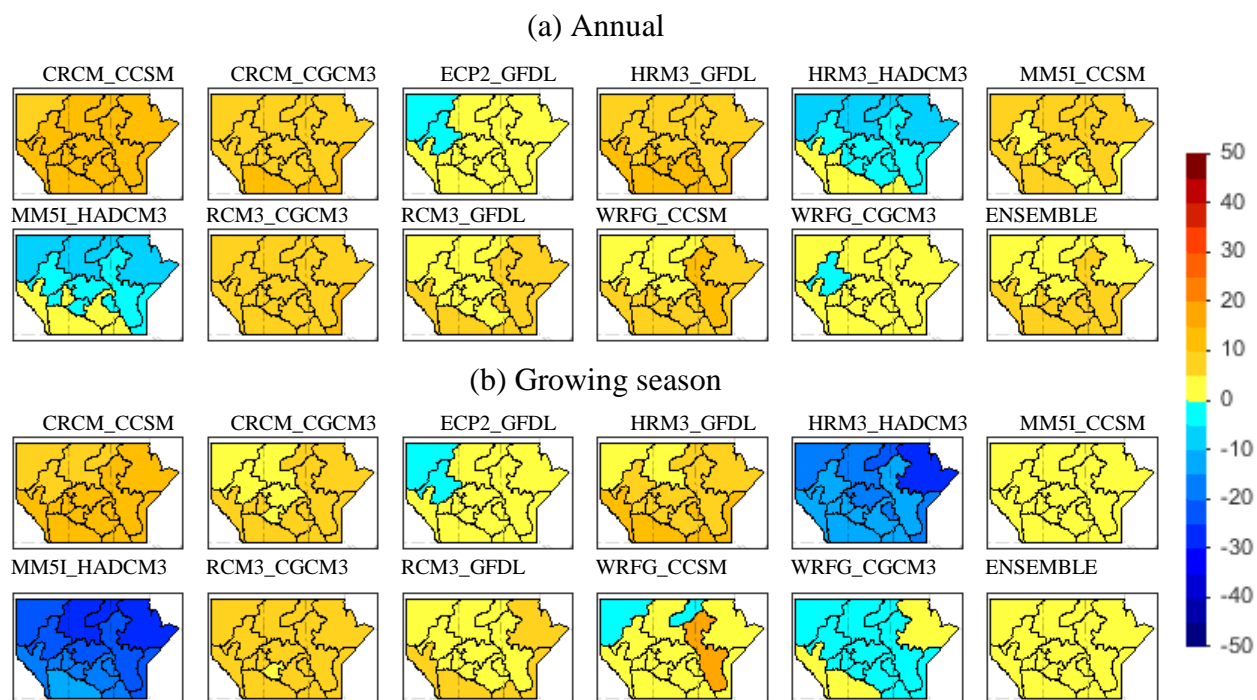


Figure B2: Projected changes (in %) to annual and growing seasonal potential evapotranspiration as simulated by various RCM-AOGCM combinations along with the ensemble averaged values for the 2041-2070 period with respect to the current 1970-1999 period.

APPENDIX C: SUPPORTING MATERIALS FOR CHAPTER 4

This appendix contains four sections. Section C.1 consists of Figs. C1 and C2 describing the comparison of observed and RCM_NCEP simulated return levels of 6-, 12- and 24-h seasonal (April to October) precipitation extremes for the current 1981–2000 reference period. Section C.2 illustrates the projected changes in selected grid-point based return levels of precipitation extremes as simulated by different RCM_AOGCM combinations for the 2041–2070 period with respect to the 1971–2000 period. Sections C.3 and C.4 contain the RCM_NCEP and RCM_AOGCM simulated regional precipitation intensity-duration-frequency plots, respectively.

C.1 Comparison of observed and RCM_NCEP simulated return levels

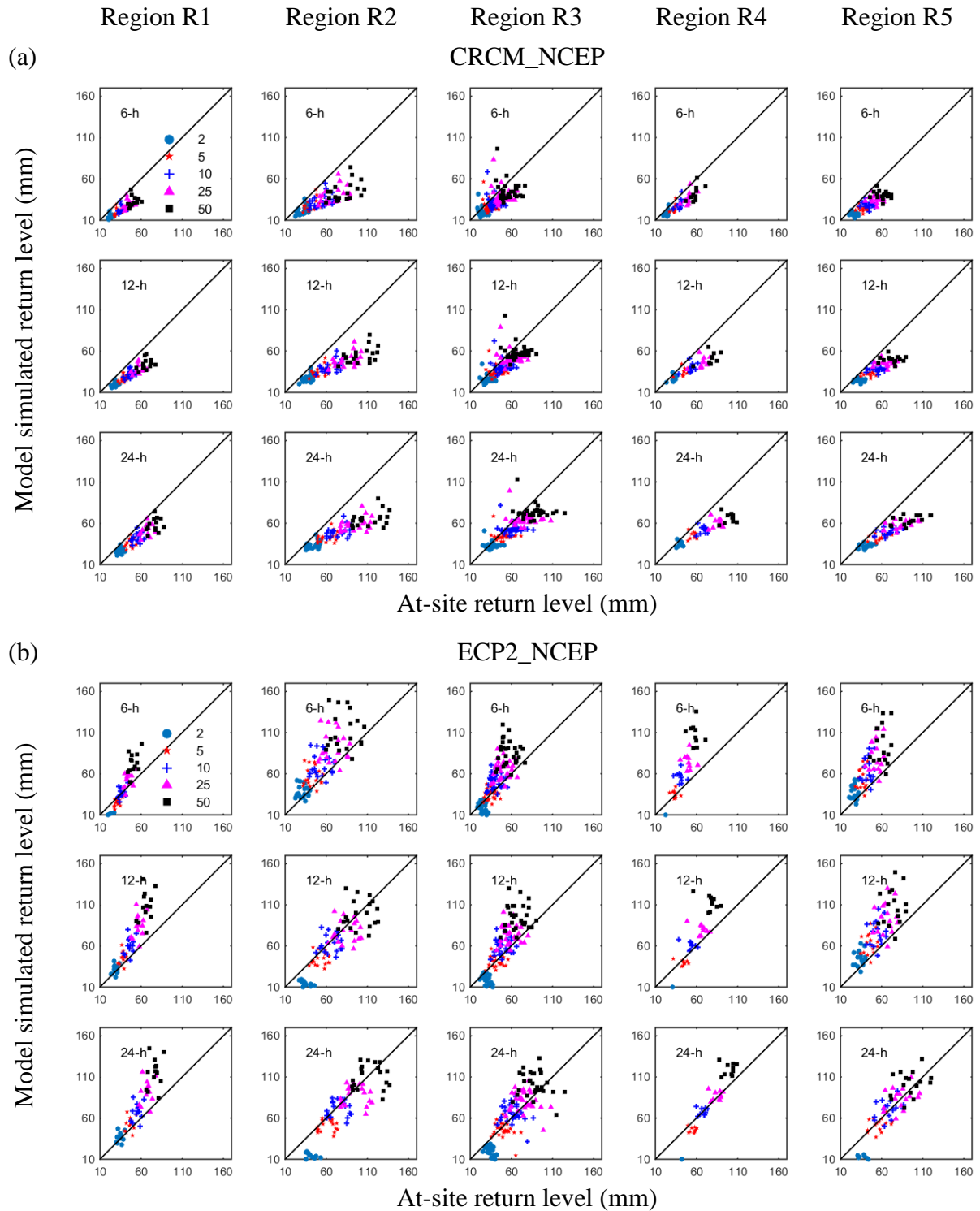


Figure C1: Comparison of 2-, 5-, 10-, 25-, and 50-yr observed and (a) CRCM_NCEP (b) ECP2_NCEP simulated return levels of 6-, 12- and 24-h seasonal (April to October) precipitation extremes for the current 1981–2000 reference period.

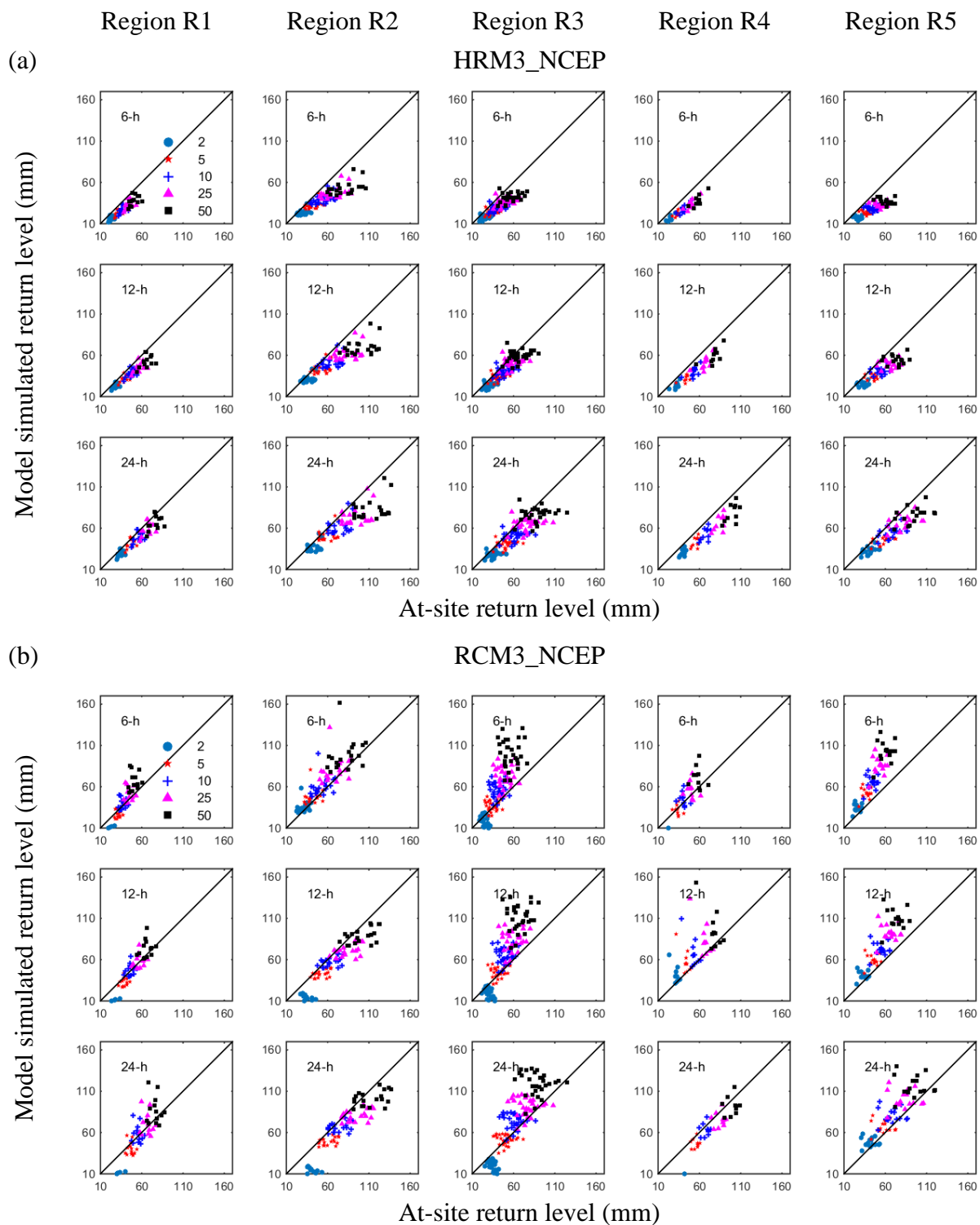


Figure C2: Comparison of 2-, 5-, 10-, 25-, and 50-yr observed and (a) HRM3_NCEP (b) RCM3_NCEP simulated return levels of 6-, 12- and 24-h seasonal (April to October) precipitation extremes for the current 1981–2000 reference period.

C.2 Projected changes (in %) in grid-point based return levels 2041-2070 vs 1971-2000

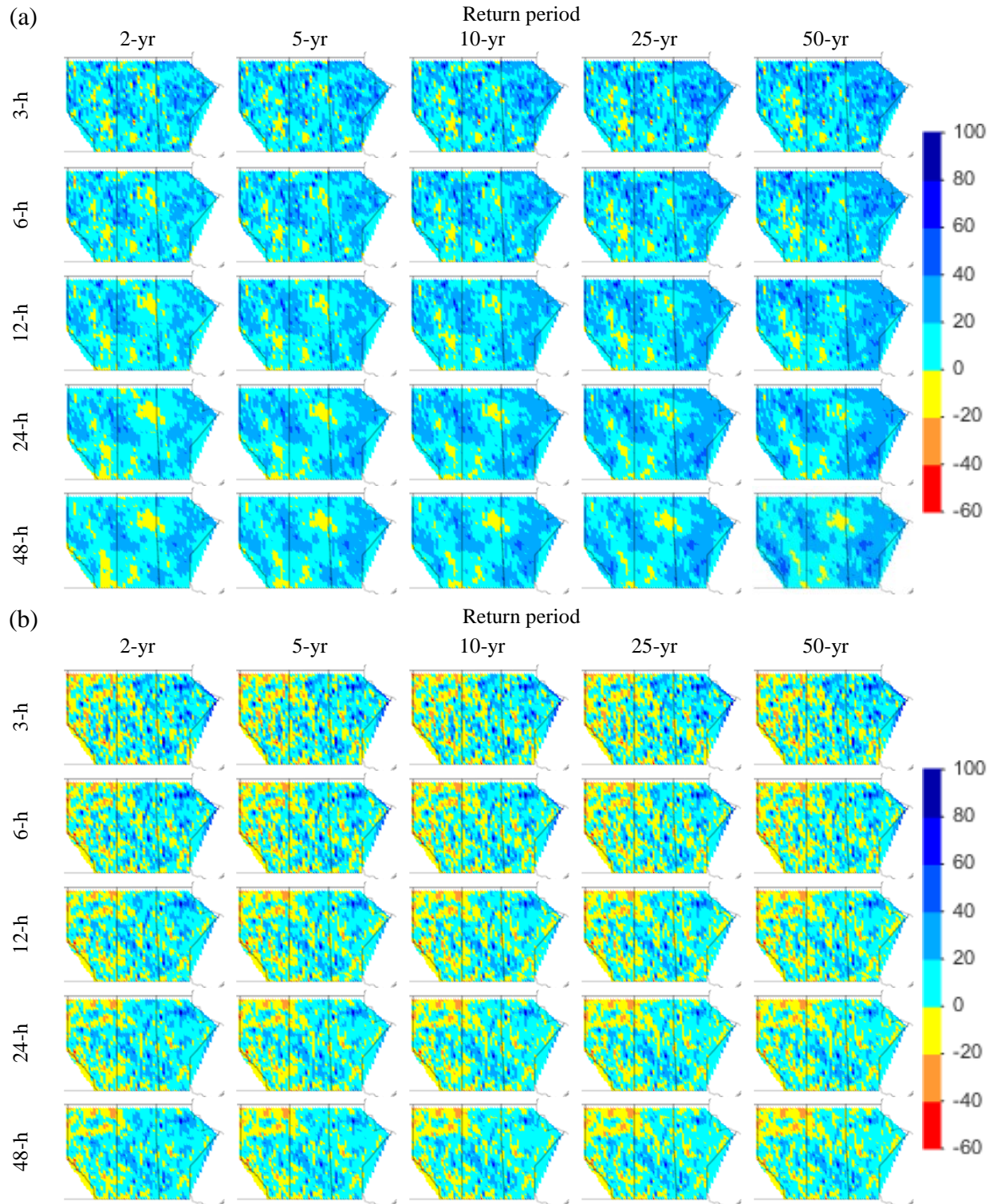


Figure C3: Projected changes in selected grid-point based return levels of 3-, 6-, 12-, 24-, and 48-h precipitation extremes as simulated by (a) CRCM_CGCM3 and (b) ECP2_GFDL.

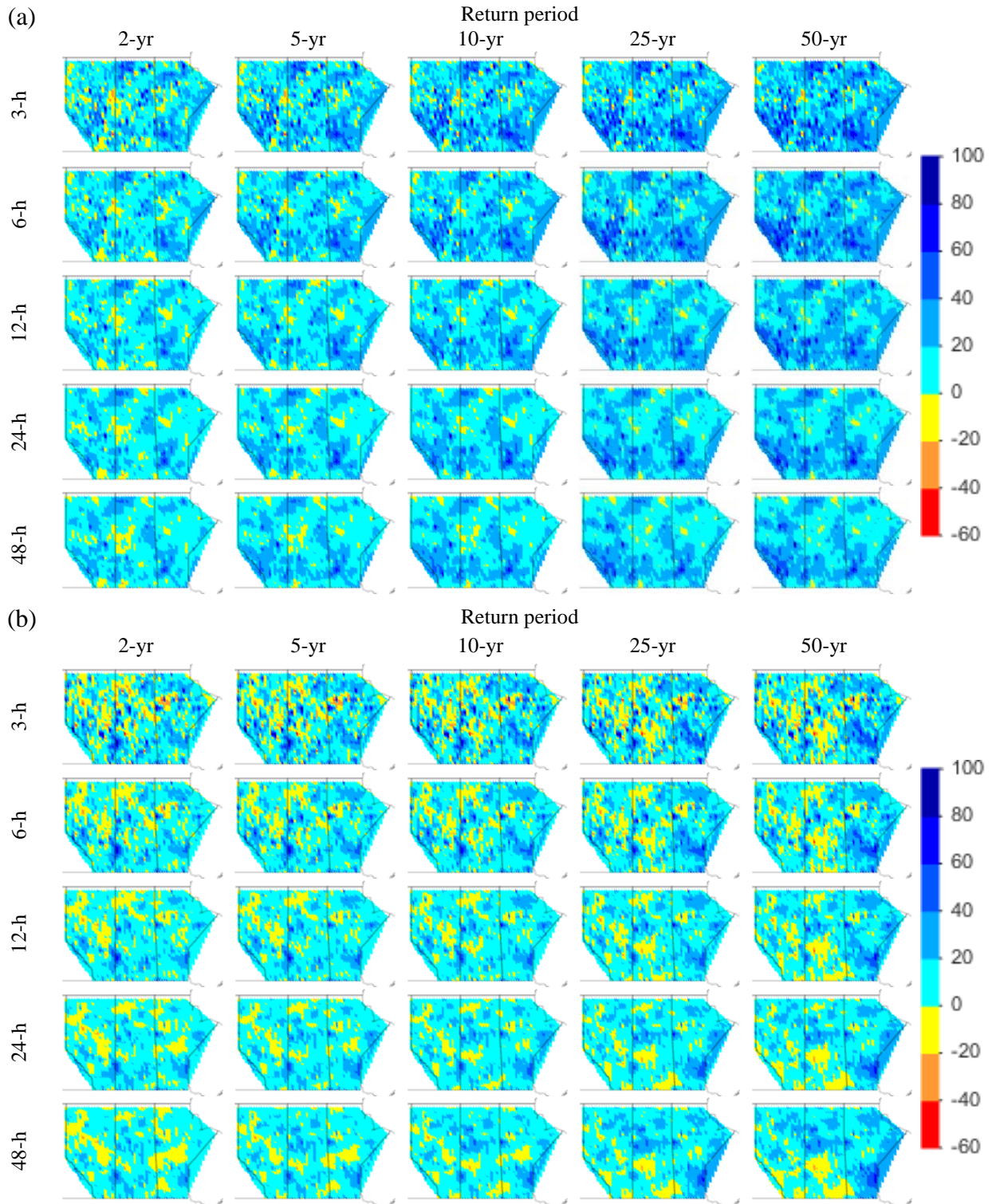


Figure C4: Same as Figure C3 but for (a) HRM3_GFDL and (b) HRM3_HADCM3.

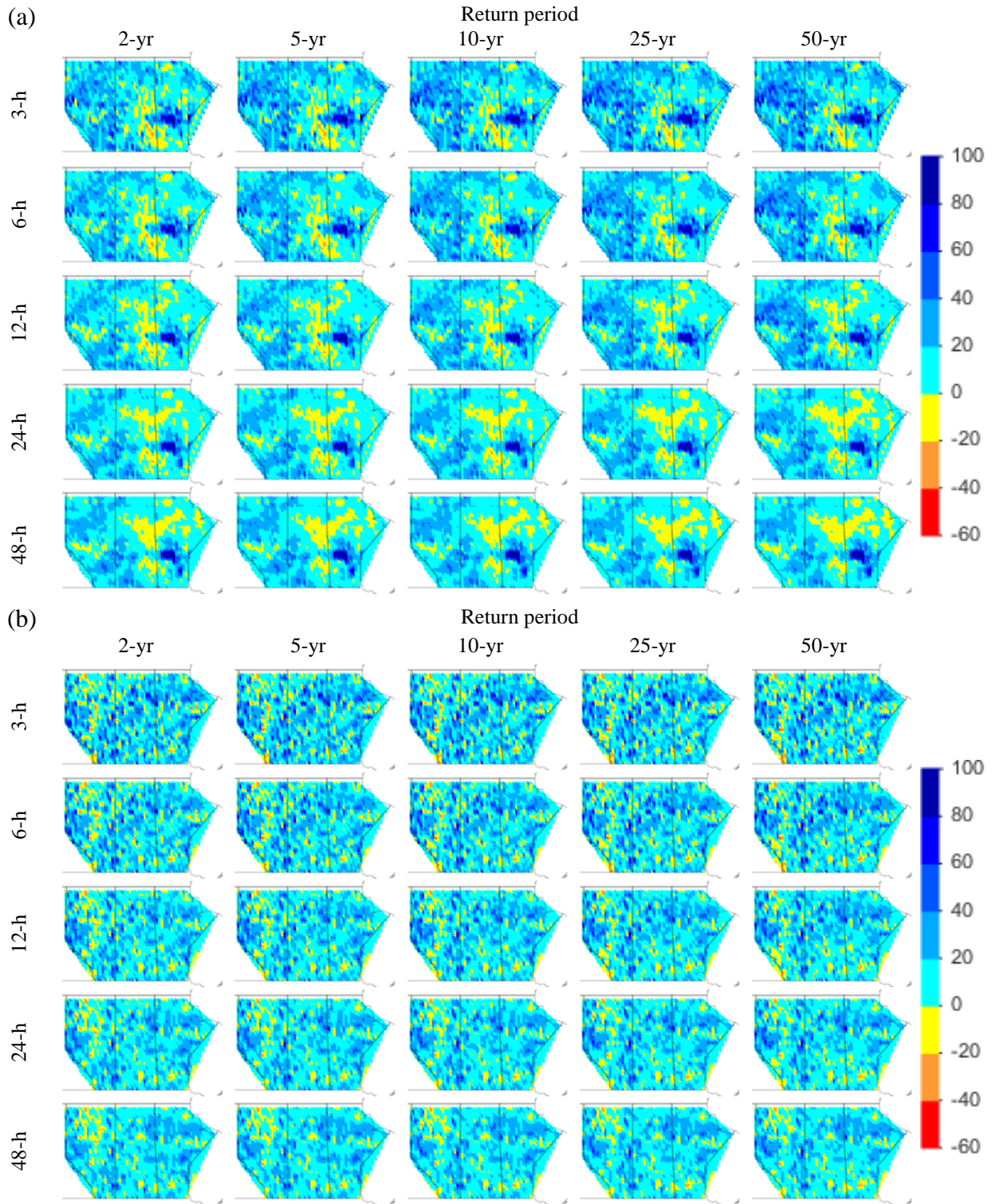


Figure C5: Same as Figure C3 but for (a) MM5I_HADCM3 and (b) RCM3_CGCM3.

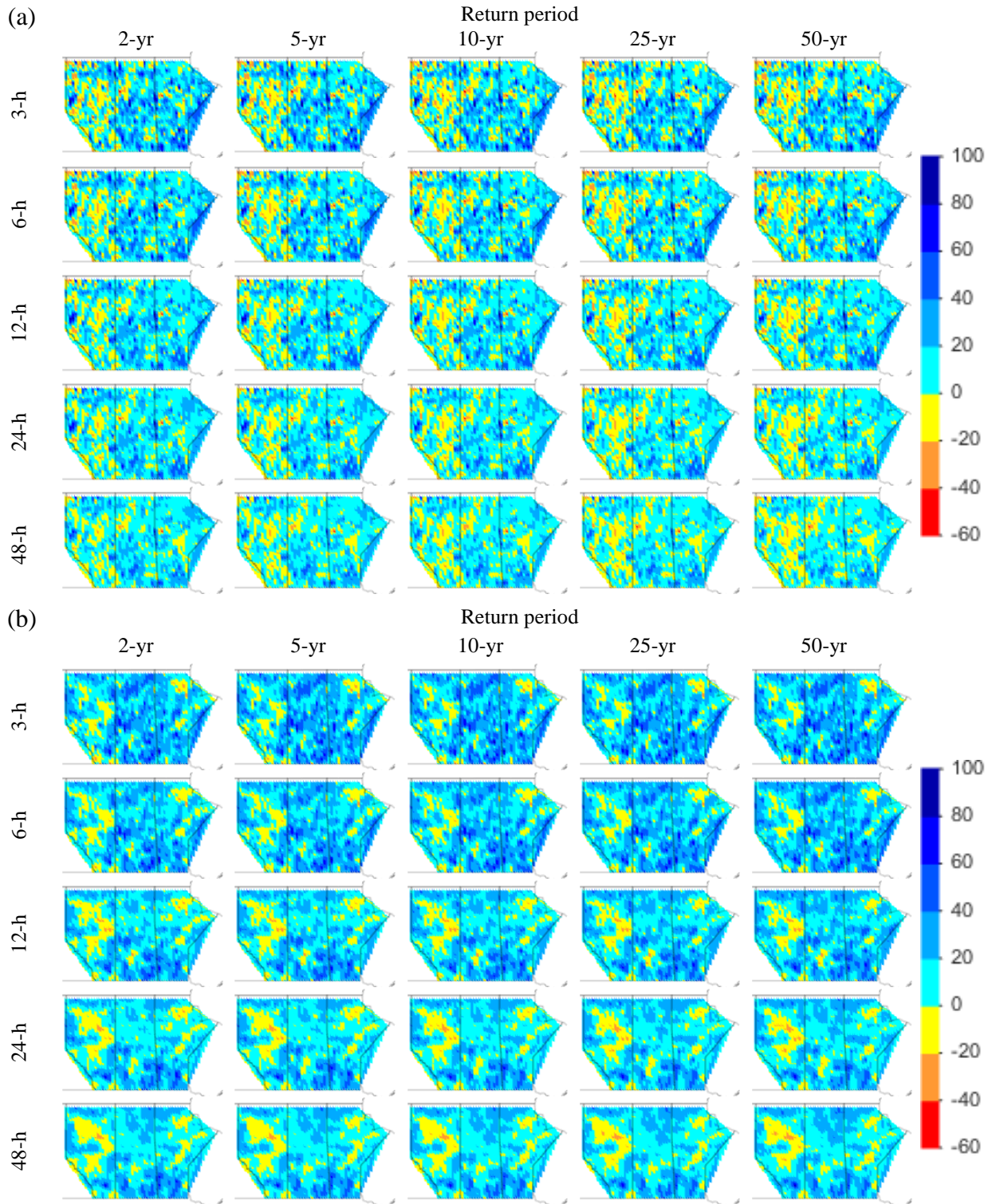


Figure C6: Same as Figure C3 but for (a) RCM3_GFDL and (b) WRFG_CCSM.

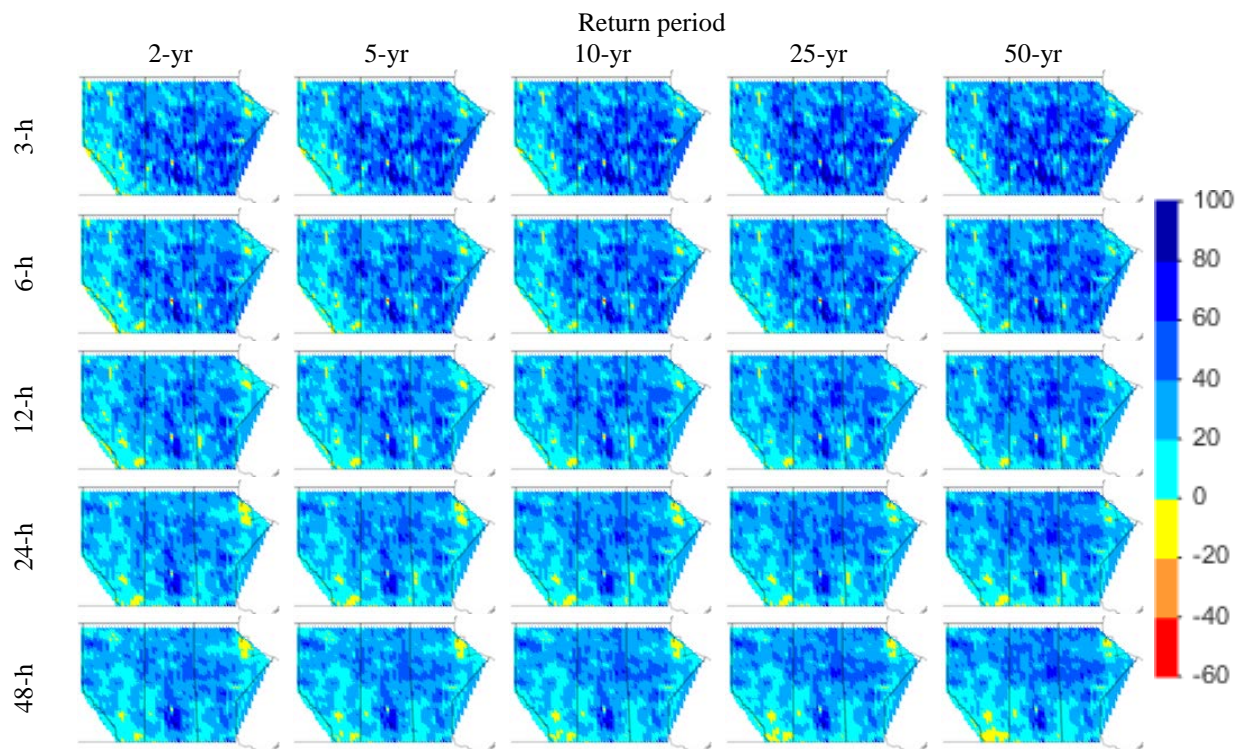


Figure C7: Same as Figure C3 but for WRFG_CGCM3.

C.3 RCM_NCEP simulated regional precipitation intensity-duration-frequency (IDF) plots

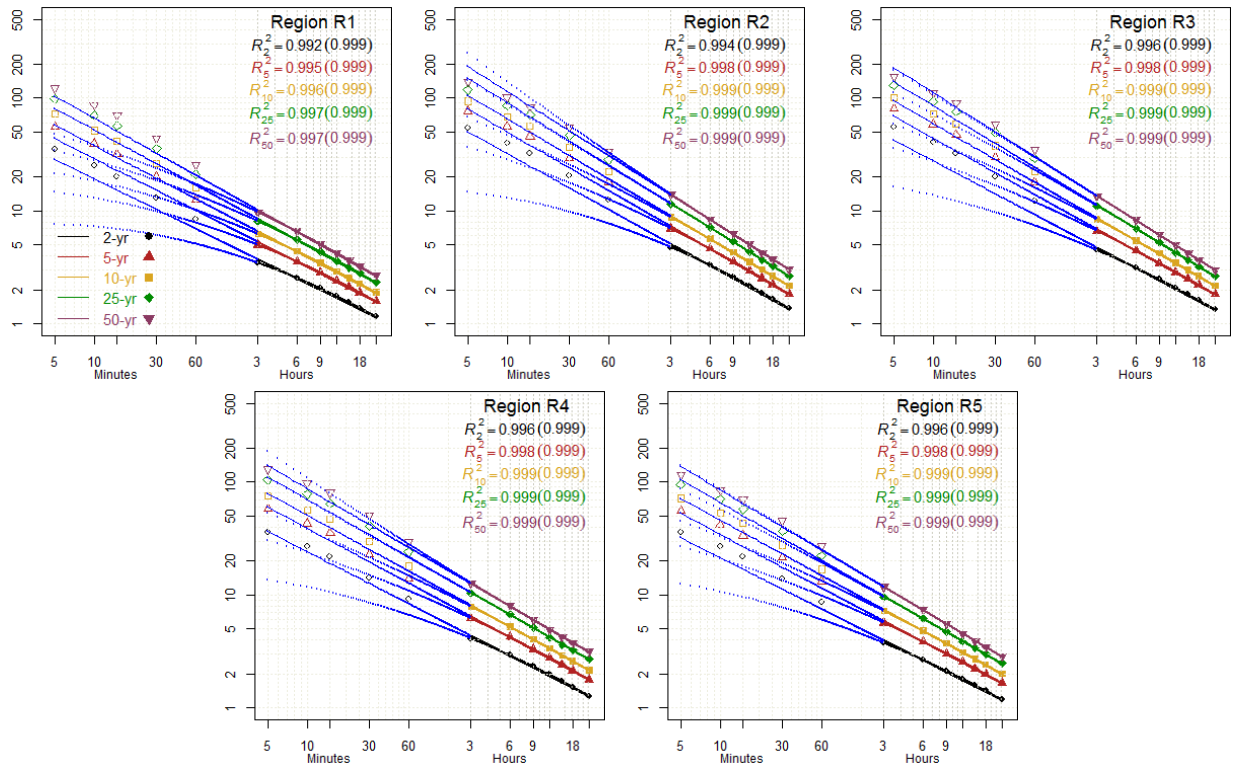


Figure C8: CRCM_NCEP simulated regional precipitation IDF plots (filled symbols) for regions R1 to R5 based on precipitation extremes of 3-, 6-, 9-, 12-, 15-, 18-, and 24-h durations (shown along the x-axis). Linear and non-linear scaling relationships (colored solid lines) estimated using the least-squares algorithm and the corresponding coefficient of determination (i.e. R^2) values are shown in each panel first for the linear case and then for the nonlinear case in brackets. Trajectories of extrapolated linear (solid blue lines) and nonlinear (dotted blue lines) relationships for each return period are also plotted. Estimated return levels based on the quantile mapping approach are shown using corresponding unfilled symbols for 2-, 5-, 10-, 25-, and 50-year return periods.

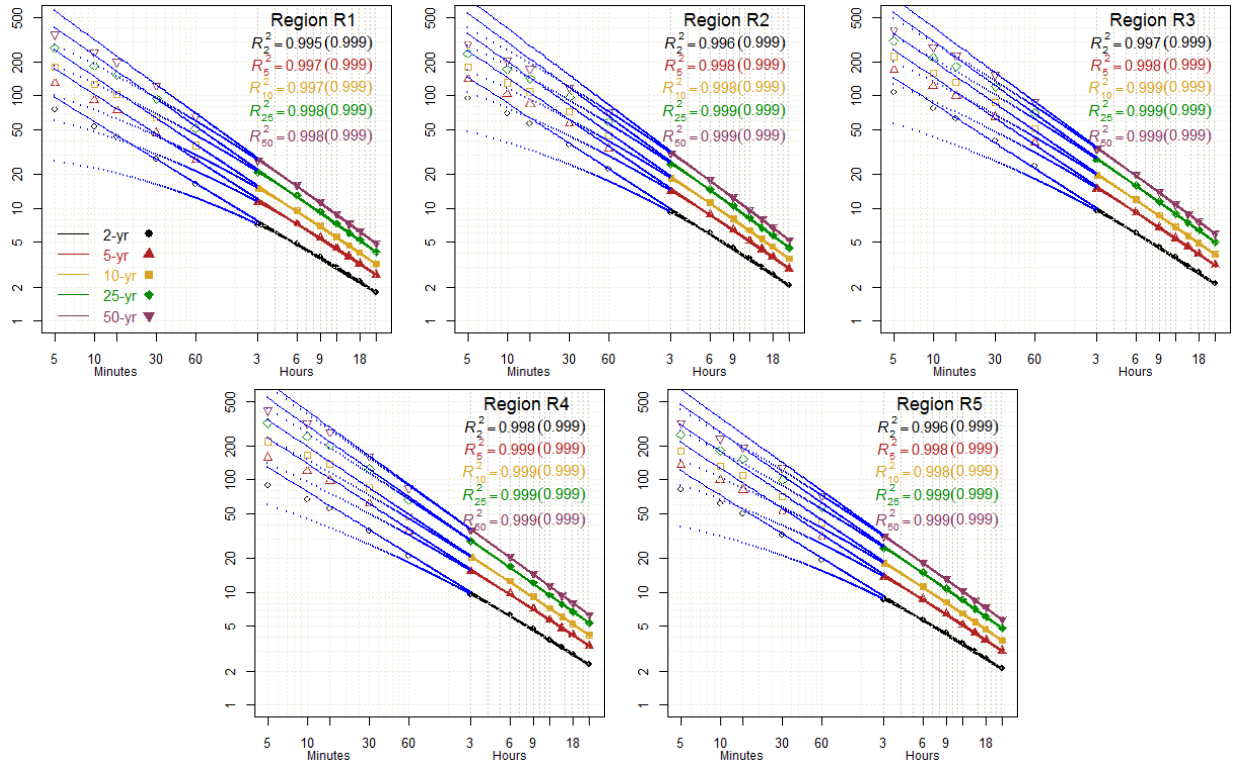


Figure C9: Same as Figure C8 but for ECP2_NCEP.

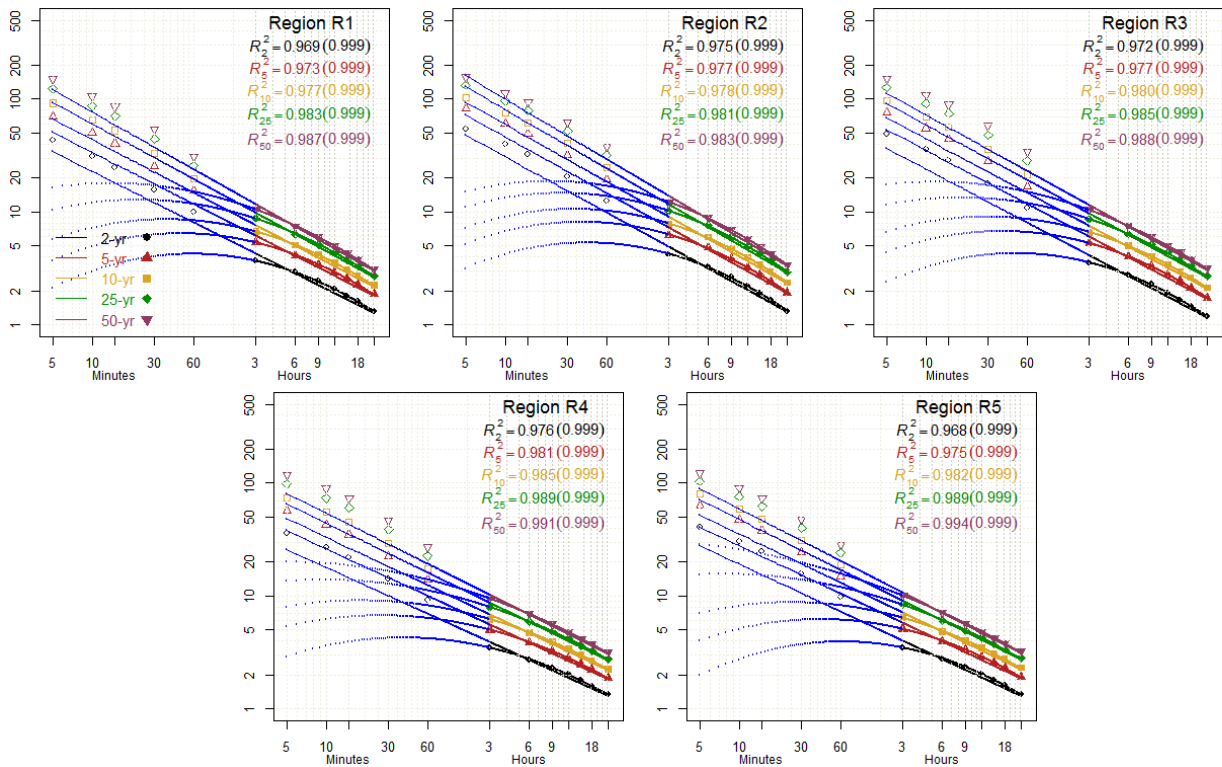


Figure C10: Same as Figure C8 but for HRM3_NCEP.

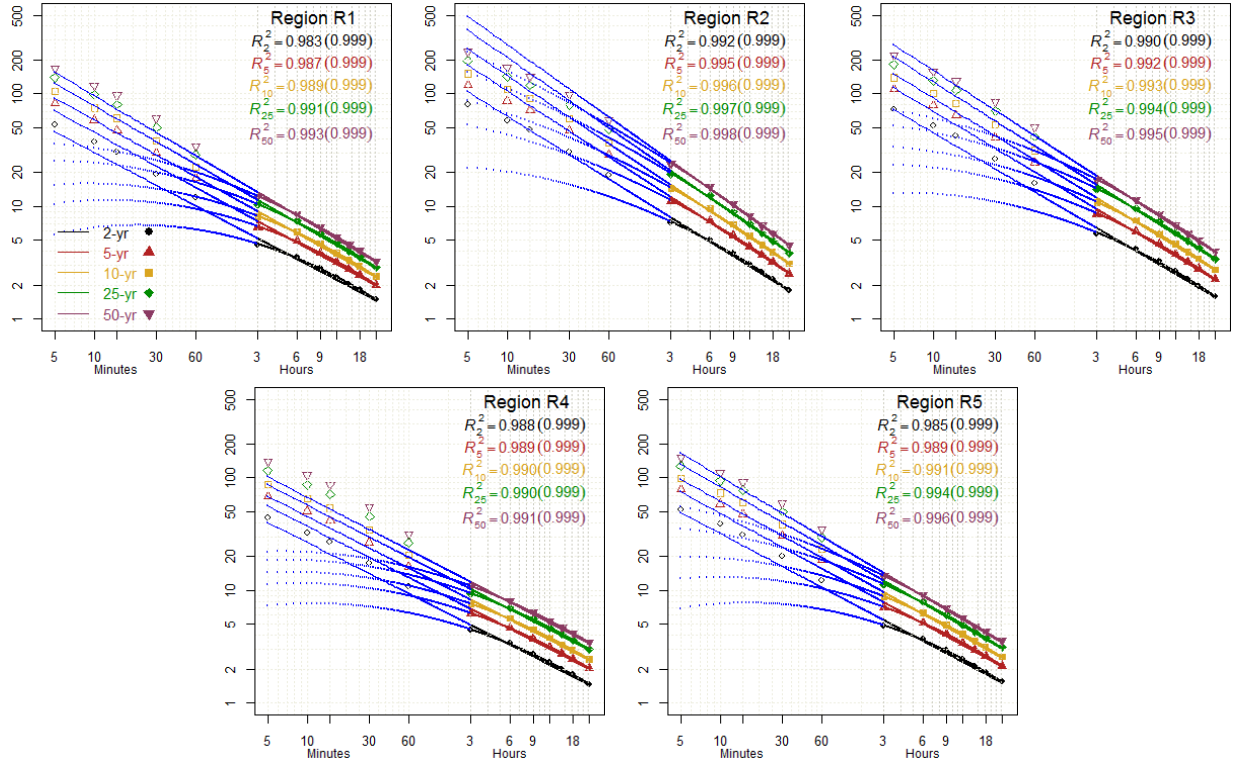


Figure C11: Same as Figure C8 but for MM5I_NCEP.

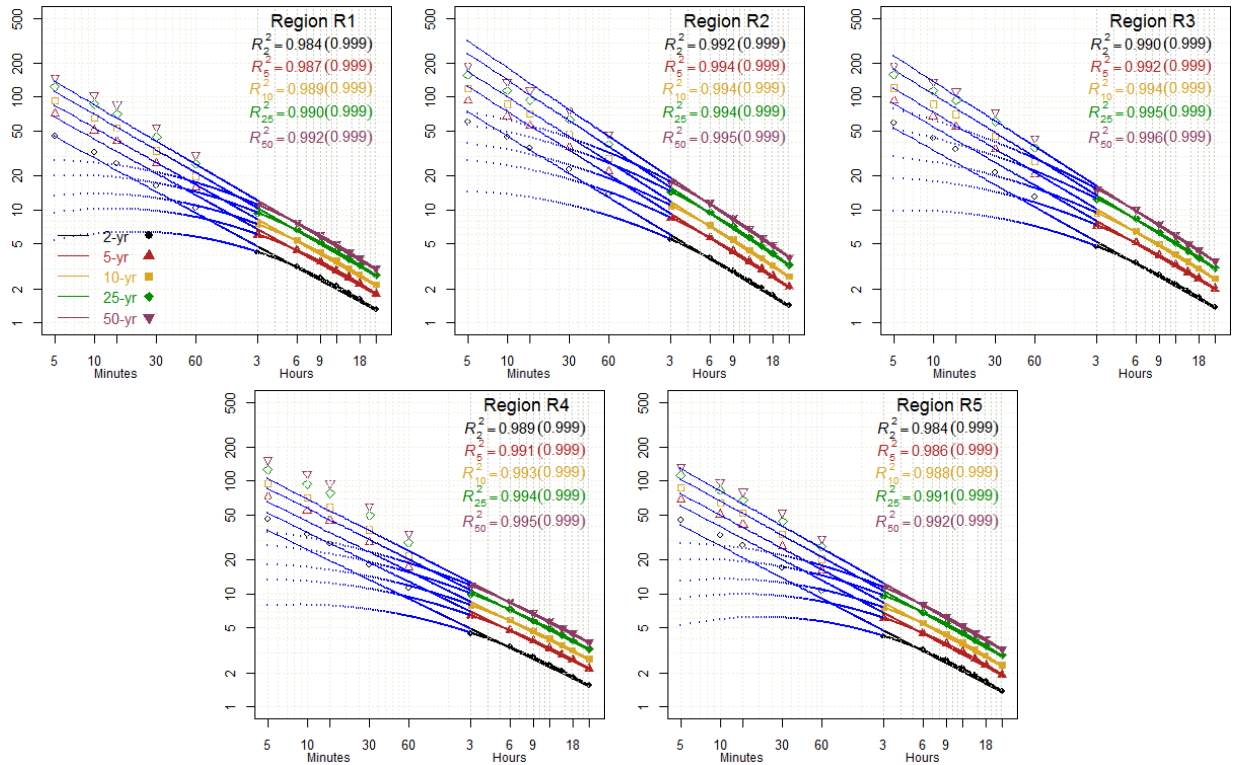
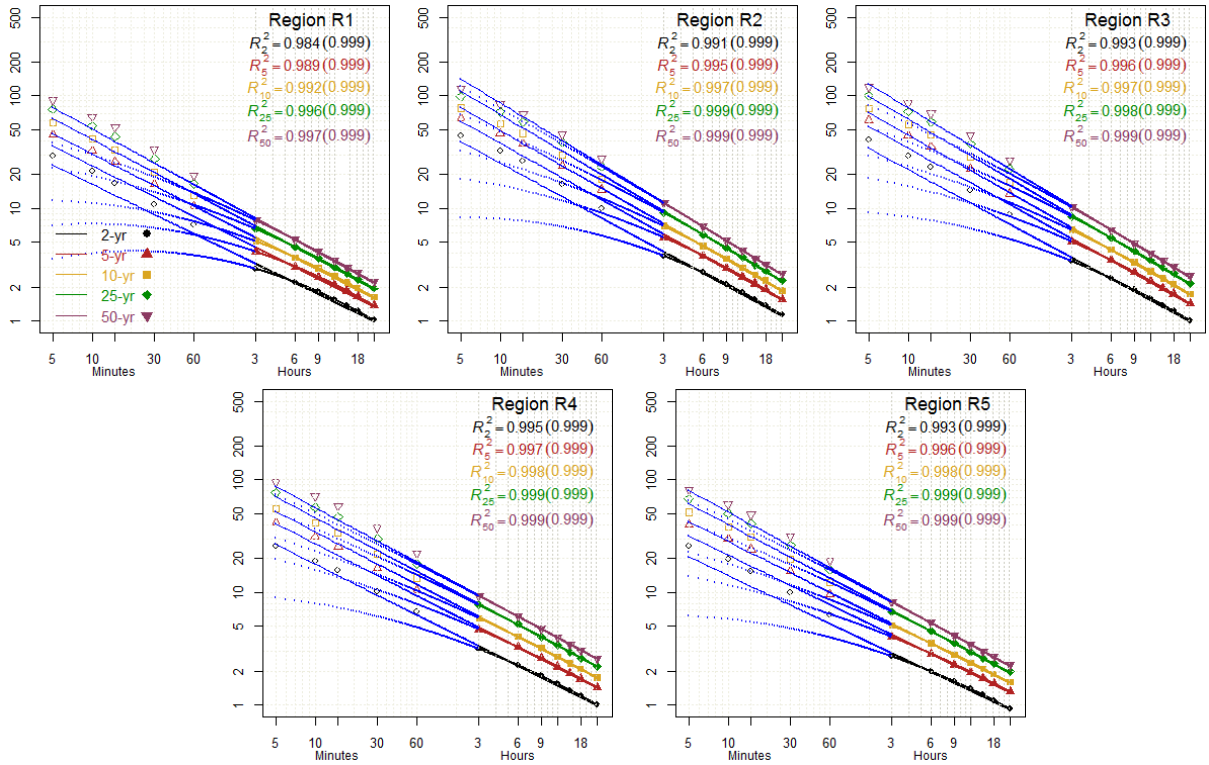


Figure C12: Same as Figure C8 but for WRFG_NCEP.

C.4 RCM_AOGCM simulated current and future period regional precipitation intensity-duration-frequency (IDF) plots

Following Figures C13 to C23 represent the RCM_AOGCM simulated (a) current 1971–2000 and (b) future 2041–2070 period regional precipitation IDF plots (filled symbols) for regions R1 to R5 based on precipitation extremes of 3-, 6-, 9-, 12-, 15-, 18-, and 24-h durations (shown along the x-axis). Linear and non-linear scaling relationships (colored solid lines) estimated using the least-squares algorithm and the corresponding coefficient of determination (i.e. R^2) values are shown in each panel first for the log-log linear case and then for the nonlinear case in brackets. Trajectories of extrapolated linear (solid blue lines) and nonlinear (dotted blue lines) relationships for each return period are also plotted. Estimated return levels based on the quantile mapping approach are shown using corresponding unfilled symbols for 2-, 5-, 10-, 25, and 50-year return periods.

(a) 1971–2000



(b) 2041–2070

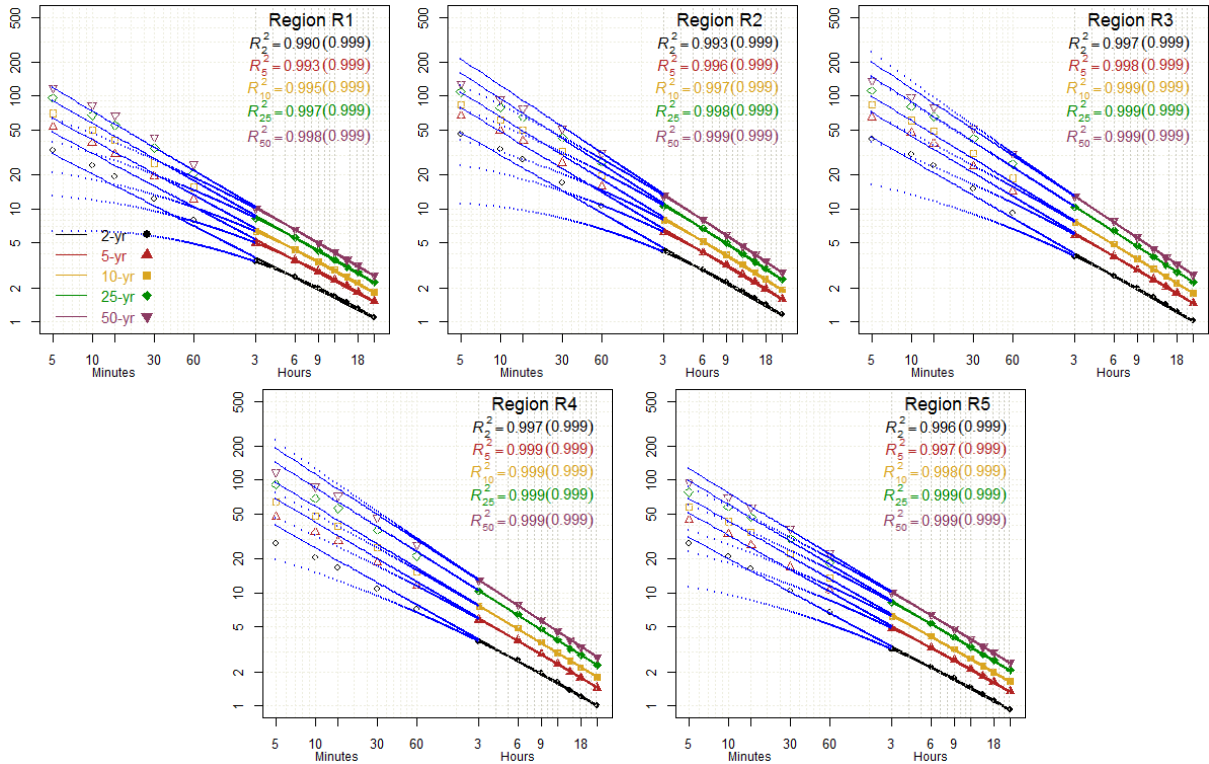
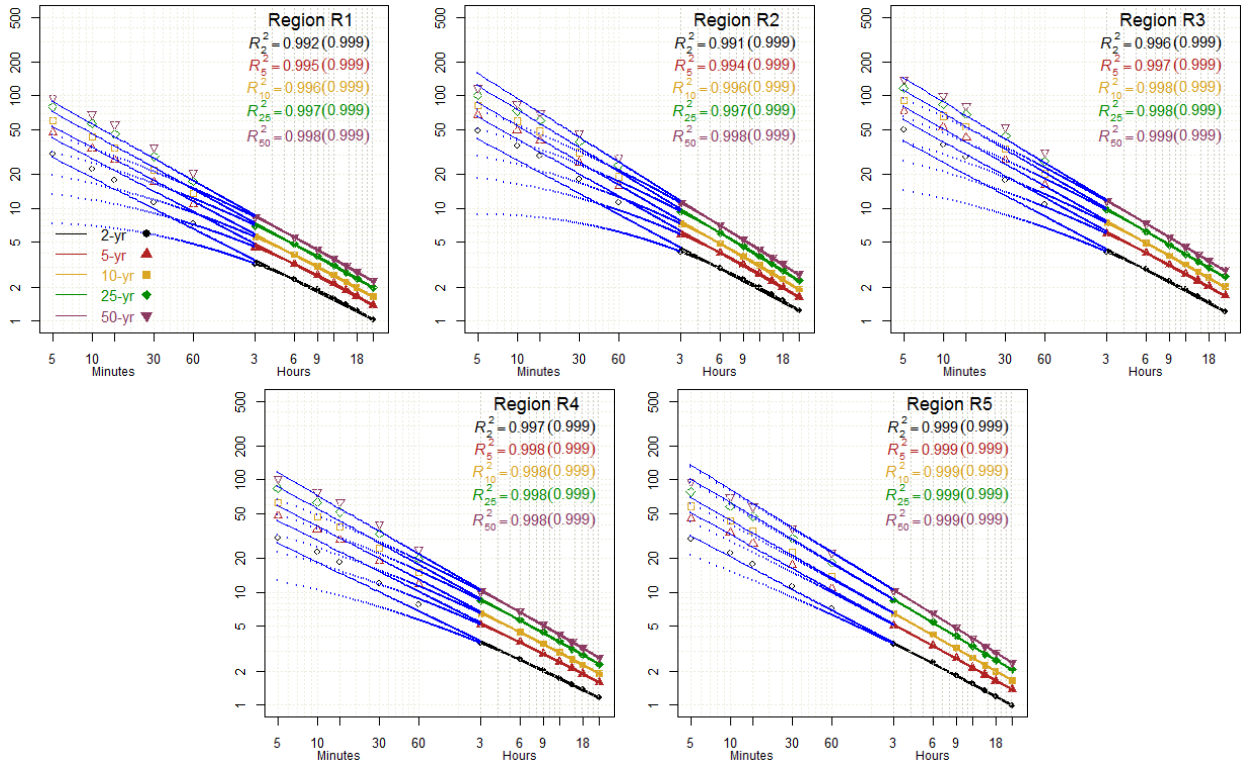


Figure C13: CRCM_CCSM simulated (a) current and (b) future IDF plots.

(a) 1971–2000



(b) 2041–2070

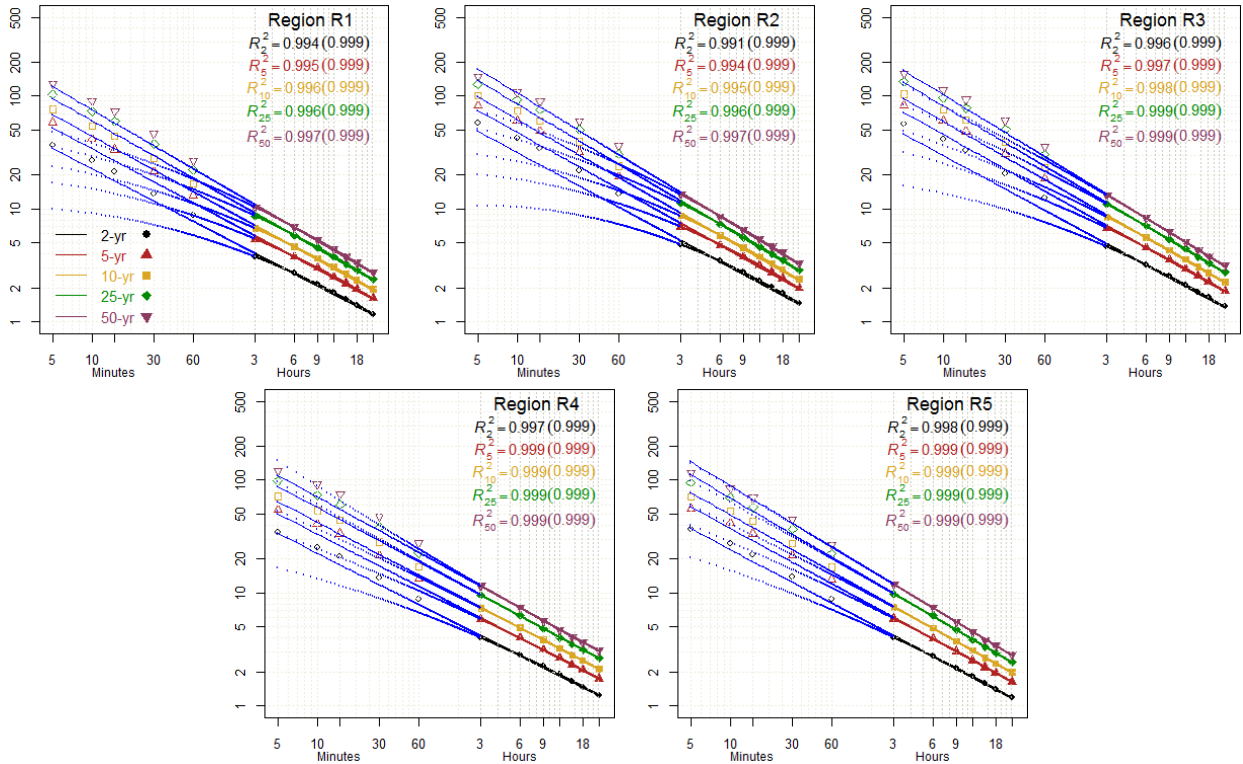
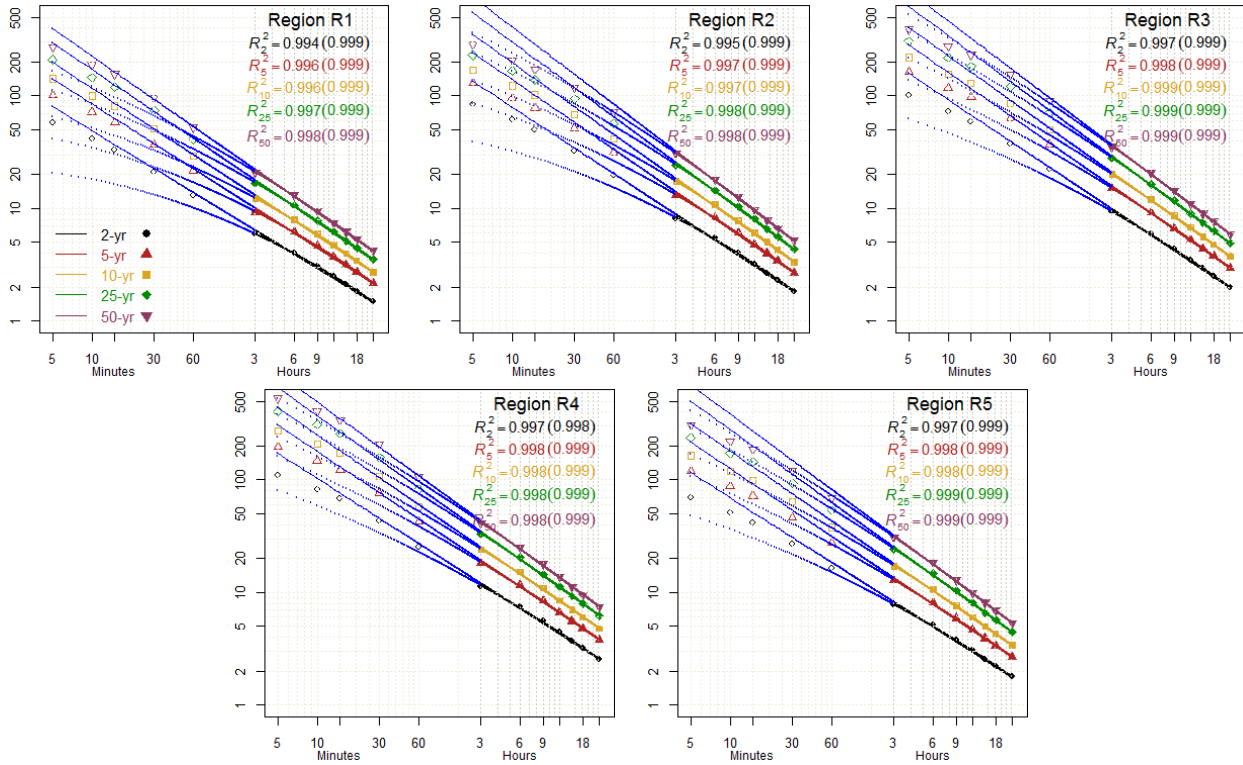


Figure C14: CRCM_CGCM3 simulated (a) current and (b) future IDF plots.

(a) 1971–2000



(b) 2041–2070

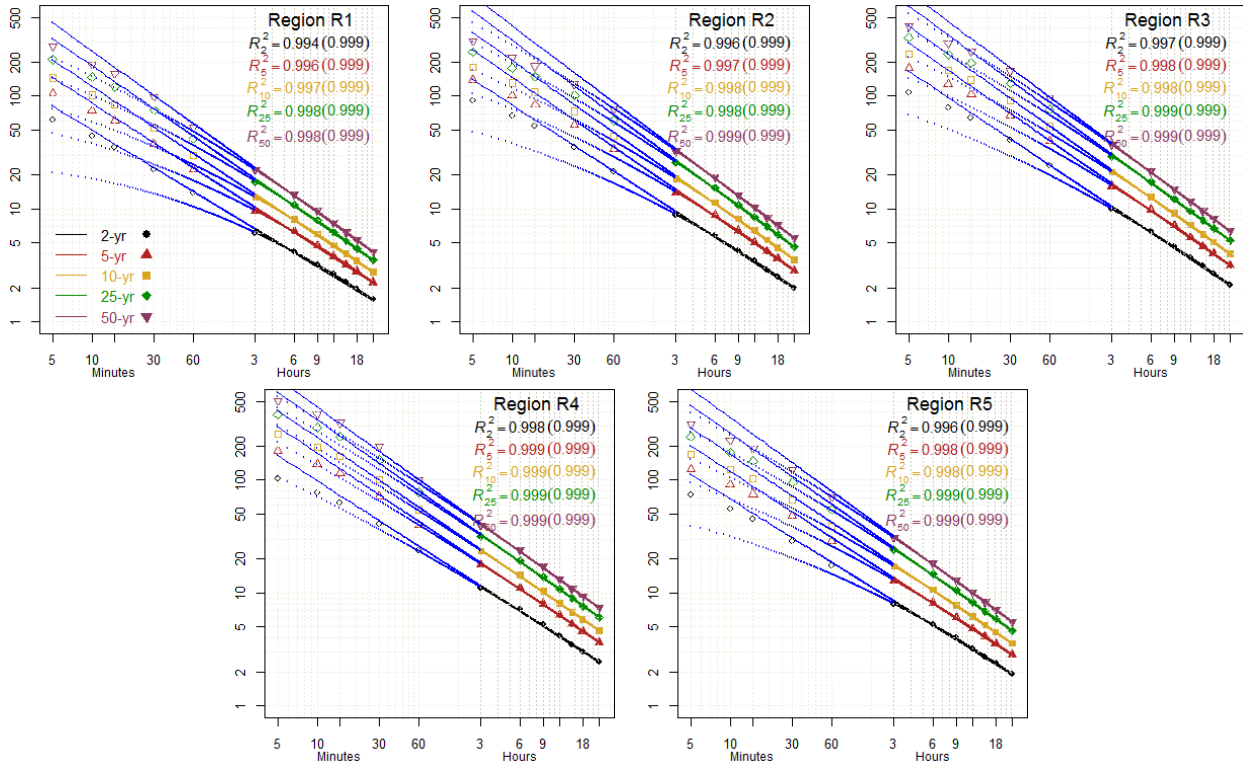
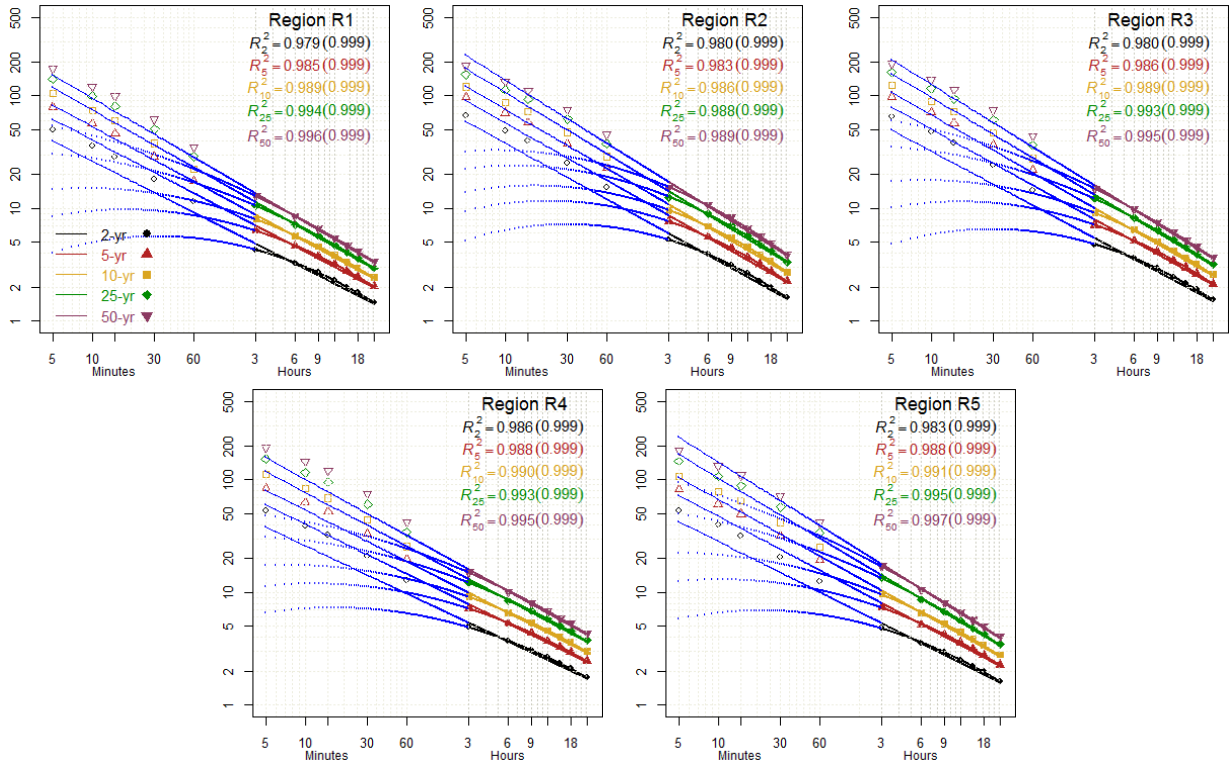


Figure C15: ECP2_GFDL simulated (a) current and (b) future IDF plots.

(a) 1971–2000



(b) 2041–2070

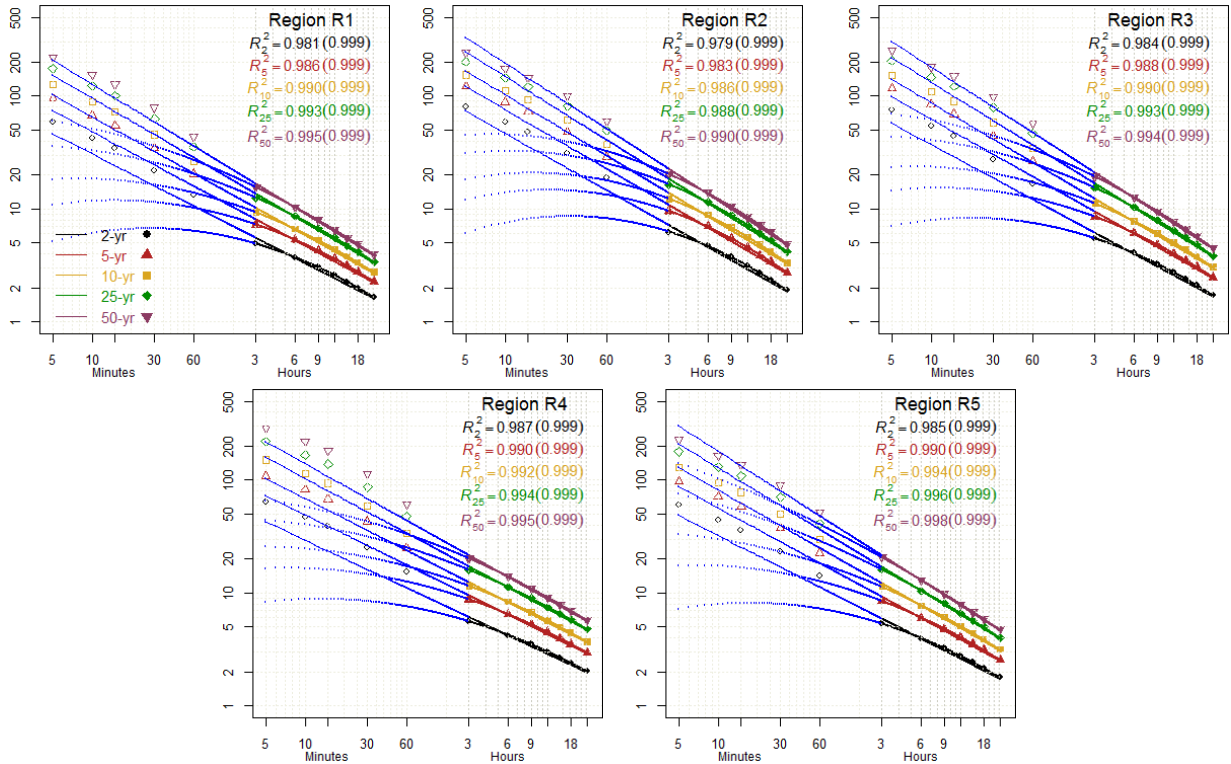
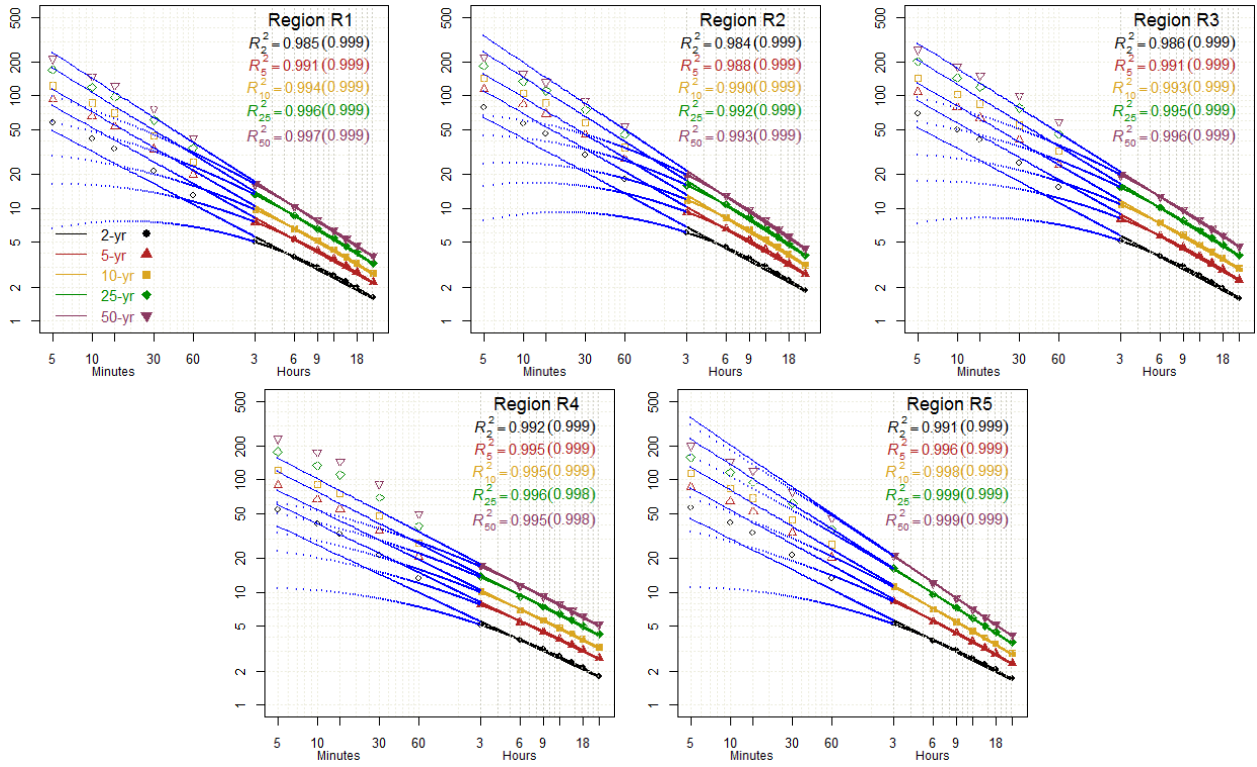


Figure C16: HRM3_GFDL simulated (a) current and (b) future IDF plots.

(a) 1971–2000



(b) 2041–2070

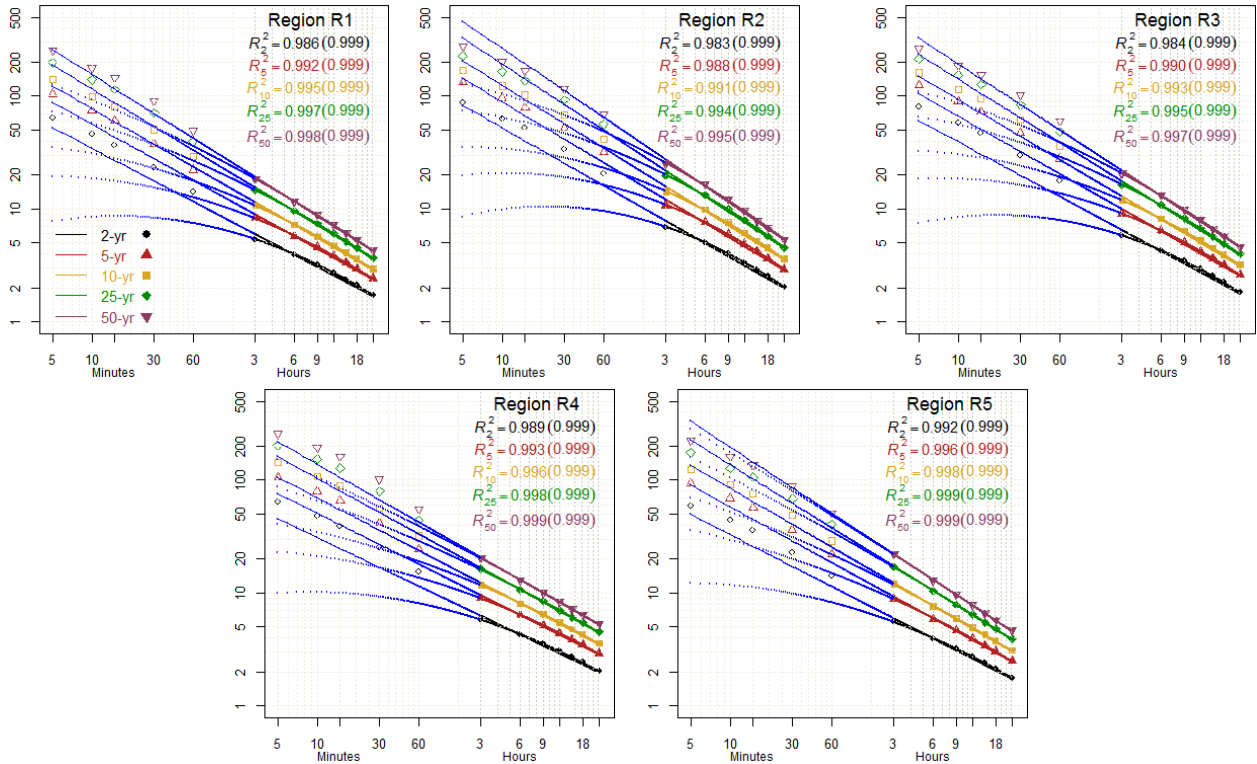
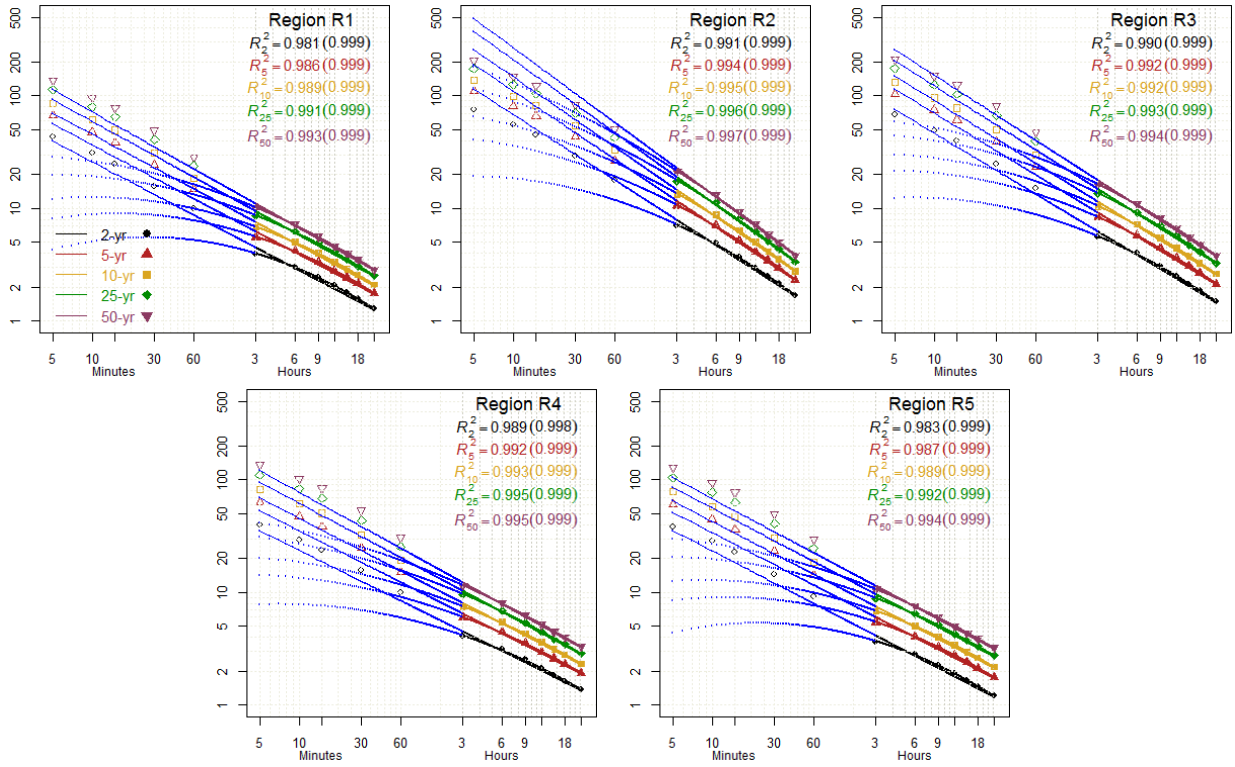


Figure C17: HRM3_HADCM3 simulated (a) current and (b) future IDF plots.

(a) 1971–2000



(b) 2041–2070

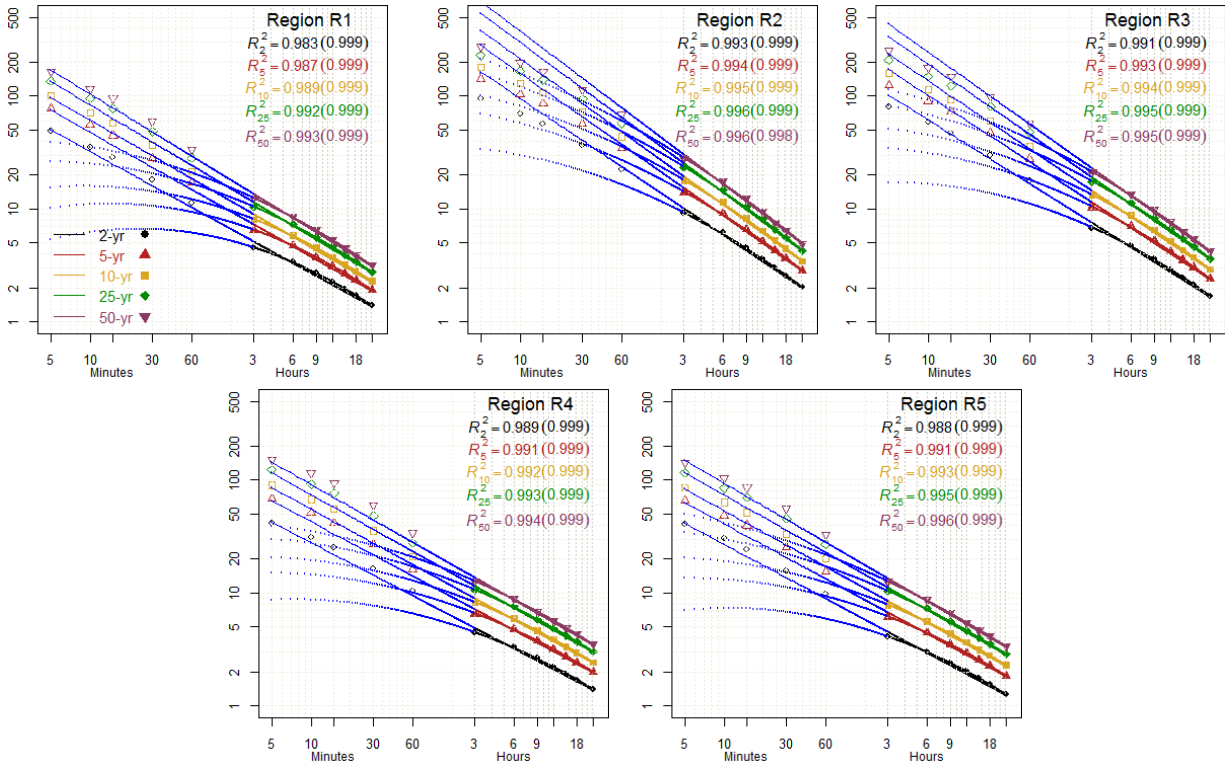
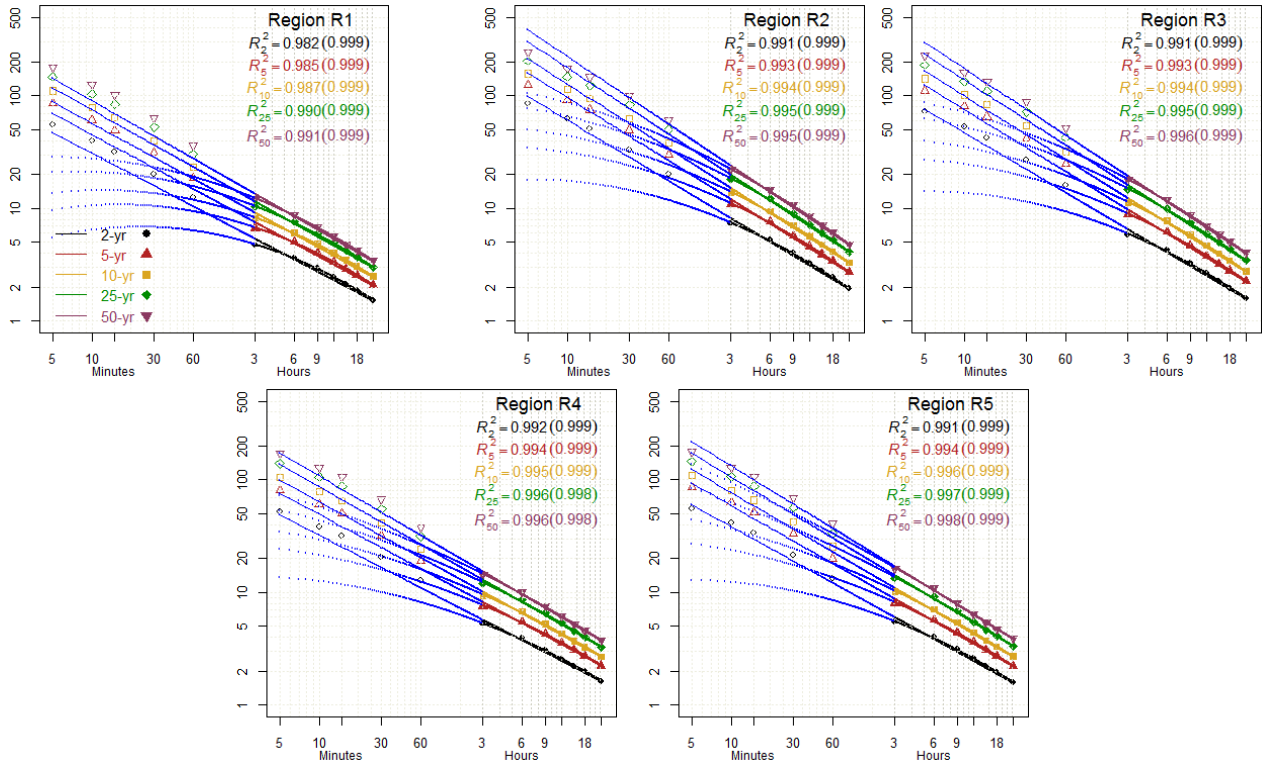


Figure C18: MM5I_CCSM simulated (a) current and (b) future IDF plots.

(a) 1971–2000



(b) 2041–2070

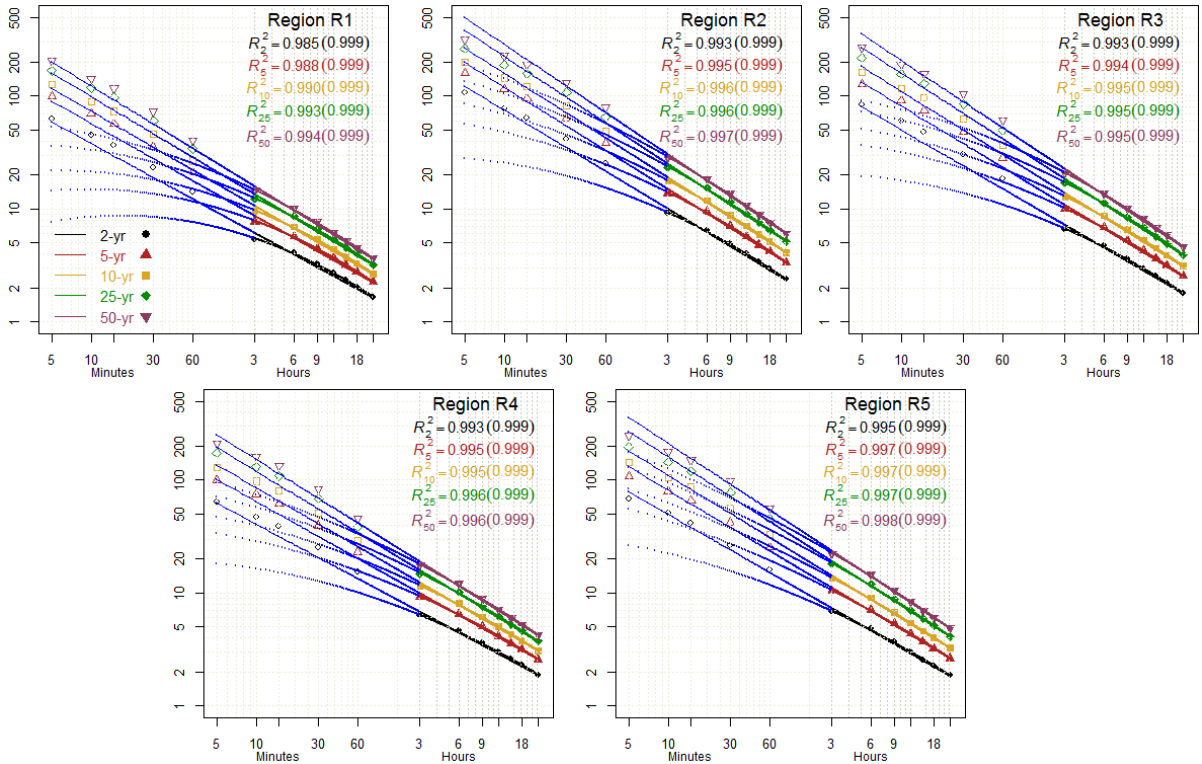
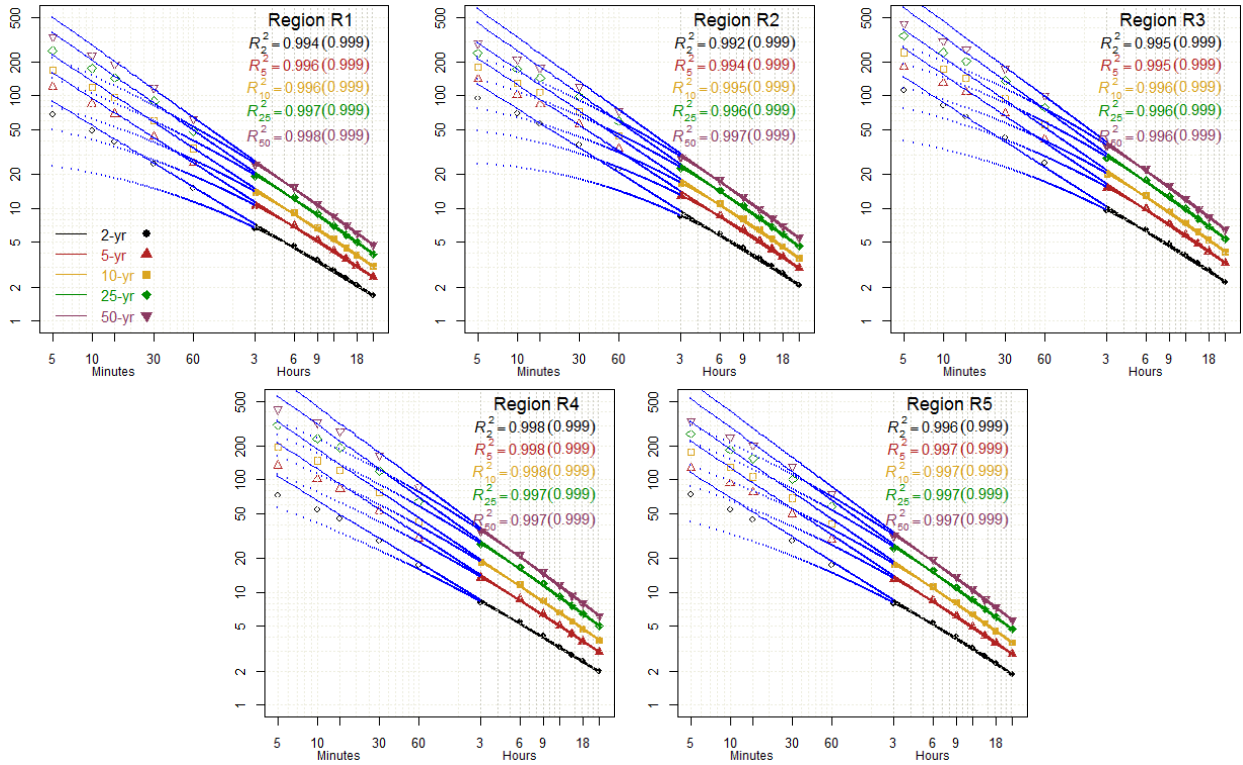


Figure C19: MM5I_HADCM3 simulated (a) current and (b) future IDF plots.

(a) 1971–2000



(b) 2041–2070

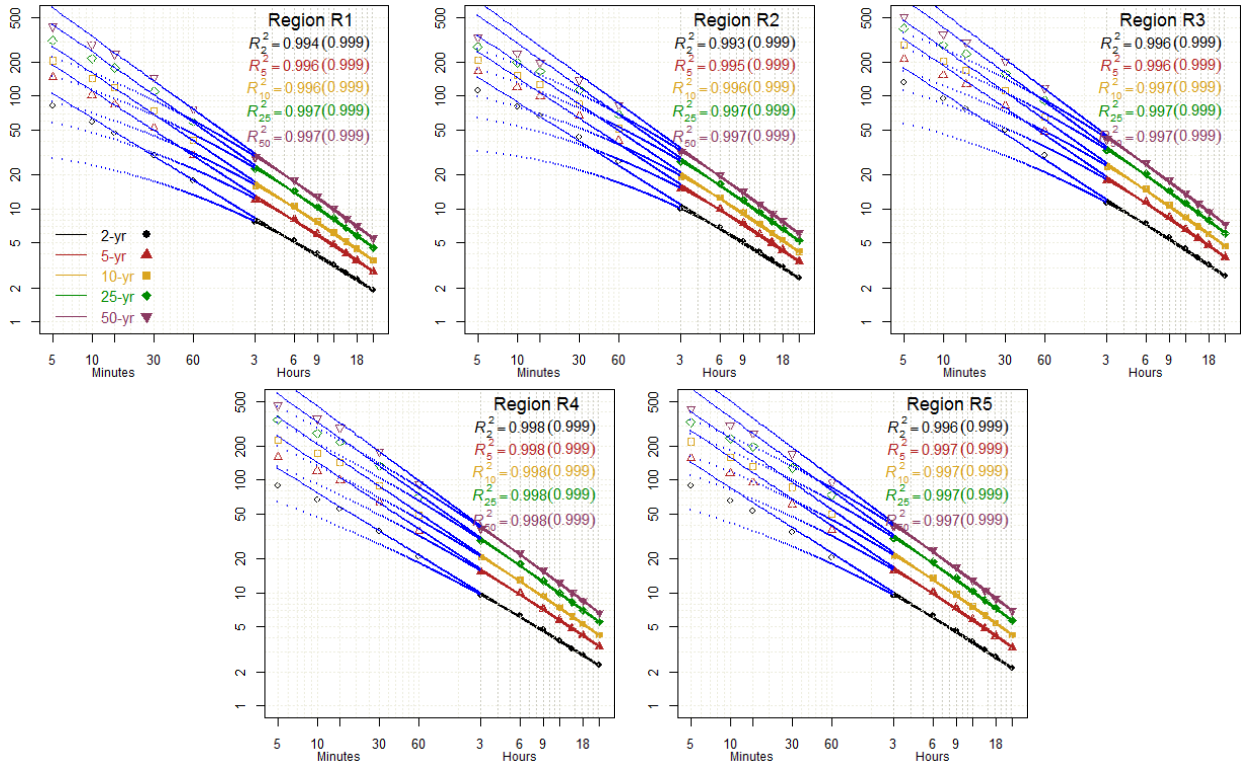
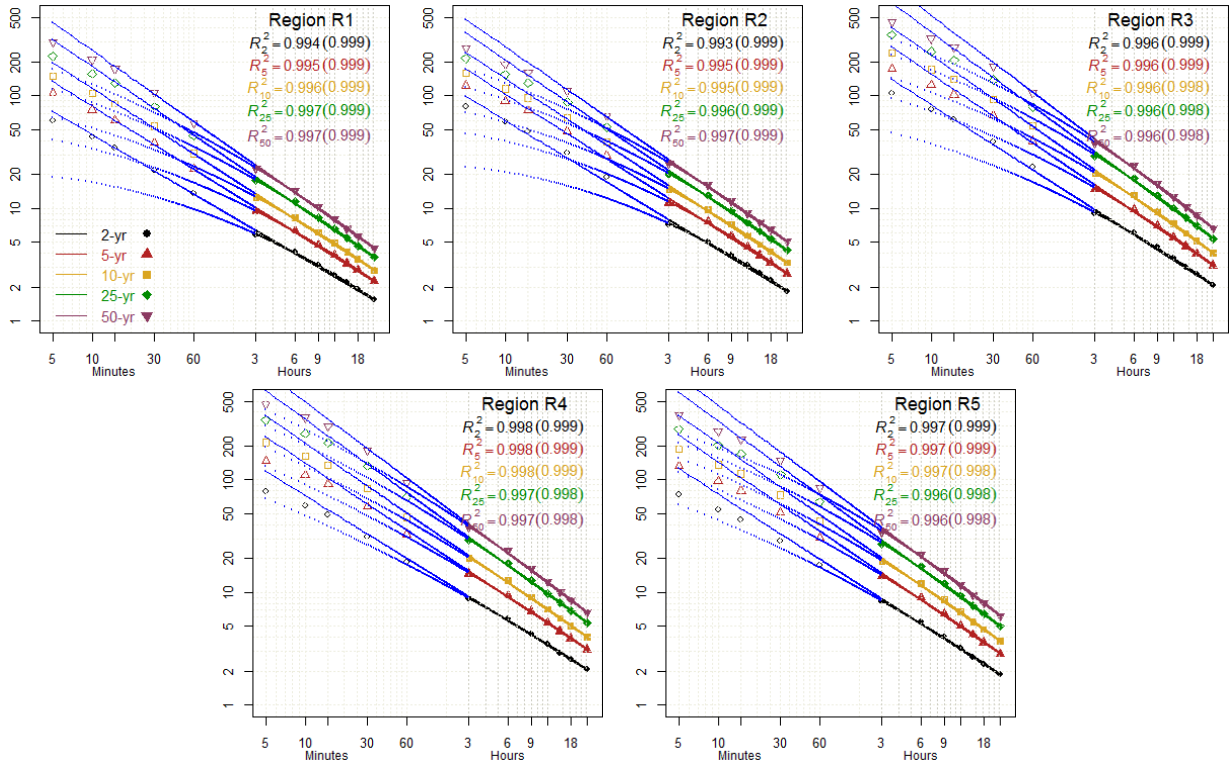


Figure C20: RCM3_CGCM3 simulated (a) current and (b) future IDF plots.

(a) 1971–2000



(b) 2041–2070

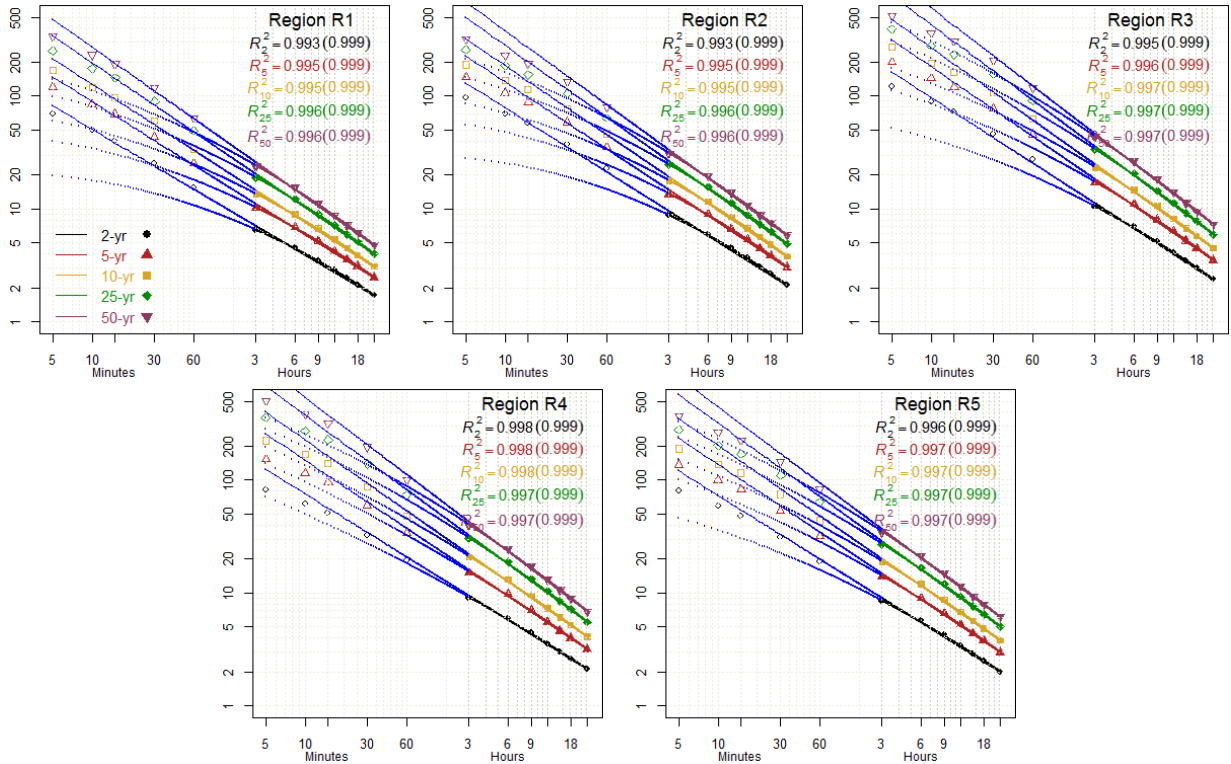
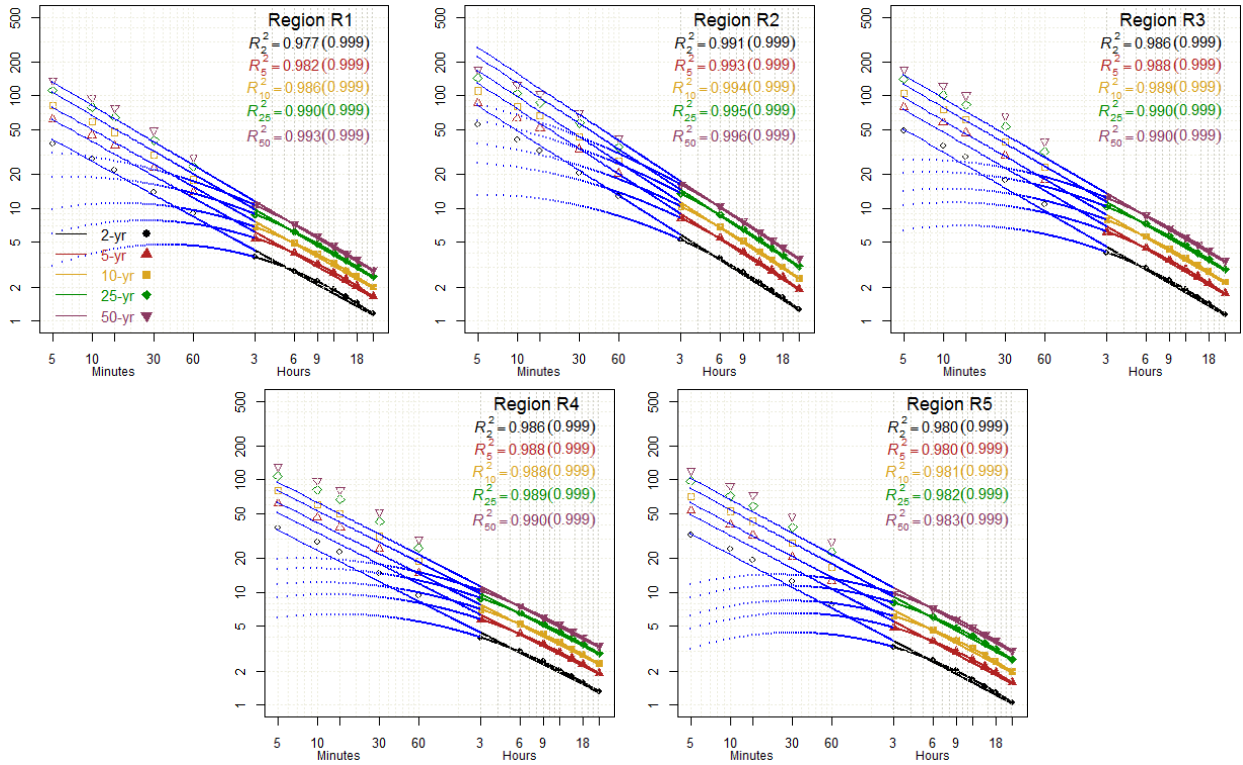


Figure C21: RCM3_GFDL simulated (a) current and (b) future IDF plots.

(a) 1971–2000



(b) 2041–2070

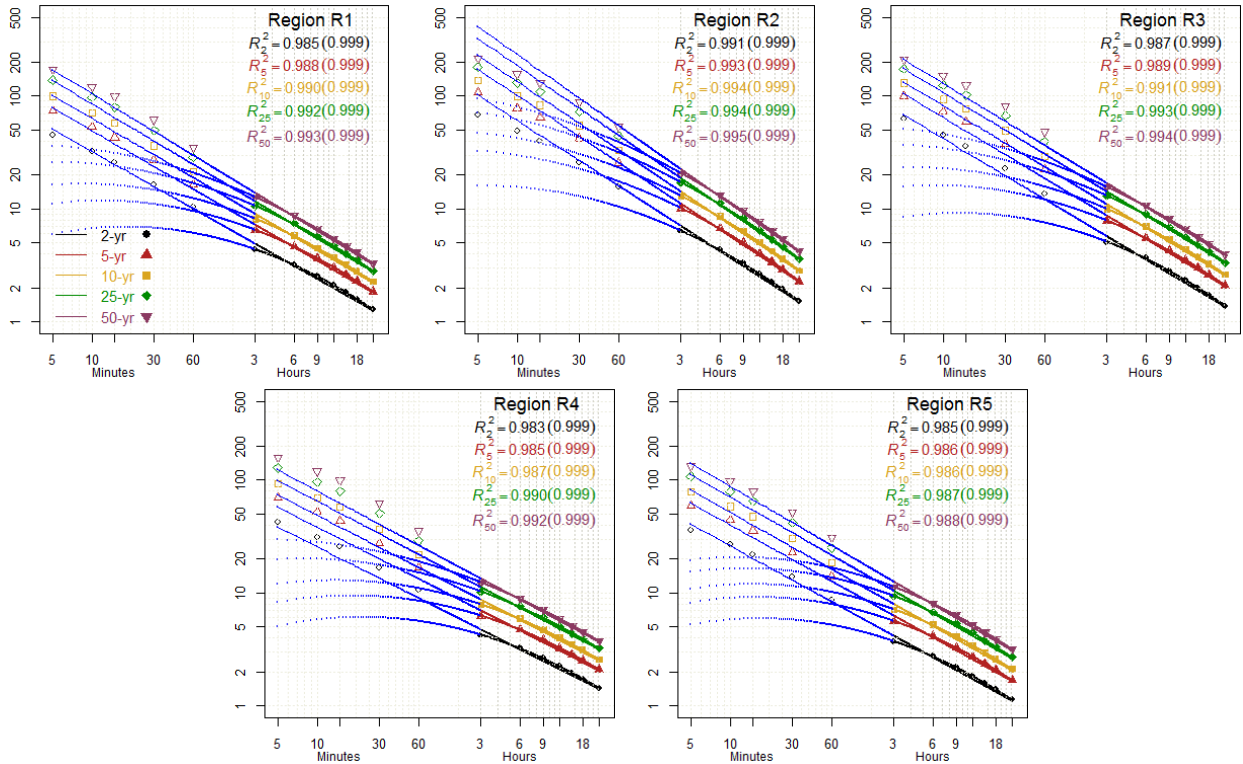
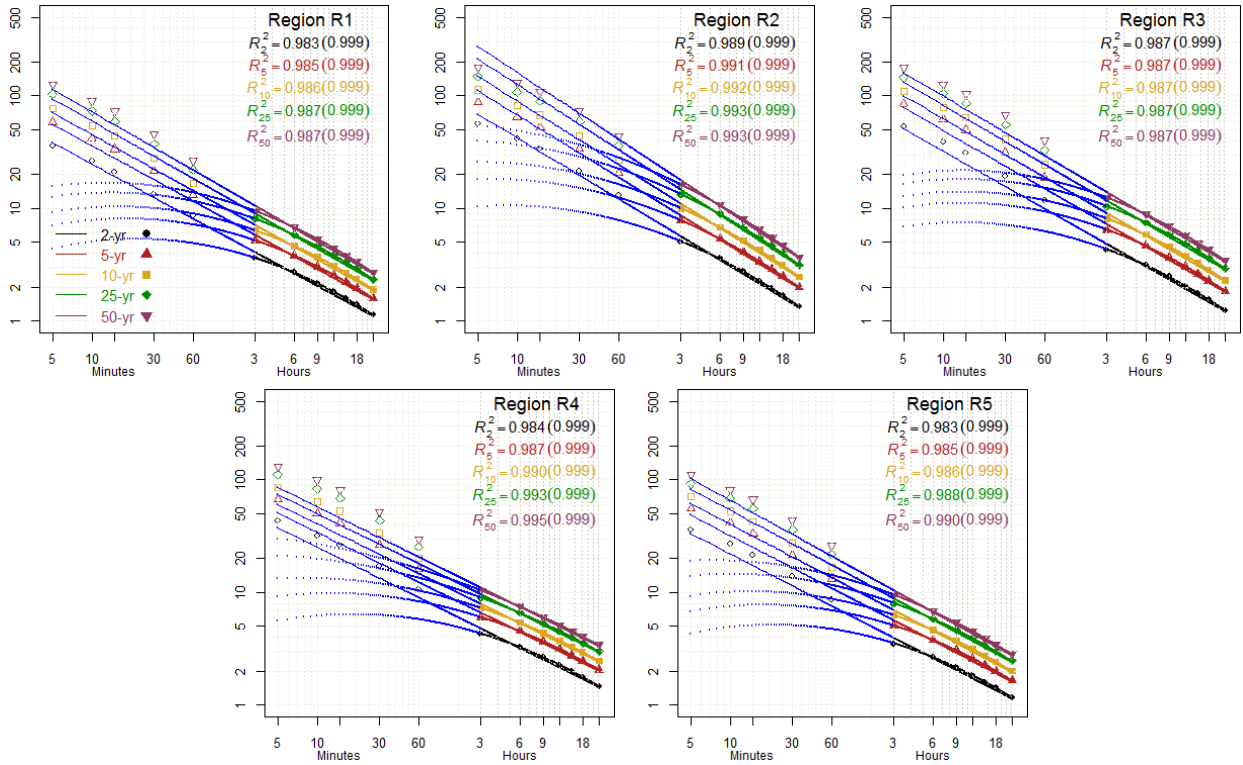


Figure C22: WRFG_CCSM simulated (a) current and (b) future IDF plots.

WRFG_CGCM3
(a) 1971–2000



(b) 2041–2070

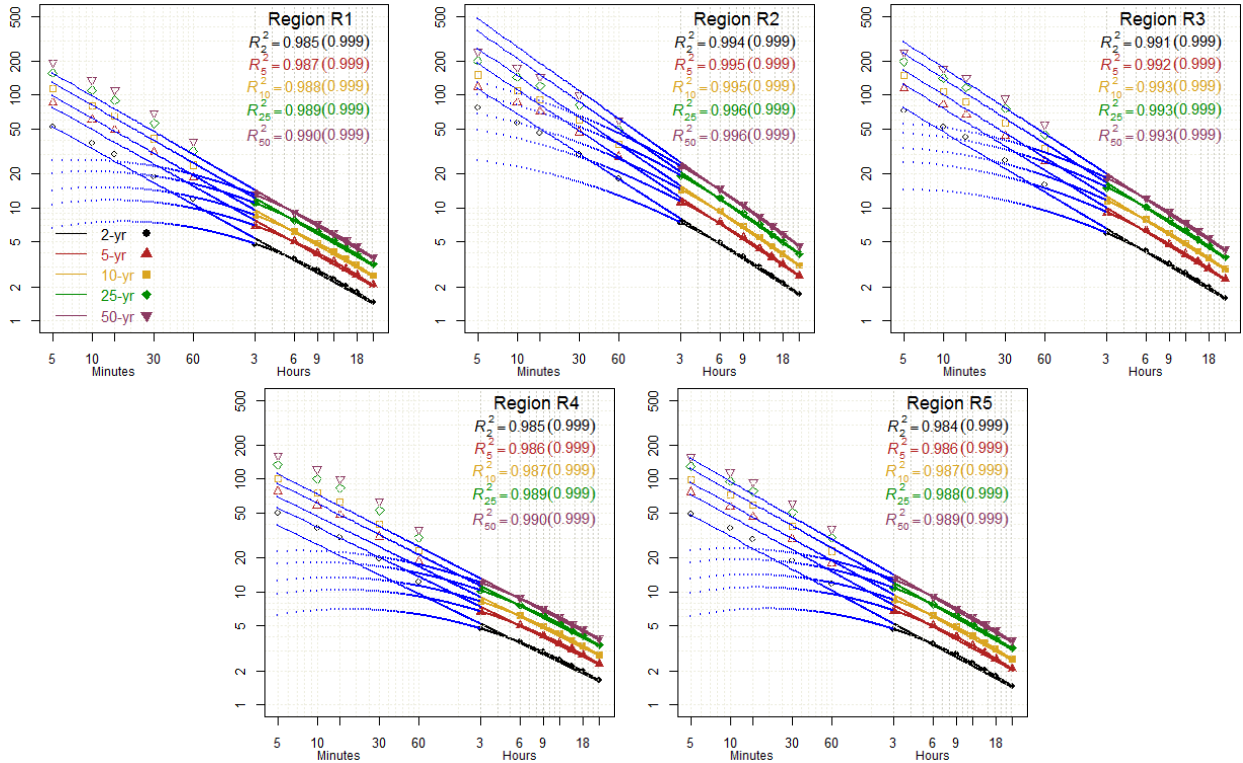


Figure C23: WRFG_CGCM3 simulated (a) current and (b) future IDF plots.

APPENDIX D: ATTRIBUTES OF OBSERVATION STATIONS

Table D.1. Attributes of observation stations (Dataset 1: DS1) used in the study. The homogeneous region associated with each station is also indicated.

ID	Site ID	Station name	Region	Eastings	Northings	Elevation (m)
1	GG89	HUDSON BAY	R1	-102.58	52.88	422
2	GG90	PELLY	R1	-101.87	52.08	509
3	GG93	CYPRESS RIVER	R1	-99.08	49.55	374
4	GG95	PORTAGE PRAIRIE	R1	-98.27	49.95	259
5	GG96	EMERSON AUT	R1	-97.23	49.00	242
6	GG98	MORDEN	R1	-98.08	49.18	298
7	GG99	SPRAGUE	R1	-95.60	49.02	329
8	G100	STEINBACH	R1	-96.77	49.53	254
9	G101	WINNIPEG	R1	-97.23	49.92	239
10	G102	ARBORG	R1	-97.08	50.93	224
11	G103	BERENS RIVER	R1	-97.03	52.35	222
12	G104	BISSETT	R1	-95.70	51.03	259
13	G105	GIMLI	R1	-97.02	50.63	223
14	G106	GRAND RAPIDS	R1	-99.28	53.15	223
15	G107	GREAT FALLS	R1	-96.00	50.47	249
16	G108	INDIAN BAY	R1	-95.20	49.62	327
17	G109	PINAWA WNRE	R1	-96.07	50.18	267
18	G110	DAUPHIN	R1	-100.05	51.10	305
19	G111	SWAN RIVER	R1	-101.23	52.12	335
20	G112	LANGRUTH WEST	R1	-98.80	50.42	264
21	G113	NEEPAWA MURRAY	R1	-99.57	50.15	412
22	G115	THE PAS	R1	-101.10	53.97	270
23	G119	NORWAY HOUSE	R1	-97.85	53.97	224
24	GG35	FORT MCMURRAY	R2	-111.22	56.65	369
25	GG40	FORT CHIPEWYAN	R2	-111.12	58.77	232
26	GG41	FORT VERMILION	R2	-116.03	58.38	289
27	GG43	KEG RIVER RS	R2	-117.62	57.75	405
28	GG79	URANIUM CITY	R2	-108.48	59.57	318
29	GG80	COLLINS BAY	R2	-103.70	58.18	490
30	GG81	CREE LAKE	R2	-107.13	57.35	495
31	GG82	ISLAND FALLS	R2	-102.35	55.53	299
32	GG83	KEY LAKE	R2	-105.62	57.25	509
33	GG84	LA RONGE	R2	-105.27	55.15	379
34	GG87	WHITESAND DAM	R2	-103.15	56.23	344
35	G114	FLIN FLON	R2	-101.88	54.77	320
36	G116	CHURCHILL	R2	-94.07	58.73	29
37	G117	GILLAM	R2	-94.72	56.35	145
38	G118	LYNN LAKE	R2	-101.08	56.87	357
39	G120	THOMPSON	R2	-97.87	55.80	222
40	GGG3	CORONATION	R3	-111.45	52.07	791
41	GG11	JENNER	R3	-111.20	50.72	755
42	GG14	SCOTFIELD	R3	-111.35	51.58	762
43	GG24	ONEFOUR	R3	-110.47	49.12	935
44	GG47	BANGOR	R3	-102.28	50.90	526
45	GG48	CEYLON	R3	-104.65	49.38	753
46	GG49	COTE	R3	-101.78	51.52	450
47	GG50	DAVIDSON	R3	-105.98	51.27	619
48	GG51	ESTEVAN	R3	-102.97	49.22	581
49	GG52	INDIAN HEAD	R3	-103.65	50.55	579
50	GG53	KELLIHER	R3	-103.75	51.25	676
51	GG54	MANOR	R3	-102.10	49.62	633
52	GG55	MOOSE JAW	R3	-105.55	50.33	577
53	GG56	MOOSOMIN	R3	-101.67	50.13	576
54	GG57	PASWEGIN	R3	-103.92	51.98	533
55	GG58	REGINA	R3	-104.67	50.43	577
56	GG59	YELLOW GRASS	R3	-104.18	49.82	580
57	GG60	TONKIN	R3	-102.23	51.20	527
58	GG61	ANEROID	R3	-107.30	49.72	754
59	GG62	LEADER	R3	-109.50	50.90	676

ID	Site ID	Station name	Region	Eastings	Northings	Elevation (m)
60	GG63	CHAPLIN	R3	-106.65	50.47	672
61	GG64	HIGH POINT	R3	-107.93	50.98	645
62	GG65	KLINTONEL	R3	-108.92	49.68	1074
63	GG66	SWIFT CURRENT	R3	-107.73	50.27	825
64	GG67	VAL-MARIE	R3	-107.85	49.37	808
65	GG68	WEST POPLAR	R3	-106.38	49.00	876
66	GG69	KINDERSLEY	R3	-109.18	51.52	694
67	GG70	BATTLEFORD	R3	-108.25	52.77	548
68	GG71	SCOTT	R3	-108.83	52.37	660
69	GG72	WASECA	R3	-109.40	53.13	638
70	GG73	MELFORT	R3	-104.60	52.82	490
71	GG74	OUTLOOK	R3	-107.05	51.48	541
72	GG75	PILGER	R3	-105.15	52.42	552
73	GG76	PRINCE ALBERT	R3	-105.67	53.22	428
74	GG77	SASKATOON	R3	-106.72	52.17	504
75	GG86	WASKESIU LAKE	R3	-106.07	53.92	569
76	GG88	NIPAWIN	R3	-104.00	53.33	372
77	GG91	BIRTLE	R3	-101.05	50.43	522
78	GG92	BRANDON	R3	-99.95	49.92	409
79	GG94	PIERSON	R3	-101.27	49.18	469
80	GG97	NINETTE	R3	-99.65	49.42	419
81	GGG1	CALMAR	R4	-113.85	53.28	720
82	GGG2	CAMROSE	R4	-112.82	53.03	739
83	GGG4	EDMONTON	R4	-113.58	53.32	723
84	GGG5	ELK POINT	R4	-111.07	53.88	605
85	GGG6	RANFURLY	R4	-111.73	53.42	673
86	GGG8	SION	R4	-114.12	53.88	701
87	GG30	ATHABASCA	R4	-113.28	54.72	515
88	GG32	CAMPSIE	R4	-114.68	54.13	671
89	GG34	ENILDA-BERG	R4	-116.30	55.42	591
90	GG36	SLAVE LAKE	R4	-114.78	55.28	583
91	GG37	WHITECOURT	R4	-115.78	54.15	782
92	GG38	BEAVERLODGE	R4	-119.40	55.20	745
93	GG39	FAIRVIEW	R4	-118.53	56.08	604
94	GG42	GRANDE PRAIRIE	R4	-118.88	55.18	669
95	GG44	PEACE RIVER	R4	-117.45	56.23	571
96	GG45	WABASCA RS	R4	-113.83	55.97	545
97	GG46	COLD LAKE	R4	-110.28	54.42	541
98	GG78	BUFFALO NARROWS	R4	-108.43	55.83	440
99	GG85	LOON LAKE	R4	-109.10	54.05	543
100	GGG7	ROCKY MT HOUSE	R5	-114.92	52.42	988
101	GGG9	STETTLER NORTH	R5	-112.72	52.33	821
102	GG10	DRUMHELLER	R5	-112.87	51.47	719
103	GG12	LACOMBE 2	R5	-113.75	52.45	860
104	GG13	OLDS	R5	-114.10	51.78	1040
105	GG15	CALGARY	R5	-114.02	51.12	1084
106	GG16	CLARESHOLM	R5	-113.73	49.93	1035
107	GG17	CARWAY	R5	-113.38	49.00	1354
108	GG18	GLEICHEN	R5	-113.05	50.88	905
109	GG19	LETHBRIDGE	R5	-112.80	49.63	929
110	GG20	MEDICINE HAT	R5	-110.72	50.02	717
111	GG21	MOUNTAIN VIEW	R5	-113.63	49.13	1339
112	GG22	PINCHER CREEK	R5	-113.98	49.52	1190
113	GG23	VAUXHALL	R5	-112.13	50.05	779
114	GG25	BANFF	R5	-115.55	51.20	1397
115	GG26	BEAVER MINES	R5	-114.18	49.47	1257
116	GG27	CROWSNEST	R5	-114.48	49.63	1303
117	GG28	HIGHWOOD	R5	-114.37	50.55	1580
118	GG29	JASPER WARDEN	R5	-118.03	52.93	1020
119	GG31	HINTON VALLEY	R5	-117.53	53.40	1011
120	GG33	EDSON	R5	-116.45	53.58	927

Table D.2. Attributes of engineering climate stations (Dataset 2: DS2) used in the study. The homogeneous region associated with each station is also indicated.

Region	Province	Site ID	Station Name	EnvCanID	Eastings	Northings	Elevation (m)
R1	AB	25	FORT CHIPEWYAN A	3072658	-111.7	58.46	232
R1	AB	27	HIGH LEVEL A	3073146	-117.1	58.37	338
R1	MB	56	LYNN LAKE A	5061646	-101.5	56.52	356
R1	SK	81	STONY RAPIDS A	4067PR5	-105.5	59.15	245
R1	SK	83	CLUFF LAKE	4061590	-109.31	58.22	330
R1	SK	84	COLLINS BAY	4061630	-103.42	58.11	491
R1	SK	85	CREE LAKE	4061861	-107.8	57.21	494
R1	SK	86	ISLAND FALLS	4063560	-102.21	55.32	299
R1	SK	87	LA RONGE A	4064150	-105.16	55.9	379
R1	SK	89	URANIUM CITY A	4068340	-108.29	59.34	318
R1	MB	53	CHURCHILL A	5060600	-94.4	58.44	29
R1	MB	54	GILLAM A	5061001	-94.43	56.22	145
R1	MB	57	THOMPSON A	5062922	-97.52	55.48	223
R2	MB	33	PORTAGE SOUTHPORT A	5012320	-98.16	49.54	269
R2	MB	34	ST ANDREWS A	50225DP	-97.2	50.3	231
R2	MB	35	DEERWOOD	5020720	-98.19	49.24	338
R2	MB	36	GLENLEA	5021054	-97.7	49.39	234
R2	MB	37	MIAMI THIESSEN	5021737	-98.15	49.27	297
R2	MB	38	MORDEN CDA	5021848	-98.5	49.11	297
R2	MB	39	PILOT MOUND (AUT)	5022125	-98.54	49.11	470
R2	MB	40	WINNIPEG HANGARLINE ROAD	5023224	-97.14	49.55	238
R2	MB	42	WINNIPEG STP	5023261	-97.6	49.57	232
R2	MB	43	BERENS RIVER A	5030202	-97.1	52.22	222
R2	MB	44	BISSETT	5030282	-95.42	51.2	259
R2	MB	45	GIMLI	5031038	-97.1	50.38	222
R2	MB	48	DAUPHIN A	5040680	-100.3	51.6	304
R2	MB	49	NEEPAWA WATER	5042005	-99.28	50.13	358
R2	MB	50	FLIN FLON A	5050960	-101.41	54.41	303
R2	MB	51	THE PAS A	5052880	-101.6	53.58	270
R2	MB	52	NORWAY HOUSE FORESTRY	506B0M7	-97.48	54	217
R2	MB	55	ISLAND LAKE A	5061376	-94.39	53.51	235
R2	SK	92	HUDSON BAY A	4083321	-102.19	52.49	359
R3	AB	2	CORONATION A	3011880	-111.27	52.4	791
R3	AB	14	MEDICINE HAT A	3034480	-110.43	50.1	716
R3	AB	17	MANYBERRIES CDA	3044200	-110.28	49.7	934
R3	MB	31	BRANDON A	5010480	-99.57	49.55	409
R3	MB	32	BRANDON CDA	5010485	-99.59	49.52	362
R3	SK	58	BROADVIEW	4010879	-102.34	50.22	599
R3	SK	59	DAVIN 5	4012164	-104.1	50.22	655
R3	SK	60	ESTEVAN A	4012400	-102.58	49.13	580
R3	SK	61	INDIAN HEAD CDA	4013480	-103.39	50.33	579
R3	SK	62	INDIAN HEAD PFRA	4013490	-103.41	50.3	604
R3	SK	63	MOOSE JAW A	4015320	-105.34	50.2	576
R3	SK	64	ORMISTON	4015680	-105.22	49.43	685
R3	SK	65	REGINA INT'L A	4016560	-104.4	50.26	577
R3	SK	66	WEYBURN	4018760	-103.5	49.39	569
R3	SK	67	WYNYARD	4019035	-104.12	51.46	560
R3	SK	68	YORKTON A	4019080	-102.28	51.16	498
R3	SK	69	SWIFT CURRENT A	4028040	-107.41	50.18	816
R3	SK	70	SWIFT CURRENT CDA	4028060	-107.44	50.16	825
R3	SK	71	BAD LAKE IHD 102	404037Q	-108.25	51.19	637
R3	SK	72	KINDERSLEY A	4043900	-109.11	51.31	693
R3	SK	73	NORTH BATTLEFORD A	4045600	-108.16	52.46	548
R3	SK	74	SCOTT CDA	4047240	-108.5	52.22	659
R3	SK	75	MELFORT CDA	4055085	-104.36	52.49	480
R3	SK	76	OUTLOOK PFRA	4055736	-107.3	51.29	541
R3	SK	77	PRINCE ALBERT A	4056240	-105.4	53.13	428
R3	SK	78	SASKATOON DIEFENBAKER INT'L A	4057120	-106.43	52.1	504
R3	SK	80	SASKATOON WATER TP	4057202	-106.41	52.7	483
R3	SK	90	WASKESIU LAKE	4068560	-106.5	53.55	532
R3	SK	91	NIPAWIN A	4075518	-104	53.2	371

Region	Province	Site ID	Station Name	EnvCanID	Eastings	Northings	Elevation (m)
R4	AB	7	ROCKY MTN HOUSE A	3015522	-114.55	52.26	988
R4	AB	9	LACOMBE CDA	3023720	-113.45	52.28	847
R4	AB	10	RED DEER A	3025480	-113.53	52.11	904
R4	AB	11	BROOKS AHRC	3030856	-111.51	50.33	758
R4	AB	12	CALGARY INT'L A	3031093	-114.1	51.7	1084
R4	AB	13	LETHBRIDGE A	3033880	-112.48	49.38	928
R4	AB	15	PINCHER CREEK A	3035202	-114	49.31	1189
R4	AB	16	VAUXHALL CDA	3036681	-112.8	50.3	778
R4	AB	19	KANANASKIS	3053600	-115.2	51.2	1391
R4	AB	20	EDSON A	3062244	-116.28	53.35	927
R5	AB	1	CAMROSE	3011240	-112.49	53.2	739
R5	AB	3	EDMONTON INT'L A	3012205	-113.35	53.19	723
R5	AB	4	EDMONTON CITY CENTRE A	3012208	-113.31	53.34	670
R5	AB	5	EDMONTON NAMA0 A	3012210	-113.28	53.4	687
R5	AB	6	ELLERSLIE	3012295	-113.33	53.25	693
R5	AB	8	VEGREVILLE CDA	3016761	-112.2	53.29	635
R5	AB	21	FORT MCMURRAY A	3062693	-111.13	56.39	369
R5	AB	22	SLAVE LAKE A	3066001	-114.47	55.18	580
R5	AB	23	WHITECOURT A	3067372	-115.47	54.8	782
R5	AB	24	BEAVERLODGE CDA	3070560	-119.24	55.12	744
R5	AB	26	GRANDE PRAIRIE A	3072920	-118.53	55.11	669
R5	AB	28	PEACE RIVER A	3075040	-117.27	56.14	570
R5	AB	29	WATINO	3077246	-117.38	55.43	393
R5	AB	30	COLD LAKE A	3081680	-110.17	54.25	541
R5	SK	82	BUFFALO NARROWS A	4060982	-108.26	55.5	433
R5	SK	88	MEADOW LAKE A	4065058	-108.31	54.8	480

APPENDIX E. PERMISSIONS FOR USE OF PUBLISHED MANUSCRIPTS

ELSEVIER LICENSE TERMS AND CONDITIONS

Feb 11, 2016

This is a License Agreement between Mohammad Masud ("You") and Elsevier ("Elsevier") provided by Copyright Clearance Center ("CCC"). The license consists of your order details, the terms and conditions provided by Elsevier, and the payment terms and conditions.

All payments must be made in full to CCC. For payment instructions, please see information listed at the bottom of this form.

Supplier	Elsevier Limited The Boulevard, Langford Lane Kidlington, Oxford, OX5 1GB, UK
Registered Company Number	1982084
Customer name	Mohammad Masud
Customer address	11 Innovation Boulevard Saskatoon, SK S7N3H5
License number	3806090535293
License date	Feb 11, 2016
Licensed content publisher	Elsevier
Licensed content publication	Journal of Hydrology
Licensed content title	Analysis of meteorological droughts for the Saskatchewan River Basin using univariate and bivariate approaches
Licensed content author	M.B. Masud, M.N. Khaliq, H.S. Wheater
Licensed content date	March 2015
Licensed content volume number	522
Licensed content issue number	n/a
Number of pages	15
Start Page	452
End Page	466
Type of Use	reuse in a thesis/dissertation
Portion	full article
Format	electronic
Are you the author of this Elsevier article?	Yes
Will you be translating?	No
Title of your thesis/dissertation	EVALUATION OF DRY AND WET EXTREMES OVER THE CANADIAN PRAIRIE PROVINCES BASED ON THE DYNAMICAL DOWNSCALING AND MULTIVARIATE FREQUENCY ANALYSIS APPROACHES
Expected completion date	May 2016

Estimated size (number of pages)	200
Elsevier VAT number	GB 494 6272 12
Permissions price	0.00 CAD
VAT/Local Sales Tax	0.00 CAD / 0.00 GBP
Total	0.00 CAD

Terms and Conditions

INTRODUCTION

1. The publisher for this copyrighted material is Elsevier. By clicking "accept" in connection with completing this licensing transaction, you agree that the following terms and conditions apply to this transaction (along with the Billing and Payment terms and conditions established by Copyright Clearance Center, Inc. ("CCC"), at the time that you opened your Rightslink account and that are available at any time at <http://myaccount.copyright.com>).

GENERAL TERMS

2. Elsevier hereby grants you permission to reproduce the aforementioned material subject to the terms and conditions indicated.

3. Acknowledgement: If any part of the material to be used (for example, figures) has appeared in our publication with credit or acknowledgement to another source, permission must also be sought from that source. If such permission is not obtained then that material may not be included in your publication/copies. Suitable acknowledgement to the source must be made, either as a footnote or in a reference list at the end of your publication, as follows:

"Reprinted from Publication title, Vol /edition number, Author(s), Title of article / title of chapter, Pages No., Copyright (Year), with permission from Elsevier [OR APPLICABLE SOCIETY COPYRIGHT OWNER]." Also Lancet special credit - "Reprinted from The Lancet, Vol. number, Author(s), Title of article, Pages No., Copyright (Year), with permission from Elsevier."

4. Reproduction of this material is confined to the purpose and/or media for which permission is hereby given.

5. Altering/Modifying Material: Not Permitted. However figures and illustrations may be altered/adapted minimally to serve your work. Any other abbreviations, additions, deletions and/or any other alterations shall be made only with prior written authorization of Elsevier Ltd. (Please contact Elsevier at permissions@elsevier.com)

6. If the permission fee for the requested use of our material is waived in this instance, please be advised that your future requests for Elsevier materials may attract a fee.

7. Reservation of Rights: Publisher reserves all rights not specifically granted in the combination of (i) the license details provided by you and accepted in the course of this licensing transaction, (ii) these terms and conditions and (iii) CCC's Billing and Payment terms and conditions.

8. License Contingent Upon Payment: While you may exercise the rights licensed immediately upon issuance of the license at the end of the licensing process for the transaction, provided that you have disclosed complete and accurate details of your proposed use, no license is finally effective unless and until full payment is received from you (either by publisher or by CCC) as provided in CCC's Billing and Payment terms and conditions. If full payment is not received on a timely basis, then any license preliminarily granted shall be deemed automatically revoked and shall be void as if never granted. Further, in the event that you breach any of these terms and conditions or any of CCC's Billing and Payment terms and conditions, the license is automatically revoked and shall be void as if never granted. Use of materials as described in a revoked license, as well as any use of the

materials beyond the scope of an unrevoked license, may constitute copyright infringement and publisher reserves the right to take any and all action to protect its copyright in the materials.

9. **Warranties:** Publisher makes no representations or warranties with respect to the licensed material.

10. **Indemnity:** You hereby indemnify and agree to hold harmless publisher and CCC, and their respective officers, directors, employees and agents, from and against any and all claims arising out of your use of the licensed material other than as specifically authorized pursuant to this license.

11. **No Transfer of License:** This license is personal to you and may not be sublicensed, assigned, or transferred by you to any other person without publisher's written permission.

12. **No Amendment Except in Writing:** This license may not be amended except in a writing signed by both parties (or, in the case of publisher, by CCC on publisher's behalf).

13. **Objection to Contrary Terms:** Publisher hereby objects to any terms contained in any purchase order, acknowledgment, check endorsement or other writing prepared by you, which terms are inconsistent with these terms and conditions or CCC's Billing and Payment terms and conditions. These terms and conditions, together with CCC's Billing and Payment terms and conditions (which are incorporated herein), comprise the entire agreement between you and publisher (and CCC) concerning this licensing transaction. In the event of any conflict between your obligations established by these terms and conditions and those established by CCC's Billing and Payment terms and conditions, these terms and conditions shall control.

14. **Revocation:** Elsevier or Copyright Clearance Center may deny the permissions described in this License at their sole discretion, for any reason or no reason, with a full refund payable to you. Notice of such denial will be made using the contact information provided by you. Failure to receive such notice will not alter or invalidate the denial. In no event will Elsevier or Copyright Clearance Center be responsible or liable for any costs, expenses or damage incurred by you as a result of a denial of your permission request, other than a refund of the amount(s) paid by you to Elsevier and/or Copyright Clearance Center for denied permissions.

LIMITED LICENSE

The following terms and conditions apply only to specific license types:

15. **Translation:** This permission is granted for non-exclusive world **English** rights only unless your license was granted for translation rights. If you licensed translation rights you may only translate this content into the languages you requested. A professional translator must perform all translations and reproduce the content word for word preserving the integrity of the article.

16. **Posting licensed content on any Website:** The following terms and conditions apply as follows: Licensing material from an Elsevier journal: All content posted to the web site must maintain the copyright information line on the bottom of each image; A hyper-text must be included to the Homepage of the journal from which you are licensing at <http://www.sciencedirect.com/science/journal/xxxxx> or the Elsevier homepage for books at <http://www.elsevier.com>; Central Storage: This license does not include permission for a scanned version of the material to be stored in a central repository such as that provided by Heron/XanEdu.

Licensing material from an Elsevier book: A hyper-text link must be included to the Elsevier homepage at <http://www.elsevier.com> . All content posted to the web site must maintain the copyright information line on the bottom of each image.

Posting licensed content on Electronic reserve: In addition to the above the following clauses are applicable: The web site must be password-protected and made available only to bona fide

students registered on a relevant course. This permission is granted for 1 year only. You may obtain a new license for future website posting.

17. **For journal authors:** the following clauses are applicable in addition to the above:

Preprints:

A preprint is an author's own write-up of research results and analysis, it has not been peer-reviewed, nor has it had any other value added to it by a publisher (such as formatting, copyright, technical enhancement etc.).

Authors can share their preprints anywhere at any time. Preprints should not be added to or enhanced in any way in order to appear more like, or to substitute for, the final versions of articles however authors can update their preprints on arXiv or RePEc with their Accepted Author Manuscript (see below).

If accepted for publication, we encourage authors to link from the preprint to their formal publication via its DOI. Millions of researchers have access to the formal publications on ScienceDirect, and so links will help users to find, access, cite and use the best available version. Please note that Cell Press, The Lancet and some society-owned have different preprint policies. Information on these policies is available on the journal homepage.

Accepted Author Manuscripts: An accepted author manuscript is the manuscript of an article that has been accepted for publication and which typically includes author-incorporated changes suggested during submission, peer review and editor-author communications.

Authors can share their accepted author manuscript:

- immediately
 - o via their non-commercial person homepage or blog
 - o by updating a preprint in arXiv or RePEc with the accepted manuscript
 - o via their research institute or institutional repository for internal institutional uses or as part of an invitation-only research collaboration work-group
 - o directly by providing copies to their students or to research collaborators for their personal use
 - o for private scholarly sharing as part of an invitation-only work group on commercial sites with which Elsevier has an agreement
- after the embargo period
 - o via non-commercial hosting platforms such as their institutional repository
 - o via commercial sites with which Elsevier has an agreement

In all cases accepted manuscripts should:

- link to the formal publication via its DOI
- bear a CC-BY-NC-ND license - this is easy to do
- if aggregated with other manuscripts, for example in a repository or other site, be shared in alignment with our hosting policy not be added to or enhanced in any way to appear more like, or to substitute for, the published journal article.

Published journal article (JPA): A published journal article (PJA) is the definitive final record of published research that appears or will appear in the journal and embodies all value-adding publishing activities including peer review co-ordination, copy-editing, formatting, (if relevant)

pagination and online enrichment.

Policies for sharing publishing journal articles differ for subscription and gold open access articles:

Subscription Articles: If you are an author, please share a link to your article rather than the full-text. Millions of researchers have access to the formal publications on ScienceDirect, and so links will help your users to find, access, cite, and use the best available version.

Theses and dissertations which contain embedded PJAs as part of the formal submission can be posted publicly by the awarding institution with DOI links back to the formal publications on ScienceDirect.

If you are affiliated with a library that subscribes to ScienceDirect you have additional private sharing rights for others' research accessed under that agreement. This includes use for classroom teaching and internal training at the institution (including use in course packs and courseware programs), and inclusion of the article for grant funding purposes.

Gold Open Access Articles: May be shared according to the author-selected end-user license and should contain a [CrossMark logo](#), the end user license, and a DOI link to the formal publication on ScienceDirect.

Please refer to Elsevier's [posting policy](#) for further information.

18. **For book authors** the following clauses are applicable in addition to the above: Authors are permitted to place a brief summary of their work online only. You are not allowed to download and post the published electronic version of your chapter, nor may you scan the printed edition to create an electronic version. **Posting to a repository:** Authors are permitted to post a summary of their chapter only in their institution's repository.

19. **Thesis/Dissertation:** If your license is for use in a thesis/dissertation your thesis may be submitted to your institution in either print or electronic form. Should your thesis be published commercially, please reapply for permission. These requirements include permission for the Library and Archives of Canada to supply single copies, on demand, of the complete thesis and include permission for Proquest/UMI to supply single copies, on demand, of the complete thesis. Should your thesis be published commercially, please reapply for permission. Theses and dissertations which contain embedded PJAs as part of the formal submission can be posted publicly by the awarding institution with DOI links back to the formal publications on ScienceDirect.

Elsevier Open Access Terms and Conditions

You can publish open access with Elsevier in hundreds of open access journals or in nearly 2000 established subscription journals that support open access publishing. Permitted third party re-use of these open access articles is defined by the author's choice of Creative Commons user license. See our [open access license policy](#) for more information.

Terms & Conditions applicable to all Open Access articles published with Elsevier:

Any reuse of the article must not represent the author as endorsing the adaptation of the article nor should the article be modified in such a way as to damage the author's honour or reputation. If any changes have been made, such changes must be clearly indicated.

The author(s) must be appropriately credited and we ask that you include the end user license and a DOI link to the formal publication on ScienceDirect.

If any part of the material to be used (for example, figures) has appeared in our publication with credit or acknowledgement to another source it is the responsibility of the user to ensure their reuse complies with the terms and conditions determined by the rights holder.

Additional Terms & Conditions applicable to each Creative Commons user license:

CC BY: The CC-BY license allows users to copy, to create extracts, abstracts and new works

CC BY: The CC-BY license allows users to copy, to create extracts, abstracts and new works from the Article, to alter and revise the Article and to make commercial use of the Article (including reuse and/or resale of the Article by commercial entities), provided the user gives appropriate credit (with a link to the formal publication through the relevant DOI), provides a link to the license, indicates if changes were made and the licensor is not represented as endorsing the use made of the work. The full details of the license are available at <http://creativecommons.org/licenses/by/4.0>.

CC BY NC SA: The CC BY-NC-SA license allows users to copy, to create extracts, abstracts and new works from the Article, to alter and revise the Article, provided this is not done for commercial purposes, and that the user gives appropriate credit (with a link to the formal publication through the relevant DOI), provides a link to the license, indicates if changes were made and the licensor is not represented as endorsing the use made of the work. Further, any new works must be made available on the same conditions. The full details of the license are available at <http://creativecommons.org/licenses/by-nc-sa/4.0>.

CC BY NC ND: The CC BY-NC-ND license allows users to copy and distribute the Article, provided this is not done for commercial purposes and further does not permit distribution of the Article if it is changed or edited in any way, and provided the user gives appropriate credit (with a link to the formal publication through the relevant DOI), provides a link to the license, and that the licensor is not represented as endorsing the use made of the work. The full details of the license are available at <http://creativecommons.org/licenses/by-nc-nd/4.0>. Any commercial reuse of Open Access articles published with a CC BY NC SA or CC BY NC ND license requires permission from Elsevier and will be subject to a fee.

Commercial reuse includes:

- Associating advertising with the full text of the Article
- Charging fees for document delivery or access
- Article aggregation
- Systematic distribution via e-mail lists or share buttons

Posting or linking by commercial companies for use by customers of those companies.

20. Other Conditions:

v1.8

Questions? customercare@copyright.com or +1-855-239-3415 (toll free in the US) or +1-978-646-2777.
